

NASA CONTRACTOR
REPORT

NASA CR-61191

February 1968

NASA CR-61191

STUDY OF ATMOSPHERIC AND AAP OBJECTIVES
OF CROSS-BEAM EXPERIMENTS

Prepared under Contract No. NAS 8-21065 by
A. D. St. John and W. D. Glauz

MIDWEST RESEARCH INSTITUTE

FACILITY FORM 602	N 68-17200	
	(ACCESSION NUMBER)	(THRU)
	207	1
	(PAGES)	(CODE)
	CR-61191	13
	(NASA CR OR TMX OR AD NUMBER)	(CATEGORY)

For

NASA-GEORGE C. MARSHALL SPACE FLIGHT CENTER
Huntsville, Alabama

February 1968

NASA CR-61191

STUDY OF ATMOSPHERIC AND AAP OBJECTIVES
OF CROSS-BEAM EXPERIMENTS
(Final Report)

By
A. D. St. John and W. D. Glauz

Prepared under Contract No. NAS 8-21065 by
MIDWEST RESEARCH INSTITUTE

For
Aero-Astroynamics Laboratory

Distribution of this report is provided in the interest of
information exchange. Responsibility for the contents
resides in the author or organization that prepared it.

NASA-GEORGE C. MARSHALL SPACE FLIGHT CENTER

PREFACE

This report was prepared by Midwest Research Institute under Contract No. NAS8-21065 for the National Aeronautics and Space Administration, George C. Marshall Space Flight Center. The work was performed in the Mathematical Analysis Section of the Mathematics and Physics Division, Dr. S. L. Levy, Division Director.

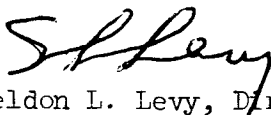
Dr. J. R. Scoggins and Mr. W. W. Vaughan, technical representatives for Marshall Space Flight Center, provided guidance and made numerous contributions to the program. Staff members of the IIT Research Institute (in particular, Drs. M. J. Fisher and A. J. Montgomery) and Dr. F. R. Krause of NASA, George C. Marshall Space Flight Center, provided briefings and helpful interpretations of their work in this area.

In the area of meteorological and atmospheric problems the writers were assisted by Dr. Ferdinand C. Bates, Dr. Alfred K. Blackadar, Dr. Richard Craig, Dr. Charles Hosler, Dr. James R. Scoggins, and Dr. Paul L. Smith who was a consultant to MRI for this project.

Contributors from the Midwest Research Institute staff include: Mr. R. Blackburn, Mr. W. Chauncey, Dr. W. D. Glauz, Dr. W. Longley, Mr. F. R. Rollins and Mr. A. D. St. John.

Approved for:

MIDWEST RESEARCH INSTITUTE



Sheldon L. Levy, Director
Mathematics and Physics Division

26 January 1968

TABLE OF CONTENTS

	<u>Page No.</u>
I. Introduction.	1
II. Summary	3
III. Rankings of Potential Applications.	6
IV. Atmospheric and Meteorological Problem Areas.	17
V. Detectors and Integration Time.	22
VI. Effects of Nonideal Environments on Cross-Beam Correlations.	23
VII. Natural Energy Sources and Optical Physics.	27
VIII. Power and Power Fluctuations in the Beam.	33
IX. Atmospheric Models.	35
X. Beam Power Calculation Results.	37
XI. Beam Size and Position.	51
XII. Critical Discussion and Future Efforts.	53
A. Critical Discussion	53
B. Future Potential of Cross-Beam Measurements in the Atmosphere.	56
C. Recommended Future Work	57
Cited References.	60
Supplementary References.	66
Appendix I - Summary of Proceedings of Cross-Beam/Meteorological Problems Symposium	69
Appendix II - Optical Physics and Atmospheric Models.	89
Appendix III - Analysis of Power Fluctuations in an Optical Beam	135

TABLE OF CONTENTS (Continued)

	<u>Page No.</u>
Appendix IV - Effects of Nonideal Environments on Cross-Beam Correlations.	159
Appendix V - Effect of Eddy Size and Beam Diameter on Beam Power.	185
Appendix VI - Detector Technology	187
Appendix VII - Integration Time Requirements.	195

List of Tables

<u>Table No.</u>	<u>Title</u>	<u>Page No.</u>
I	Ground-Based Applications for Scientific Purposes . . .	11
II	Ground-Based Applications for Operational Purposes. . .	12
III	Aircraft-Based Applications for Scientific Purposes . .	13
IV	Aircraft-Based Applications for Operational Purposes. .	14
V	Satellite-Based Applications for Scientific Purposes. .	15
VI	Satellite-Based Applications for Operational Purposes .	16
VII	Meteorological Problem Areas.	18
VIII	Results of Nonideal Environment Analyses.	26
IX	Atmospheric Models, Spectral and Weather Combinations .	36
X	Condensed Table of Beam Power Calculation Cases	39
XI	Mie Scattering Parameter, πs	141

List of Figures

<u>Figure No.</u>	<u>Title</u>	<u>Page No.</u>
1	Rayleigh Scattering Distribution.	29
2	Mie Scattering Distribution for a Wavelength of 0.45μ , Diermendjian's Haze "C"	31
3	Scattering, Absorption, and Source Characteristics. . .	32
4	Effect of Solar Zenith Angle, Clear Day, Telescope on Ground Looking Up, 0.45μ	41
5	Comparison of Ground-Based and Orbit-Based Telescopes, Clear Day, 45° Solar Zenith Angle, 0.45μ	43

TABLE OF CONTENTS (Continued)

<u>Figure No.</u>	<u>List of Figures</u> (Continued)	<u>Page No.</u>
6	Effect of Solar Zenith Angle, Hazy Day, Telescope on Ground Looking Up, 0.45μ	44
7	Telescope Pointing Down From Aircraft at 6 km. Clear Day 45° Solar Zenith Angle, 0.8 Earth Reflectance, 0.45μ	45
8	Comparison of Ground- and Aircraft-Based Telescopes, Clear Day, 45° Solar Zenith Angle, 0.45μ	47
9	Comparison of Ground-Based and Orbit-Based Telescopes, Clear Day, 0.04% H_2O Vapor, 9.5μ	48
10	Comparison of Ground-Based and Orbit-Based Telescopes, Clear Day, 4% H_2O Vapor, 9.5μ	49
11	Access to Upper Atmosphere From Orbit With Solar Ultraviolet.	50
12	Source of Power Variations From Outside Field of View. .	52
13	Rayleigh Scattering Coefficient vs. Altitude for Ultraviolet Wavelengths.	95
14	Rayleigh Scattering Coefficient vs. Altitude for Visible Wavelengths.	97
15	Rayleigh Scattering Coefficient vs. Altitude for Infrared Wavelengths	99
16	Aerosol (Mie) Scattering Coefficient vs. Altitude for Ultraviolet Wavelengths.	102
17	Aerosol (Mie) Scattering Coefficient vs. Altitude for Visible Wavelengths.	103
18	Aerosol (Mie) Scattering Coefficient vs. Altitude for Infrared Wavelengths	104
19	Haze Model Mie Scattering Coefficient vs. Altitude for a Wavelength of 0.45μ	105
20	Haze Model Mie Scattering Coefficient vs. Altitude for for a Wavelength of 9.5μ	106
21	Cloud Model Mie Scattering Coefficient vs. Altitude for a Wavelength of 0.45μ	108
22	Cloud Model Mie Scattering Coefficient vs. Altitude for a Wavelength of 9.5μ	109
23	Absorption Coefficient vs. Altitude for Ultraviolet Wavelengths.	113
24	Absorption Coefficient vs. Altitude for Visible Wavelengths.	115
25	Absorption Coefficient vs. Altitude for Infrared Wavelengths.	117

TABLE OF CONTENTS (Concluded)

<u>Figure No.</u>	<u>List of Figures (Concluded)</u>	<u>Page No.</u>
26	Haze Model Absorption Coefficient vs. Altitude for Wavelength of 9.5μ119
27	Cloud Model Absorption Coefficient vs. Altitude for a Wavelength of 9.5μ120
28	Emissivity vs. Altitude for a Wavelength of 9.5μ and Varying Atmospheric Conditions121
29	Fields of View With Multiple Limiting Apertures.132
30	Geometry of Optical Beam137
31	Location of Element of Beam.139
32	Details of Solid Angle139
33	Power Scattered but Retained Within Beam144
34	Power Scattered Into Beam.144
35	Power Scattered From a Plane149
36	Effects of Convection on Correlation Coefficient163
37	Relation Between Turbulence Region and Area of Integration.163
38	Effect of Convection on Integration Area167
39	Covariance for Turbulence Patch Centered Around Beam Normal.170
40	Effect of Cross Flow on Covariance Envelope for Turbulence Patch Centered Around Beam Normal171
41	Effect of Cross Flow on Autocorrelation for Turbulence Patch Centered Around Beam Normal.173
42	Covariance for Turbulence Patch Centered Above the Beam Normal with a Horizontal Cross Flow174
43	Effect of Cross Flow on Covariance Envelope for Turbulence Patch Centered Above the Beam Normal.175
44	Effect of Location of Turbulence Relative to Beam Normal on Integral Scale of Turbulence177
45	Determination of Cross Flow Velocity with Nonuniform Turbulence178
46	Effect of Shear, w' , on Correlation Envelope.181
47	Effect of Shear, w' , on Autocorrelation.182
48	Effect of Cross Flow Shear on Correlation Envelope183
49	Eddy Passing Through Optical Beam.186
50	Power Spectrum for Finite Beam186
51	Signal-to-Noise Ratio in the Visible Spectrum.191
52	Signal-to-Noise Ratio in the Infrared Spectrum193
53	Maximum Fractional Error, at 95% Confidence Level, in Cross Correlation for Zero Time Lag as a Function of Bandwidth and Integration Time198
54	Error in Correlation Determination vs. Time Lag for Selected Bandpasses and Integration Times.200

I. INTRODUCTION

A remote probing method, called the cross-beam technique, has been under development by the Marshall Space Flight Center and the IIT Research Institute. The cross-beam method, a new test arrangement for the remote sensing of fluid flow phenomena, employs the triangulation of two collimated light beams for local studies of a preselected region. This region is near the point of intersection of the two beams, or near the line of minimum separation between nearly intersecting beams.

The fluctuations of radiative power received at the two detectors are multiplied and averaged. The resulting "two-beam-product mean value" is then used to determine characteristics of the fluid flow which caused, or are related to, the fluctuations in optical properties along the two beams. These characteristics include convection speed, eddy lifetime, scale of turbulence, power spectrum of turbulence, and three-dimensional wave numbers. Further discussion of the basic principles is given by, for example, Fisher and Krause.^{1,2,3/}

The basic tenets of the cross-beam technique have been confirmed by a group of experiments. One series of experiments, carried out by Fisher et al.^{2-6/} involved the measurement of convection speed in flows of known direction. Both subsonic and supersonic turbulent jets were observed in the laboratory, using artificial light sources. The flow contained traces, either injected purposely or present naturally (e.g., condensed water vapor). These experiments were highly successful. Independent work by Wolff^{7/} utilized cross-beam apparatus in an atmospheric application. He determined the altitude of the 5577 Å nightglow, a naturally occurring radiation of low intensity located at about 100 kilometers. This work involved the determination of the altitude of beam crossing at which a maximum correlation, or two-beam-product mean value, was obtained -- a simpler application than is generally considered under the classification of cross-beam methods. Nevertheless, his efforts were successful, indicating the distinct possibility of using cross-beam techniques in the atmosphere.

It became obvious that the cross-beam technique was potentially a powerful tool for making remote measurements in the atmosphere, as well as in the laboratory. However, many basic differences exist in these two types of applications. For example, the use of natural, extended light sources vs. artificially generated optical beams; unknown flow properties vs. carefully produced, known flows; and potentially small correlated power fluctuations in a "noisy" background vs. large fluctuations, enhanced by tracers, occurring over a well defined portion of the beam path -- all of these

pose unanswered questions. In addition, one must consider the possibility of optical fluctuations at one point in the atmosphere being transmitted relatively unchanged to another point some distance away under varying meteorological conditions (in other words, being "visible" from afar).

A first feasibility study of atmospheric applications of the cross-beam method was carried out by Krause et al.^{8/} The present document reports the findings of a more in-depth study to aid in determining the value of the cross-beam method for atmospheric measurements. This study was primarily analytical with support by expert opinions. Guidance was obtained from experimental programs to measure near-ground-level winds. The experimental programs were being conducted concurrently with this study by NASA Marshall Space Flight Center, IIT Research Institute, and the Colorado State University, Department of Atmospheric Science.

The current study involved the separate consideration of many features relating to potential applications of the cross-beam system, such as meteorological problems and environments, optical physics, detectors, electromagnetic power fluctuations, etc. Then, these individual considerations were combined to yield a set of tables of potential applications of the system in the atmospheric environment. Each potential application is given a relative ranking as to the relative usefulness and value of the cross-beam technique.

Part II of this report presents, briefly, the main findings of the study. Part III contains the rankings and the rationale behind the ranking system. The reader is cautioned, however, that full understanding of these findings and rankings will probably require study of the remainder of the report. This is especially true if the reader is not familiar with the cross-beam concept and the work of the past several years on this subject.

Parts IV through XI contain in some detail the principal findings of the study. This material is backed up by the seven Appendices. Part XII contains a critical discussion of the work reported here, together with the authors' opinions concerning the most promising avenues of future research and development of the cross-beam system.

Following the main body of the report, and preceding the Appendices, are two bibliographies. The first, the cited references, are those reports that are explicitly mentioned in either the main body or in the Appendices. Following that is a list of supplementary references which were referred to by the authors and which had some influence on the course of the study and/or the conclusions developed.

II. SUMMARY

The goal of this project was to determine the potential value of the cross-beam technique in resolving meteorological and atmospheric problems. To attain this goal, several areas of study were undertaken. The separate studies were followed by the evaluation of the technique in relation to the chosen problem areas. The evaluation was to be supported as far as possible by authoritative opinion, and experimental and analytical results.

The major efforts in this evaluation were:

1. The identification of meteorological and atmospheric problem areas whose resolutions have scientific and/or operational importance.
2. An appraisal of the value of the cross-beam technique in resolving the problems, under ideal conditions.
3. An appraisal of the data requirements.
4. An appraisal of the cross-beam technique under nonideal conditions.
5. An appraisal of the ability to reach problem regions in the atmosphere through electromagnetic radiation which arises naturally in extended sources.
6. A codification of all these considerations in a ranking system.

In the area of problem identification it was found that there is a dearth of useful quantitative information on the atmosphere. Further, this information is in many cases prerequisite to the resolution of problems with great scientific and operational value. The problems cover all scales from the general circulation to synoptic to microscopic. In general, information is required about the transport and diffusion of energy and moisture. The measurements of convection speed and turbulence characteristics, ideally available from the cross-beam technique, would have great value especially if they could be combined with temperature and moisture measurements. Reduced but appreciable value could be derived from the ideal cross-beam measurements by themselves. Even the ability to measure remotely one component of convection velocity would in some cases be very valuable.

In a majority of operational applications there is a requirement for processed results shortly after (few seconds to minutes) the data are obtained. A somewhat longer time for processing would be available for some weather prediction applications. In addition, an "all weather" capability is required for many operational atmospheric measurement systems.

There are two considerations in the amount of data required. First, it is obvious that the quantity will depend on the geographical size of the problem, the number of grid points, the types of information required, and the temporal duration of the problem. There is also the question, how much data must be obtained at one point (or region) to define the flow properties to a suitable degree of confidence?

The amount of data (measured by the length in time of a data record) depends to a great extent on the bandwidth of the analyzed signals which, in turn, is limited by detector noise considerations. Current atmospheric cross-beam experiments indicate that at least 10 minutes of data are required to estimate the magnitude of the peak correlation within 50% with 95% confidence. This is the least demanding measurement. Measurements of more direct utility such as the wind vector component will require larger (probably significantly larger) quantities of data.

An analysis was performed for the simple, stationary (nonsweeping), two beam system in nonideal environments. It was found that the values of some flow features could be distorted by the nonideal situations. However, in all cases one component of velocity was correctly indicated. Other flow quantities obtainable in order of decreasing reliability are: the scale of turbulence, the power spectrum, and the eddy lifetime. The same analysis indicated some possibility of measuring a second component of velocity under the nonideal conditions.

An analysis was made of the flow of electromagnetic energy in a beam through the atmosphere. The analysis included accounts of scattering in and out of the beams, and absorption and emission within the beams. The analysis was applied for a variety of weather conditions, a variety of energy sources, and in three spectral regions. Two major restrictions were found.

1. A cloud will block access* to information from the far side. (The cloud becomes a pseudo plane of diffuse emission or reflectance.)

* Access refers to the capability of detection, at one location, of optical fluctuations occurring at another location. In a practical sense access depends not only on the atmosphere at the region of interest but also along the entire sight path. While there may be some effect by the optics of the detection system this is not the primary consideration.

2. The present, two-beam technique is defeated when the beams "see" successive regions of a variably lighted or variably emissive background such as a cloud surface or the earth's surface.

Within the (current) bounds above, additional results were:

1. Access to the lower atmosphere (up to 3 to 15 kilometers) is essentially the same as near-ground access.

2. Access to the lower atmosphere may be made from the ground, aircraft or orbit-based equipment. In general those systems which look at the earth have less desirable signals as a result of the back light energy input. (This is a separate consideration from the currently dis-barring effect associated with variable back lighting.)

3. Upward looking systems in aircraft can extend the accessible region to slightly higher altitudes.

4. Weather conditions and primary light sources can combine favorably or unfavorably so that the required power variations change by at least two orders of magnitude.

With less numerical substantiation it appears that:

5. Access to the upper atmosphere may be possible using air-glow as an emitting tracer.

6. Access to the upper atmosphere may be achieved from orbit using spectral regions of limited path length (i.e., high extinction coefficients).

The final effort of the evaluation was the codification of the previous considerations in a ranking system. Separate ranking tables are presented for ground-based systems, aircraft-based systems, and orbit-based systems. The scientific and operational applications are also separately ranked. The rankings in one table cannot be compared numerically with those in another table.

The potential applications are evaluated with regard to nine categories which are:

1. Value of applications,
2. Value of cross-beam (ideal),

3. Value of cross-beam with nonideal environments,
4. Accessibility of area to optical beam (ideal),
5. Accessibility of area to optical beam considering weather associated with potential application,
6. Relative ease in locating problem region,
7. Relative statistical stationarity of situation,
8. Time allowed for data reduction, and
9. Volume of data required.

Under Category 1, value of application, the authors have attempted to use the proportion of the population benefited as a weight factor. Other approaches may be equally appropriate.

It should also be noted that nowhere is the capability of the cross-beam technique set equal to zero. The present system is marginal in useful signal attained and is defeated by varying backgrounds. The first problem may be due partly to the short development period. The second problem may be amenable to resolution by additional beams or beam-spectral combinations. The moving-beam systems (aircraft- and orbit-based) also are in a less well established state. Consequently the rankings must be viewed as applicable to different time frames of development. The current experimental cross-beam system is restricted almost exclusively to the ground-based system looking up.

The rankings are shown in the tables in Section III of the report.

III. RANKINGS OF POTENTIAL APPLICATIONS

The rankings are made separately for ground-based, aircraft-based and orbit-based systems. Scientific and operational applications are also considered separately.

Each potential application is given a numerical weight in each of several categories. The product of the weights then forms a measure of the predicted usefulness and value of the cross-beam technique for the particular application.

The weight in each category varies from 0 to 1. A weight of 1 is always given to the potentially best application for the particular category, with the other applications receiving some fraction of 1. The value, 1, does not imply certainty of success for the category, however. For example, if application "B" rates twice as high as application "A", as regards category "X", then "B" would receive a weight of 1.0 and "A" would receive a weight of 0.5. The weights are, in many cases, subjective in the sense that opinions must often be used. These opinions, where possible, are based on analytical or definitive studies presented in this report or its references.

The description of each category is given below.

Category 1 - Value of Application

- a. Operational: An estimate of the relative value to society of the operational application. This value is independent of the means, cost, etc., of obtaining the data needed for the application.
- b. Scientific: An estimate of the relative value to science of obtaining the data in question. This value is also independent of the means, cost, etc., of obtaining the data. Consideration of ultimate usefulness of scientific findings to society is included.

The authors have included the fraction of society benefited in the weight factor for operational and scientific applications. Other approaches may be equally appropriate. Furthermore, subjective opinion is recognized as playing a part in ranking this category. This opinion is undoubtedly influenced by the particular scientists who contributed, in greater or lesser degree, to the present program.

Category 2 - Value of Cross-Beam

An estimate of the value of the cross-beam technique in the application. Here it is assumed that the technique is fully capable of providing the information (wind speed, scale of turbulence, eddy lifetime, power spectrum) that the idealized theory indicates. The value, therefore, considers need of other additional information, availability of simpler techniques, etc.

Category 3 - Nonideal Environments

The probability of the cross-beam technique being able to obtain the information indicated by Category 2 in the presence of nonideal local environments. Only the considerations of Appendix IV are involved here. Other factors are given in subsequent categories.

Category 4 - Ideal Accessibility of Area to Optical Beam

The effect on a generated signal due to intervening atmosphere and the atmosphere beyond the region of interest is of concern here. In this category, ideal (clear air) conditions are assumed. Factors considered are the amount and properties of the atmosphere to be traversed in reaching the region of interest and the effect on received power of a beam which broadens with distance.

Category 5 - Accessibility Degradation Due to Normal Meteorological Conditions

The weight given in this category multiplies that of Category 4 to give a combined effect of accessibility. Factors to be considered include the degree of the effect of adverse conditions and the need to obtain data under the adverse conditions.

Category 6 - Relative Ease in Locating Problem Region

Some applications involve phenomena which are localized and must be located before studying. Included in this weight is the ease of moving the beams to the site, or alternatively, of waiting for the phenomena to come within range. This category does not apply to some applications. In those cases a weight of 1.0 is assigned.

Category 7 - Relative Stationarity of Situation

A reasonable period of data collection is necessary to obtain statistically significant correlations. The longer a given situation remains statistically stationary (or, the longer data record in time that can be obtained), the larger weight that is given. Signal intensity is also a factor here.

Category 8 - Time Available for Data Reduction, i.e., Responsiveness

This factor affects only the operational applications. A small weight indicates relatively quick data processing is required. Cost of such data processing is not considered here. Responsiveness could be a significant factor for some applications.

Category 9 - Volume of Data Required

Associated with data volume is cost of data processing, although all data need not be processed. The weight considers both the volume and the costs. The weights are not linearly related to the volume of data, but more nearly to the square root of the volume. This was done to prevent the weights in Category 9 from overriding all other categories.

Attention is directed to the fact that the categories do not include an item which says unequivocally that the cross-beam technique will or will not work in the ranked application. Even with the added information provided by the present project there is no reasonable basis for making such positive distinctions. It is clear that the current system capabilities are very limited. For instance, the concurrent experimental program has shown that the correlated signal fluctuations are at best marginal. The analyses performed here confirm that variably lighted backgrounds will defeat the present system. There are, however, no analyses or experimental results which indicate that the signal levels cannot be improved or that the variably lighted background is fundamentally incapable of resolution. Consequently, in those categories which involve the probability of successful measurements the rankings are based on such factors as can be evaluated. These factors are the reliability of measurements and the electromagnetic access to the atmospheric region involved.

As a consequence of the situation described above the rankings presented here apply to the current state of the art and to projected future states of this art. Some idea of current and future states can be summarized as follows:

1. The current state shows a marginal capability to measure one wind component near ground level using a ground-based system.
2. Short range projection for the state of the art should show improved confidence levels in wind component measurements and the inclusion of turbulence-descriptive quantities.
3. Short to medium projection for the state of the art would extend the capabilities to a moving system.

4. The resolution of the variably lighted background is most likely a relatively long range goal.

These time frames should be considered when interpreting the tabular rankings.

Tables I to VI give the rankings of potential applications for the current and projected cross-beam systems. Due to the "normalization" of each category within each of the six types of applications (ground-, air- or orbit-based; scientific or operational) it is not possible to compare one table with another. Even if the normalization is modified, it would still be necessary to assign a relative worth (weight) to operational vs. scientific applications and a weight (cost?) to the orbit-based vs. aircraft-based or ground-based systems. The authors have not done this.

TABLE I

GROUND-BASED APPLICATIONS
FOR SCIENTIFIC PURPOSES

RATING CATEGORY	APPLICATION									RELATIVE USEFULNESS AND VALUE OF THE CROSS-BEAM TECHNIQUE
	1	2	3	4	5	6	7	8	9	
APPLICATION	VALUE OF APPLICATION	USEFULNESS OF IDEAL CROSS-BEAM	INFLUENCE ON 2. OF NONIDEAL ENVIRONMENTS	IDEAL ACCESSIBILITY OF AREA TO BEAM	INFLUENCE ON 4. OF ADVERSE MET. CONDITIONS	EASE OF LOCATING PROBLEM REGION	RELATIVE LENGTH OF STATIONARY DATA RECORD AVAILABLE	TIME AVAILABLE FOR DATA REDUCTION	AMOUNT OF DATA REQUIRED	
	MESOSCALE AND MICROSCALE WINDS (LOW ALTITUDE)	0.5	1.0	1.0	1.0	1.0	0.8	-	0.3	6×10^{-2}
	SURFACE FRICTION EFFECTS ON LOW LEVEL WINDS	0.4	1.0	1.0	1.0	0.5	1.0	-	0.3	3×10^{-2}
	UPPER ATMOSPHERE WIND MEASUREMENTS	0.2	1.0	1.0	0.8	1.0	0.8	-	1.0	3×10^{-2}
	ENERGY DISSIPATION IN THE ATMOSPHERE	1.0	1.0	0.3	0.3	1.0	0.8	-	0.3	2×10^{-2}
	STATISTICAL PROPERTIES OF ATMOSPHERIC TURBULENCE	0.5	1.0	0.1	0.3	1.0	0.8	-	0.3	3×10^{-3}
	DENSITY & COMPOSITION OF UPPER ATMOSPHERE	0.3	0.1	0.1	1.0	1.0	1.0	-	1.0	6×10^{-4}
	CLOUD STUDIES FOR WEATHER MODIFICATION	0.9	0.5	0.8	0.5	0.05	0.2	-	0.3	4×10^{-4}
	AIRGLOW STUDIES	0.05	0.3	0.5	1.0	0.5	0.3	-	1.0	2×10^{-4}

TABLE II

GROUND-BASED APPLICATIONS
FOR OPERATIONAL PURPOSES

RATING CATEGORY	APPLICATION									RELATIVE USEFULNESS AND VALUE OF THE CROSS-BEAM TECHNIQUE
	1	2	3	4	5	6	7	8	9	
WIND MONITORING NEAR AIRPORTS AND LAUNCH FACILITIES	0.5	0.1	1.0	1.0	1.0	1.0	1.0	0.3	1.0	8×10^{-3}
	1.0	1.0	1.0	0.5	1.0	0.1	0.1	0.3	0.3	5×10^{-4}
	0.3	0.1	0.5	1.0	0.5	0.3	1.0	1.0	0.2	5×10^{-4}
	0.3	0.3	0.3	0.3	0.3	0.1	0.3	1.0	0.1	7×10^{-6}
CLOUD STUDIES FOR WEATHER MODIFICATION										
AIR POLLUTION STUDIES										
LOCATING CLEAR AIR TURBULENCE										

TABLE III
AIRCRAFT-BASED APPLICATIONS
FOR SCIENTIFIC PURPOSES

RATING CATEGORY	APPLICATION									RELATIVE USEFULNESS AND VALUE OF THE CROSS-BEAM TECHNIQUE
	1	2	3	4	5	6	7	8	9	
UPPER ATMOSPHERE WIND MEASUREMENTS CLOUD STUDIES FOR WEATHER MODIFICATION DENSITY AND COMPOSITION OF UPPER ATMOSPHERE THUNDERSTORM RESEARCH	VALUE OF APPLICATION	USEFULNESS OF IDEAL CROSS-BEAM	INFLUENCE ON 2. OF NONIDEAL ENVIRONMENTS	IDEAL ACCESSIBILITY OF AREA TO BEAM	INFLUENCE ON 4. OF ADVERSE MET. CONDITIONS	EASE OF LOCATING PROBLEM REGION	RELATIVE LENGTH OF STATIONARY DATA RECORD AVAILABLE	TIME AVAILABLE FOR DATA REDUCTION	AMOUNT OF DATA REQUIRED	6 X 10 ⁻² 3 X 10 ⁻³ 1 X 10 ⁻³ 6 X 10 ⁻⁴
	0.2	1.0	1.0	0.3	1.0	1.0	1.0	-	1.0	
	1.0	0.3	0.8	1.0	0.3	0.5	0.3	-	0.3	
	0.3	0.1	0.1	0.3	1.0	1.0	1.0	-	1.0	
	0.3	0.5	0.8	1.0	0.3	0.2	0.3	-	0.3	

TABLE IV

AIRCRAFT-BASED APPLICATIONS
FOR OPERATIONAL PURPOSES

RATING CATEGORY	APPLICATION									RELATIVE USEFULNESS AND VALUE OF THE CROSS-BEAM TECHNIQUE
	1	2	3	4	5	6	7	8	9	
	VALUE OF APPLICATION	USEFULNESS OF IDEAL CROSS-BEAM	INFLUENCE ON 2. OF NONIDEAL ENVIRONMENTS	IDEAL ACCESSIBILITY OF AREA TO BEAM	INFLUENCE ON 4. OF ADVERSE MET. CONDITIONS	EASE OF LOCATING PROBLEM REGION	RELATIVE LENGTH OF STATIONARY DATA RECORD AVAILABLE	TIME AVAILABLE FOR DATA REDUCTION	AMOUNT OF DATA REQUIRED	
CLOUD STUDIES FOR WEATHER MODIFICATION	1.0	0.5	1.0	1.0	0.3	1.0	0.3	0.3	1.0	1×10^{-2}
SEVERE THUNDERSTORM WARNING/MODIFICATION	0.3	1.0	1.0	1.0	0.1	1.0	0.3	0.3	1.0	3×10^{-3}
AIR POLLUTION STUDIES	0.3	0.05	1.0	1.0	1.0	0.5	0.3	1.0	0.3	7×10^{-4}
LOCATING CLEAR AIR TURBULENCE	0.3	0.2	0.3	0.8	1.0	0.2	1.0	1.0	0.1	3×10^{-4}

TABLE V
SATELLITE-BASED APPLICATIONS
FOR SCIENTIFIC PURPOSES

RATING CATEGORY	APPLICATION									RELATIVE USEFULNESS AND VALUE OF THE CROSS-BEAM TECHNIQUE
	1	2	3	4	5	6	7	8	9	
APPLICATION	VALUE OF APPLICATION	USEFULNESS OF IDEAL CROSS-BEAM	INFLUENCE ON 2. OF NONIDEAL ENVIRONMENTS	IDEAL ACCESSIBILITY OF AREA TO BEAM	INFLUENCE ON 4. OF ADVERSE MET. CONDITIONS	EASE OF LOCATING PROBLEM REGION	RELATIVE LENGTH OF STATIONARY DATA RECORD AVAILABLE	TIME AVAILABLE FOR DATA REDUCTION	AMOUNT OF DATA REQUIRED	
	UPPER ATMOSPHERE WIND MEASUREMENTS	0.2	1.0	0.1	1.0	1.0	1.0	-	1.0	2×10^{-2}
	ENERGY DISSIPATION IN THE ATMOSPHERE	1.0	1.0	0.8	0.3	1.0	1.0	-	0.3	7×10^{-3}
	WORLD-WIDE ATMOSPHERIC STABILITY MEASUREMENTS	0.8	0.3	0.8	0.3	1.0	1.0	-	0.3	2×10^{-3}
	DENSITY & COMPOSITION OF UPPER ATMOSPHERE	0.3	0.1	0.1	1.0	1.0	1.0	-	1.0	3×10^{-4}
	STUDY OF AIRGLOW	0.05	0.3	0.5	1.0	0.5	0.3	-	0.3	2×10^{-4}
	FORMATION AND LIFE OF HURRICANES	0.3	0.3	1.0	0.3	0.2	0.3	-	0.3	1.5×10^{-4}

TABLE VI

SATELLITE-BASED APPLICATIONS
FOR OPERATIONAL PURPOSES

RATING CATEGORY	VALUE OF									APPLICATION	RELATIVE USEFULNESS AND VALUE OF THE CROSS-BEAM TECHNIQUE
	1	2	3	4	5	6	7	8	9		
	APPLICATION	USEFULNESS OF IDEAL CROSS-BEAM	INFLUENCE ON 2. OF NONIDEAL ENVIRONMENTS	IDEAL ACCESSIBILITY OF AREA TO BEAM	INFLUENCE ON 4. OF ADVERSE MET. CONDITIONS	EASE OF LOCATING PROBLEM REGION	RELATIVE LENGTH OF STATIONARY DATA RECORD AVAILABLE	TIME AVAILABLE FOR DATA REDUCTION	AMOUNT OF DATA REQUIRED		
	1.0	1.0	1.0	1.0	0.1	1.0	1.0	1.0	0.2		2×10^{-2}
WORLD-WIDE WIND MEASUREMENTS FOR WEATHER PREDICTION	0.3	0.5	1.0	1.0	0.3	0.5	0.3	0.5	1.0		4×10^{-3}
PREDICTION OF HURRICANE MOTION	0.1	0.3	0.3	0.2	1.0	0.1	0.1	0.1	0.1		2×10^{-7}
LOCATING CLEAR AIR TURBULENCE											

IV. ATMOSPHERIC AND METEOROLOGICAL PROBLEM AREAS

A search was made to locate problems whose resolution would have significant scientific or operational value. Further, an attempt was made to determine the value of the cross-beam measurements in resolving these problems. Candidate problem areas were defined by a group of authoritative meteorologists at a small symposium held for this purpose. In addition, questionnaires were sent to a broad spectrum of meteorologists and scientists in universities, government, and industry.

Two salient facts emerged from the results of this search.

(1) There is a dearth of useful quantitative information about the atmosphere. (2) The acquisition of atmospheric data is prerequisite to numerous scientific and operational activities which have great potential value.

The most valuable potentials of the cross-beam appeared to be the abilities to measure remotely the wind or wind components, and the characteristics of turbulence. These measurements have value in a variety of applications as shown in Table VII.

The list in Table VII is not exhaustive for terrestrial meteorology applications. In addition there are other potential applications which, for one or more reasons, are outside this project scope. Among these are extra-terrestrial atmosphere studies, underwater applications and probes of cloud interiors. There is great meteorological interest in the cloud interior both for the winds and the size and motion of precipitates. A microwave adaption of the cross-beam technique with artificial sources is conceivable. The use of more than one wavelength might permit sizing of precipitates and, by their motions, the driving winds might be inferred.

TABLE VII

METEOROLOGICAL PROBLEM AREAS

<u>Atmospheric Region</u>	<u>General Subject Area</u>	<u>Specific Interest</u>	<u>Measurements Required</u>	<u>Comments</u>
Upper atmosphere	Winds	Correlation with tidal and gravity waves	Winds over 24 hour periods	All these items reflect current lack of knowledge about upper atmosphere behavior. Relation to or effect on lower atmosphere is unknown but thought to be small.
	Turbulence characteristics		Eddy lifetime, scale, power spectrum	
	Properties		Density composition	Measurements required not part of current cross-beam capability. Measurements have value for space vehicles and possibly supersonic transport.
	Airglow	Time and space variations	Intensities, power spectrum of radiation	Airglow can be seen with cross-beam optical and detector elements. Measurements required are not part of cross-beam capability but system should be adaptable for altitude identification.
	Radio propagation	Effects of refractive variations	Scale and intensities of refractive variations	Cross-beam not presently capable of distinguishing sources of observed variations. Subject has value scientifically and operationally for surface to surface and surface - space communications.
Primarily lower atmosphere	World weather watch	Winds	Averages over 500 km grids with resolution of values at up to 9 altitudes. One measurement in 12 or 24 hours useful. All values measured within one hour most desirable.	Global measurements are prerequisite to effective mathematical prediction (by simulation). Great operational value. Scientific value also in supplying partial information on flux of energy and moisture. Less than global coverage useful for improving weather forecasts over extensive (continent sized) regions.
		One component of winds	One measurement in 6 hours	The north-south component at small latitudes would be useful for estimating convective fluxes on a global scale. The east-west component along meridians would have value for weather forecasting.
	Stability		Direct measurement of turbulence or wind measurements plus temperature	Has operational value for forecasting turbulence and weather. Has scientific value for identifying the diffusion of energy and moisture in the atmosphere.

TABLE VII (continued)

Atmospheric Region	General Subject Area	Specific Interest	Measurements		Comments
			Required	Available	
Primarily lower atmosphere (concluded)	World weather watch (continued)	Clear air turbulence	Same as above plus ozone detection in upper atmosphere	There is a possibility of detecting CAT of significance by aircraft if the spectral energy is sufficiently distinctive. However, regions of high probability are more likely to be amenable to detection and forecast.	
	Hurricanes	Origins	Winds and eddy scale as measured in world weather watch & energy spectrum	Stored data could be used to trace back in time from established hurricane to origins. Initially scientific, the measurements might ultimately have forecast value.	
		Mechanics of storm	Winds around elements of overall storm, Associated energy and moisture fluxes.	The interaction of elements or cells within the storm are not well understood. Initial value would be scientific.	
Lower atmosphere		Path prediction	Winds around but outside of overall storm	Values are needed to implement the currently available "steering method". Has high operational, forecast value.	
	Severe thunderstorms	Prediction	World weather watch winds	High operational value.	
		Mechanics and interaction with environment	Winds, temperatures and moisture contents around storm boundary. Turbulence and mixing at storm boundaries	Crossbeam capability restricted to winds and turbulence measurements which would be valuable by themselves. Numerous and simultaneous measurements desirable, however, as few as three would be valuable if taken within a 5-minute period. Vertical wind compounds under clouds desirable. Cross boundary component has some value. Operational value (to predict intensification, etc.) would require quick (5 minutes to 30 minutes) data reduction.	
	Tornadoes	Area prediction	Same as severe thunderstorms		

TABLE VII (continued)

Atmospheric Region	General Subject Area	Specific Interest	Measurements Required	Comments
Lower atmosphere (continued)	Tornadoes	Invisible vortices	High spatial resolution winds	Current evidence indicates the occurrence of high speed vortices below and in cumulus congestus. The vortices below the cloud (an extreme hazard to aircraft) may be of insufficient intensity to cause local condensation and identification. These conditions may also be precursors to full strength vortices with destructive intensities at the ground. Scientific and ultimately operational value.
	Clouds	Weather modification	Same as thunderstorm mechanisms and interaction	Similar distinction between scientific and operational use in that operational use requires data acquisition and reduction in approximately 5 minutes.
	Aircraft operations	Clear air turbulence	Presented above	
		Wind shear	Wind measurements at fine vertical scale near ground	During approach and landing, large mass aircraft may descend into reduced headwinds so that flying speed is compromised or lost. Operational value.
		Wake turbulence	Energy in scales likely to affect aircraft control	Heavy aircraft trail vortices which are especially intense at the low speeds in approach, landing take off. Lighter aircraft may be uncontrollable in these vortices. Scientific value lies in identification of weather and terrain effects on persistence of vortices with subsequent application to operations. Direct sensing above runway would constitute another operational application of value.
	Launch facilities application	Vehicle security on pad and in flight	Winds and turbulence versus altitude	Winds and turbulence induce vehicle loads while on the launch site and in flight. Direct operational use requires fast data processing. Indirect application may relax time requirement but necessitates knowledge of persistence of local atmospheric behavior.
	Other mesoscale and microscale studies	Topographic and surface roughness effects	Wind speeds and turbulence as a function of altitude	Local small-scale roughness has an effect on the coupling between earth surface and air mass. Energy and moisture transfers are affected. Predominant features such as mountains have similar effects on a larger scale. Initially of scientific value.

TABLE VII (continued)

<u>Atmospheric Region</u>	<u>General Subject Area</u>	<u>Specific Interest</u>	<u>Measurements Required</u>	<u>Comments</u>
Lower atmosphere (concluded)	Other mesoscale and microscale studies.	Statistical proper- ties of turbulence and energy dissipa- tion	Wind speeds and turbulence prop- erties as a function of alti- tude	The energy balance in the atmosphere is strongly dependent on these mechanisms. Significant scientific value.
		Effects of small variations of sea temperature	Winds and turbu- lence character- istics	Fraction of a degree variations in sea temperature are sus- pected to be influential in the types of weather systems which are evolved. Scientific value.

V. DETECTORS AND INTEGRATION TIME

In analyzing the usefulness of an optical detector, three sources of noise must be considered. One source is detector signal shot noise, a second is detector dark noise. The first source is signal-dependent while the second is purely a property of the detector. The third noise source is the atmosphere itself. Part (in fact, most) of the intensity fluctuations arriving at the detector are uncorrelated and must be considered as noise.

The atmospheric noise cannot be eliminated, although it can be minimized by proper selection of optical frequency, detector altitude, etc. It is therefore highly desirable, if not mandatory, that the two detector-related noise sources be small compared to the atmospheric noise sources. Based on conservative estimates of atmospheric and optical parameters, and detector properties available from the open literature, it appears that in the visible range, the detector-related noise sources can be neglected. In the infrared range, the situation is only marginal with the dark noise being nearly as large as the atmospheric noise. Future detector developments may relax this marginal situation, however.

The detector considerations are based on the assumption that no time restriction is placed on the data collection effort. However, atmospheric phenomena are not stationary, so that only a finite amount of time is available for the data collection. The time available depends on the phenomena studied, and typically will range from a few minutes to a few hours.

The effect of a finite integration time on the accuracy of cross-correlation coefficients is examined. The results of these preliminary estimates indicate that the magnitude of the peak correlation can be calculated with acceptable accuracy in the current ground-based studies of ground winds.* However, the accuracy deteriorated rapidly with increasing time lags measured from the peak. An optimum filter bandwidth exists which will minimize the error. This bandwidth depends on time lag and is given by the expression:

$$B = \frac{1}{2\pi\tau}$$

* The location, in time, of this peak is, however, much more difficult and is not yet resolved in the current studies.

which leads to the relative error

$$P_{\min} = 51.4 \sqrt{\tau/t}$$

with 95% confidence. t is the integration time.

The accuracy, for fixed bandwidth, is strongly dependent on time lag, being sharply peaked at the time lag corresponding to the peak in the correlation curve. It may be that this phenomenon will be useful in locating the peak. That is, the variance of the correlation estimate may be a stronger indicator of the peak than the correlation itself.

Further theoretical work should be done to develop better understanding and more realistic estimates of integration time requirements. Factors to be considered include the actual atmospheric power spectrum and the true filter transfer function.

VI. EFFECTS OF NONIDEAL ENVIRONMENTS ON CROSS-BEAM CORRELATIONS

The basic theory of cross-beam correlation techniques is based on simplifying assumptions leading to what might be considered an ideal environment. This portion of the overall study on the feasibility of applying cross-beam techniques to atmospheric problems is concerned with studying several types of departures from ideality which are to be expected in the atmosphere.

The approach is based on mathematical simulation. That is, a mathematical model containing reasonable but simple approximations to the expected behavior of the extinction coefficient is postulated, and then applied to a variety of physical situations. A combination of numerical integrations performed on a digital computer and analytical proofs developed where possible is utilized. The details of the approach and the results obtained are given in Appendix IV. The results are summarized here.

The mathematical model includes the effects of axial velocities (along the beam normal) and cross flow (perpendicular to the beam normal). The intensity of the extinction coefficient may vary (inhomogeneous turbulence) and the convection speed need not be uniform. The mathematical model takes the form

$$G(\Delta z, \tau) = \langle I_1 \rangle \langle I_2 \rangle \int_{y_1}^{y_2} \int_{x_1}^{x_2} \left\{ \overline{k^2(x)} \overline{k^2(y, \Delta z)} \right\}^{1/2} R(x, y, \Delta z, \tau) dx dy$$

$$R(x, y, \Delta z, \tau) = e^{-\tau/T_e} - \left\{ \left[(x+u\tau)^2 + (y-v\tau)^2 + (\Delta z-w\tau)^2 \right]^{1/2} / L \right\}$$

where G is the covariance of the signal intensities from the two beams, the first of which is aligned along the x -axis and the second along the y -axis; Δz is the distance of minimum separation between the two beams (measured along the beam normal); τ is the time by which the signal from the y -beam is delayed relative to the x -beam; $\langle I_1 \rangle$ and $\langle I_2 \rangle$ are the time-averaged signal intensities from the two beams; k the extinction coefficient; T the eddy lifetime; L the integral scale of turbulence; w the component of convection along the common beam normal; and u and v the components of the cross flow. The expression is written such that the beams would intersect (if $\Delta z = 0$) at $x = y = 0$. The limits on the integrals represent, then, the position of the detectors and the opposite ends of the beams (the limit of the atmosphere, say). The above expression is written for the case where the y -beam is "downstream" of the x -beam so that τ is always taken as positive. Other arrangements are readily obtained.

The nonideal situations are defined by including the following possibilities:

- a. Isolated bands of turbulence as opposed to turbulence of uniform intensity throughout space.
- b. Nonzero cross flow velocities.
- c. Nonconstant wind speed in direction of beam normal. A uniform shear, w' , is postulated where w is horizontal and the derivative is with respect to y or, to within a multiplicative constant,* with respect to the vertical.
- d. A cross flow velocity which varies in the vertical direction, in the same way as does w in case c above.

* The secant of the inclination of the y -axis from the vertical.

The results of the numerical studies are given in Table VIII. These are stated in terms of the effect of the nonideal situation on the various parameters which are measurable in an ideal environment with the cross-beam correlation technique. In each case where the answer no appears, analytical proofs or demonstrations based on the mathematical form of R given above verified that the parameter in question is, indeed, independent of the variable in that particular situation.

The following conclusions regarding estimates of turbulent flow parameters obtained from cross-beam correlations may be drawn from this analysis:

1. The axial component of wind speed at the altitude of the beam normal is correctly predicted, even though the turbulence and wind speeds are not uniform in space.
2. The scale of turbulence is correctly determined in the presence of cross flow or nonuniform wind speeds, but will be incorrectly determined in the presence of nonuniform turbulence of unknown distribution.
3. Generally, the eddy lifetime and power spectrum of turbulence cannot be obtained unless ideal, uniform turbulence and wind speeds prevail.
4. Under special circumstances, it appears possible to estimate cross flow velocities or shears -- an achievement not possible under uniform conditions.

The above conclusions are based on the empirical form of R chosen for the analysis, and may need to be modified for other forms not studied. However, the general trends are expected to remain true in any case. That is, the estimates of turbulent flow parameters may be ranked in order of expected reliability in the following order, most reliable first:

1. Axial component of wind speed,
2. Scale of turbulence,
3. Power spectrum,
4. Eddy lifetime, and
5. Cross flow velocity components and/or shears.

TABLE VIII

RESULTS OF NONIDEAL ENVIRONMENT ANALYSES

<u>Situation</u>	<u>Quantity Varied</u>	<u>Is Estimate of This Parameter Affected?</u>				<u>Can Cross Flow Be Determined? **</u>
		<u>Axial Wind Component*</u>	<u>Eddy Lifetime</u>	<u>Auto Correlation, Power Spectrum</u>	<u>Scale of Turbulence</u>	
Isolated band of turbulence centered around beam normal	Cross flow velocity	No	Yes	Slightly	No	No
Isolated band of turbulence located above or below beam normal	Cross flow velocity	No	Yes	Yes	No	Maybe
Isolated band of turbulence, no cross flow velocity	Location of turbulence	No	No	Yes	Yes	--
Uniform turbulence, no cross flow velocity	Wind shear for axial velocity	No	Yes	Slightly	No	--
Uniform turbulence, uniform axial velocity	Wind shear for cross flow velocity	No	Yes	Yes	No	Maybe

* Velocity component along beam normal.

** Velocity component perpendicular to beam normal.

VII. NATURAL ENERGY SOURCES AND OPTICAL PHYSICS

The cross-beam applications considered here are to make use of natural, extended sources of electromagnetic radiation. The most powerful source is solar radiation which becomes extended in skylight through scattering. The second most powerful source is the thermal radiation of the earth and atmospheric constituents. A considerably weaker source is airglow, an emission which takes place nonuniformly in the upper atmosphere.

About half of the solar power lies in the visible range, 0.4 to 0.7 μ . This radiation is scattered by molecules and particles (aerosols) in the atmosphere. On the lighted side of the earth skylight is the dominant extended source. And since the atmosphere is essentially transparent over this wide spectral band it is possible to intercept a large amount of energy which has been affected in a similar but not exactly equal fashion in traversing the atmosphere.

Solar radiation extends into the ultraviolet and the infrared. The atmosphere is opaque to many ultraviolet wavelengths due to absorption by ozone (0.22 to 0.29 μ), oxygen ($< 0.25 \mu$), and water vapor (especially 0.16 to 0.18 μ). However, in the upper atmosphere some ultraviolet wavelengths may be suitable for use with scattered solar radiation. The solar power within the ultraviolet domain will be much less than in the visible range so that a relatively large collector would be required.

The atmosphere is also variably opaque over a large part of the infrared spectrum where solar power is significant.

At wavelengths greater than 3 μ the thermal radiation from the earth and atmosphere become predominant over solar radiation. In the "window" near 9.5 μ the solar radiation is insignificant. The total power available in an infrared band is somewhat restricted by the bandwidths. However, at 9.5 μ a bandwidth of 2 μ would be reasonable. On this basis the earth as a background source supplies power of about one order of magnitude lower than the visible skylight observed at sea level. Consequently, larger collector elements would be required for a cross-beam system designed for the infrared.* Power is, however, added to the beam by atmospheric emissions as well as lost by absorption.

Airglow is an emission from excited elements of the upper atmosphere. The emissions are thought to come from relatively thick layers,

* Power collection should be tailored in the system to minimize the effects of detector and amplifier noise while not overdriving components into nonlinear response.

on the order of 25 kilometers, generally located between 50 kilometers and 120 kilometers altitude. The emissions extend from the near ultraviolet through the visible and into the near infrared range. There is a faint background intensity, at least in the visible range; however, most of the energy is emitted in lines or narrow bands characteristic of the emitting substance and the excited energy state.* The power in these emissions is low compared to either skylight in the visible range or thermal radiations in the infrared. As a background source the airglow power is about six to eight orders of magnitude lower than skylight at the ground. As a tracer emission where measurements are sought within the emission altitudes the airglow may be more attractive. Here the comparison should be made on power emitted per unit volume and the airglow can be compared to the infrared emissions in the 9.5μ region, due primarily to ozone and water vapor. The airglow power is down about four orders of magnitude from the ozone emission.

In summarizing natural energy sources, then, it appears that scattered sunlight and thermal emission from earth and atmosphere are the most desirable and dependable sources. Airglow may be useful; however, very large collectors would be needed together with minimum noise detectors and amplifiers. It is also true that potentially useful spectral regions include the ultraviolet, visible, and infrared.

In passage through the atmosphere electromagnetic energy is subject to scattering and absorption. Also, energy may be added by emitting species.

Scattering occurs when the radiation encounters particles with dimensions either less or greater than the wavelength. Scattering results in changed directions of propagation for the energy which is intercepted. When the particle is much smaller than the wavelength (particle size/wavelength < 0.01) a special case called Rayleigh^{9/} scattering occurs. The distribution of Rayleigh-scattered energy is shown in Figure 1 where it is seen that forward and back scattering distributions are equal. Theta (θ) is the angle between the incident and the scattered directions, being zero for forward scatterings. Scattering to the side is significant here. There is also symmetry around the initial direction vector. The magnitude of Rayleigh scattering depends, of course, on the number of particles encountered. It also varies as the fourth power of the expression (particle size/wavelength).

* Some of the airglow emissions are also observed in aurorae which would constitute an overpowering interference. Aurorae cannot be used as a tracing emission because the excitation mechanism does not depend exclusively on the atmospheric component involved. Instead the location of aurorae depends on the impingement of high energy particles from space.

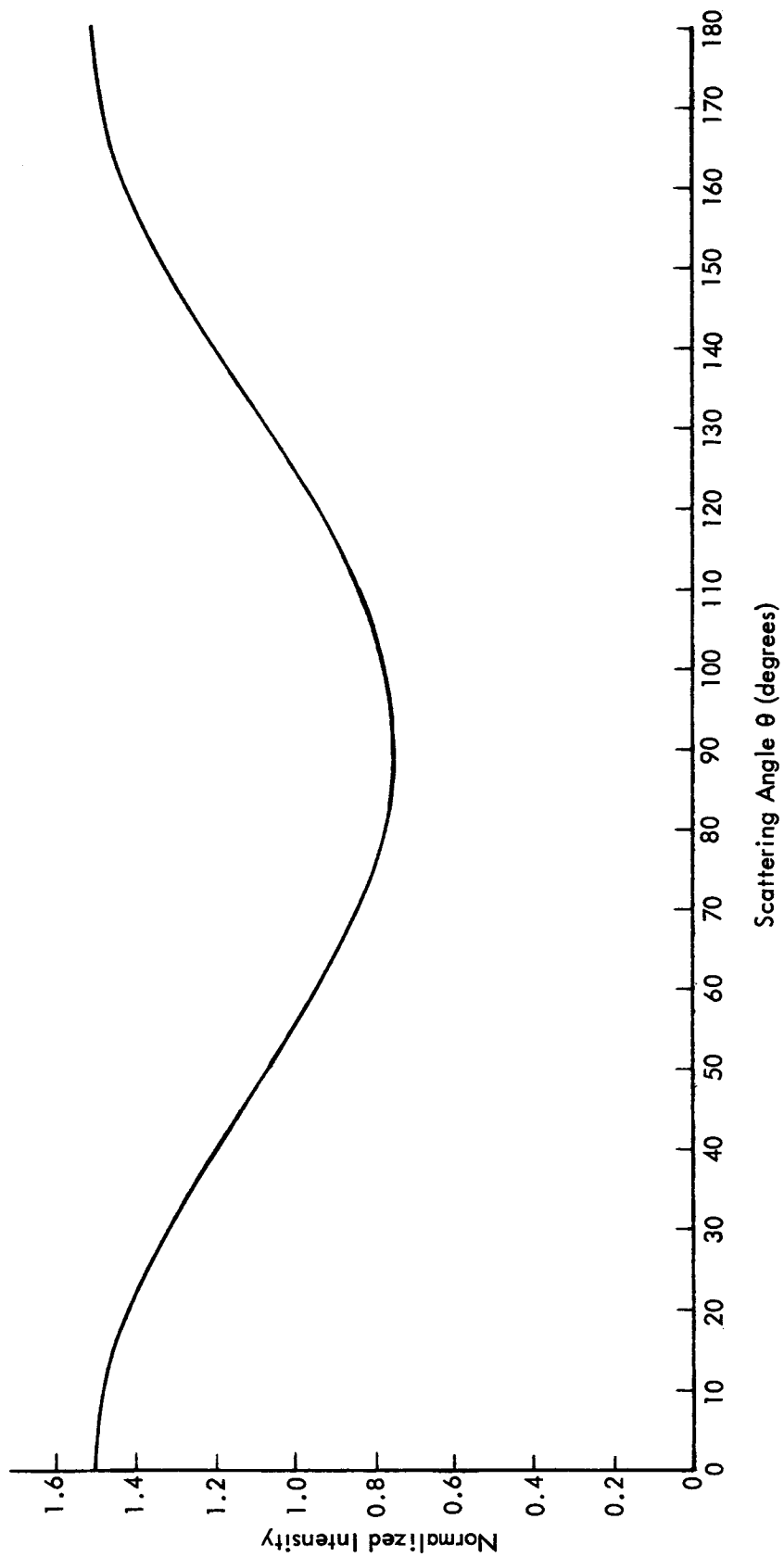


Figure 1 - Rayleigh Scattering Distribution

When the particle size is more nearly equal* to the wavelength a more inclusive theory due to Mie^{10/} is needed. The energy is scattered primarily in the forward direction, close to the original direction of propagation. There is a small amount directed to the sides and back scattered. When the scattering from a single particle is treated, the diagram of Mie-scattered energy contains sharp spikes whose orientation and magnitude depend on the ratio (particle size/wavelength) and the indices of refraction. For groups of particles as found in the atmosphere this particle size distribution averages out all but the common features. The result is a diagram such as the one shown in Figure 2, taken from D. Deirmendjian.^{11/} Notice that the ordinate scale is logarithmic. The magnitude of Mie scattering tends to vary as the ratio (particle size/wavelength)^N, where N varies from 0 to 1. The shape of the "averaged" scattered intensity function becomes more peaked in the forward direction as the above ratio increases.

A summary of scattering, absorption, and energy sources is shown in Figure 3 versus spectral region.

* Or, up to two orders of magnitude greater than the wavelength.

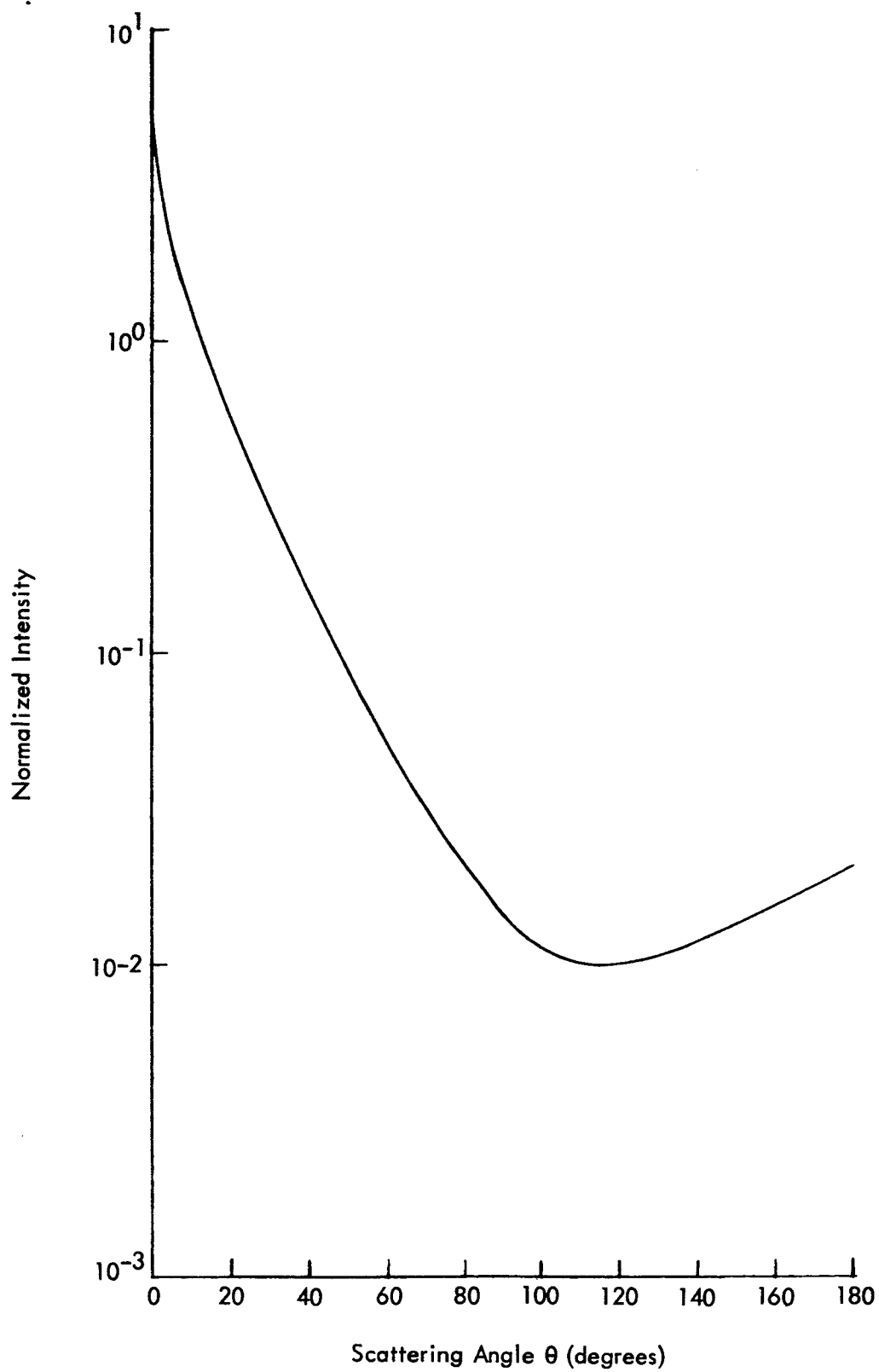


Figure 2 - Mie Scattering Distribution for a Wavelength of 0.45μ ,
Diermendjian's Haze "C"

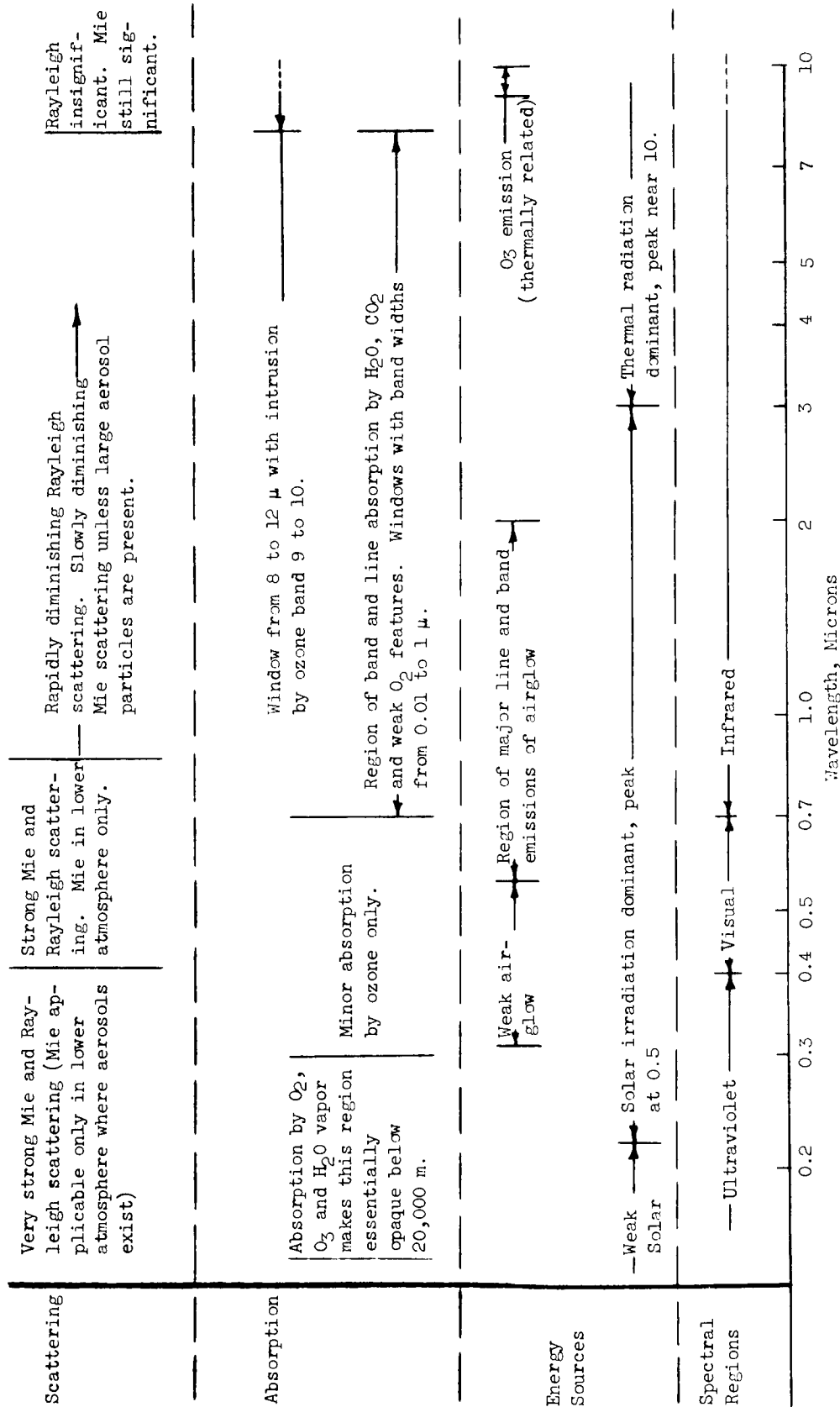


Figure 3 - Scattering, Absorption, and Source Characteristics

VIII. POWER AND POWER FLUCTUATIONS IN THE BEAM

The power and power fluctuations which reach a detector depend on the optical system, the light sources, scattering, absorption, emission, and refractive effects in the atmosphere. We choose here to consider the average refractive effects and the fluctuations about the average separately. When this is done the optical system characteristics can be used to define a beam-like volume which is "seen." The power at the detector consists of energy which satisfies several requirements. It must

1. Traverse or be emitted in the beam volume,
2. Be directed (or redirected) into the optical system entrance, and
3. Not be removed by absorption or by redirection away from the optical entrance.

A model of the above situation has been constructed and an associated analysis developed and employed. The analysis accounts for scattering in and out of the beam (Rayleigh and Mie), absorption and emission, and the input derived from a background such as the earth's surface. The scattering, absorption and emission characteristics are allowed to vary along the beam simulating the changes with altitude. Some effects of multiple scattering are included implicitly, although a complete multiple-scattering model is not formulated.

The approximations employed include central and averaged values, small angle equivalents and the like. Approximations have been made with care so that the basic analysis is thought to be a good description of the actual situations.

The analysis provides a differential equation which can be integrated and perturbed to produce the forms applicable to the cross-beam study. The gain in power approaching the entrance pupil along the beam is

$$\frac{dE}{dg} = - \left\{ \sum_{i=1}^6 k_i(g) F_i(g) \right\} E + \sum_{i=1}^6 k_i(g) I_i(g)$$

where E is the power in the beam at the location, g , along the beam. The first group of terms represents the losses due to scattering out and absorption; the second group represents gains due to scattering in and emission. The k_i have the following meanings:

k_1 = coefficient for Rayleigh scattering out of beam, (length)⁻¹

k_2 = coefficient for Mie scattering out of beam, (length)⁻¹

k_3 = absorption coefficient, (length)⁻¹

k_4 = k_1 but in term for Rayleigh scattering into beam, (length)⁻¹

k_5 = k_2 but in term for Mie scattering into beam, (length)⁻¹

k_6 = emission, watts/unit volume.

The functions F_i and I_i contain geometrical effects and the like. In particular, $F_4 = F_5 = F_6 = I_1 = I_2 = I_3 = 0$.

The differential equation can be formally integrated to provide the beam power at the entrance pupil, $g = g_p$:

$$E(g_p) = e^{-G(g_p)} \left\{ E_0 + \int_0^{g_p} e^{G(g)} \left[\sum_{i=1}^6 k_i(g) I_i(g) \right] dg \right\}$$

where

$$G(g) = \int_0^g \left[\sum_{i=1}^6 k_i(g) F_i(g) \right] dg$$

and E_0 is the power in the beam at $g = 0$. E_0 can be used to represent power added at a surface or pseudo surface such as the top or bottom of a dense cloud.

While we are interested in total power at the detector, our prime interest is in the power variations which result from small local changes in the atmosphere at some position out in the beam. The solution for small incremental changes then provides

$$\delta_j E(g) = \delta k_j \delta g \left\{ e^{-G(g_p)} / e^{-G(g_v)} \right\} \left\{ I_j(g_v) - F_j(g_v) E(g_v) \right\} .$$

Here the left-hand side is the change in beam power at $g = g_p$ due to the change (δk_j) of the j^{th} k over a distance (δg). The change occurs at the position $g = g_v$. If g_p is taken as the value of g at the detector the above expression provides the sought power variation due to a well defined and located variation out in the beam.*

The above expression has been evaluated by numerical integrations for a number of atmospheric conditions with values appropriate to the ultraviolet, visible, and infrared regions. These calculations also cover a variety of prime light sources, considerations which affect the character and magnitudes of the I_i and E_0 .

IX. ATMOSPHERIC MODELS

The atmospheric models consist of the coefficients (altitude-dependent) which are required to carry out the beam power calculations. These coefficients are presented in the Appendices together with a description of sources and bases for extrapolations used. The spectral and weather combinations are given here in Table IX.

* Notice that the equation can be divided through by $\delta k_j \delta g$, yielding $\delta_j E(g_p) / (\delta k_j \delta g)$ on the left side. This expression may be interpreted as the power change at $g = g_p$ due to a unit change in k_j over a unit of beam length at $g = g_v$.

TABLE IX

ATMOSPHERIC MODELS, SPECTRAL AND WEATHER COMBINATIONS

Spectral Region	Center Wave Length (microns)	Weather Character	Comments
Ultraviolet	0.15	Clear	Weather here is unimportant since the only useable path lengths are in the upper atmosphere.
Ultraviolet	0.245	Clear	
Visible	0.45	Clear	The "clear" day atmosphere does contain particulate Mie scatterers up to 30 km with stratification as indicated in references.
	0.45	Hazy	A dense continental haze (Mie scatterers) is added to the clear day atmosphere. Haze extends from sea level to 6 km with gradual return to clear day conditions between 6 km and 9 km.
	0.45	Cloud (with haze)	A cloud (100 particles/cm ³ and 4 μ mode radius) is added to the hazy day between 2 and 3 km. Characteristics taper to hazy day values outside the main cloud. The cloud provides greatly increased Mie scattering.
Infrared	9.5	Clear day, .04% H ₂ O vapor (by volume)	Water vapor contents affect absorption and emission. The values used here are very near to extremals.
		Clear day, 4% H ₂ O vapor	
		Hazy day, .04% H ₂ O vapor	The haze increases locally the Mie scattering, absorption, and emission since the haze consists primarily of liquid water droplets.
		Hazy day, 4% H ₂ O vapor	
		Cloud (with haze)	Cloud adds to local Mie scattering, absorption and emission. (The emission values are suggested but not plotted in the appendix.)

X. BEAM POWER CALCULATION RESULTS

Calculations have been made for the power at the detector and the power variations there under a variety of conditions. The intent of these calculations is to determine the access to information in various parts of the atmosphere through the received power fluctuations.

Access to an atmospheric region means that the atmospheric fluctuations occurring there produce at the detector power fluctuations which are useable in the cross-beam technique. There are two requirements for usefulness.

1. The power fluctuations arising in the atmospheric region must be sufficiently large with respect to the steady power which is received by the detector.
2. The power fluctuations arising in the atmospheric region must not be "swamped" by larger fluctuations which arise in other regions along the same line of sight. (To avoid swamping it is likely that power fluctuations should be down not more than one order of magnitude from those produced over appreciable lengths in other atmospheric regions.)

Ideally it should be possible to calculate the received power variations which arise along the system line of sight and use them to determine "access" as defined above. To do this the atmospheric variations at each station along the beam would be assigned, and the associated local optical variations would be used in the beam power calculation. Unfortunately, the local atmospheric variations are not known for many meteorological environments and the relations between atmospheric and optical variations are not quantified. Consequently, the present analysis and calculations are performed using typical atmospheric properties and the associated optical coefficients (functions of altitude).

The results are obtained as Relative Specific Power Variations (RSPV) versus altitude. These values may be interpreted as the decimal percent change in received power arising from optical fluctuations at the indicated altitude. The RSPV values provide the best current indicators of access to an altitude region. The RSPV value itself indicates if a region meets the first requirement in the paragraph above. (The current experimental conditions and results provide a basis for required values.) Conformance with the second requirement must be judged by examining RSPV values along the line of sight and comparing them with the RSPV value in the region of interest.

It is clear that all the power fluctuations depend on the location of the optical and detector system, the spectral region, sources of light energy, and the atmospheric conditions. Calculations have been made for a variety of these situation parameters as shown in Table X. All calculations are for vertically oriented beams (looking up or down). There is a capability for handling inclined beams; however, this was not considered necessary in the initial survey of electromagnetic access. In the present calculations extended backgrounds were treated as infinite lambert planes.*

The calculation results have been studied for the major implications. They are:

1. The access to the lower atmosphere (up to 3,000 to 15,000 meters) is essentially the same as access to elements close to the ground.

2. Access to slightly higher elements of the atmosphere is afforded by upward-looking aircraft-based systems.

3. Access to the lower atmosphere (not cloud blocked) from orbit and ground is generally comparable. Somewhat less desirable RSPV values are obtained for the orbit-based system due to earth back lighting (see No. 4 following).

4. Background and primary radiation sources can combine favorably or unfavorably to produce RSPV values which vary by at least two orders of magnitude.

5. In its present state the cross-beam technique is defeated when the system looks at and sees a varying background such as the earth's surface or a cloud boundary. Variations in transmission, reflectivity or emissivity in these backgrounds produce power variations which are several orders of magnitude greater than variations due to the atmosphere.

6. There is a possibility of access to the upper atmosphere from orbit using short-path-length spectral regions in the ultraviolet.

7. Calculation of the scattering out and absorption in the cloud model shows that the 1 kilometer thick cloud is somewhat translucent but not transparent to a visible and infrared beam. Consequently, thick clouds must be considered at their surfaces as diffuse radiators or reflectors.

* The basic analysis is not restricted to such infinite planes. However, they do provide the simplest forms and are considered adequate for the present purposes.

TABLE I
CONDENSED TABLE OF BEAM POWER CALCULATION CASES

Wavelength (microns)	Telescope		Weather and Other Factors
	Location	Orientation	
0.45 (Visible)	ground	look up	Clear day and no cloud, various solar zenith angles and ground reflectances.
	ground	look up	Clear day with cloud at 6 km, no direct sunlight.
	ground	look up	Hazy day but no cloud, various solar zenith angles and ground reflectances.
	ground	look up	Hazy day with cloud at 6 km, no direct sunlight, one ground reflectance value.
	6 km	look up	Clear day, two ground reflectances, one solar zenith angle.
	6 km	look up	Hazy day, one ground reflectance value, one solar zenith angle.
	6 km	look down	Clear day, two ground reflectances, one solar zenith angle.
	6 km	look down	Clear day, but cloud above 6 km so no <u>direct</u> sunlight is available, two earth reflectances, beam "looking at" average reflectance area and area of twice average reflectance.
	6 km	look down	Hazy day, one ground reflectance, one solar zenith angle.
	6 km	look down	Hazy day with cloud above 6 km so there is no direct sunlight, one earth reflectance value, beam "looking at" average reflectance area and area of twice average reflectance.
	200 km	look down	Clear day, two earth reflectances, three solar zenith angles, beam looking at average reflectance area and area with twice average reflectance.
	200 km	look down	Hazy day, one earth reflectance, one solar zenith angle, beam looking at average reflectance area and area with twice average reflectance.
	200 km	look down	Same as above.
9.5 (Infrared)	ground	look up	Clear day, 0.04 percent H ₂ O vapor, typical ground radiation (1 μ band width).
	ground	look up	Clear day, 0.04 percent H ₂ O vapor, cloud at 6 km, typical (equal) radiation from ground and cloud.
	ground	look up	Hazy day, 0.04 percent H ₂ O vapor, typical ground radiation.
	ground	look up	Hazy day, 0.04 percent H ₂ O vapor, typical ground and typical (equal) radiation from cloud.
	ground	look up	Above combinations with 4 percent H ₂ O water vapor.
	6 km	look up	Typical ground (or cloud) radiation from below: all combinations of clear and hazy day, 0.04 and 4 percent H ₂ O vapor.
	6 km	look down	Typical ground emission, beam "looking at" ground area of typical emission and at ground area of twice typical emission. All combinations of clear day, hazy day and 0.04 percent and 4 percent H ₂ O vapor.
0.245 (Ultraviolet)	200 km	look down	45° solar zenith angle; assume zero beam power at 20 km altitude. (Solution is less accurate than visible and infrared cases due to approximate boundary conditions.)
	200 km	look down	45° solar zenith angle; assume zero beam power at 120 km altitude. (Solution is less accurate than visible and infrared cases due to approximate boundary conditions.)

8. No specific calculations were made using airglow; however, related calculations indicate this source should be accessible as an emitting tracer for the 50 to 100 kilometer regions.

The results of several calculations have been plotted and will be presented to illustrate the sources of the generalizations given above. However, it is necessary first to describe the quantities which are plotted versus altitude.

The beam power analysis provided a perturbation solution which is: The power variation at the detector due to a unit change in a specified coefficient (atmospheric property) over a unit length along the beam at a specified location (altitude).

Since the coefficients change drastically with altitude the result of a unit change is not illustrative of the variation magnitude which might be expected in the atmosphere. It would be more logical to expect that the variation in a coefficient at some altitude would be proportional to the average size of the coefficient there. This kind of value can be obtained by multiplying the original power variation by the coefficient at the perturbation altitude. This provides: The power variation at the detector due to a 100% increase in a specified coefficient over a unit length along the beam at a specified location (altitude). We might call this the specific power variation.

For the cross-beam technique the power variations are important. However, the final utility of a power variation depends on its comparison with the average power received. Thus a more informative quantity is obtained by dividing the above quantity by the power at the detector. This provides the relative specific power variation which is: The power variation at the detector due to a 100% increase in a specified coefficient over a unit length along the beam at a specified location (altitude), divided by the unperturbed power at the detector.*

This is the quantity which is plotted and discussed. The adequacy of signal strengths can then be judged using the current experiments as a reference.^{12,13/} These experiments were conducted at near-ground levels (400 feet) on essentially clear days.

Figure 4 shows the results from two clear-day visible-region calculations. In both runs the telescope is located at ground level.

* This quantity has the dimensions (length)⁻¹ arising from the "unit length along the beam." The meter was used as the unit of length in calculations and in the plotted results.

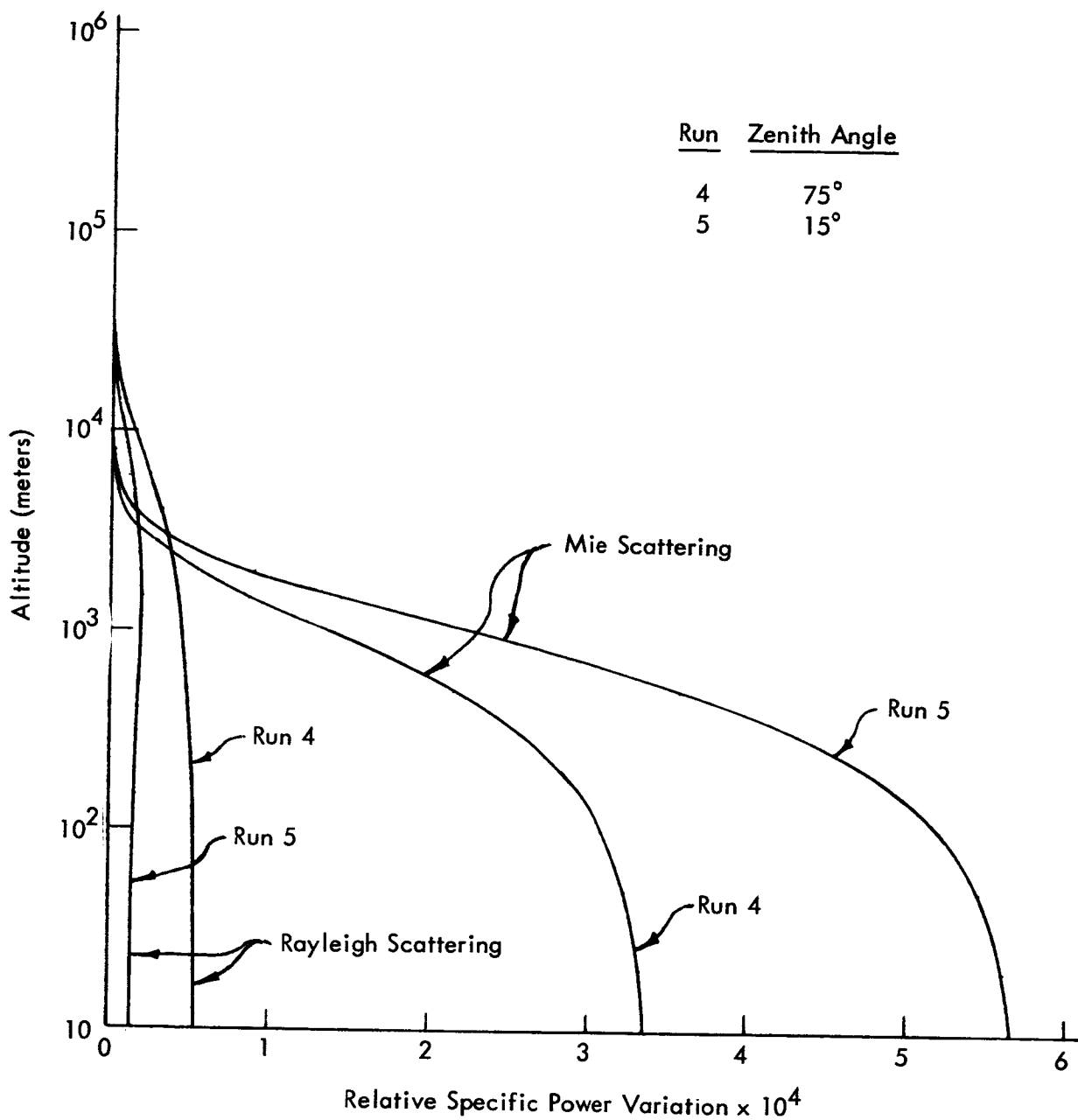


Figure 4 - Effect of Solar Zenith Angle, Clear Day, Telescope on Ground Looking Up, 0.45μ

The only difference is the solar zenith angle. (Recall that the telescopes look straight up or down in all runs presented here.) These results can be used as a reference since they correspond to conditions in the current experimental program. In addition, comparison between runs shows the increased sensitivity to Mie scattering perturbations when the sun is close to the telescope field of view.

It is clear in Figure 4 that the RSPV (relative specific power variations) have fallen one order of magnitude at 3,000 meters for Mie scattering and at 15,000 meters for Rayleigh scattering. Absorption effects are several orders of magnitude lower than those plotted.

Figure 5 compares clear-day access from the earth and from orbit (200 kilometers). Access is essentially equal with a factor of four advantage to the earth-based system in Mie scattering. This advantage is due, of course, to the preponderant forward components in the aerosol (Mie) scattering. The orbiting telescope receives only side or back scattering from the solar input. The accessible altitudes are approximately the same from ground and orbit.

Figure 6 shows the effects of solar zenith angle with a hazy day. The telescopes are ground-based, using the visible region. Here, some RSPV are negative. This means that a local increase in the indicated coefficient reduces power to the detector. Two of the curves cross through zero. This behavior shows that the power in the beam has an equilibrium-like character with respect to scattering processes. For instance, in Run 21 at high altitude both Rayleigh and Mie scattering are adding power to the beam. Following the beam down it is seen that the Rayleigh scattering continues to add power as the net effect of scattering in and out. Now, however, due to the amount of power in the beam the Mie scattering begins to remove more power than it adds. The converse is true in Run 22 where the zenith angle is only 15° . This interaction between scattering mechanisms suggests that there may be situations where the RSPV are much lower or higher than the values shown thus far.

Figure 7 shows the results for a case in which the combination of beam power inputs combine unfavorably to produce small RSPV. The telescope is aircraft-based, at 6 kilometers altitude and looking down over an area of the earth with relatively high reflectance (0.8). The large direct power input from the earth (in the area seen by the telescope) causes the scattering losses to predominate. However, the balance of scattering in and out is so nearly equal that the RSPV are two or more orders of magnitude below the values previously shown.

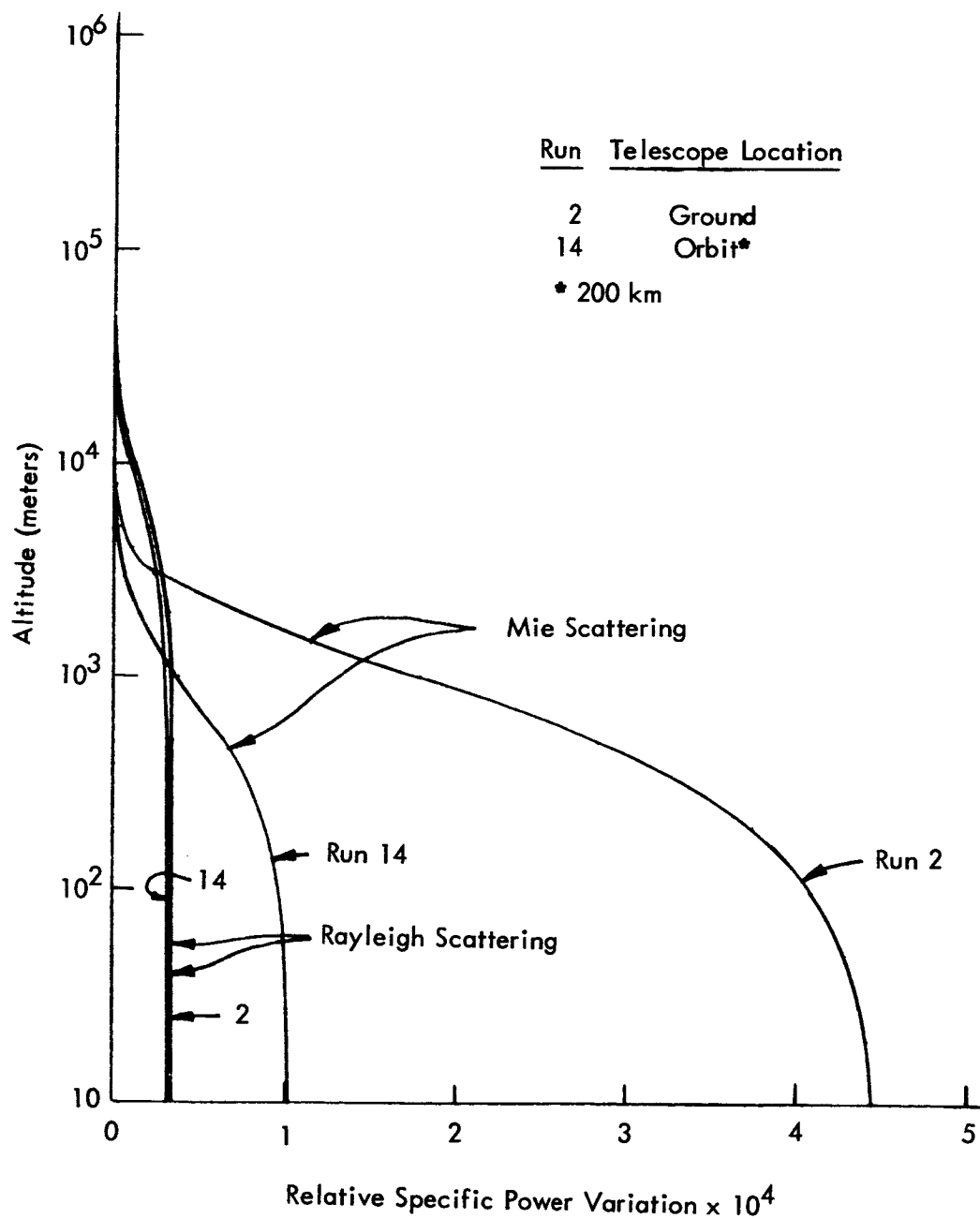


Figure 5 - Comparison of Ground-Based and Orbit-Based Telescopes,
Clear Day, 45° Solar Zenith Angle, 0.45 μ

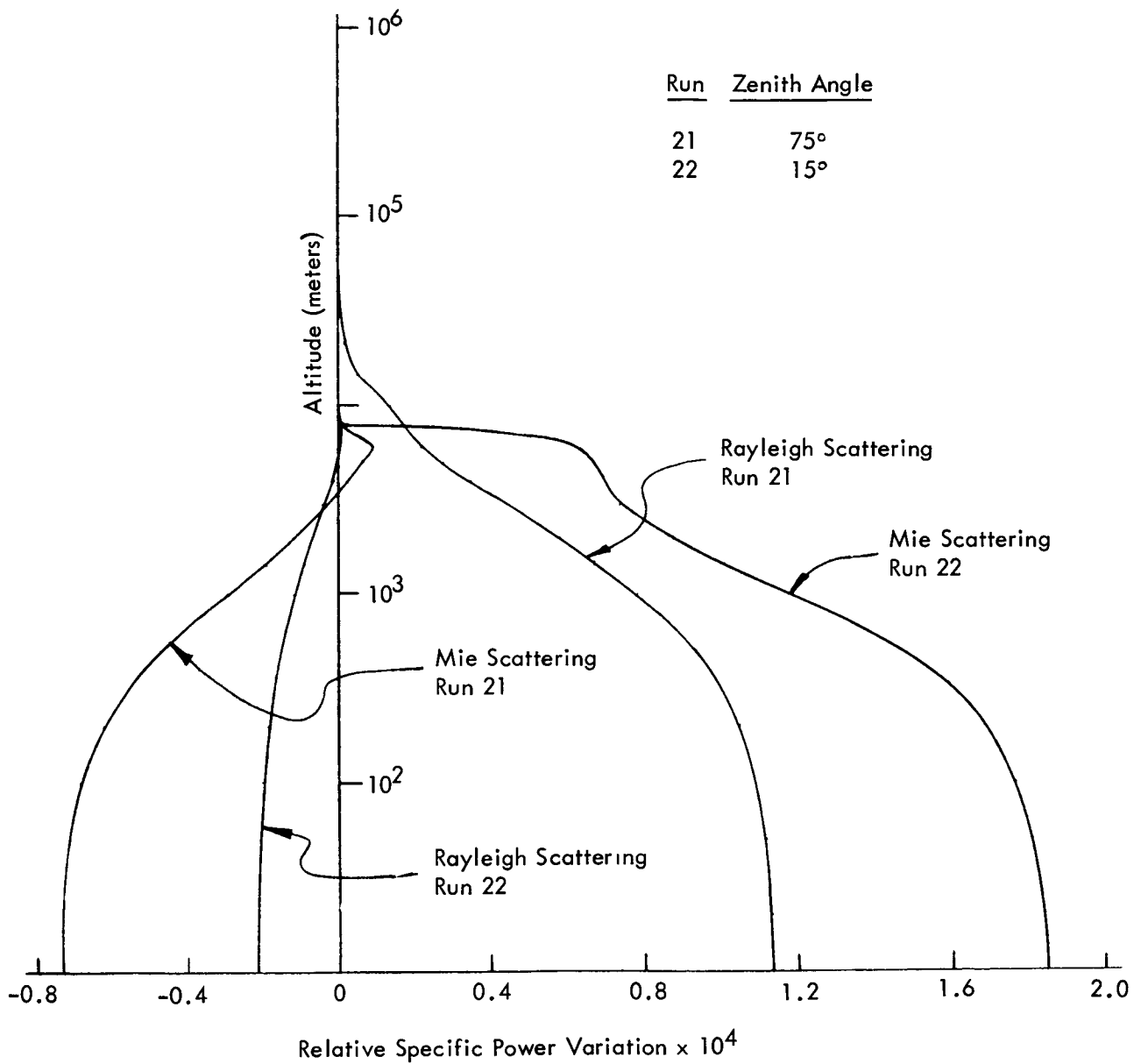


Figure 6 - Effect of Solar Zenith Angle, Hazy Day, Telescope on Ground Looking Up, 0.45μ

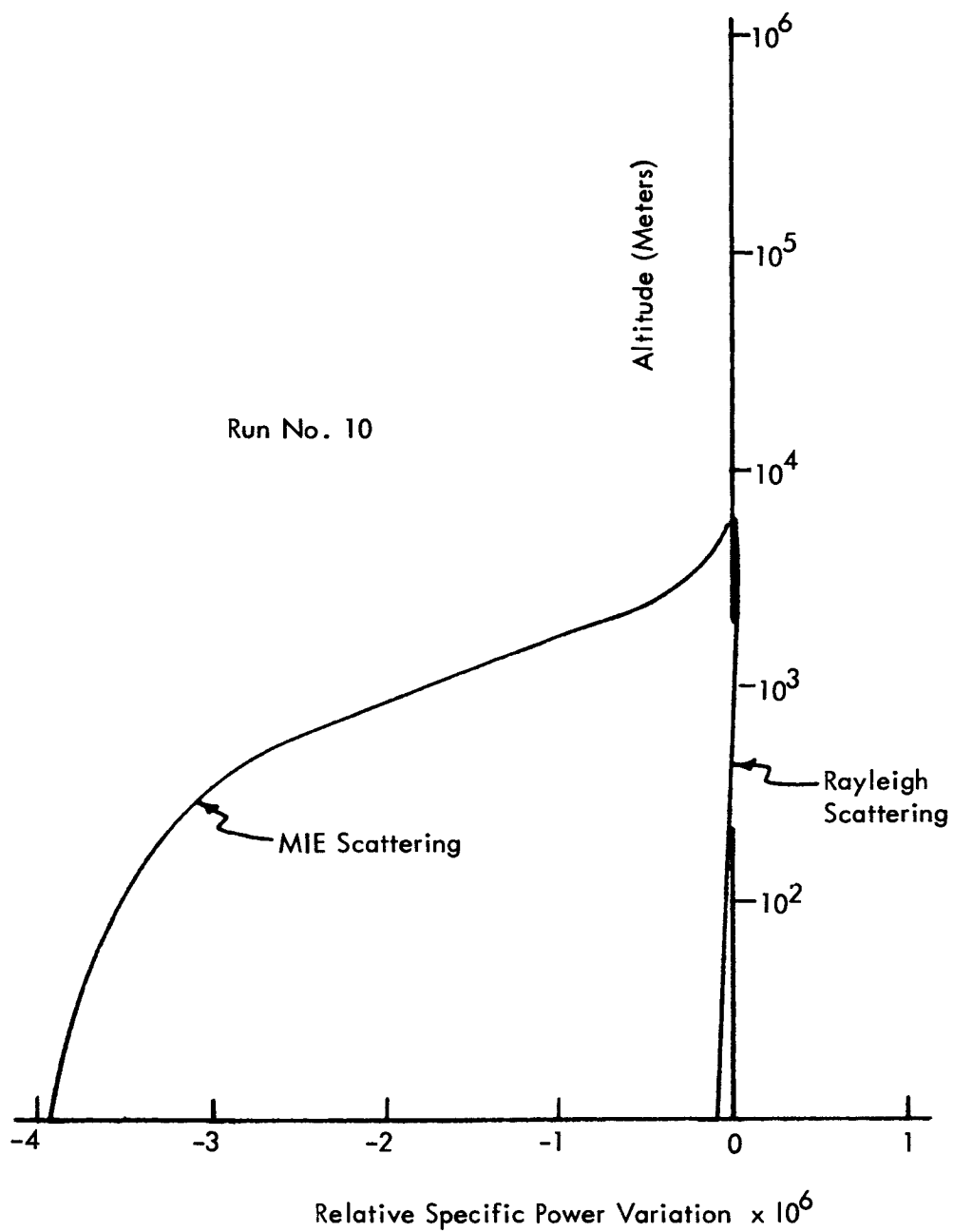


Figure 7 - Telescope Pointing Down From Aircraft at 6 km. Clear Day,
 45° Solar Zenith Angle, 0.8 Earth Reflectance, 0.45μ

Figure 8 compares results for an earth-based and aircraft-based system, both looking up, and both in the visible region. It appears that the aircraft-based system can gain useable access to somewhat higher altitudes than the ground-based system.

Figures 9 and 10 both show comparisons of earth- and orbit-based systems operating in the infrared window at 9.5μ . Figure 9 is for a very dry atmosphere and indicates a possibility of access to the 10-kilometers to 30-kilometer altitude region from the ground under these atmospheric conditions. The orbit-based system has a less attractive RSPV because of the direct beam input from the earth's surface. In both cases the lower altitude RSPV are down approximately one order of magnitude from the visible-region results. Notice that the factors of importance here are Mie scattering, absorption and emission.

Figure 10 shows the results for an atmosphere with relatively high water-vapor content. The RSPV are comparable with the visible-region results. The orbit-based system is again penalized by the direct earth input but may have slightly better access above 10 kilometers. The Mie scattering effects have been greatly reduced in importance due to the increase in water vapor absorption and emission.

None of the visible and clear window infrared (9.5μ) results showed access to the region above 30 kilometers. The upward looking aircraft-based system at 6 kilometers (Figure 5) extended the visible-region access somewhat. A similar but smaller improvement is attained with aircraft-based infrared systems. Since only small additional access seemed realizable from below, a different strategy was tried.

With the long-path-length spectral regions the orbit-based systems see the perturbations in the atmosphere below 10 to 30 kilometers. A short-path-length system used in orbit would not be able to "see" this far and could not be swamped by lower atmosphere variations. There are several potential regions in both the ultraviolet and infrared.

Figure 11 shows the results for two narrow spectral bands in the ultraviolet with an orbit-based system. The primary power here comes from solar radiation (45° zenith angle in these runs). Rayleigh back and side scattering together with absorption are the important mechanisms. These results are more approximate than those for the visible and infrared presented previously. (The basic analysis is capable of handling the short path problem; however, the limited boundary conditions and capabilities in the present computer program are not well suited to this problem.) The results do indicate this possibility of access to the upper atmosphere from orbit using spectral regions of limited path lengths.

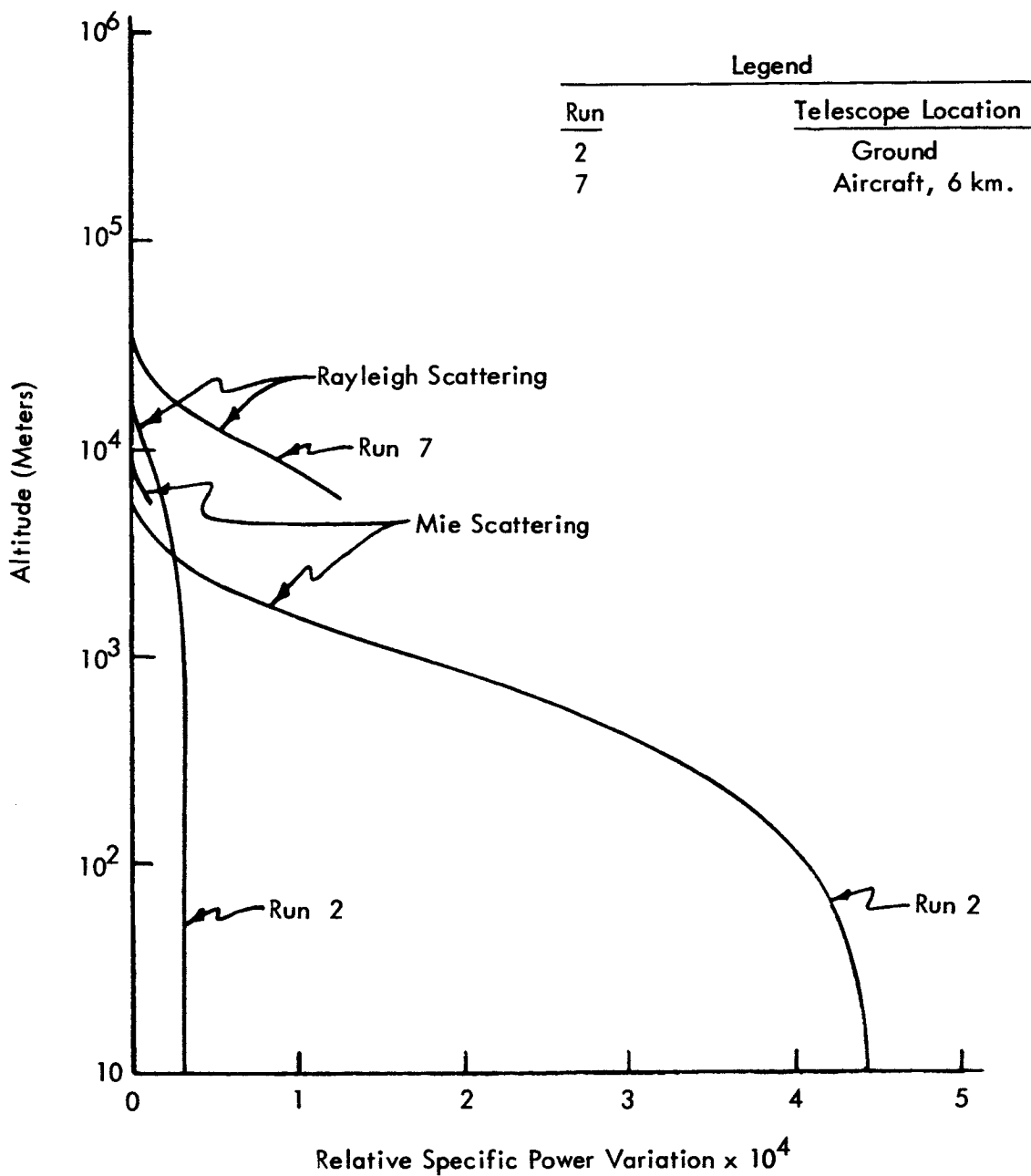


Figure 8 - Comparison of Ground- and Aircraft-Based Telescopes,
Clear Day, 45° Solar Zenith Angle, 0.45 μ

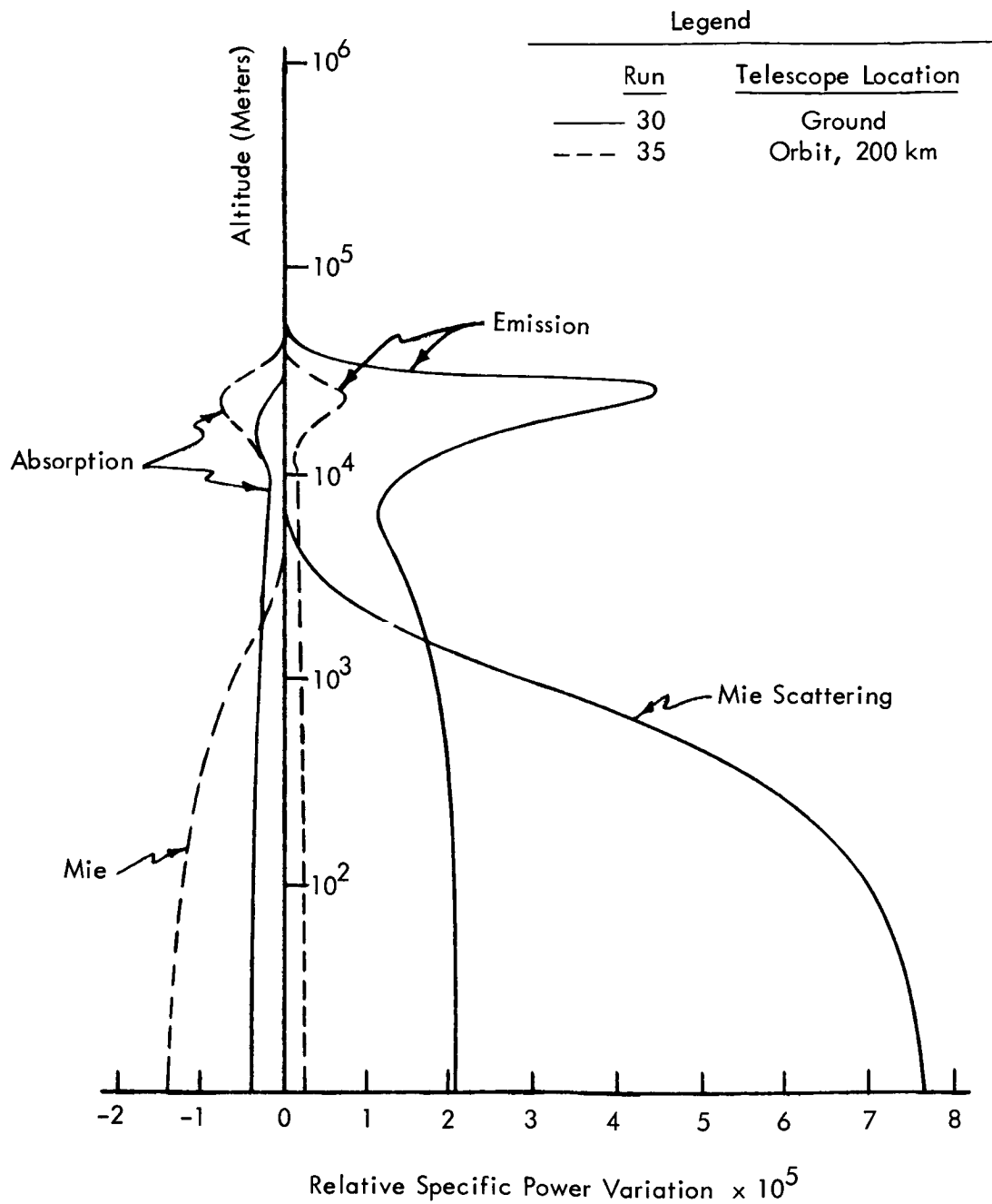


Figure 9 - Comparison of Ground-Based and Orbit-Based Telescopes,
Clear Day, 0.04% H₂O Vapor, 9.5 μ

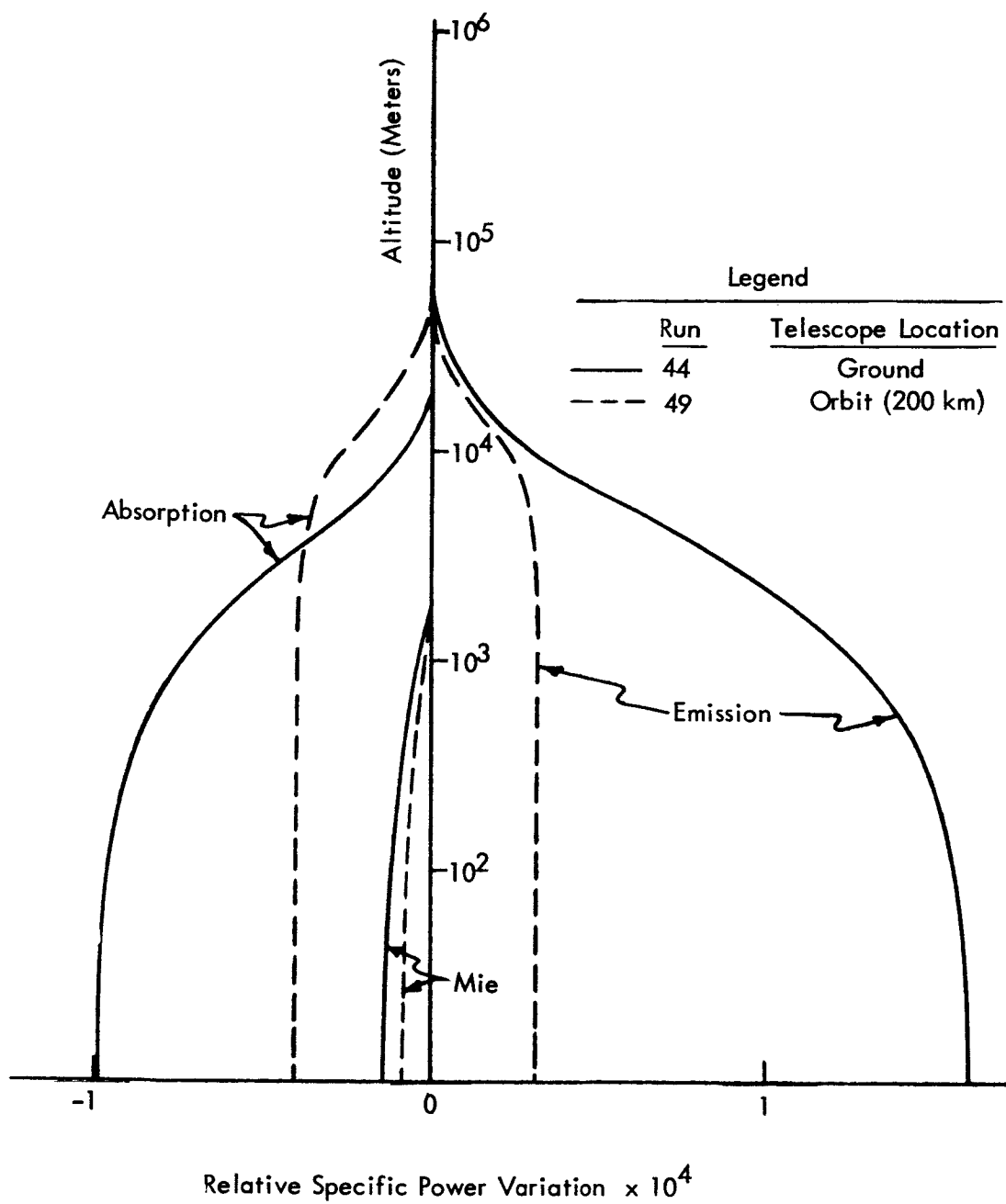


Figure 10 - Comparison of Ground-Based and Orbit-Based Telescopes,
Clear Day, 4% H₂O Vapor, 9.5 μ

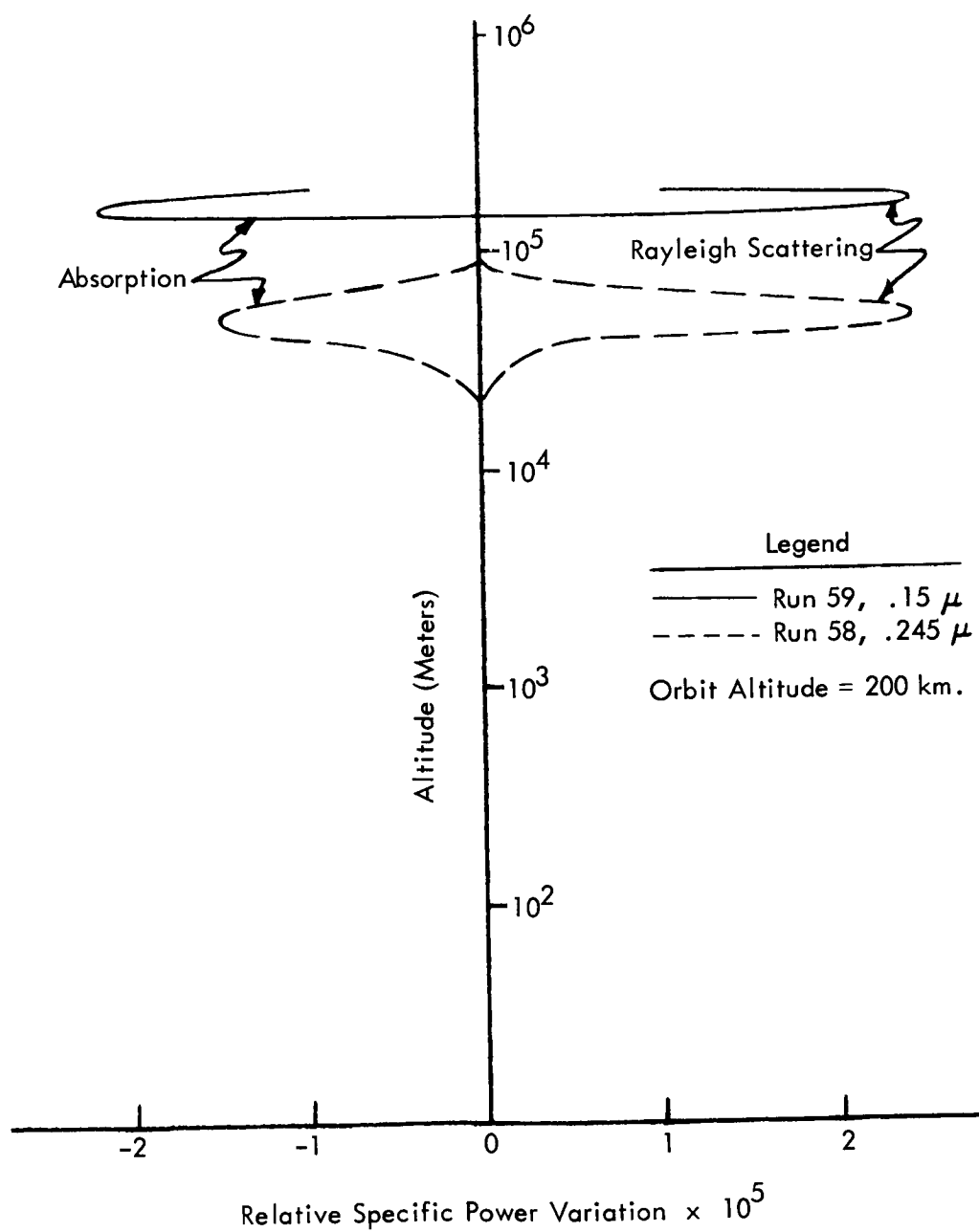


Figure 11 - Access to Upper Atmosphere From Orbit With Solar Ultraviolet

XI. BEAM SIZE AND POSITION

A simple analysis, presented in Appendix V, shows that atmospheric disturbances affect the received power only when the size of the disturbance is comparable to or larger than the beam transverse dimension. This feature provides a geometric filter which can be used to advantage by averaging out the power fluctuations associated with small scale turbulence. This facet needs consideration in comparing access from ground, aircraft, and orbit. It also requires knowledge of energy-scale relations which are not well known for most of the atmosphere.

Consideration has been given to the actual beam cross section as compared with the ideal, right circular cone element. In a more general fashion this question is simply from what volumes in space do the power fluctuations arise? This question can be treated in two parts, the scattered-in and the refractive contributions.

The scattered-in contribution is illustrated in Figure 12 where a column of solar radiation is shown passing through the geometrically defined beam volume. Some of the incident solar radiation will be scattered into the beam. (This is the first order process which has been modeled, solved numerically, and reported under Beam Power Calculation Results.) However, the solar radiation column has passed through the atmosphere and will contain variations similar to those observed at the detector. This second order process provides some power variations which arise in volumes outside the ideal beam geometry. In the depicted situation the variations external to the beam will arise in a slab-like volume extending from the ideal beam boundaries, through the atmosphere, toward the sun. In this case the effective beam geometry consists of the ideal volume plus the slab-like volume taken with a very small weight factor. Even though this is a second order process, detrimental, spurious cross correlations might be obtained if both beams of a complete system had a common slab-like region.

When the primary radiation is emitted or reflected from a plane the individual geometric elements external to the beam are conical shells. In summing over all such primary radiation paths the volumes just outside the ideal beam will be emphasized. The effective beam geometry then consists of the ideal beam plus closely adjunct volumes taken with a very small weight factor.

Scattering mechanisms underlie both of the above weak extensions of the effective beam geometry. Consequently the potential importance of the effect is related to the relative importance of scattering in the specific application.

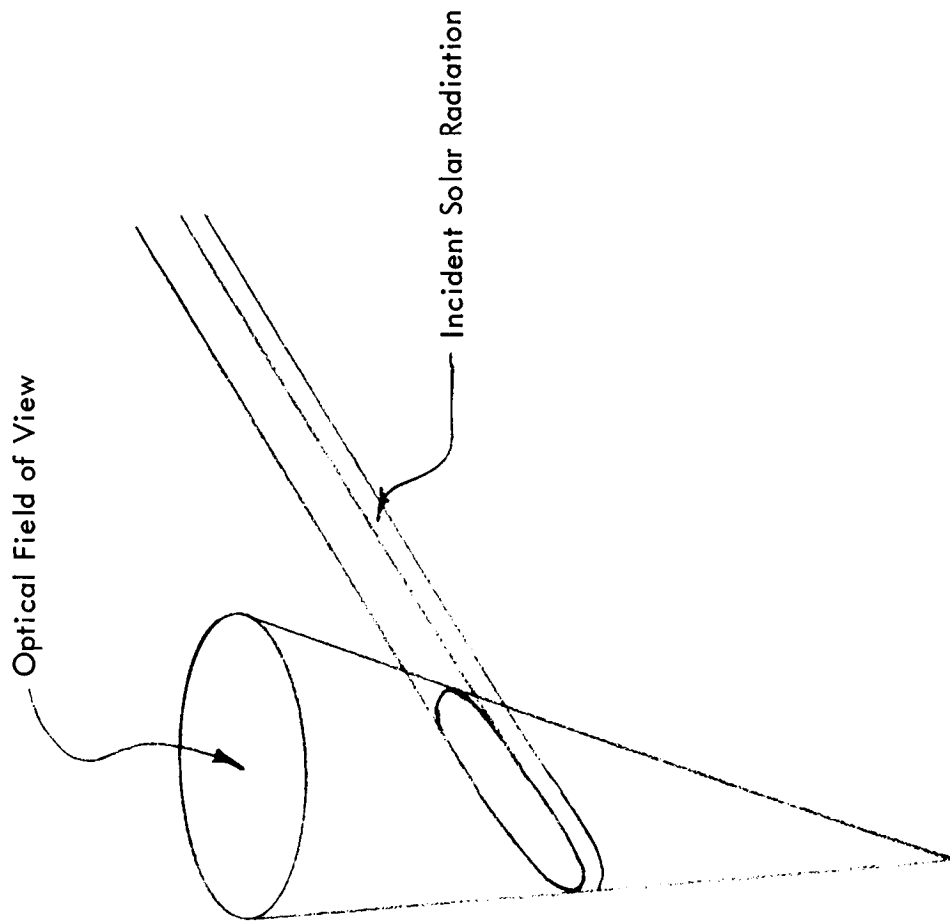


Figure 12 - Source of Power Variations From Outside Field of View

A fifth perturbation solution was obtained in the beam power analysis to evaluate the potential importance of the scattered in signals discussed above. The perturbation is treated as a 100% increase in incident radiation over a unit beam length. The RSPV (relative specific power variations) obtained for this perturbation are generally equal in magnitude to the most important of the other perturbed coefficients. (However, in cases where these incident power fluctuations arise from typical atmospheric fluctuations their final net effect at the detector should be down several orders of magnitude from those fluctuations produced inside the beam geometry.)

Refractive effects in the atmosphere cause a variety of beam perturbations none of which appear serious. The largest scale refractive effect arises from the average gradients in the overall atmosphere. This is a relatively steady effect and will divert the entire beam (visible spectrum) about 1 arc minute in a near horizon passage through the atmosphere.

Smaller scale variations may still be large compared to beam cross section and will cause beam wander. Measurements near sea level indicate beam bending of 10^{-4} to 10^{-3} radians over paths of several kilometers. For a path length of 354 meters, 5×10^{-5} radians was obtained.

Variations at a scale small with respect to the beam cross-sectional dimensions will deflect out part of the beam power and replace it with power traveling at a very small inclined angle. This, in effect, will make the boundaries of the beam wiggle slightly and slightly reduce the power from the ideal beam volume. As witnessed by visual and photographic image, these effects are not highly disruptive except in the presence of extreme temperature gradients, such as might occur in CAT.

XII. CRITICAL DISCUSSION AND FUTURE EFFORTS

In this section the authors appraise the work presented here, express their personal opinions, and recommend the direction of future efforts.

A. Critical Discussion

The analyses developed and employed here are thought to be fundamentally sound. The reader has been informed of approximations and simplifications which are for the most part considered adequate for the purposes of this project.

There are two rather fundamental gaps which do reduce the benefits otherwise obtainable from this project, as well as several remaining questions of less importance. The major gaps are:

1. Quantitative knowledge of the relations between local atmospheric fluctuations and local optical characteristics.

2. The characteristics of local fluctuations in various regions of the atmosphere under a variety of general environmental conditions.

If there were more information in these two areas it would be possible to make much stronger statements about the adequacy of power fluctuations (electromagnetic access) received from atmospheric regions. In this case the beam power calculations would be combined with data in (1) and (2) above to provide more explicit numerical results. In the absence of data in (1) and (2) the reported results using relative specific power variations (RSPV) are thought to provide reasonable engineering guides.

The guidance provided by the RSPV values is probably more reliable in the lower than the upper atmosphere. Current experiment cross-beam work is conducted in the lower atmosphere and other investigators have performed related experiments in the lower atmosphere. Here it is necessary to recognize that the lower atmosphere contains water vapor and solid aerosols in concentrations not found elsewhere. These constituents appear to play significant or dominant roles in the optical property fluctuations which are being observed. Consequently, the upper atmosphere, which lacks these high concentrations, must be considered a different environment in which there is currently no reliable experimental base for the RSPV values.*

The computed RSPV values change smoothly with altitude and imply that similar power fluctuations will be obtained from closely adjunct altitude regions. However, these RSPV values do not contain the mesoscale atmospheric variations which may make plateaus or peaks and valleys in the actual RSPV versus altitude relation. This means that the received signal fluctuations from adjunct altitude regions may differ considerably. These variations can arise from adjunct air masses with distinctive species concentrations (ozone, water vapor, or aerosols) or with critical and non-critical psychrometric states. Interactions between air masses may create boundary regions of large RSPV due to constituent inhomogeneities or to condensation processes.

* This statement does not apply to measurements in airglow regions where local emission is the dominant factor.

There are several other areas which the current work did consider, but probably not in sufficient depth or generality. Also, some effects were not considered in any detail because it was expected that they were of higher order. These other areas are discussed below.

The RSPV values for the ultraviolet spectrum in the upper atmosphere are less accurate than similar calculations using spectral regions with longer sight distances. The ultraviolet results do imply potential utility for the short sight distance spectral regions in the upper atmosphere. Calculations with more realistic boundary and forcing functions are needed to reinforce this implication.

Gross refractive perturbations are not included in the beam power analysis.* It appears that associated power and beam geometry fluctuations should be small. The idea of relatively low significance seems supported by scintillation studies and studies in photographic resolution. However, the idea of relative insignificance is not demonstrated here by a model and numerical calculations.

The current project did not formally treat the problem of distinguishing between atmospheric waves and fluid motions. It is apparent that these phenomena may be distinguishable by characteristics such as spectral content, persistence with altitude variation, and apparent life time. The additional models which are recommended later in this section would permit a formal evaluation of this distinction during data processing.

In the analysis of cross-beam results with nonideal environments a steady wind component was generally specified. Consequently, the present work cannot illuminate some interpretative questions such as the meaning of convection speed in a turbulent environment. By extension to a more complete model, described later in this section, the relations between measured quantities and associated atmospheric behavior can be explored and defined in revealing detail.

In the beam power analysis the account of scattering is best described as first order. That is, examination of the model shows that the account of scattering cannot be described as single scattering, but that some aspects of multiple scattering should be and are included. For instance, power from a source such as the sun may be scattered into the beam at one station and become part of the beam power. However, the beam power is subject to scattering out at subsequent stations on the way to the optical system and detector. Consequently, some of the energy scattered in may later be scattered out.

* By gross refractive perturbations we mean those which affect a significant fraction of the beam as opposed to the refractive effects at individual aerosol particles. The particle-related effects are included in scattering.

This same type of situation can be used to illustrate the most serious neglect of multiple scattering. The direct sunlight is not the 'only radiant power which traverses the beam geometry or volume. Sunlight which has been scattered in other volume elements of the atmosphere also traverses the beam volume and may suffer a second scattering there which places it in the beam. The incident, previously scattered, power could be well described by a reversed scattering diagram. In a clear earth atmosphere the previously scattered power may be one-sixth to one-fifth of the unscattered solar power at sea level. Haze may increase this fraction; however, in any situation where previously scattered power becomes dominant, the region of intense scattering may become a barrier to the beam. This is what happens in a cloud.

It appears that the beam power analysis could be refined by adding second order effects involving the most important aspects of multiple scattering. However, these changes would most likely not alter the pre-dominate aspects of electromagnetic access obtained with the present analysis.

B. Future Potential of Cross-Beam Measurements in the Atmosphere

During the course of this project the principal investigators have formed opinions which are similar. In our opinion the cross-beam technique will become useful for some atmospheric measurements. Initial application will most likely be as a scientific rather than an operational tool. This opinion is based on:

- The great need for remote probing measurements in the atmosphere;
- The considerable variety of atmospheric regions and conditions in which the measurements are valuable;
- The marginal, but still clearly correlated signals which have been obtained in the current attempts to measure winds;
- The considerable array of beam geometries and spectral regions (or combinations) which might be employed; and
- The complexities of data reduction and interpretation. (Which indicates the scientific applications as being more probable.)

C. Recommended Future Work

It is our opinion that the best course of action in the near future is purposeful experimentation with guidance and interpretive support from analysis. The purposeful experimentation should include attempts to make actual measurements, such as in the current wind study program. This forces a "practical systems approach" in that no item or activity can be overlooked. In addition it appears desirable to reduce the fundamental gap on the quantitative relations between local atmospheric disturbances and the associated perturbations of local optical properties.

The current ground level experimentation with analytical support will provide added knowledge about the fundamental fluid and optical mechanisms which underlie the cross-beam applications in the atmosphere. This added knowledge can be applied for improved estimates on applicability in other atmospheric regions.

However, it may be desirable to consider some future experimentation which bypasses the step-by-step acquisition of fundamentals. Two such experiments are presented for consideration.

The first added experiment would be designed to answer the question, Is the current wind measurement work a relatively difficult application of the cross-beam technique? Two facets of the current experimental application suggest that it may be difficult. First, the optical systems look up through the entire atmosphere. Second, the beam diameter is small near the ground and increases with altitude just as do the dominant scales of turbulence. Thus the beams may be seeing the entire atmosphere and be strongly coupled by geometric matching to the fluctuations in every atmospheric region. An experiment to answer the question of relative difficulty might take one of several forms. A horizontal-looking system might be used with a natural or interposed background. Alternately, an aircraft-based, upward-looking system could be used. Each of these possibilities would need careful analytical appraisal and experiment design.

The second added experiment would be designed to answer the question, Can cross-beam measurements (other than airglow) be made in the upper atmosphere? Here there are two subsidiary questions. (1) Are atmospheric fluctuations in the upper atmosphere accompanied by significant optical effects? (2) Will the intensities of the atmospheric-optical mechanisms provide useful signal levels?* An orbit-based system might be used to

* The analysis performed in this project implies that signal levels would be low relative to lower atmosphere levels. However, the signals may still be useable if the altitude region "seen" is not too extensive.

obtain the answer. With the current state of the art it would probably employ a spectral region of reduced sight distance. Again, the experiment would require a significant preparatory effort.

In conjunction with, or in addition to, the experimental programs, certain analytical work should be carried out. Some of the analyses and computer programs developed in this project can be extended and exploited for significant benefits to the cross-beam development. In particular the following five categories of effort should be considered.

1. Analysis of relationships between atmospheric phenomena and optical perturbations.
2. Extensions of the beam power fluctuations work.
3. Generalization of correlations under nonideal environmental situations.
4. More realistic appraisal of integration time requirements.
5. Documentation of existing and/or new computer programs.

The analysis of related atmospheric and optical phenomena was considered and dropped during the reported project due to time and fund limitations. A simple engineering analysis appears essential to identify the mechanisms of potential importance and as a prerequisite to experimental design.

The analysis of beam power fluctuations at the detector was based on a sound model, but the boundary conditions and forcing functions were kept simple in order to satisfy project objectives. The analysis and associated computer program can be modified to contain more complete and realistic conditions. The program would become a powerful and flexible tool providing results for experimental planning and interpretation.

The analyses and computer programs for correlations under nonideal environmental situations can be extended and employed to provide more complete answers to the questions, What can be measured? How can measurements best be made? and What is the most unfavorable environment? Revisions and capabilities of most value appear to be:

1. Applications to a moving beam system.
2. Improvements of the correlation function to

- a. Possess power-scale characteristics.
- b. Be associated with a physically depictable model of turbulence.
- c. Be associated with a physically depictable model of atmospheric waves.

3. Provision for frequency dependent filtering in the simulated data processing (where power-scale characteristics are treated).

The appraisal of integration time requirements employed existing statistical techniques. These techniques are limited to a flat power spectrum and ideal filtering. A more flexible technique is needed which will permit more realistic analysis.

The computer programs which have been or will be developed would be valuable tools for organizations engaged in cross-beam experimentation and application. These programs should be cleaned up and documented for transmission to potential users.

CITED REFERENCES

1. Fisher, M. J., and F. R. Krause, "Local Measurements in Turbulent Flows Through Cross-Correlation of Optical Signals," NASA TM X-53295, April 1965.
2. Krause, F. R., and M. J. Fisher, "Remote Sensing With Optical Cross-Correlation Methods," Interdisciplinary Symposium on AAP, Society of Engineering Science, Huntsville, Alabama, January 1966.
3. Fisher, M. J., and F. R. Krause, "The Crossed-Beam Correlation Technique," J. Fluid Mech., 28, p. 705, June 1967.
4. Fisher, M. J., and R. J. Damkevala, "Optical Measurements With High Temporal and Spatial Resolution," IIT Research Institute Final Report, Contract NAS8-11258, September 1967.
5. Fisher, M. J., and R. J. Damkevala, "Shock Wave Shear Layer Interaction on Clustered Rocket Exhausts," IIT Research Institute Final Report, Contract NAS8-20408, October 1967.
6. Krause, F. R., "Mapping of Turbulent Fields by Crossing Optical Beams," 20th Anniversary Meeting, Division of Fluid Mechanics, Am. Phys. Soc., Bethlehem, Pennsylvania, November 1967.
7. Wolff, M. M., "A New Attack on Height Measurement of the Nightglow by Ground Triangulation," J. Geophys. Res., 71, No. 11, June 1966.
8. Krause, F. R., J. C. LaFrance, S. V. Paranjape, and J. B. Stephens, "Feasibility and Potential of Atmospheric Cross-Beam Experiments," NASA TM X-53568, October 1966.
9. Lord Rayleigh, "On the Scattering of Light by Small Particles," Phil. Mag., 41, p. 447 (1871).
10. Mie, G., "Optics of Turbid Media," Ann. Physik., 25, p. 377 (1908)
11. Diermendjian, D., "Scattering and Polarization Properties of Water Clouds and Hazes in the Visible and Infrared," Appl. Opt., 3, p. 187 (1964).
12. IITRI Final Report, Contract NAS8-20107, to be published.

13. Colorado State University, Department of Atmospheric Science, Final Report, Contract NAS8-21049, to be published.
14. Elterman, L. "Aerosol Measurements in the Troposphere and Stratosphere," Appl. Opt., 5, 1769 (1966).
15. van de Hulst, H. C., Light Scattering by Small Particles, J. Wiley & Sons (1957).
16. Dave, J. V., "Importance of Higher Order Scattering in a Molecular Atmosphere," J. Opt. Soc. Am., 54, 307 (1964).
17. Dave, J. V., and P. M. Furukawa, "Intensity and Polarization of the Radiation Emerging from an Optically Thick Rayleigh Atmosphere," J. Opt. Soc. Am., 56, 394 (1966).
18. Chandrasekhar, S., Radiative Transfer, Oxford Univ. Press (1950).
19. U. S. Standard Atmosphere, 1962, U. S. Government Printing Office, Washington, D. C.
20. Elterman, L., in Handbook of Geophysics and Space Environments edited by S. L. Valley, Air Force Cambridge Research Laboratories (1965).
21. de Bary, E., and F. Rössler, "Size Distributions of Atmospheric Aerosols Derived from Scattered Radiation Measurements Aloft," J. Geophys. Research, 71, 1011 (1966).
22. Fraser, R. S., "Computed Intensity and Polarization of Light Scattered Outwards from the Earth and an Overlying Aerosol," J. Opt. Soc. Am., 54, 157 (1964).
23. Eldridge, R. G., "A Comparison of Computed and Experimental Spectral Transmissions Through Haze," Appl. Opt., 6, 929 (1967).
24. de Bary, E., "Influence of Multiple Scattering on the Intensity and Polarization of Diffuse Sky Radiation," Appl. Opt., 3, 1293 (1964).
25. Blau, H. H., R. P. Espinola, and E. C. Reifenshtein, "Near Infrared Scattering by Sunlit Terrestrial Clouds," Appl. Opt., 5, 555 (1966).
26. Carlon, H. R., "The Apparent Dependence of Terrestrial Scintillation Intensity Upon Atmospheric Humidity," Appl. Opt., 4, 1089 (1965).

27. Carrier, L. W., G. W. Cato, K. J. von Esser, "The Backscattering and Extinction of Visible and Infrared Radiation by Selected Major Cloud Models," Appl. Optics, 6, No. 7, pp. 1209-1216, July 1967.
28. Watanabe, K., E. C. Y. Inn, and M. Zelikoff, "Absorption Coefficients of Oxygen in the Vacuum Ultraviolet," J. Chem. Phys., 21, 1026 (1953).
29. Goldstein, R., and F. N. Mastrup, "Absorption Coefficients of the O₂ Schumann-Runge Continuum from 1270 Å \longleftrightarrow 1745 Å using a New Continuum Source," J. Opt. Soc. Am., 56, 765 (1966).
30. Ditchburn, R. W., and P. A. Young, "The Absorption of Molecular Oxygen between 1850 and 2500 Å," J. Atmosph. Terr. Phys., 24, 127 (1962).
31. Inn, E. C. Y., K. Watanabe, and M. Zelikoff, "Absorption Coefficients of Gases in the Vacuum Ultraviolet. Part III. Carbon Dioxide," J. Chem. Phys., 21, 1648 (1953).
32. Stull, V. R., P. J. Wyatt, and G. N. Plass, "The Infrared Transmittance of Carbon Dioxide," Appl. Opt., 3, 243 (1964).
33. Herzberg, G., Molecular Spectra and Molecular Structure. III. Electronic Spectra and Electron Structure of Polyatomic Molecules, D. Van Nostrand (1966).
34. Tanaka, Y., E. C. Y. Inn, and K. Watanabe, "Absorption Coefficients of Gases in the Vacuum Ultraviolet. Part IV. Ozone," J. Chem. Phys., 21, 1651 (1953).
35. Vigroux, E., "Contributions a l'étude expérimentale de l'absorption de l'ozone," Ann. Phys., 8, 709 (1953).
36. Herzberg, G., Molecular Spectra and Molecular Structure, II. Infrared and Roman Spectra of Polyatomic Molecules, D. Van Nostrand (1945).
37. Brinkmann, R. T., A. E. S. Green, and C. A. Barth, "Atmospheric Scattering of the Solar Flux in the Middle Ultraviolet," Appl. Opt., 6, 373 (1967).
38. Watanabe, K., and M. Zelikoff, "Absorption Coefficients of Water Vapor in the Vacuum Ultraviolet," J. Opt. Soc. Am., 43, 753 (1953).

39. Wyatt, P. J., V. R. Stull, and G. N. Plass, "The Infrared Transmittance of Water Vapor," Appl. Opt., 3, 229 (1964).
40. Winch, G. T., M. C. Boshoff, C. J. Kok, and A. G. duToit, "Spectroradiometric and Colorimetric Characteristics of Daylight in the Southern Hemisphere: Pretoria, South Africa," J. Opt. Soc. Am., 56, 456 (1966).
41. Henderson, S. T., and D. Hodgkiss, "The Spectral Energy Distribution of Daylight," Brit. J. Appl. Phys., 14, 125 (1963) and 15, 947 (1964).
42. Judd, D. B., D. L. MacAdam, and G. Wyszecki, "Spectral Distribution of Typical Daylight as a Function of Correlated Color Temperature," J. Opt. Soc. Am., 54, 1031 (1964).
43. Sastri, V., and S. Das, "Spectral Distribution and Color of North Sky at Delhi," J. Opt. Soc. Am., 56, 829 (1966).
44. Jones, L. A., and H. R. Condit, "Sunlight and Skylight as Determinants of Photographic Exposure. I. Luminous Density as Determined by Solar Altitude and Atmospheric Conditions," J. Opt. Soc. Am., 38, 123 (1948).
45. Sharp, W. E., J. W. F. Lloyd, and S. M. Silverman, "Zenith Skylight Intensity and Color During the Total Eclipse of 20 July 1963," Appl. Opt., 5, 787 (1966).
46. Gordon, J. I., and P. V. Church, "Sky Luminances and the Directional Luminous Reflectance of Objects and Backgrounds for a Moderately High Sun," Appl. Opt., 5, 793 (1966).
47. Lloyd, J. W. F., S. Silverman, L. J. Nardone, and B. L. Cochran, "Day Skylight Intensity from 20 km. to 90 km. at 5500 Å," Appl. Opt., 4, 1602 (1965).
48. Kondratiev, K. Ya., G. A. Nicolsky, I. Ya. Badinov, and S. D. Andreev, "Direct Solar Radiation up to 30 km. and Stratification of Attenuation Components in the Stratosphere," Appl. Opt., 6, 197 (1967).
49. Kuers, G., "Investigation of the Infrared Emission Spectrum of the Atmosphere and Earth," Report under Contract AF 61(052)-778, 28 July 1966.
50. Coulson, K. L., "Effects of Reflection Properties of Natural Surfaces in Aerial Reconnaissance," Appl. Opt., 5, 905 (1966).

51. Bauer, K. G., and J. A. Dutton, "Albedo Variations Measured from an Airplane Over Several Types of Surface," J. Geophys. Research, 67, 2367 (1962).
52. Kung, E. C., R. A. Bryson, and D. H. Lenschow, "Study of a Continental Surface Albedo on the Basis of Flight Measurements and Structure of the Earth's Surface Cover over North America," Monthly Weather Rev., 92, 543 (1964).
53. Boileau, A. R., and J. I. Gordon, "Atmospheric Properties and Reflectances of Ocean Water and Other Surfaces for a Low Sun," Appl. Opt., 5, 803 (1966).
54. Hovis, W. A., and W. R. Callahan, "Infrared Reflectance Spectra of Igneous Rocks, Tuffs and Red Sandstone from 0.5 to 22 μ ," J. Opt. Soc. Am., 56, 639 (1966).
55. Hovis, W. A., "Optimum Wavelength Intervals for Surface Temperature Radiometry," Appl. Opt., 5, 815 (1966).
56. Garing, J. S., in Handbook of Geophysics and Space Environments edited by S. L. Valley, Air Force Cambridge Research Laboratories, (1965).
57. Vigroux, E., M. Migeotte, and P. Vermande, "Variations saisonnieres de l'ozone atmospherique," Ann. Geophys., 21, 500 (1965).
58. Vigroux, E., M. Migeotte, and P. Vermande, "Variations de l'ozone atmospherique," Ann. Geophys., 22, 15 (1966).
59. Bell, E. E., L. Eisner, J. Young, and R. A. Oetjen, "Spectral Radiance of Sky and Terrain at Wavelengths Between 1 and 20 Microns. II. Sky Measurements," J. Opt. Soc. Am., 50, 1313 (1960).
60. Silverman, S. M., G. J. Hernandez, A. L. Carrigan, and T. P. Markham in Handbook of Geophysics and Space Environments edited by S. L. Valley, Air Force Cambridge Research Laboratories (1965).
61. Ivanov, A. P., and A. Ya. Khairullina, "On the Determination of the Extinction Coefficient of Turbid Media," Atmosph. and Oceanic Phys., 2, 436 (1966).
62. Steward, H. S., and J. A. Curcio, "The Influence of Field of View on Measurements of Atmospheric Transmission," J. Opt. Soc. Am., 42, 801 (1952).

63. Subramanian, M., and J. A. Collinson, "Modulation of Laser Beams by Atmospheric Turbulence - Depth of Modulation," Bell System Tech. J., 46, 623 (1967).
64. Buck, A. L., "Effects of the Atmosphere on Laser Beam Propagation," Appl. Opt., 6, 704 (1967).
65. Herrick, R. B., and J. R. Meyer-Arendt, "Interferometry Through the Atmosphere at an Optical Path Difference of 354 m," Appl. Opt., 5, 981 (1966).
66. Krause, F. R., S. S. Hu, and A. J. Montgomery, "On Cross-Beam Monitoring of Atmospheric Winds and Turbulence with Two Orbiting Telescopes," NASA TM X-53538, November 14, 1966.
67. Hinze, J. O., Turbulence, McGraw-Hill (1959).
68. Secrest and Stroud, Gaussian Quadrature Formulas, Prentice-Hall, Inc., (1966).
69. Johnson, G., and A. J. Montgomery, "Survey of Detectors and Dynamic Calibration Methods for Remote Sensing Systems," NASA CR-751, April 1967.
70. IITRI Report No. M6187, "Special Report: Crossed-Beam Resolution of Ground Winds at Launch Sites," August 1967.
71. IITRI Report No. M6187-5, "Crossed-Beam Resolution of Ground Winds at Launch Sites," August 1967.
72. Bendat, J. S., Principles and Applications of Random Noise Theory, John Wiley & Sons, New York (1958).
73. IITRI Report No. M6187-6, "Crossed-Beam Resolution of Ground Winds at Launch Sites," September 1967.

SUPPLEMENTARY REFERENCES

(Listed Alphabetically)

1. Anderson, A., A. T. Chai, and D. Williams, "Self-Broadening Effects in the Infrared Bands of Gases," J. Opt. Soc. Am., 57, 240 (1967).
2. Bauer, E., "The Scattering of Infrared Radiation from Clouds," Appl. Opt., 3, 197 (1964).
3. Cann, M. W. P., and A. J. Montgomery, "Survey of Light Sources for Remote Sensing Systems," Special Supplementary Report, IIT Research Institute Project A6139, September 1966.
4. Chandrasekhar, F. R. S., "The Fluctuations of Density in Isotropic Turbulence," Proc. Roy. Soc., A, Vol. 210 (1951-1952).
5. Coulson, K. L., J. V. Dave, and Z. Sekera, Tables Related to Radiation Emerging from a Planetary Atmosphere with Rayleigh Scattering, University of California Press, Berkeley (1960).
6. Croom, D. L., "The Possible Detection of Atmospheric Water-Vapor from a Satellite by Observations of the 13.5 mm and 1.64 mm H₂O Lines," J. Atmosph. Terr. Phys., 28, 323 (1966).
7. Davies, P. O. A. L., and N. W. M. Ko, "The Near Field Generated by Intense Turbulence," Paper L-53 presented at Fifth Inter. Cong. on Acoustics, Liege, Belgium, September 1965.
8. Davies, W. O., and R. W. Deuel, "Atmospheric Applications of the Cross-Beam Technique," NASA TM X-53568, October 1966.
9. Dianov-Klokov, V. I., "Absorption by Gaseous Oxygen and Its Mixtures with Nitrogen in the 2800-2350 Å Range," Opt. Spectry., 21, 233 (1966).
10. Gibbons, M. G., "Radiation Received by an Uncollimated Receiver from a 4π Source," J. Opt. Soc. Am., 48, 550 (1958).
11. Herzberg, G., Molecular Spectra and Molecular Structure I. Spectra of Diatomic Molecules, 2nd edition, D. Van Nostrand (1950).
12. Heybey, W. H., "On the Wind Component Measurable by Crossed-Beam Arrangement," NASA - George C. Marshall Space Flight Center, Internal Note, IN-AERO-7-67, October 1967.

13. Heybey, W. H., "Product Mean Values and Convection Speed," NASA - George C. Marshall Space Flight Center, Internal Note, IN-AERO-67-8, November 1967.
14. Holland, A. C., and J. S. Draper, "Analytical and Experimental Investigation of Light Scattering from Polydispersions of Mie Particles," Appl. Opt., 6, 511 (1967).
15. Hoover, G. M., C. E. Hathaway, and D. Williams, "Infrared Absorption by Overlapping Bands of Atmospheric Gases," Appl. Opt., 6, 481 (1967).
16. Hughes, J. V., "Sky Brightness as a Function of Altitude," Appl. Opt., 3, 1135 (1964).
17. Kelly, K. L., "Lines of Constant Correlated Color Temperature Based on MacAdam's (u,v) Uniform Chromaticity Transformation of the CIE Diagram," J. Opt. Soc. Am., 53, 999 (1963).
18. Krause, F. R., "A Passive Optical Technique for Remote Sensing of Horizontal Wind Profiles and Atmospheric Turbulence," Oral presentation to American Geophysical Union, April 1967.
19. Krause, F. R., W. O. Davies, and M. W. P. Cann, "The Determination of Average Thermodynamic Properties with Optical Cross Correlation Methods," AIAA Paper No. 67-149, presented at Fifth Aerospace Sciences Meeting, New York, January 1967.
20. Krause, F. R., and M. J. Fisher, "Optical Integration Over Correlation Areas in Turbulent Flows," Paper K-65, presented at Fifth Inter. Cong. on Acoustics, Liege, Belgium, September 1965.
21. Krause, F. R., A. J. Montgomery, W. O. Davies, and M. J. Fisher, "Optical Methods for Remote Sensing of Local Thermodynamic Properties and Turbulence," NASA TM X-53568 (1966).
22. Lichtenstein, M., V. E. Derr, and J. J. Gallagher, "Millimeter Wave Rotational Transitions and the Stark Effect of the Water Molecule," J. Mol. Spectry., 20, 391 (1966).
23. MacLay, G. J., and H. J. Babrov, "Errors in Spectral Absorption Measurements Due to Absorbing Species in the Atmosphere," J. Opt. Soc. Am., 54, 301 (1964).

24. Plyler, E. K., and N. Griff, "Absolute Absorption Coefficients of, Liquid Water at 2.95 μ , 4.7 μ , and 6.1 μ ," Appl. Opt., 4, 1663 (1965).
25. Rozenberg, G. V., "Light Scattering in the Earth's Atmosphere," translation in Soviet Phys. - Uspekhi, 3, 346 (1960).
26. Stergis, C. G., et al. Handbook of Geophysics and Space Environments, edited by S. L. Valley, Air Force Cambridge Research Laboratories (1965).
27. Stergis, C. G., "Rayleigh Scattering in the Upper Atmosphere," J. Atmosph. Terr. Phys., 28, 273 (1966).

APPENDIX I

SUMMARY OF PROCEEDINGS OF CROSS-BEAM/METEOROLOGICAL PROBLEMS SYMPOSIUM

A. Introduction

On September 7-8, 1967, a conference on meteorological problems was held at Midwest Research Institute. The purpose of the meeting was to bring to light the problem areas of current concern in meteorology and atmospheric physics whose solution might conceivably be aided by a remote sensing technique known as the cross-beam method. In addition to the problem areas, information, in depth, concerning such matters as data needed, space and time scale of collection effort, characteristics of the data, and much more was elicited.

The entire two-day symposium was tape recorded. The tapes were then transcribed, yielding a rather bulky document. The transcription was then carefully edited and indexed. From this indexed volume, the following summary was prepared. It remains, however, the opinions of the panel of meteorologists. That is, care has been taken not to add to the transcriptions, or to omit any agreed upon problem area or description. At times, the wording of the panelist has been retained. In places, the problem descriptions may seem incomplete or hesitant--this is because there are simply many unknown features in our atmosphere and, in fact, is the reason for the study in the first place.

The authorities who served on the panel are listed below in alphabetical order:

Dr. Ferdinand C. Bates, St. Louis University
Dr. Alfred K. Blackadar, Pennsylvania State University
Dr. Richard Craig, Florida State University
Dr. Charles Hosler, Pennsylvania State University
Dr. James R. Scoggins, Texas A & M University
Dr. Paul L. Smith, South Dakota School of Mines and Technology

Also present at the conference, not as meteorologists, but to guide the discussion and relate the topics to the cross-beam technique were Mr. Andrew D. St. John and Dr. William D. Glauz of Midwest Research Institute. They, together with Dr. Smith, were responsible for summarizing the discussions.

Appreciation is expressed to Miss Joanne Jackson and Mrs. Jane Hess, who transcribed the tapes, and to Miss Mary Beyer, who aided in the indexing.

B. The Upper Atmosphere

1. Winds

Relatively few measurements have been made of the winds in the upper atmosphere. The measurement technique currently used is the radiosonde. The balloon borne radiosonde provides data to about 30 km. altitude. Above this altitude relatively small meteorological rockets are employed. For wind measurements, one technique utilizes a rocket releasing chaff which is then tracked by radar. The result is a point rather than an area measurement. That is, only the wind along the path of the chaff can be measured.

The wind versus height is not a smooth curve and the farther up you go the more wiggles it has. An important theoretical question is to what extent are these wind variations with a 12 to 24 hour period and a large horizontal scale, and to what extent are they small scale--for example, gravity waves with periods of hours and a scale of a couple of hundred kilometers. It would be desirable to determine the eddy lifetime, scale of turbulence, and power spectral density. These measurements are not possible with the current meteorological rocket and radiosonde data.

A first step in a measurement program using a remote measuring device would be to determine the wind at one point. We need to know what parts of the wind are of 12 to 24 hour periods and therefore are tidal waves and which have shorter periods and are therefore gravity waves. Perhaps some of the eddies have a smaller period and are what we might think of as turbulence. It would be important to make these measurements simultaneously with conventional meteorological soundings, initially. The time resolution (averaging time) of these first tests would be on the order of hours to days.

It is expected that a large contributor to the upper atmospheric winds is the phenomena of gravity waves. These waves arise from a basically stable layer in the atmosphere. Any of a number of influences such as conductive, thermal, etc., may temporarily displace fluid from its equilibrium state. The fluid tends to return to its equilibrium state due to the influence of gravity. In so doing, an oscillation is set up. These oscillations are termed gravity waves.

The wavelength of the gravity waves varies, but typically is on the order of 10's to 100's of kilometers. In the lower atmosphere the predominant scale consists of a wavelength of 6 to 7 kilometers. The amplitude of the density or velocity differences due to the gravity waves, from peak to trough, is expected to be on the order of 10 percent.

The atmospheric tidal waves, another contributor to the total winds, have basically a 12-hour period and a horizontal wavelength of 20,000 kilometers. The vertical wavelength is estimated to be on the order of 5 to 10 kilometers.

Care must be taken when interpreting results of a cross-beam experiment in terms of a convection speed when studying gravity waves. This is because in these wave motions it is not the fluid that is being convected, but rather some property such as density. Oftentimes, there is actually cloudiness associated with these density changes. At times, one sees decided bands of clouds on the crests of the waves.

The practical effects of the gravity waves on society are not known. It is generally agreed that gravity waves at, say, the 30-kilometer level in themselves produce negligible effects at the surface. Some people feel that while these gravity waves in themselves are not important, there may be occasions when through reinforcement, interference, etc., there may be an effect on the upper level divergence or convergence and thus they may contribute to other phenomena down in the troposphere. Certainly, gravity waves traveling at these very high altitudes would be of interest to those who are concerned with UHF radio propagation. Furthermore, if the kinetic energy associated with gravity waves in the upper atmosphere is roughly of the same magnitude as that for gravity waves in the lower atmosphere, then one might expect that the gravity waves are a major feature of the upper atmosphere. Although this is above the level of the SST, it might be that future vehicles would regularly use this portion of the atmosphere--necessitating a better knowledge of the wind and turbulence environment at this level.

2. Properties of the Upper Atmosphere

It is presently felt that the one property of most practical significance at the present time is that of density. There are quite a number of satellites that have their perigee at 140 to 180 kilometers. Some of these have a lifetime of months to years if they have a very large apogee. In addition, ballistic problems such as reentry of a capsule or firing accurately an ICBM or an ABM depend on the density of the upper atmosphere. Thus, many classes of vehicles currently spend short time periods in this environment and are affected by it.

The efficiency of a jet engine depends to a large degree on the density of the atmosphere at flight level. This effect is often more important than winds on overall operating economy. Thus, the continuing measurement of density at the 20 kilometer level could have a direct economic impact on SST flight.*

A second major property of the upper atmosphere is its composition. The component which is most well known (and is also felt to be the most important) is ozone. The ozone absorbs the ultraviolet radiation. Without the ozone, life as we know it on earth would not be possible. However, it has a corrosive effect on vehicles, such as the SST, flying through it. Furthermore, it is dangerous in any but the most minute quantities when breathed by human beings. It must, therefore, be removed from the air by heating and subsequent cooling before being used in the cabin of the SST.

There are other species which are known and could be measured, for example, nitric oxide, atomic oxygen, hydroxyl, sodium, and others. The economic effects of these constituents are not known. One feature of some of these trace constituents which might make the cross-beam technique particularly useful in their study is the identifying emission associated with them. In this way the main contributor to the extinction coefficient, it is hoped, would be fluctuations in the emission.

In addition to the existence of many chemical species in the molecular form, the upper atmosphere also contains particulate matter. Very little is known about this, however. There is presumably some sort of layer at about 22 kilometers. But nobody knows exactly what it is or how it got there. It is also presumed that the particulate matter is probably sulfates.

3. Other Features

Airglow emissions are phenomena which might conceivably be studied by the cross-beam technique. Airglow is a source of electromagnetic radiation of very low intensity which can be observed at the ground at night. It appears that the airglow emission occurs as the result of several previous steps. The sun, the basic energy source, disassociates oxygen molecules into atomic oxygen. One theory is that the atomic oxygen

* There is no clear-cut distinction between upper and lower atmosphere. Oftentimes, the SST altitude is considered as the lower fringe of the upper atmosphere, so is considered here.

then recombines at night in three body collisions ($O + O + M \longrightarrow O_2 + M$, where M is any other molecule), and that the third body in this process of collision is excited to a metastable state. The majority of this emission originates at about 100 kilometers. By careful study of these phenomena, it is hoped that more can be learned about the energy exchange process and the composition at this level of the upper atmosphere. Also, it is known that much patchiness in the sense that you get time variations on the order of 10's of minutes to an hour as well as space variations exists. We would like to know more about the size or scale of this system.

One would like to state that better knowledge of the upper atmosphere would lead to more accurate weather prediction. Such, however, does not appear to be the case, at least in the immediate future. Most meteorologists feel that the upper atmosphere, due to its small mass, can have little effect on the lower atmosphere in which the weather occurs. There is statistical evidence which indicates that certain features of our weather on earth are correlated, for example, to the lunar cycles, solar disturbances, and meteor showers. It may be that the upper atmosphere plays a role in this correlation. It must be stated, however, that the probability of finding a significant cause and effect relationship between the upper atmosphere and weather which would have a large economic benefit is small.

It is known that almost any altitude affects some frequency of radio propagation in one way or another. Therefore, any property of that altitude which varies may change the efficiency with which one can propagate radio waves. This question of radio propagation effects may deserve a closer look. This would require a collaboration between upper atmosphere meteorologists and specialists in wave propagation and transmission.

C. World Weather Watch and Related Topics

1. Wind Measurements in General

The world weather watch or global observing system requires the measurement of atmospheric properties over the entire earth surface on a 500 kilometer grid. The ideal measurement would be that which is representative in some way of conditions over the entire 500-kilometer square. This information is needed (and is not currently available) as initial conditions for mathematical weather prediction models.

A first approximation to the desired measurement would be a point measurement, say at the midpoint of each 500-kilometer square. This, basically, is the type of measurement currently being made over

limited areas of the earth's surface. One would be better off, for example, by taking four measurements over the grid and averaging. A continuous average would, of course, be better still.

The mathematical weather models require not only wind data but also state data such as temperature, moisture, pressure, etc. The cross-beam technique would be directly applicable only to obtaining the wind data. The remainder of this section, therefore, will be concerned only with wind data and not the state variables.

The wind, in addition to being measured over a horizontal grid of 500 kilometers square, must also be measured on a vertical grid. Currently, at those locations where wind measurements are made, the vertical grid is determined not by altitude, but rather by pressure level.* This undoubtedly is the way in which they would prefer it to be done in the future. However, measurements taken at equal altitudes would probably be satisfactory. The current mathematical models have up to 9 altitude (pressure) levels or layers, the upper layer extending up to 50 millibars. A single value, representative of each layer, is what is required in the models.

The timing of the measurements has two considerations: the period between measurements, and the simultaneity of measurements. Currently, over the limited regions where winds are measured they are usually observed at 12-hour intervals, occasionally at 6-hour intervals. It would be desirable if these were monitored continuously. However, 12-hour intervals or perhaps even 24-hour intervals would be useable if on a global basis. As for simultaneity, all measurements should be taken within a one-hour interval. Lacking this, it would be acceptable to interpolate or extrapolate the measured data to a common point in time.

A major consideration in a global weather watch scheme is the effect of missing data. Currently, adequate data are available only over the U.S. and a few other areas. There are virtually no data over the oceans, over the southern hemisphere, etc. To make use of such data in numerical weather prediction techniques, an essentially complete matrix of information is required. The existence of more than a few gaps in the data would make it practically useless for this purpose. Partial data would, however, be useful for dealing with more localized weather phenomena. For example, information on the winds aloft over the eastern Pacific or over Mexico would be of extreme usefulness in severe local storm forecasting in the United States.

* Some, however, have their equations written in terms of isentropic surfaces rather than constant pressure surfaces so would like to know the wind as a function of potential temperature.

Also in regions around tropical storms such as hurricanes and typhoons the wind information would be useful. These problem areas are discussed in subsequent sections.

Although it would not be of use in itself in world wide weather prediction techniques, the measurement of only one component of the wind velocity vector on a global basis would aid in other areas. The North-South component would be of most use to the scientific world. Knowing the latitudinal flux of any property on a global basis would be beneficial in refining our knowledge of the energy balance and conversion of one type of energy to another. Of particular interest would be the transport of moisture, momentum and energy. On the other hand, the East-West wind component would be of most use to the operational people. This is because the East-West component is generally bigger and therefore more important for air travel considerations, for example. All in all, however, it is more valuable by a factor greater than two to obtain both the East-West and North-South components than it is to obtain only one of them.

Again, it is emphasized that care must be taken in the interpretation of convection speed data as wind speed. That is, the propagation speed of a disturbance, which might be detected by the cross-beam technique, may not be equal to the wind speed.

2. Atmospheric Stability

It would be extremely valuable both to the scientific world as well as to the operational people to have a direct measurement, on a world wide basis, of the stability versus altitude. The stability or instability depends primarily on two factors: first, the lapse rate or comparison of the temperature change with height with the adiabatic potential temperature changes; and second, the wind shears. Stable layers imbedded in an otherwise unstable atmosphere can lead to smog problems if at low altitude and can limit cumulus development at higher altitudes even though the stable layer might be quite thin. On the other hand, a layer of extreme instability could be associated with turbulence and in particular clear air turbulence. (See subsequent section for further information.)

A common, but not universally accepted, method of measuring the instability is by means of the Richardson number, which is the ratio of the vertical temperature gradient to the square of the wind shear. It would be necessary to obtain this number at intervals on the order of 300 meters in the vertical direction. Wind measurements without the temperature gradients would be a help in this direction but both are really required.

It might be possible to estimate the stability of the atmosphere by knowing the power spectral density or the scale of turbulence or eddy lifetime. This would enable direct determination of atmospheric stability, which is not currently possible.

3. Hurricanes

Unfortunately, there is much that is unknown about the growth and decay of hurricanes. Studies of such storms are not hindered so much by lack of data as they are by lack of knowledge of what data would be useful in determining the course of events.

It is felt that one phenomenon which has a large role in the growth and subsequent development of hurricanes is the energy distribution among the various eddies. It is thought to be important to know the predominant size of the eddies that contain the energy of the system and the way in which the energy changes. That is, does it go from big eddies to little eddies or vice versa and in what stages and in what places in the hurricane?

As far as prediction of hurricanes is concerned, a first step would be to collect data on a global scale of the winds and, more importantly, the eddy scale. This quantity, the eddy scale, is something that has probably not been used before as a synoptic parameter simply because there was no convenient way to measure it. Measurements which consist of averages over a 500-kilometer grid would be acceptable for this purpose. These historical data would then be used to trace backward in time the development of existing hurricanes.

Once a hurricane has developed there is much that should be measured. Everyone is interested in circulation and the measurement of the flux of water vapor and energy in and out of the system. There is apparently a lot of smaller scale organizations within a hurricane. One can't think of it in the same way as one thinks of an individual storm. Here it is very important to see how the individual cells interact with one another. We recognize that the flux of water vapor from the surface is one of the very important sources of energy of the storm. After the storm moves over land this tends to be cut off and is one of the reasons that they dissipate so quickly over land. Also, the wind profiles and the boundary layer which tell us a lot about friction and momentum transfer near the surface are important. It is not implied that these are operational requirements. We need to know them in order to understand the mechanics of the storms.

An important economic problem is that of predicting the path of an existing hurricane. The only technique currently believed valid for this purpose is known as the "steering method." The technique involves the computation of the flow field external to the hurricane and then assumes that the hurricane is a vortex imbedded in and carried with the external flow.* The use of the steering technique requires the knowledge of the wind field external to the storm, and measurements taken, for example, along with the world weather watch studies would be useful for this purpose.

The study on a smaller scale of a developed hurricane would also be of interest. Within the hurricane is an organized system of convective cells. One can't think of them as simply individual storms since they interact with one another. One would, therefore, want to make his study first on a scale of the order of the distance between cells, in order to better determine the interactions between the cells. Later one could study the individual cells in much the same way as one might study an individual thunderstorm. (See later section.) They are basically of the same size as a thunderstorm, perhaps a little wider with lower tops. Items to be measured include the vertical component of the wind and the circulation.

4. Clear Air Turbulence (CAT)

Conceivably, one of the most directly beneficial uses of a remote sensing device would be in detecting or forecasting CAT. CAT is turbulence in clear air, that is, without any visual evidence. This presents different problems from turbulence associated with, for example, thunderstorms and squall lines primarily because it is difficult to detect and less is known about it. It is more common at the higher altitudes (12 to 18 kilometers), and is, therefore, important to the military and, with the advent of the SST, to commercial aircraft. Currently, there are many theories and research projects under way which attempt to relate CAT to atmospheric parameters which can be measured. Several such parameters which might be amenable to the cross-beam technique are discussed below.

* This neglects the effect of propagation wherein if there were an energy source on one side and not on the other there would be a tendency for the hurricane to propagate towards the energy source.

First, we will consider the detection of existing patches of CAT. The obvious and most direct approach would be to simply ascertain the intensity of turbulence throughout the air space of interest. This might be done, for example, on the basis of a one-mile grid. There may be situations where such information would be useful. However, it does not appear to be a feasible scheme when carried out on a world wide or even country wide basis. This is because the isolated pockets of turbulence do not remain fixed, but tend to dissipate and reappear elsewhere. Therefore, the sampling would have to be repeated at relatively frequent intervals on the order of 15 to 30 minutes. The amount of data required would thus become astronomical.

An approach aimed at locating the general vicinity of CAT rather than pinpointing the phenomena may be of more practical use. A possibility along this line would be to measure and determine the power spectral density of the air as part of the world wide weather watch. Those portions of the atmosphere containing CAT would have a different power spectral density than the remainder of the atmosphere. Presumably, if there was a significant amount of CAT in a 500-kilometer square area, the average power spectral density over the area would be detectably different from that of a like area without CAT. Of particular interest in such a power spectral analysis would be those wavelengths which would elicit undesirable responses from the aircraft. Such measurements would probably be indicative of general conditions several hours in the future.

There is evidence indicating that the occurrences of ozone and radioactivity at levels lower than usual may be correlated with CAT. Normally, the ozone and radioactive portions of the atmosphere are in the stratosphere. It apparently gets down into the upper troposphere on occasions which can be correlated with periods of clear air turbulence. Again, areas of the order of 500 kilometers on a side could be averaged over for purposes of detecting ozone or radioactivity. The turbulence layer itself may be rather thin, say, on the order of 600 meters; therefore, several scans with altitude would be necessary.

In addition to the problem of detecting existing CAT is the associated problem of forecasting the future occurrence of CAT. This is thought to be related to the Richardson number (see Section II B). An altitude band which contains a large wind shear which is not compensated by a large positive temperature gradient (compared with the adiabatic case) may be expected to form turbulence. Therefore, the measurement of the wind as a function of altitude which would yield the wind shear would be a start in the right direction. This should, however, be complemented with temperature gradient measurements.

D. Clouds and Local Storms

1. Thunderstorms

The distinction between a severe thunderstorm and a lesser storm or cumulus cloud is based primarily on size and intensity. An isolated severe thunderstorm may affect an area on the order of 40 kilometers in diameter, and may, in extreme cases, have internal updrafts on the order of over 50 meters per second. It is this severe type of storm that is of interest in this section.

Data can be obtained for both operational and research uses. That is, there are some data which if made available quickly enough are believed to be of operational use in the prediction and tracking of severe storms. Most suggested studies, however, are aimed at obtaining a more basic understanding of the behavior and life cycle of a thunderstorm. Those studies more nearly related to obtaining operational data will be discussed first.

The prediction of severe thunderstorms could be enhanced by more complete wind information. For example, if as part of a world weather watch we had coverage of the eastern Pacific and Mexico we could improve the accuracy of severe storm forecasts in the United States by 10 to 15 percent. In general the inputs to severe local storm prediction are the large scale wind fields, stability, and temperature measurements.

The detailed interaction of a thunderstorm and its environment is not completely understood. This is particularly of interest in the smaller stages where the interaction between the cloud and its environment is critical to the fate of the cloud. Therefore, in addition to studying the environment near the storm (see below), it would be necessary to observe the atmosphere that is unaffected by the appearance of the thunderstorm. This would require measurements outside of the affected region of, say, 40 kilometers in diameter. This relationship between a cloud and its environment is also of extreme importance in weather modification, discussed in a subsequent section.

Moving closer to the storm, the measurement of the wind environment surrounding the cloud is important. Ideally, temperature and moisture data would be obtained simultaneously from, for example, radiosonde measurements. However, the wind data have value in themselves. The ideal wind measurement experiment would consist of measuring the wind speed and direction on a three-dimensional network. The grid spacing in this network would be on the order of 300 meters between points both

vertically and horizontally. This spacing could be relaxed for the very large storms. If the data obtained from such a study were to be used operationally, it would be necessary to be able to reduce the data within 5 minutes of the time they were taken. The time period between measurements should be from 1 to 5 minutes. It is doubtful that much could be learned with longer periods between measurements since the storms change so rapidly. The total cycle or time period over which measurements should be taken is about one hour. It would be desirable to be able to measure the convection speeds to within 10 kilometers per hour.

There are less ambitious experiments involving the measurements of winds around thunderstorms which would provide useful information. One of these is to determine the convergence. The minimum requirement for this, which would not be very satisfactory but would be better than nothing, would be measurements at three points around the cloud. Anything more than that improves the value, such as several different altitudes, more points, etc. The ideal measurement would be that which circumscribes the entire cloud and performs an integral of the normal component of velocity. Another study would be that of measuring the vertical wind under the base of the thunderstorm. In this case anything from a single measurement to a detailed map of the updraft would be of interest. In conjunction with other observations, it would fix certain features of the storm.

Aside from the wind field measurement problems, another area of study would be to measure the turbulence adjacent to a thunderstorm. Measurements of the turbulence variables would be related to the rate of mixing and, therefore, of value in helping parameterize the mixing of the air within and without the storm. It might also be operationally important in helping aircraft avoid particularly severe turbulence. In this regard, it has been recently determined that the most severe turbulence so often found within a mile or two of the storm on the southern or southwestern flank. It would be desirable to locate these regions of severe turbulence so as to be able to vector aircraft around them. In addition to the turbulence it would be most desirable to be able to measure the eddy flux of water vapor or other flux through the edge of the cloud.

Another class of measurements is concerned with what goes on inside of the thunderstorm cloud. A beginning study might concern itself with making measurements at a single point within the cloud. Later, one would hope to be able to map the interior of the cloud by a sequence of measurements. Again, wind velocities, turbulence, etc., would be of interest. It would be desirable to measure eddy sizes, for example, as small as 100 feet. Such studies would be primarily of scientific benefit rather than having immediate operational usefulness.

One of the questions which might be studied is the relationship between eddy size at the top of the cumulus and the diameter, d , of the vertical draft. It is felt that the median eddy size is proportional to $1/d$. Another question concerns a class of storms recently recognized to be associated with a rotating updraft over sufficiently smooth terrain. As yet, we have no good measurements of this draft rotation.

Another point of critical importance which appears in the mechanics of treating a severe thunderstorm would be to measure water droplet spectra and density of water particles. It is not clear how the cross-beam technique would be directly applicable to this problem. It is clear, however, that fluctuations of water droplet density will lead directly to fluctuations in the extinction coefficients. The water droplets may not be used, however, as simple tracer objects. There is the additional problem here that large size water droplets or ice particles do not move at the same speed as the air because of the influence of gravity. Thus, a measurement of water droplet motion may not correspond to motion of the air masses.

A potentially useful and interesting feature of the cross-beam technique would appear if the technique could be used to measure the speed of propagation of acoustic disturbances. In this instance, it would be of interest to detect the propagation of small density or pressure fluctuations. Since acoustic waves propagate at a speed proportional to the square root of the absolute temperature, a means of remote measurement of the temperature as well as the wind speed around the thunderstorm might be possible. To be useful, the acoustic speed would need to be determined within a few tenths of a percent, that is, within a few feet per second.

A phenomenon often associated with the severe thunderstorm is the tornado. Special studies related to this event are presented in the next section.

2. Tornadoes

The detailed interpositioning of a tornado and the parent thunderstorm remains uncertain. This is due primarily to the difficulties in making accurate, simultaneous measurements. It has been found, however, that the tornado appears consistently, except for one infrequent type, on the southern or southwestern flank of the squall line of thunderstorms, and can appear up to a considerable distance from the parent thunderstorm--as much as 30 kilometers. Vortices other than tornadic, which are invisible structures, also exist below these cloud bases and are a hazard to aviation. They do not stop abruptly at the cloud base, but extend into the cloud for some distance. We need to know how far into

the cloud and in what configurations these tornadic vortices exist. This must be done by a remote sensing operation due to the hazards involved". Furthermore, it must be done by means of airborne equipment. It can be shown that the probability of being able to make such a measurement from a ground station might be once in eight years. On the other hand, with airborne equipment, one might expect to be able to make measurements in about one out of five tries.

3. Weather Modification

The study of cumulus clouds for purposes of weather modification closely resembles the study of severe storms except that the systems involved here are much smaller. Again, the primary measurement would be that of wind speeds. It would be desirable, but not mandatory, to supplement wind speed data with temperature and moisture data.

In an operational cloud seeding program, where you want to treat cumulus clouds as individuals, you would want very detailed observations on a total grid something like 10 to 15 kilometers on a side. Within this grid, measurements should be made at intervals on the order of 300 to 1500 meters. One prime purpose of these measurements is to determine where is the inflow into the storm and what is the size of the inflow area, so that one knows where to put in materials to alter the cloud. The data must, of course, be analyzed in real time. In other words, the data would be of no use for more than about a 5-minute period. These measurements are taken within 300 to 600 meters of the physical cloud.

From a research standpoint, the requirement of the 5-minute analysis period may be relaxed. Here, the emphasis would be on collecting detailed data of many types, and then analyzing them at leisure, the aim being to increase our knowledge of cloud physics. The difference in whether a cloud produces rain or not is often not the overall stability or anything that we observe about the gross characteristics of the atmosphere, but is the relationship between that individual cloud and the environment and the rate of entrainment of additional air. In this regard, then, measurements which illuminate the mixing process, fluxes of all kinds, etc., are of primary value in a scientific sense.

The above paragraphs all discuss phases of weather modification which involve the modification of clouds so as to produce rain. Another technique of weather modification that hasn't been exploited or explored concerns precipitation that evaporates before reaching the ground. Oftentimes some, if not all, of the moisture which is precipitated out of the cloud never reaches the ground due to evaporation. It appears that one could increase rainfall greatly if the evaporation could be reduced. A study program would be necessary to learn more about the particle size

distribution, falling speed, and evaporation rate. Conceivably the cross-beam technique might be used to aid in this purpose.

4. Radio Frequency Emission

There are radio frequency emissions from clouds due to mechanical and electrical processes. A great number of electron transfer processes occur in the process of growth, evaporation, and collision of water droplets and ice crystals. Many of these give off emissions in radio frequencies which if monitored and studied might give vital information about the composition and processes going on in the cloud. These emissions are not in the optical range so, therefore, are perhaps beyond the scope of the cross-beam technique. Conceivably, however, a similar device operating in the proper frequency range might be of use as a remote sensing tool in cloud physics studies.

E. Mesoscale and Microscale Studies

1. Wind Profile Measurements

The measurement of winds on a scale smaller than global has many direct and indirect benefits to society. In a direct way, such measurements would be of use in special regions such as near launch facilities, large smokestacks, airports, etc. Other problem areas involving wind profile measurements, which are just as important although perhaps of less direct usefulness at the present time, include the study of surface friction, of winds near thunderstorms, their relationship to turbulence and stability, etc. These problem areas are discussed individually in subsequent sections. The measurement of wind profiles is discussed on a more general basis here.

Low altitude winds are being measured today as a matter of course by many techniques. These techniques all possess two major flaws. First, of course, the presence of a tower or other structure on which the measurement device is mounted may disrupt the flow pattern. Second, and just as important, is the fact that these devices give basically a point measurement. Generally, the wind measurement desired is not a point value but rather a volume or area average over some region. If the cross-beam device would actually integrate the winds and their statistical characteristics over an area, it would represent a tool which doesn't exist now.

A suggested approach is to start by making point measurements in the vicinity of a tower and using standard instruments mounted on the

tower as a basis of comparison.* These measurements should be made up to an altitude of about 150 m.; that is, within the earth's boundary layer. Then, a measurement program without towers and utilizing area averages would be in order. The area size would depend on the problem, ranging from a few hundred feet to a kilometer.

We would also like to have detailed wind profiles up to 1 kilometer or more. Above 120 to 150 m., however, the wind is so nearly geostrophic that for practical purposes it isn't too important to get the fine resolution. Beyond the 1-kilometer altitude, it would be desirable to obtain wind profile measurements at intervals of 300 to 600 m. in the vertical, to obtain wind shear data. This, of course, would be of use in determining the Richardson number which was previously discussed in regard to CAT.

The motions of the mesoscale are vertical as well as horizontal and both ought to be measured. The vertical motions on a smaller scale that contribute to evaporation and fluxes of heat and momentum, that is, what we normally think of as turbulence, should also be measured.

2. Statistical Properties of Turbulence

Various aspects of turbulence are discussed in sections on clear air turbulence, storms, and the upper atmosphere. These features will not be repeated here. The emphasis in this section is the study of turbulence in a general, scientific sense. It has been said that one of the most important problems on all scales is to identify the characteristic motions of the atmosphere.

The problem of describing motions on the microscale has to be done statistically. One wishes to know the frequency distribution of velocities, and the spectrum of velocities. That is to say, we desire the energy distribution of the velocities according to time frequency. Ultimately, one would hope to be able to relate these factors to other meteorological parameters. We must know how to relate the statistical properties of turbulence to parameters we can measure on a larger scale.

Initial studies of turbulence could be carried out in conjunction with the studies of wind profiles, energy dissipation, and surface roughness effects. One would probably start with point measurements at tower

* This approach is currently being followed by people from IIT Research Institute in conjunction with other researchers from the NASA Marshall Space Flight Center and Colorado State University.

altitudes and expand from this to area averages which are expected to be more useful.

The properties of the small scale components such as power spectrum, etc., tend to be isotropic. That is, their statistical properties do not depend on direction. This is generally true in the horizontal plane and true of the vertical also if the wavelengths involved are small compared to the altitude. There are, of course, situations in which anisotropy exists. For example, in squall lines the properties along the line are expected to differ from those perpendicular to the line. These organized systems should be recognized as such and not confused with the more unorganized turbulence.

3. Energy Dissipation

Related to the study of turbulence is a special topic--that of energy dissipation. Most of the kinetic energy in the atmosphere is dissipated into heat in the turbulent scale. If we can measure the rate of dissipation of energy, we may be in a better position for forecasting on a large scale. We must know specifically how the energy is being dissipated, where it's being dissipated, and we must try to relate this to large scale parameters. We must measure fluctuations on a very small scale and then try to relate the dissipation to things we can measure over large areas.

It had been largely thought that most of the energy dissipation in the atmosphere takes place in the boundary layer near the ground. But recent estimates on a continental scale have suggested that the dissipation in the free atmosphere may be equally important in magnitude. There is, therefore, a great need to measure energy dissipation in a free atmosphere. We have no way of determining the distribution of this energy dissipation; that is, where it takes place geographically, and whether it occurs in connection with clear air turbulence zones. (This is suspected.)

The turbulence scales which must be measured depend on the height. Near the surface, scales that are very small compared to height are important. We must concern ourselves with fluctuations of the order of 1 sec. Out of the boundary layer, however, not enough is known about the frequency distribution of the dissipation to say precisely what scales are important. This determination would be a goal of a measurement program.

4. Friction Effect of Surface Roughness

A problem that we don't know how to tackle, mainly because of its complexity, is the way in which the wind profile changes as the wind moves from one kind of terrain to another. It is known that these changes are large and can have significant effects on weather. For example, in a big storm system we know there is going to be large scale convergence and uplift and that there will be cloudiness and precipitation. The details within this storm cannot generally be predicted, however. In other words, we cannot tell whether there will be lines or bands and where they will be located. These lines or bands may cause quite intense rainfall some places and nothing elsewhere. These patterns are determined not only by thermal influences (which may actually be secondary) but by changes in the wind profile dictated by frictional characteristics of the surface.

The study of these frictional effects is currently under way in this country. Initial studies involve the change in wind profile that results from wind going from a uniformly rough surface to a uniformly smooth surface. The studies are hampered, however, by the lack of remote wind measuring apparatus and the consequent need of towers. The effects of friction are generally close to the ground and are thought to disappear at about 1 kilometer under normal circumstances. In extreme types of situations, such as hurricanes, the effects could go to 3 kilometers or higher. It is important to characterize the difference in the winds over different types of land surfaces, and how the wind changes in going from one surface to another. It is conceivable that such studies might even lead to a new philosophy of weather modification.

5. Aircraft Operating Problems

Several potential applications of the cross-beam technique which are applicable to problems involving aircraft have been discussed in other sections. Primarily these involve the SST and the effects on it of CAT, ozone, and atmospheric density measurements. There are two other problem areas, both associated with measurements near airports, which should be mentioned.

One critical problem is the mean wind shear at the lowest layers of the atmosphere, at night particularly. This is extremely critical in landing jet aircraft where they let down from recent very strong head winds into a layer of much more slowly moving air very close to the ground.

An associated problem is that concerning the turbulent wake behind the large jet aircraft. This wake may extend a mile or more behind the aircraft, and not be visible to other air traffic. This is particularly serious for small airplanes following or crossing behind the large jets.

6. Launch Facilities

There are two areas of wind measurements which are particularly important to the launching of large space vehicles. One of these concerns the measurements of the winds and wind shears prior to launch to which the vehicle will be subjected. The second is the measurement of the structure of the turbulence and gusts at the time of launching. The problem of predicting the appearance of specific gusts or gusty situations from measurements made some distance away should be studied.

7. Other Problem Areas

Problem areas of potential application of the cross-beam method which have not been covered in previous sections are mentioned briefly here. The first, a problem on the mesoscale, concerns the effects of topography on the air flow and wave phenomena set off by mountains. This is, in a way, related to the frictional effects of rough surfaces except for the much different scale involved.

A second problem, one which is beginning to be realized, is that of the effect of small variations in the sea surface temperature on mesoscale convection patterns. This is one area where measurements have apparently never been made. The problem is associated with temperature variations on the order of one-fourth of a degree and the resulting distribution of winds. Some people think this has an important bearing on the determination of the types of weather structures that develop.

Another research area that might be explored is that of measuring the speed of propagation of acoustic waves in the atmosphere. This was discussed previously under the subject of thunderstorms, but is mentioned again here because of its potentially more general application. The atmospheric temperature can be determined if the speed of propagation of acoustic waves is known. This then opens a whole new area of possible usefulness of remote measurement techniques.

Finally, it should be indicated that one need not rule out extraterrestrial applications. As an example, it is suggested that the circulation of the Martian atmosphere is similar to earth's. Therefore, at least a good part of the time there should be cyclones involved. But, if there are, apparently they are not visible by water phenomena, lifting of dust, etc. A remote sensing technique that would detect these would provide useful information.

APPENDIX II

OPTICAL PHYSICS AND ATMOSPHERIC MODELS

A. Introduction

A description is given in this Appendix of the optical physics considerations important to the atmospheric application of the cross-beam correlation method. The employment of the cross-beam techniques in atmospheric research requires the investigation of a number of areas. These areas are related to the selection of useable spectral regions, optical sources and possible tracers. The selection of useable spectral regions involves the study of atmospheric intensity changing mechanisms resulting from scattering (both Rayleigh and Mie), absorption, and emission properties of the environment. Except for techniques which rely on backscattering, the study of the atmosphere by use of electromagnetic signals requires either a sharply defined volume of study (transmission studies between a searchlight and a detector) or an extended source. The possible general extended sources will be considered.

The cross-beam correlation technique requires a change in extinction or emission properties within the atmospheric volume under study. Tracers are items whose temporal and/or spatial variations cause these changes in or near the region of interest. Consequently, it is advantageous to examine possible useable tracers within the volume in conjunction with the selection of favorable spectral regions.

Techniques which use a single optical path can be generalized to cross-beam techniques. The simplest system is one in which a restricted source of radiation, a path, and a detector are used, as in searchlight transmission measurements, pyrometry, and similar single beam measurements. A more complex system which depends on backscattering of radiation from a specific source to a proximate detector, e.g., radar and lidar systems, could conceivably be developed for studies in which natural light sources could not be used. The searchlight scattering technique^{14/} which depends on a variable scattering angle suggests some of the difficulties to be encountered in the use of cross-correlation measurements. In all of the single path experiments, the extinction properties of the intervening medium must be accounted for in data analysis. The cross-beam technique has the capability of reducing the need for estimates of signal variations that are not directly related to the volume under consideration. The present study considers natural radiation sources, as well as tracers and atmospheric limitations which apply to both natural and man-made sources.

The scattering properties of various types of particles expected in the atmosphere are dependent on the light wavelength and number density (also particle size distribution for aerosols). Rayleigh scattering is applicable when the ratio of the diameter of the molecule, D , to the wavelength of the scattered light, λ , is small ($D/\lambda < 0.01$). Mie scattering must be considered for D/λ ratios larger than 0.01. (Rayleigh scattering is the small particle limit of Mie scattering.)

The scattering distribution is usually expressed in polar coordinates with axis along the direction of the incident light. The angular distribution diagram for a distribution of particle sizes is called an indicatrix. The indicatrix will show a wavelength dependence when the particles are large enough to require Mie theory application. The permanent gas and water vapor molecules are small enough that Rayleigh theory can be used for wavelengths longer than X-rays.

Scattering properties are important in the consideration and use of extended sources. This is particularly evident in the case of diffuse transmission of sunlight resulting from a combination of Rayleigh scattering and aerosol scattering.

The intensity changing mechanisms as a function of altitude are an important consideration in the application of the cross-beam correlation technique to atmospheric research. Rayleigh scattering and oxygen, ozone, and carbon dioxide absorption variations with altitude can be readily predicted because of their strong dependence on gas molecular number density. However, Mie scattering and the effects of water vapor content on absorption are highly variable and must be designed for specific conditions. Mie scattering varies with aerosol stratification, composition and size distribution within the atmosphere. The effects of water vapor content on absorption can best be described by the influence of extremals in concentration. The scattering due to molecular water vapor is included in the Rayleigh scattering model.

There are some areas within the electromagnetic spectrum where absorption due to normally present gases and aerosols will tend to restrict useable distances between the source and detector. This is particularly evident in the O_2 and O_3 absorption bands in the ultraviolet range and in the infrared region when large water vapor concentrations are present.

Part B of this Appendix discusses the extinction and emission mechanisms which are important to cross-beam studies of the atmospheric environment. Scattering (both Rayleigh and Mie) is described. Total absorption due to gases present in the atmosphere is discussed. Plots of representative altitude variations of Rayleigh and Mie scattering and

absorption coefficients are presented for the ultraviolet, visible and infrared wavelength regions. The Mie scattering coefficients are given for three specific aerosol models. The effects of haze and cloud models on the infrared absorption coefficients are also presented.

Part C is a detailed discussion of possible sources of radiation. The information in the visible and near-visible spectrum suggests that aerosol variation is important in both skylight and surface reflectance. The use of thermal emission from either the ground or atmospheric ozone as an infrared source is complicated by interference from atmospheric water, both cloud and vapor. Airglow emitters are a highly specialized source, being intimately related to the presence of chemically excited species which may serve as tracers.

The information in Parts B and C suggest that an experimental evaluation of water vapor as a tracer could be helpful, especially since it is so variable in amount and distribution. Other natural tracers are not as widespread, but this does not rule out their potential usefulness.

Part D summarizes some of the problems related to the difficulty of collimating extended natural sources. Additional problems discussed include triangulation error due to beam wander, and experimental error due to multiple scattering resulting from large turbulent cells outside the two beam volumes.

Part E describes some pertinent features of collimating systems.

B. Localized Mechanisms Changing Intensity

The concept of the cross-beam system requires a variation in electromagnetic power received at the detector. This variation is due to both source variations and changing conditions along the optical path. The optical path can have intensity changes resulting from 1) scattering into or out of the path, 2) absorption, and 3) emission of energy by particles within the volume of the beam.

The change in intensity of a beam in going along a pathlength ℓ is ideally given by

$$I = I_0 e^{-B\ell} + I_c$$

where $\beta = \beta_S + \beta_A$ consists of both a scattering contribution, β_S , (which sums all scattering processes out of the beam) and an absorptive contribution, β_A . I_c corrects for scattering into the beam, and for emission into the path. Since the in-scattering and emission are independent of I_o , the correction term, I_c , is required. Scattering, absorption and emission are discussed and quantified in the following.

1. Scattering Mechanisms

When electromagnetic radiation encounters particles whose size is comparable with or less than the wavelength of the radiation, the phenomenon known as scattering occurs. This scattering is a change in direction of energy flow resulting from the interaction between the particle and the radiation. The size of particles in the atmosphere and the size distribution encountered for large particles suggest that for wavelengths between 0.15μ and 25μ the scattering can be treated in two areas: (a) molecular scattering, and (b) aerosol scattering. Coherent scattering or diffraction effects are not anticipated as long term effects, so the common treatments of incoherent scattering are adequate.

a. Rayleigh scattering coefficients: Since the characteristic dimensions of gas molecules are much less than 0.15μ , the Rayleigh scattering theory can be used to describe the molecular scattering from the gaseous part of the atmosphere. Since the scattering effect is averaged over all gases, quantum mechanical transitions sufficiently close to a wavelength which might excite resonance in one molecular type will not significantly affect scattering behavior. The basic scattering cross section, σ , for a single particle and unpolarized light¹⁵ is

$$\sigma = 8 \frac{\pi^3}{\lambda^4} \frac{(n-1)^2}{N^2} \frac{2+\Delta}{6-7\Delta},$$

while the differential scattering cross section, $\frac{d\sigma}{d\omega}$, becomes

$$\frac{d\sigma}{d\omega} = 3 \frac{\pi^2}{\lambda^4} \frac{(n-1)^2}{N^2} \frac{1+\Delta+(1-\Delta)\cos^2 \phi}{6-7\Delta}$$

where n is the index of refraction (which depends on the molecular number density N), λ is the wavelength, Φ is the scattering angle and Δ is the depolarization factor. (For isotropic polarizable particles, Δ is zero, while for O_2 , $\Delta = 0.054$.)

For atmospheric scattering under conditions of low sun and short wavelength, the loss of energy by single Rayleigh scattering is great enough that multiple scattering also becomes important. Dave^{16/} presents an example in which secondary scattering provides at least 16 percent of the intensity of primary scattering, while tertiary scattering is about 3 percent of primary. Further work on a molecular atmosphere with optical thickness near unity shows that the ratio of diffuse to direct transmittance rises significantly as optical thickness goes from 0.2 to 1.^{17/} Chandrasekhar^{18/} has treated the problem of molecular atmospheres including multiple scattering and polarization effects. The angular distribution is affected by the optical path, the relative weighting of primary and multiple scattering, and the extent of the primary source. A two order of magnitude change in total intensity between a minimum near the source and the horizon is found for thin atmospheres.^{17/}

Rayleigh scattering coefficients as a function of wavelength and altitude can be developed from the scattering cross section, which is dependent on the wavelength of the radiation, and the atmospheric number density (1962 standard atmosphere^{19/}). The tables in Handbook of Geophysics and Space Environment^{20/} have been extended beyond the original 0.27μ to 4.0μ wavelength range and 0 to 50 kilometers altitude range in order to develop the material presented in Figures 13, 14, and 15. Figure 13 is for the ultraviolet wavelengths (0.15μ to 0.38μ), 14 for the visible wavelength range (0.4μ to 0.7μ), and 15 for the infrared wavelength region (0.8μ and longer).

The altitude variation is separable from the wavelength variation, thus explaining the close similarity of the figures. However, there is a wide variation in Rayleigh scattering coefficients from 2.4 km^{-1} at 0.15μ and sea level to $2.7 \times 10^{-13} \text{ km}^{-1}$ at 11.7μ and 85 kilometers.

b. Aerosol scattering coefficients: For particles with sizes comparable to the wavelength of the radiation, the Mie scattering formulae should be used. Aerosol particles fall in this range. Although the Mie expressions reduce to the Rayleigh form in the limit of very small particles, the differential scattering cross section for aerosol particle sizes of interest shows a strong forward peak and a number of subsidiary maxima in contrast to the Rayleigh scattering. The averaging of the Mie formulae over a model particle size distribution will tend to smooth the variation of differential scattering cross section for a given wavelength and to suppress strongly wavelength dependent features. However, the strong preponderance of forward scattering remains. For water-based aerosols, the Mie theory leads to both scattering and absorption when the index of refraction of

water is complex. Only the averaged scattering effects will be considered for the aerosol scattering coefficients.

The Mie scattering of radiation by a single particle of spherical shape is reviewed by van de Hulst.^{15/} The extension of this theory to systems of identical particles in random orientation is made difficult only when multiple scattering has to be included. For a distribution of particle sizes and for sufficient optical thickness that multiple scattering must be considered, the problem is attacked by a variety of approximate methods. de Bary and Rössler^{21/} have shown that a variety of particle size distributions for haze at 25 kilometers altitude can approximate measurements of the ratio of aerosol scattering at two angles. A more stringent requirement exists if not only the angular scattering function but also the number of measurable particles (radius greater than 0.08μ) must be approximated or the ratio of scattering functions at different wavelengths must be matched. de Bary and Rössler^{21/} suggest that improved agreement between theoretical model and experiment resulted from a division of the aerosol size spectrum into Aitken nuclei (less than 0.06μ radius) and measurable particles with application of a modified Junge distribution to the large haze particles. A choice of $dN/d \log r$ proportional to $r^{-3.5}$ seems reasonable at 25 kilometers altitude.

Other aerosol models have been proposed. Fraser^{22/} discusses two aerosol models for particles in the size range 0.03μ to 20μ . One model has an order of magnitude more particles per unit volume than the other, but the extinction coefficient in the visible spectrum is more dependent on the number of particles with radii between 0.03μ and 20μ than on the total number of particles including Aitken nuclei. Using a model with neither multiple scattering nor aerosol absorption, Fraser indicates that polarization and intensity data on outward scattered light was insufficient to adequately define the aerosol present. Eldridge^{23/} suggests that aerosols to fit specific spectral distributions of transmittance can be created by modifying the size distribution of particles. One approximation to multiple scattering by aerosols assumes that the effect for the smaller aerosol particles is similar to multiple Rayleigh scattering for an atmosphere of optical thickness comparable to that of the aerosol.^{24/} However, to the authors' knowledge a satisfactory multiple scattering treatment for the entire aerosol size spectrum is nonexistent.

Additional studies of the effect of changing size distribution profiles of model aerosols and model clouds are available. A particularly interesting summary by Deirmendjian^{11/} compares two haze distributions and one cloud distribution. Comparable scattering results were obtained from haze with an r^{-4} distribution for particles above 0.15μ radius, no particles below 0.03μ and with a particle density 23 times greater than

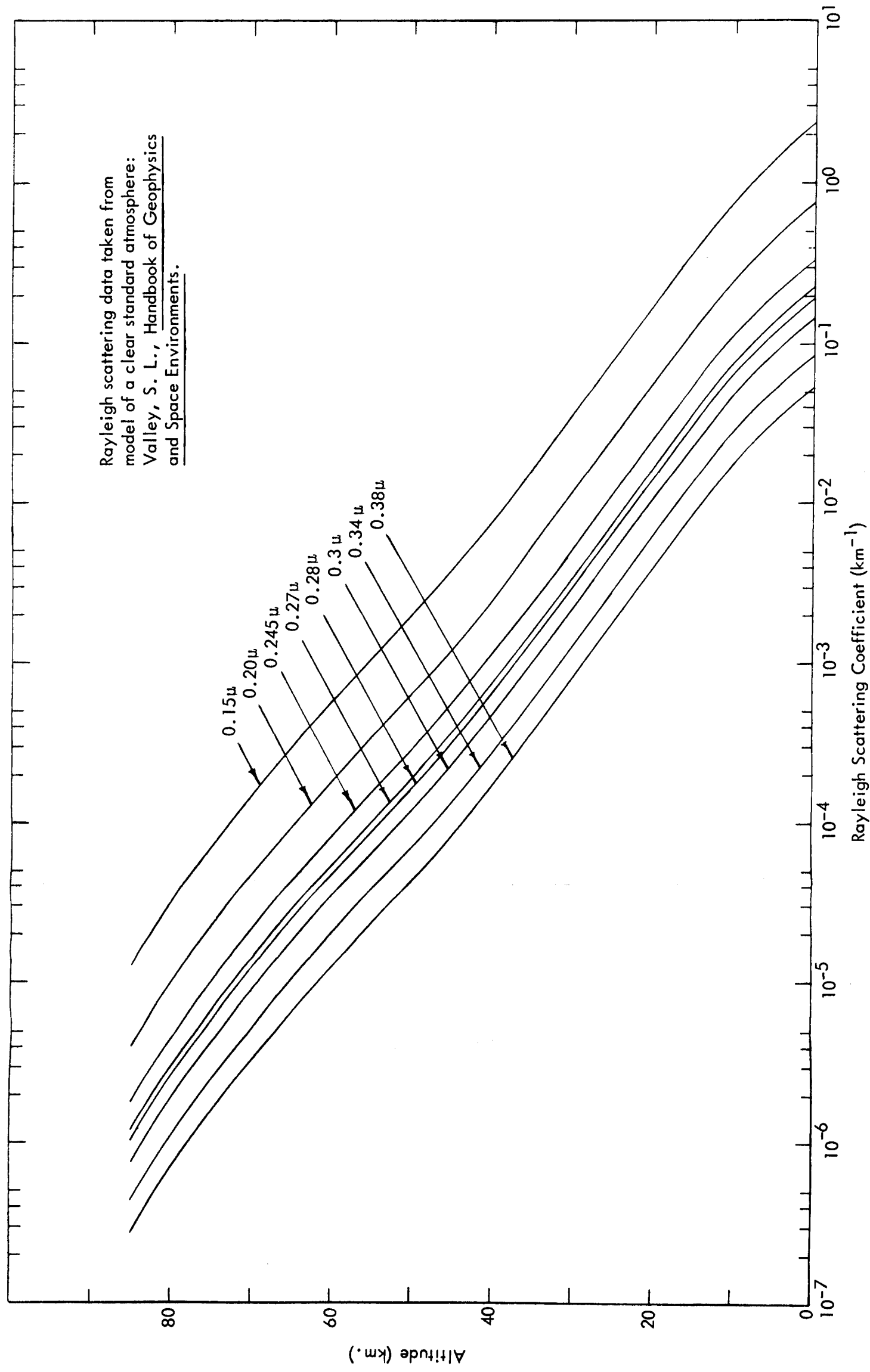


Figure 13 - Rayleigh Scattering Coefficient vs. Altitude for Ultraviolet Wavelengths

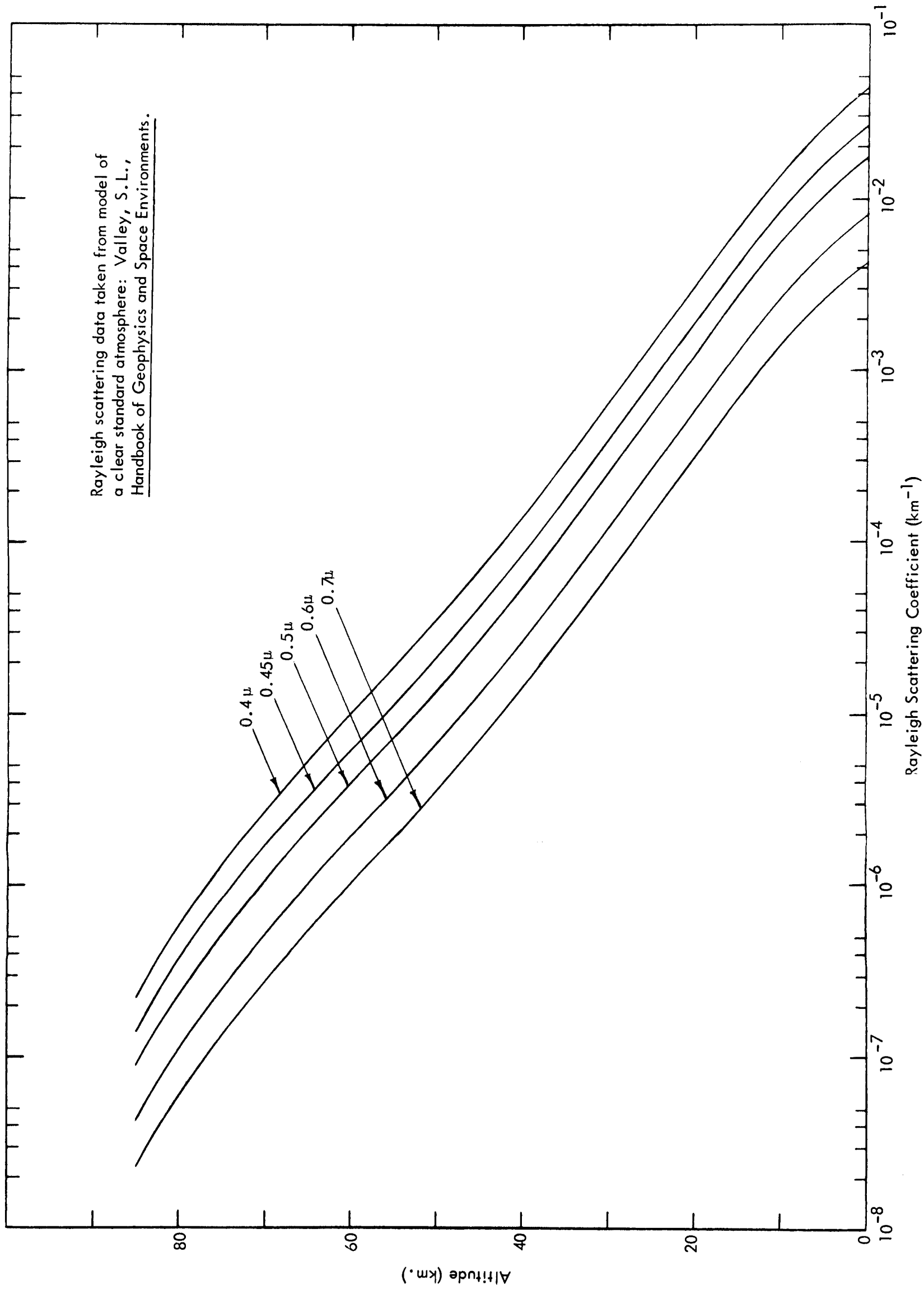


Figure 14 - Rayleigh Scattering Coefficient vs. Altitude for Visible Wavelengths

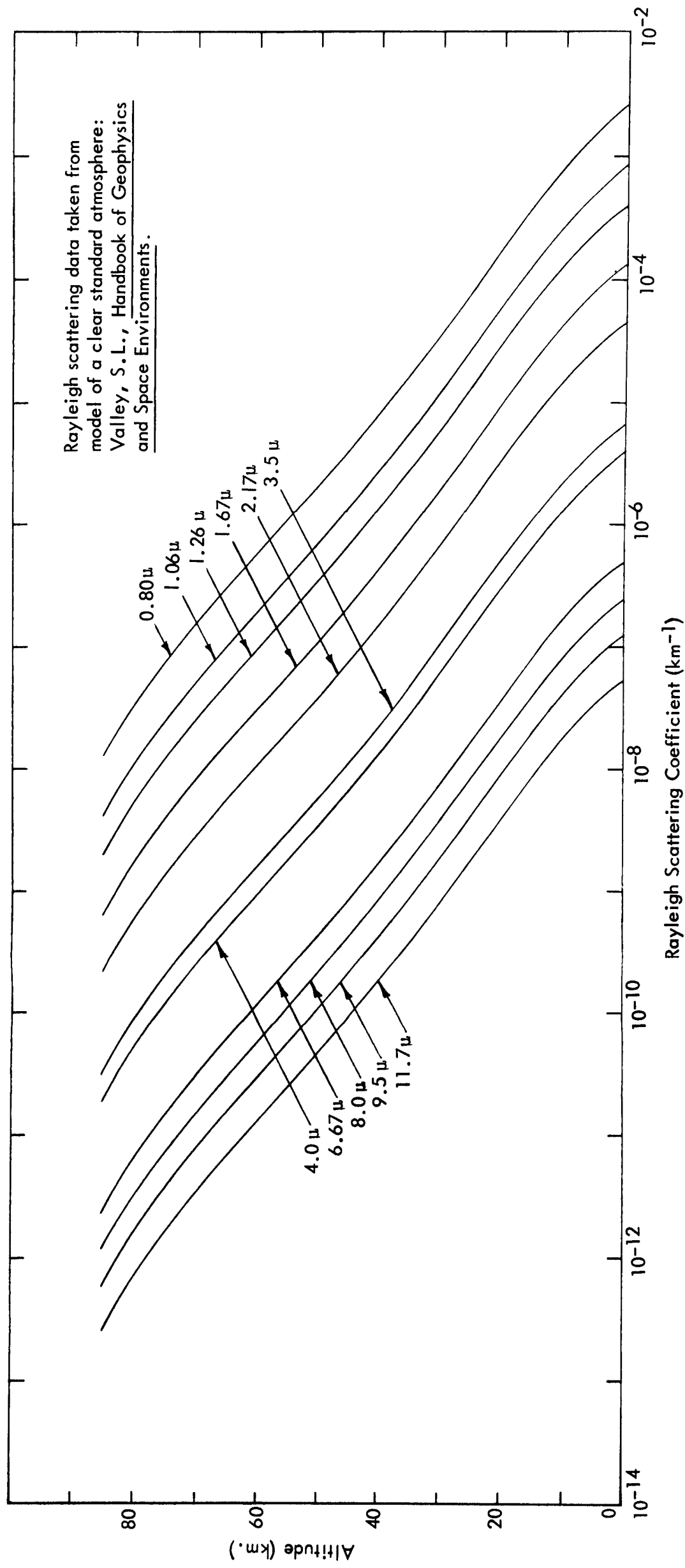


Figure 15 - Rayleigh Scattering Coefficient vs. Altitude for Infrared Wavelengths

that of another haze with an $re^{-a\sqrt{r}}$ distribution having mode radius at 0.05μ . The difference is due to particles at the upper end of the size range. The cloud model has an $r^6e^{-1.5r}$ distribution for $n(r)$ with a mode radius of 4μ . The cloud model shows more scattering in the visible range than either haze model.

One haze and the cloud from this reference^{11/} are used in the atmospheric models. It is important to note that the scatter diagrams obtained by the author agree well with experimental measurements on natural haze and fog.

The lack of an adequate solution for ice crystal geometry has led to the use of approximate values of size parameters on the argument that the ice crystals will be large enough that the highly variable portion of the Mie angular distribution is not needed.^{25/}

There is a greater transparency in the 0.7 to 4μ infrared region than in the visual range for thin clouds and a possible difference between ice crystal and water droplet reflection at 1.48 and 1.97μ . There is, however, a wide change between the effects of water in the near infrared and in the 10μ window. In the latter the optical density due to water droplets seems very important.^{26/}

Three different aerosol models are presented in this Appendix. The first is an extension of a model developed by Elterman^{20/} and tabulated for 0.27μ to 4.0μ . This is called a clear-day aerosol and is assumed to apply to a nonabsorbing medium with an altitude-dependent number density. The angular distribution of scattering was not defined, but should show a preference for forward scattering. The model was extended to 0.15μ and 9.5μ by extrapolating on a wavelength dependent graph, but the aerosol number density curve has not been extended above 30 kilometers. Figures 16, 17, and 18 show the ultraviolet, visible, and infrared wavelength regions. This model varies through five orders of magnitude in the aerosol scattering coefficient with a much stronger dependence on altitude variation of aerosol number density than on wavelength.

A haze model has been developed by assuming the addition of Deirmendjian's "Haze C"^{11/} to the clear-day aerosol between ground level and 6 kilometers altitude (a constant haze particle number density for this range) and a decrease to the clear-day aerosol at 9 kilometers altitude. The dense haze is characterized by particles in the 0.03μ to 5μ radius range with a number density of 2300 cm^{-3} and a distribution approximating continental hazes. Two wavelengths, 0.45μ and 9.5μ , were chosen for the illustrations in Figures 19 and 20. The clear-day aerosol coefficients are used between 9 and 30 kilometers.

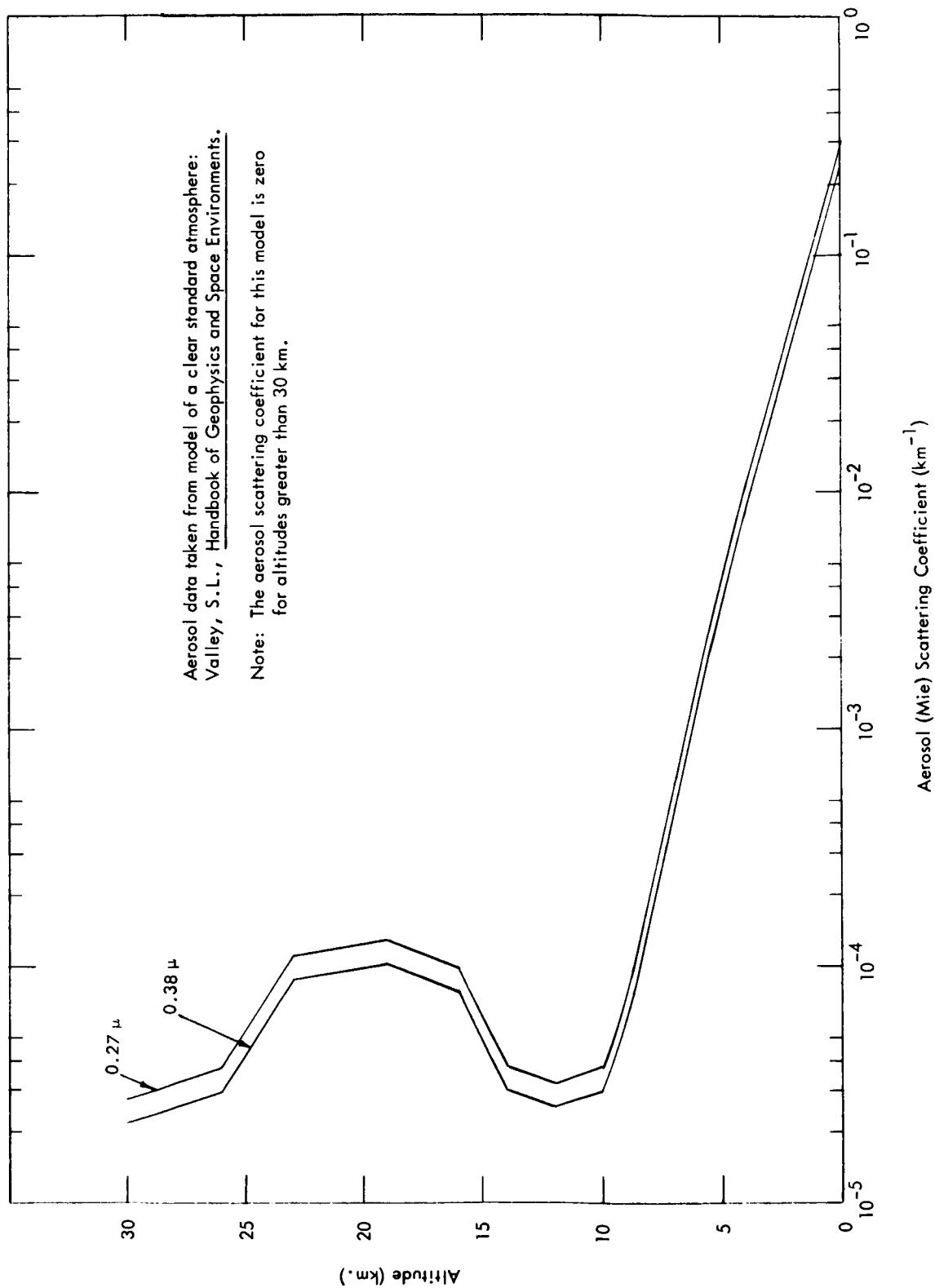


Figure 16 - Aerosol (Mie) Scattering Coefficient vs. Altitude
 for Ultraviolet Wavelengths

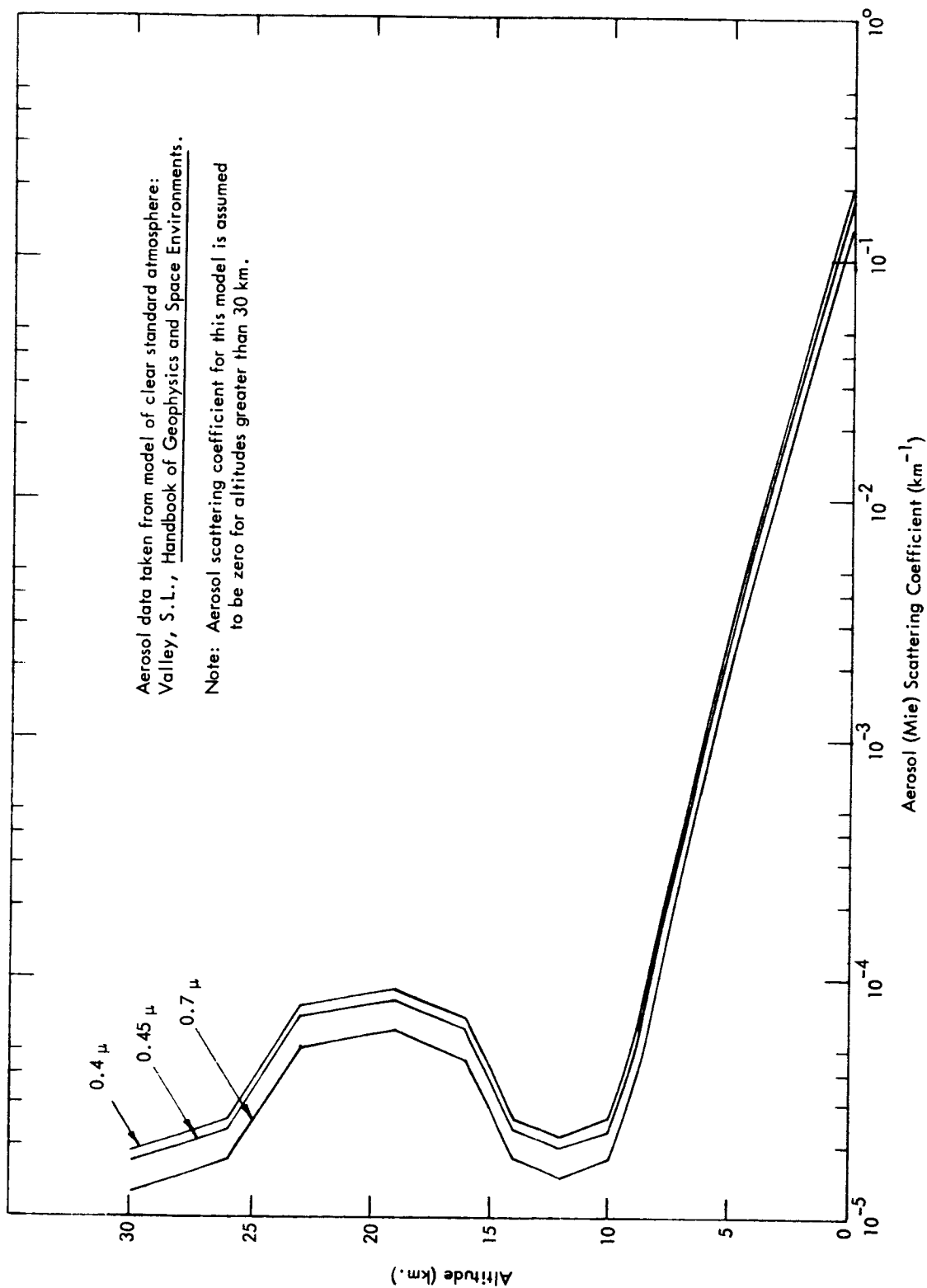


Figure 17 - Aerosol (Mie) Scattering Coefficient vs. Altitude for Visible Wavelengths

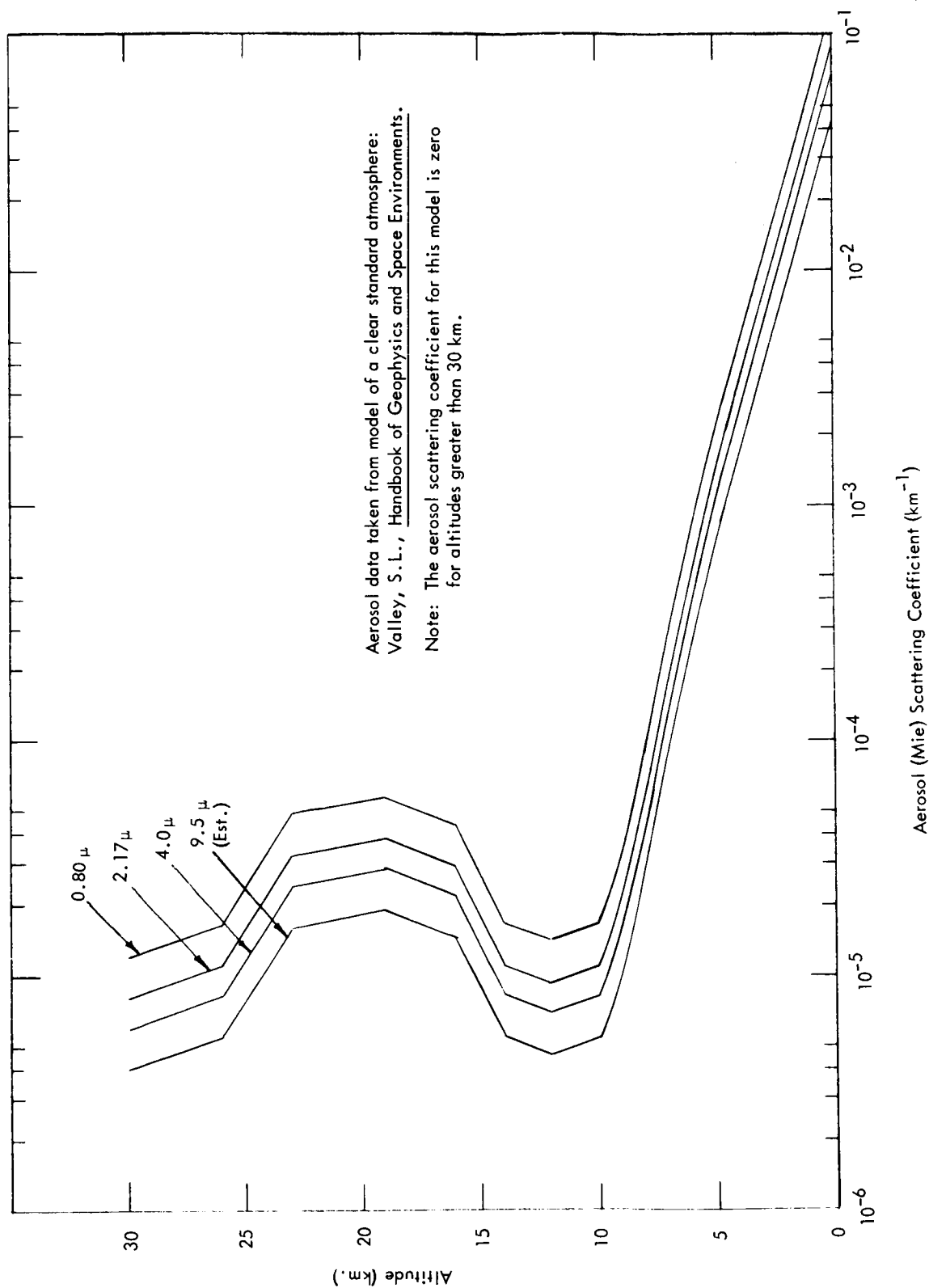


Figure 18 - Aerosol (Mie) Scattering Coefficient vs. Altitude for Infrared Wavelengths

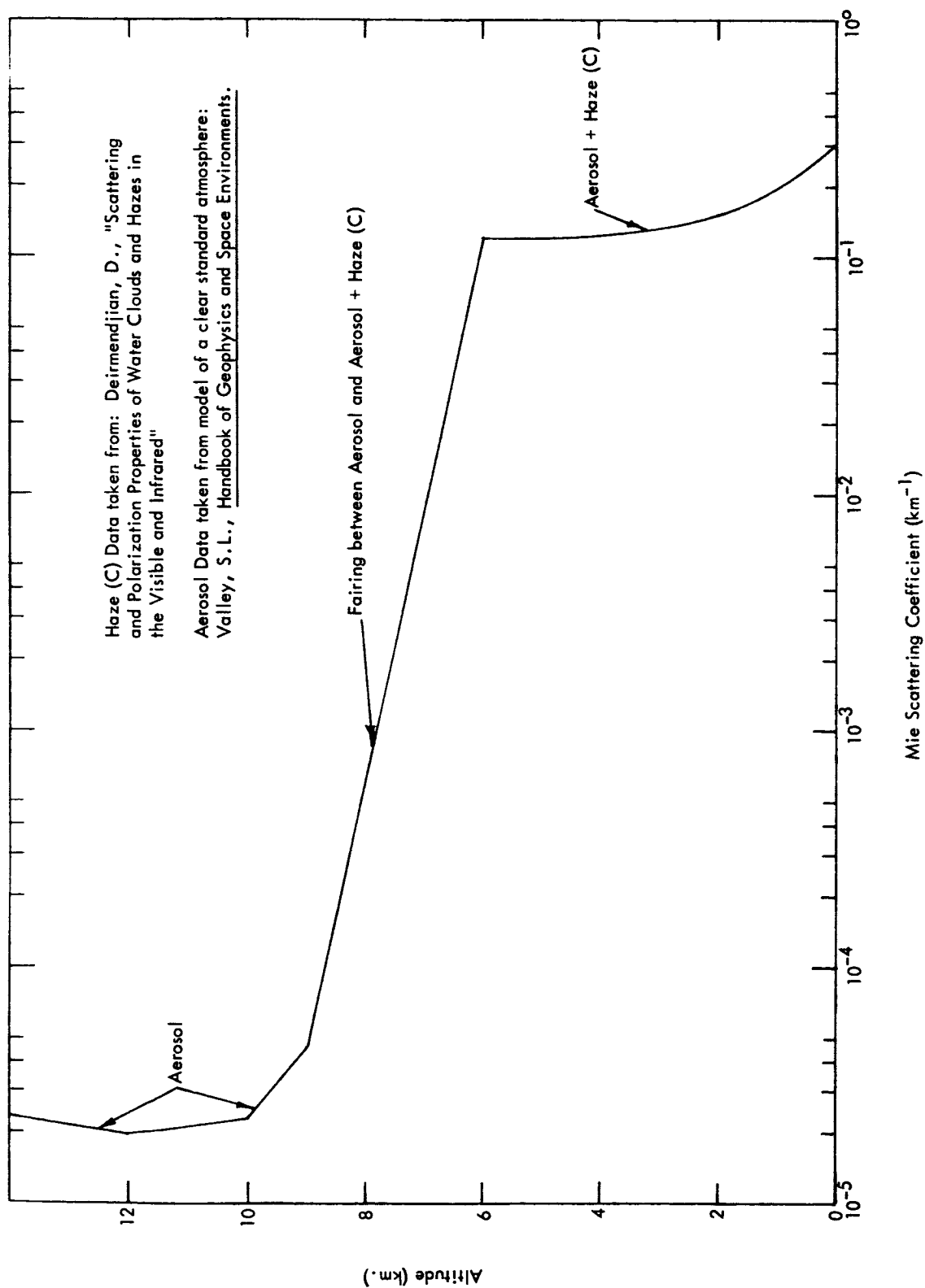


Figure 19 - Haze Model Mie Scattering Coefficient vs. Altitude for a Wavelength of 0.45μ

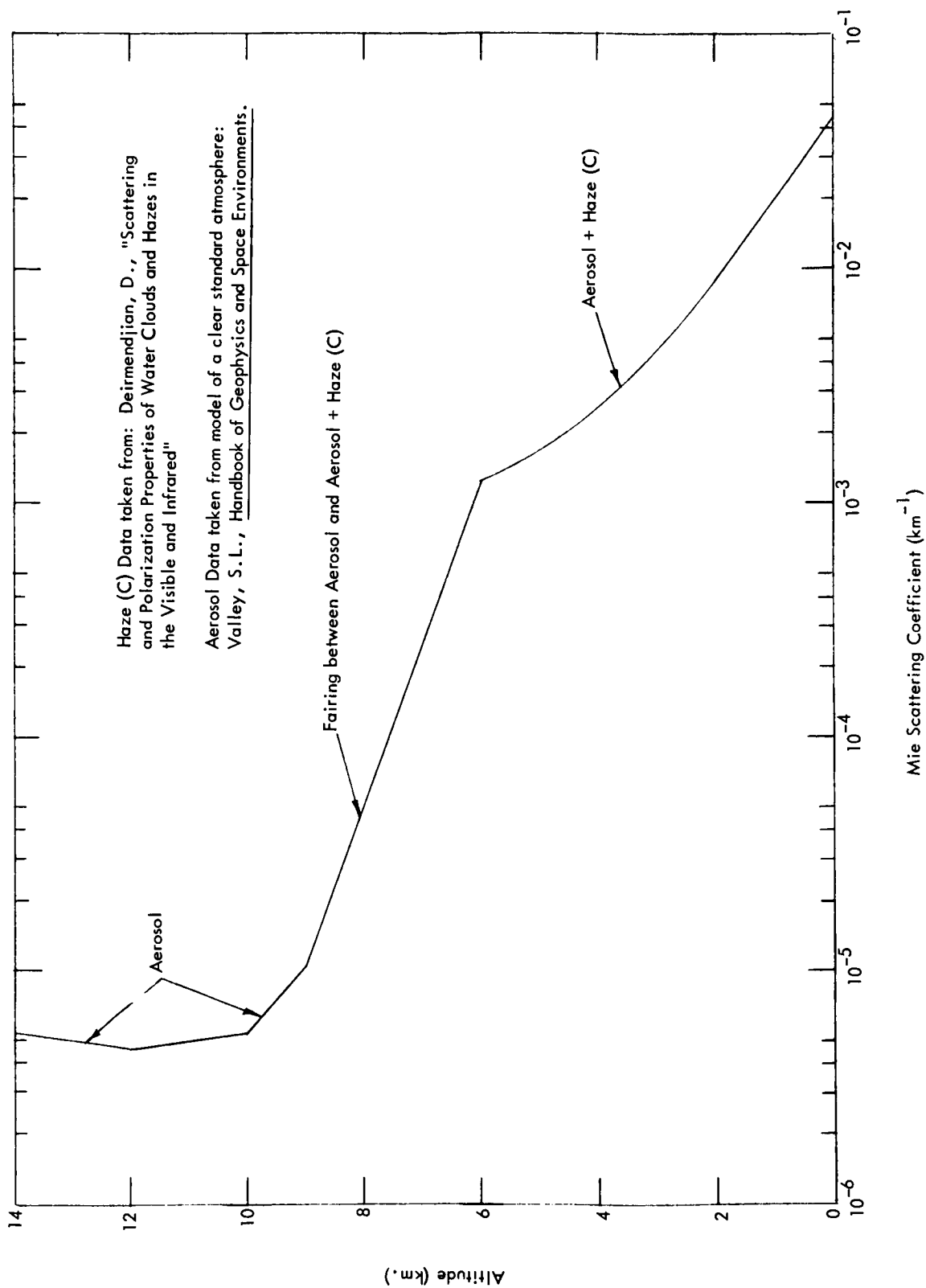


Figure 20 - Haze Model Mie Scattering Coefficient vs. Altitude for a Wavelength of 9.5μ

A cloud model was developed from the following assumptions: 1) between 2 and 3 kilometers altitude the cloud particle number density and size distribution (100 particles/cm³ and 4μ mode radius)^{11/} are supplemented by the haze model; 2) at ground level only a clear-day aerosol is used; 3) at 1 kilometer altitude the haze value represents an appropriate transition; 4) between 5 and 30 kilometers the clear-day aerosol is adequate; and 5) the various points can be connected by straight line segments on semi-log graphs. The 1 kilometer cloud thickness is within the range reported in papers on optical properties of clouds, while the chosen cloud model^{11/} is near the lower limit of the variations discussed by Carrier et al.^{27/} Figure 21 shows this cloud model's scattering coefficient for 0.45μ. Figure 22 shows that at 9.5μ the cloud has half as large a scattering coefficient as at 0.45μ, while the aerosol is somewhat more transparent.

2. Absorption Mechanisms

In addition to transfer of energy from a ray by scattering, hence changing the intensity of the ray, there is also loss of energy by absorption within particles. There are two basic types of absorption to consider, depending on the phase of the particle. Various types of gas molecules have possible structural rearrangements which permit them to convert certain wavelengths of radiative energy into internal energy. Liquid and solid particles will show collective effects which can lead to absorption (aerosol absorption). Several of the gases present in air show absorption in various areas, while water-based aerosols have many strong absorption features in the infrared.

a. Gas phase absorption coefficients: For signal evaluation purposes, the total absorption coefficient for the gas molecules is the important factor. This absorption will show dependence on gas composition, altitude and wavelength. For the 0.15μ to 25μ wavelength range some gases will be unimportant due to weak or negligible absorption while other gases will show highly localized regions of importance. Some gases will show essentially uniform mixing ratios, while others will show altitude-dependent or time-dependent mixing ratios. The total absorption coefficient used in this study will be presented after a discussion of various parts of the model.

Nitrogen has no absorption features in the 0.15μ to 25μ wavelength region which are strong enough to be seen in a nitrogen-oxygen atmosphere. Oxides of nitrogen are minor constituents and usually are not strong enough to change total absorption coefficients appreciably.

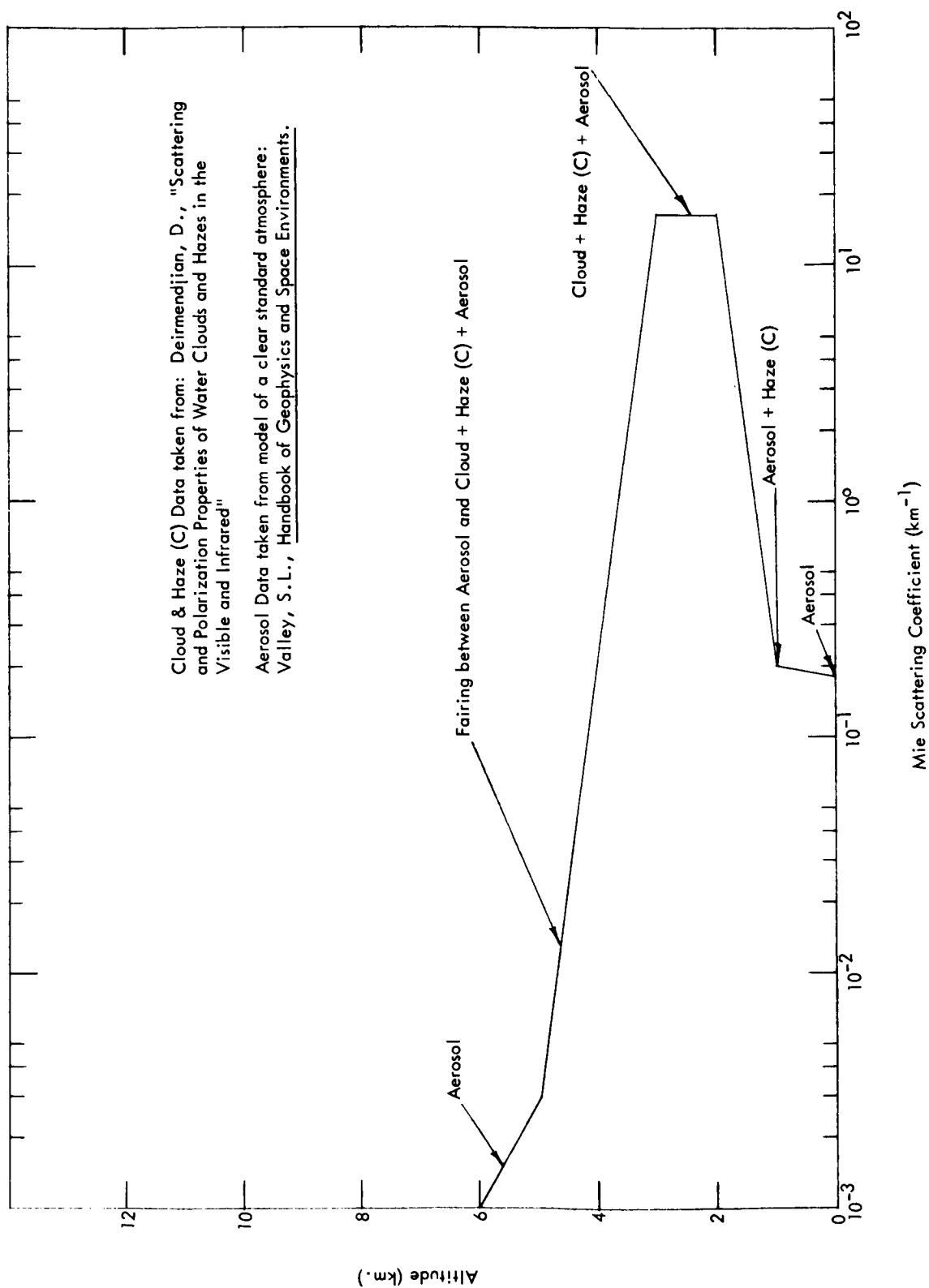


Figure 21 - Cloud Model Mie Scattering Coefficient vs. Altitude for a Wavelength of 0.45μ

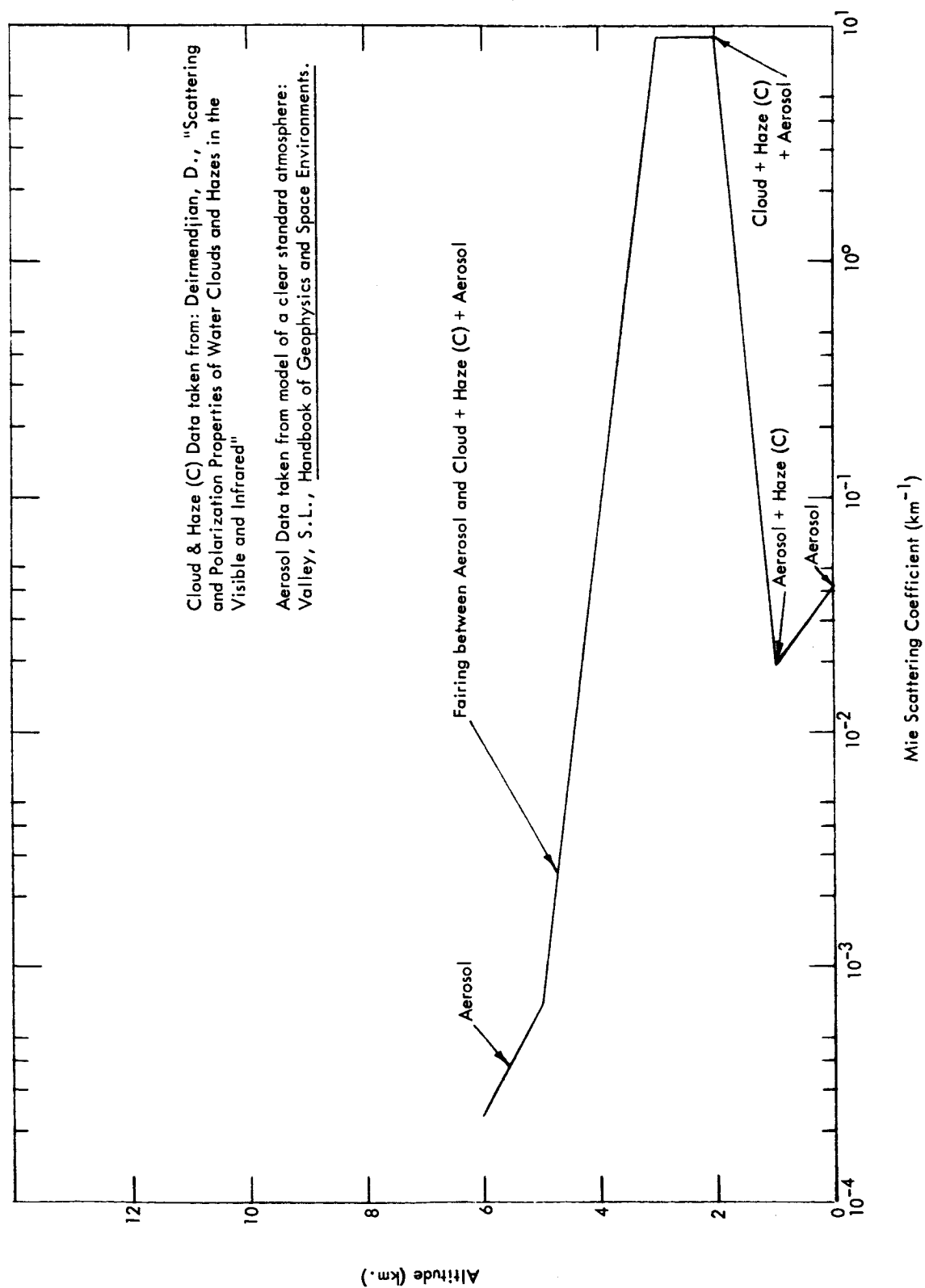


Figure 22 - Cloud Model Mie Scattering Coefficient vs. Altitude for a Wavelength of $9.5\text{ }\mu$

Oxygen shows strong absorption in the Schumann-Runge continuum (0.13 to 0.175 μ), the Schumann-Runge band spectrum (0.175 to 0.20 μ) and the Herzberg band system (0.20 to 0.28 μ). The oxygen absorption used is based on laboratory measurements of absorption coefficients by Watanabe et al.,^{28/} Goldstein and Mastrup,^{29/} and Ditchburn and Young.^{30/} Specification of absorption coefficients in the Herzberg bands is complicated by the Wulf bands of O₂-O₂ complexes, which cause pressure dependent terms to appear. Absorption coefficients were not available for the weak infrared oxygen bands.

Carbon dioxide is another molecule which can absorb in the vacuum ultraviolet and infrared portions of the spectrum, but it shows no absorption in the visible region. The vacuum ultraviolet spectrum shows various diffuse bands superimposed on continua. The ultraviolet absorption coefficients were developed from measurements by Inn et al.^{31/} These measurements could not be extended by him beyond 0.175 μ due to equipment limitations on determining small k values. A carbon dioxide content of 0.03% by volume was assumed at all altitudes. Estimates of absorption coefficients for various infrared wavelengths can be made from the 50 cm⁻¹ bandpass table of Stull et al.^{32/}

Ozone is an important factor for removing solar and skylight radiation in the 2200 to 2900Å wavelength range. It also produces significant absorption in the vacuum ultraviolet and diffuse bands in the regions 2200 to 3740Å, 5500 to 6100Å, and 7000 to 10,000Å.^{33/} The ozone absorption coefficients, k , are based on Tanaka et al.^{34/} and Vigroux.^{35/} An estimate of k for the 9.6 μ vibration-rotation band based on Herzberg's^{36/} collection is 0.5 cm⁻¹, which seems consistent with data on infrared radiation from the sky. Other ozone vibration bands are less intense and less accessible. The ozone profile used appears in Ref. 4 for 0 to 50 kilometers and has been extended to 85 kilometers altitude by adapting Brinkmann's^{37/} distribution. The ozone profile will show variation at all altitudes with the greatest variation near ground level as notable in comparing Refs. 4 and 22 below 5 kilometers.

Water vapor is a particularly troublesome problem in vacuum ultraviolet, infrared, and microwave regions. Many diffuse bands, isolated bands, and Rydberg series are seen in the 750 to 1400Å range. A continuous absorption in the range 1450 to 1860Å, with maximum k for 124 cm⁻¹ at 1655Å,^{38/} is not the most intense vacuum ultraviolet feature. The infrared spectrum shows very strong vibration-rotation features at 6.27 μ and 2.66 μ where less than 0.01 precipitable centimeters of water will lead to significant attenuation in the more intense portions of the bands. Wyatt, Stull, and Plass^{39/} have calculated infrared transmittances for water vapor with a 100 cm⁻¹ bandpass and various amounts of water using a quasi-random assignment of weak

lines within the bands. There are many other vibration-rotation bands of water vapor in the 0.57μ to 3.2μ region. The water vapor spectrum also includes many features between 10 and 13.5μ which can be problems on long paths.

The main problem with developing a water model is the large variation in mixing ratio at all altitudes. The water vapor level was taken as either ~ 0.3 gm/kg (0.04% by volume) or ~ 30 gm/kg (4% by volume), thus not quite approaching the dry condition 0.01 gm/kg near 15 kilometers suggested for mean midlatitude mixing ratio but including the upper range of surface mixing ratios.

The total absorption coefficient for gas phase species has been obtained by summation at various wavelengths. Figure 23 shows the wide variation with wavelength in the ultraviolet range (0.15 to 0.38μ). The effects of water vapor concentration are quite pronounced at 0.18μ and noticeable at 0.16 and 0.17μ in the ultraviolet. The change from a total density dependent curve to an ozone density profile as the wavelength reaches 0.245μ is apparent.

The numerical results from the beam power analysis showed that a restricted sight length might be useful to obtain significant signal levels from the upper atmosphere. Two narrow bands near 0.15μ and 0.245μ might be suitable for instrumentation above the atmosphere. The absorption coefficients are shown in Figure 23. There it is seen that the lower atmosphere is essentially opaque in these spectral regions.

Figure 24 shows absorption in the visible wavelength range by ozone, the principal absorber there. A few wavelengths in the infrared have been used for preparing Figure 25. The 4.26μ curve is illustrative of CO_2 bands. The effect of ozone in the 9 to 10μ range is illustrated in the 9.5μ curve. The prevalence and variation of water effects in the infrared are shown by the number of wavelengths at which the variation in water vapor causes major variation in the total absorption coefficient.

b. Aerosol absorption coefficients: The aerosol models discussed in the section on scattering can also show absorption if the component particles can absorb. The clear-day aerosol was assumed to be nonabsorptive. However, since water can absorb in liquid form as well as in vapor form in much of the infrared, the haze and cloud models presented here show a greater absorption than the clear day aerosol for wavelengths greater than 2μ . At 9.5μ the curve in Figure 25 is adequate for clear-day aerosol, while Figure 26 illustrates the slight changes necessary below 9 kilometers for the haze model (where the ozone is as important as the total water content for low mixing ratios and the water effects are predominant for higher mixing ratios). Figure 27 shows the effect of the cloud model with the great absorption capability of the large droplets.

3. Emission Mechanisms

Radiation emitted from atmospheric constituents may be of either resonant or black body origin. The gaseous state does not exhibit normal black body radiation but the ambient temperature does affect the population of excited states and thus the resonant emission. However, there are also nonthermal methods of populating the radiating states such as photodissociation, collisional excitation, and similar mechanisms. The emission mechanisms of atmospheric importance include both gray body (emissivity less than 1) and resonance mechanisms. A major problem in the use of thermally excited resonance radiation as a source is due to competing absorption by other molecules (both of the same species in appropriate energy states and other species with overlapping bands) located between the emitter and the detector. This difficulty is also found in nonthermal radiation when the source is of significant optical thickness.

The monatomic gases of most interest in the possible application of cross-beam correlation to atmospheric studies are the airflow emitters O, N, Na, Ca⁺, K, H, Li, and He. In addition, three band systems of O₂, one band system of N₂⁺, and the vibrational spectrum of the OH radical are known in airglow. All of these airglow emitters result from nonthermal excitation and are generally strong at altitudes near 100 kilometers. The emission strengths are fairly low, but a study of specific emitters such as Wolff's⁷ study of OI 0.5577 μ airglow is possible.

Ozone also shows emission in the 9.6 μ band due to various exciting mechanisms which seem important in the stratosphere. Figure 28 shows the emission in the atmosphere in the 9.5 μ region. This figure was obtained by assuming that water vapor has the same relative population of emitting molecules as ozone.

Gray body thermal radiation, which has an intensity equal to a wavelength-dependent emissivity times the black body intensity for the same temperature, is a reasonable approximation to the infrared behavior of absorbing aerosols. The major problem with clouds and heavy hazes results because they both absorb and re-emit infrared radiation. For thick cloud cover, where the absorptive optical thickness exceeds unity, the radiation from the cloud is proportional to that from a black body at the mean cloud temperature regardless of whether the cloud is backed by a warm body or empty space.

Except for the cloud emission, which has a temperature dependence that tends to favor wavelengths longer than 10 μ and has spotty altitude and breadth characteristics, the only emitters of interest to atmospheric cross-beam exploration are better used as tracers in and near the volume being studied than as sources beyond the volume of interest.

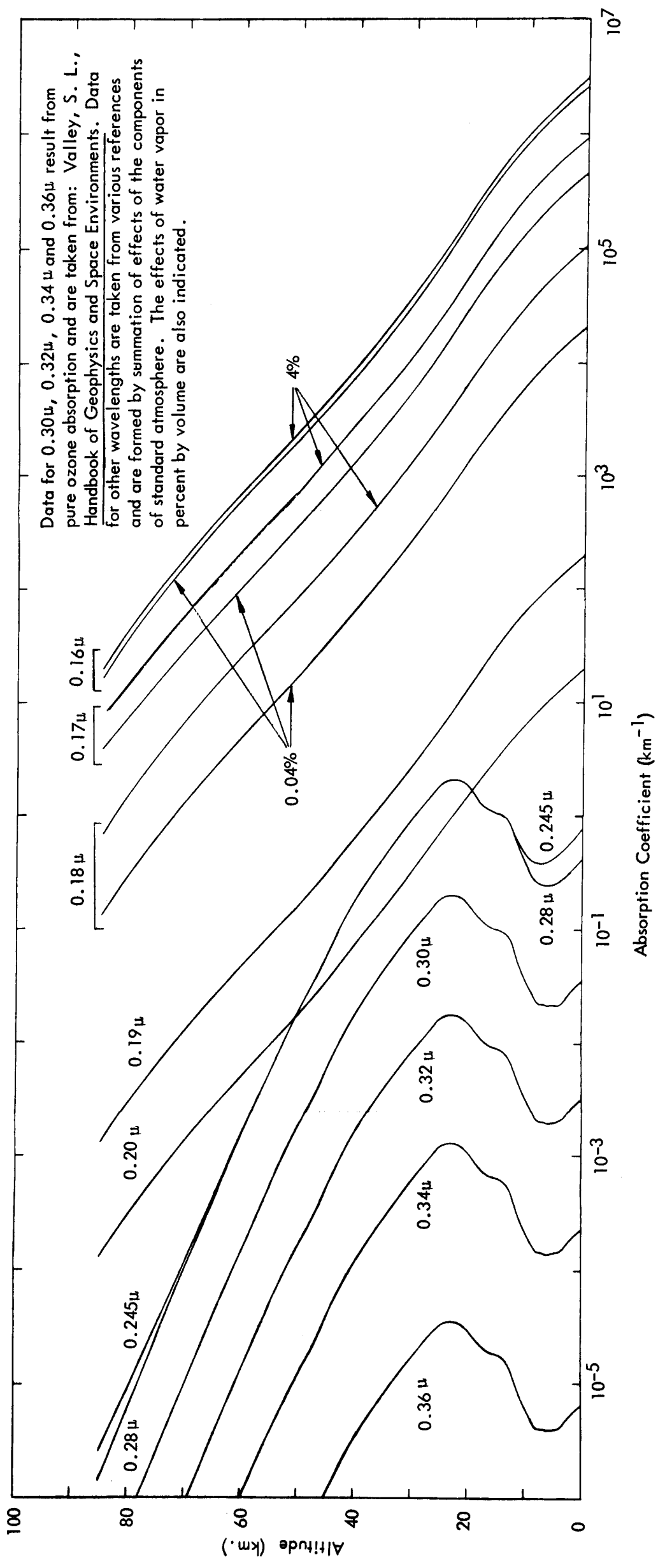


Figure 23 - Absorption Coefficient vs. Altitude for Ultraviolet Wavelengths

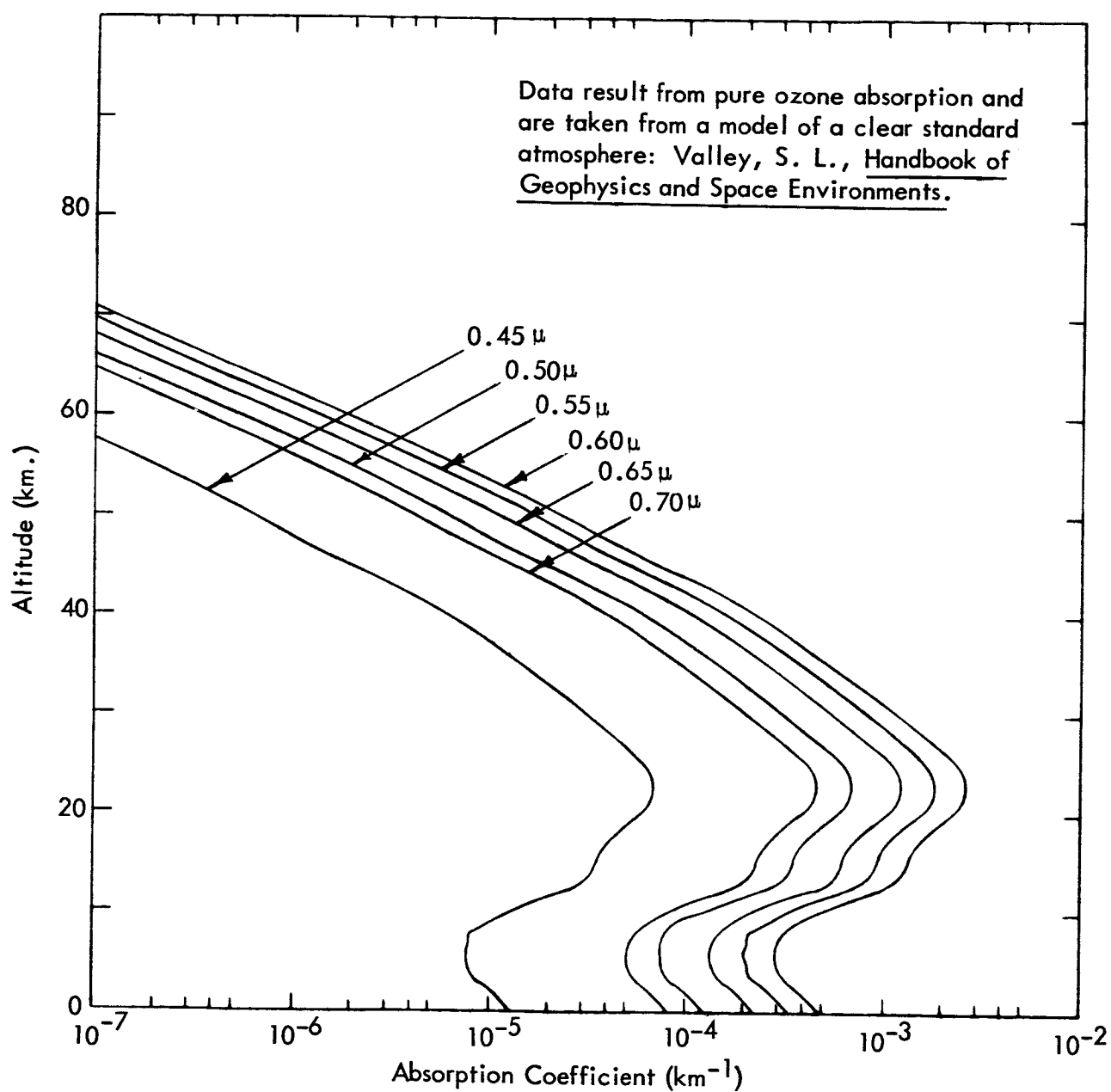


Figure 24 - Absorption Coefficient vs. Altitude for Visible Wavelengths

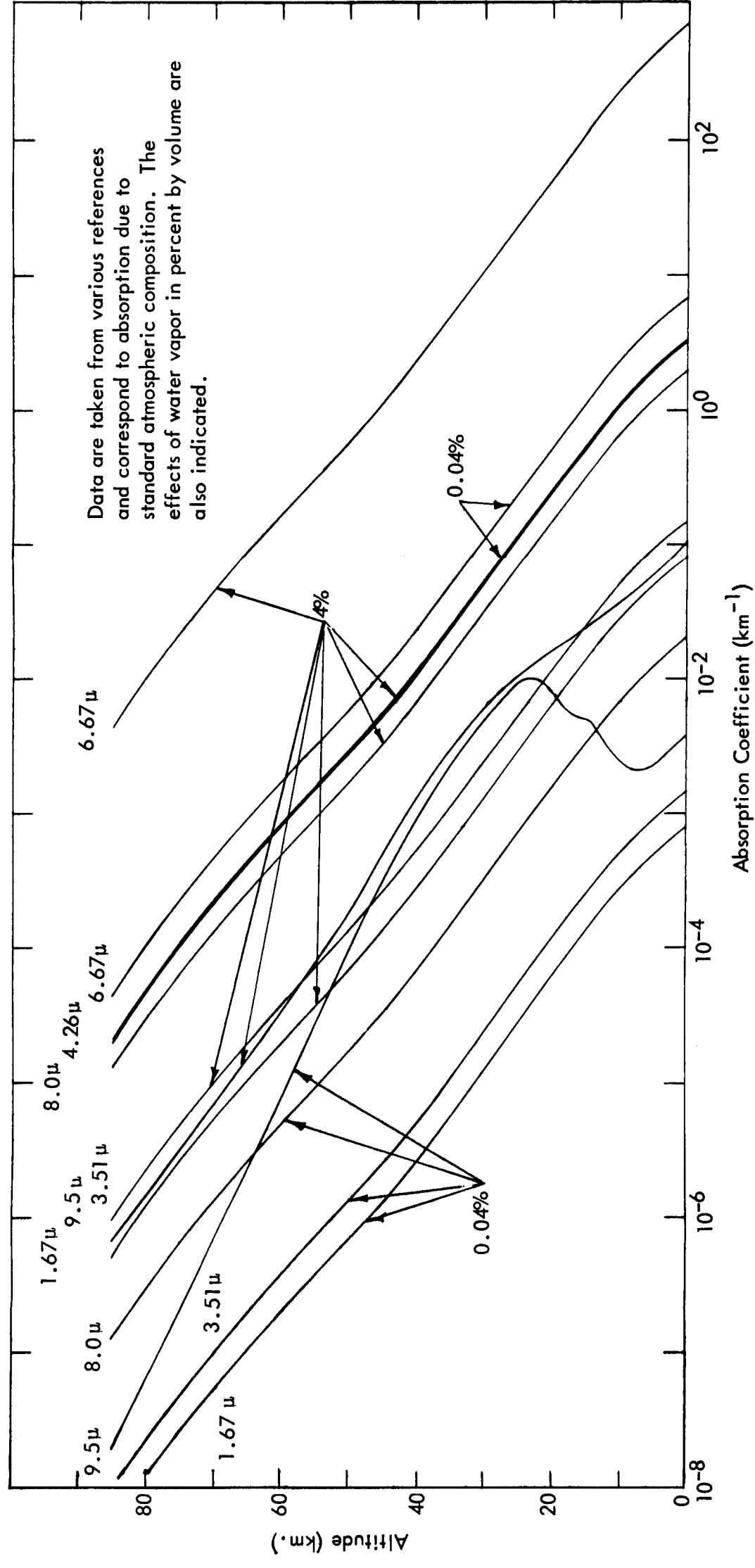


Figure 25 - Absorption Coefficient vs. Altitude for Infrared Wavelengths

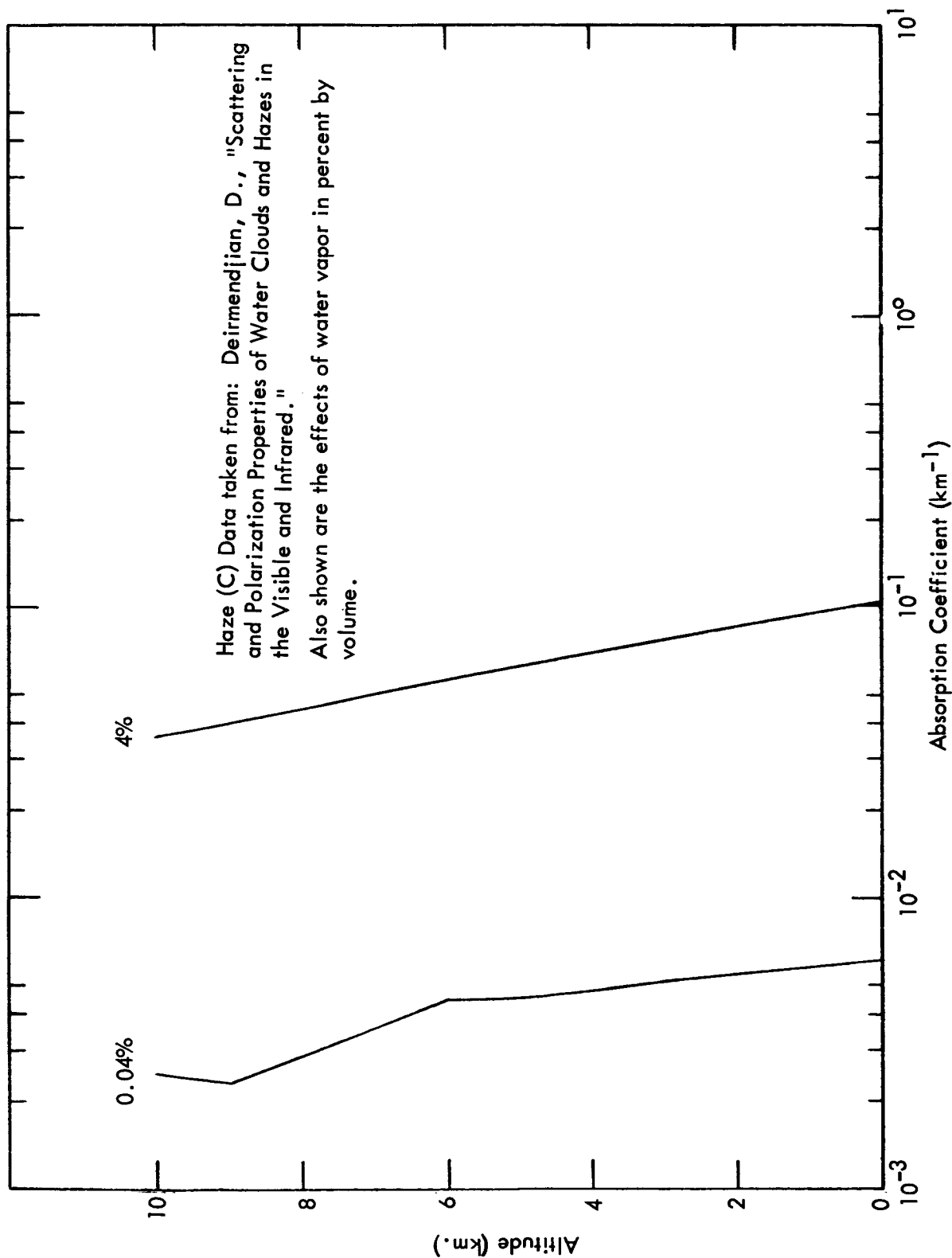


Figure 26 - Haze Model Absorption Coefficient vs. Altitude for Wavelength of 9.5 μ

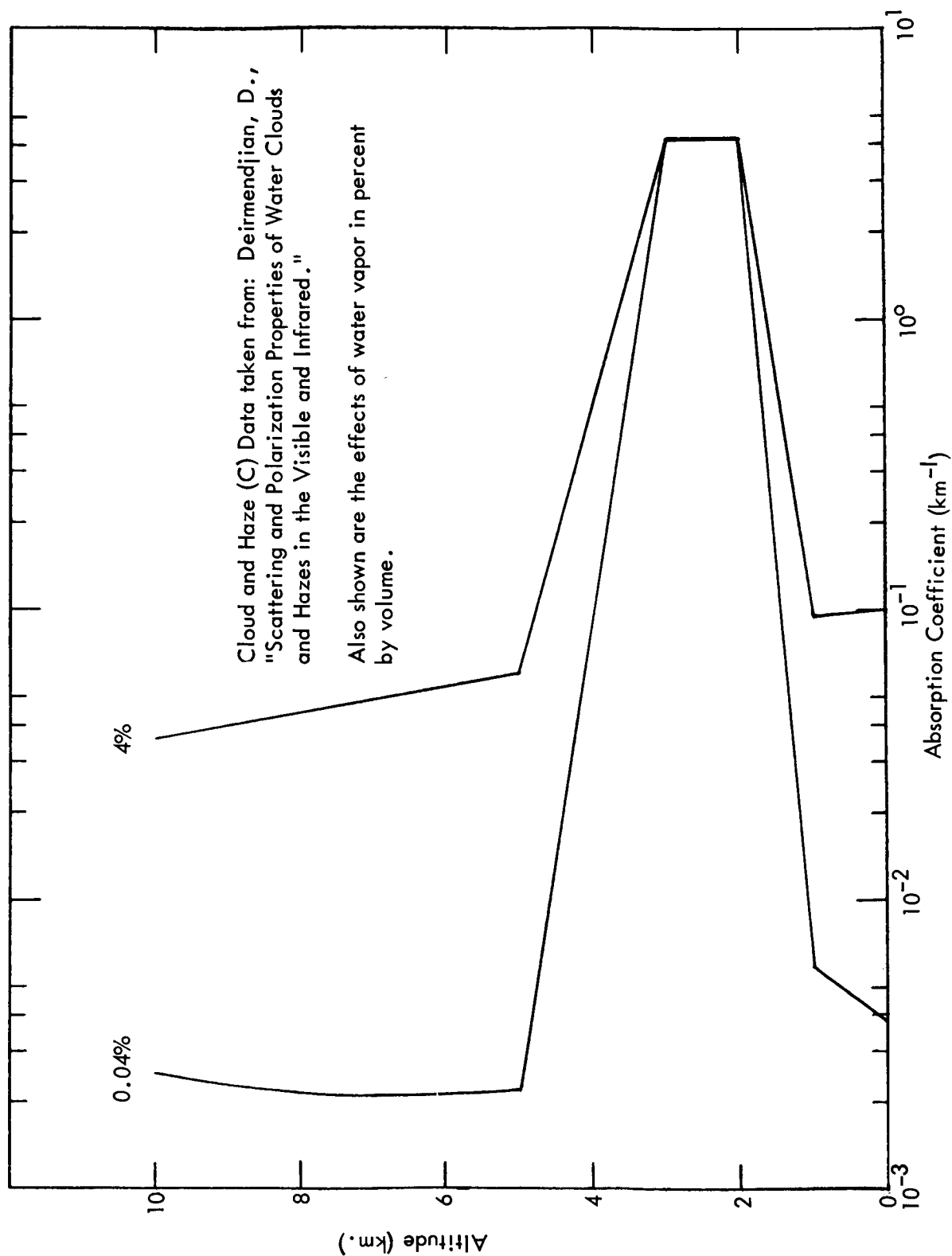


Figure 27 - Cloud Model Absorption Coefficient vs. Altitude for a Wavelength of 9.5 μ

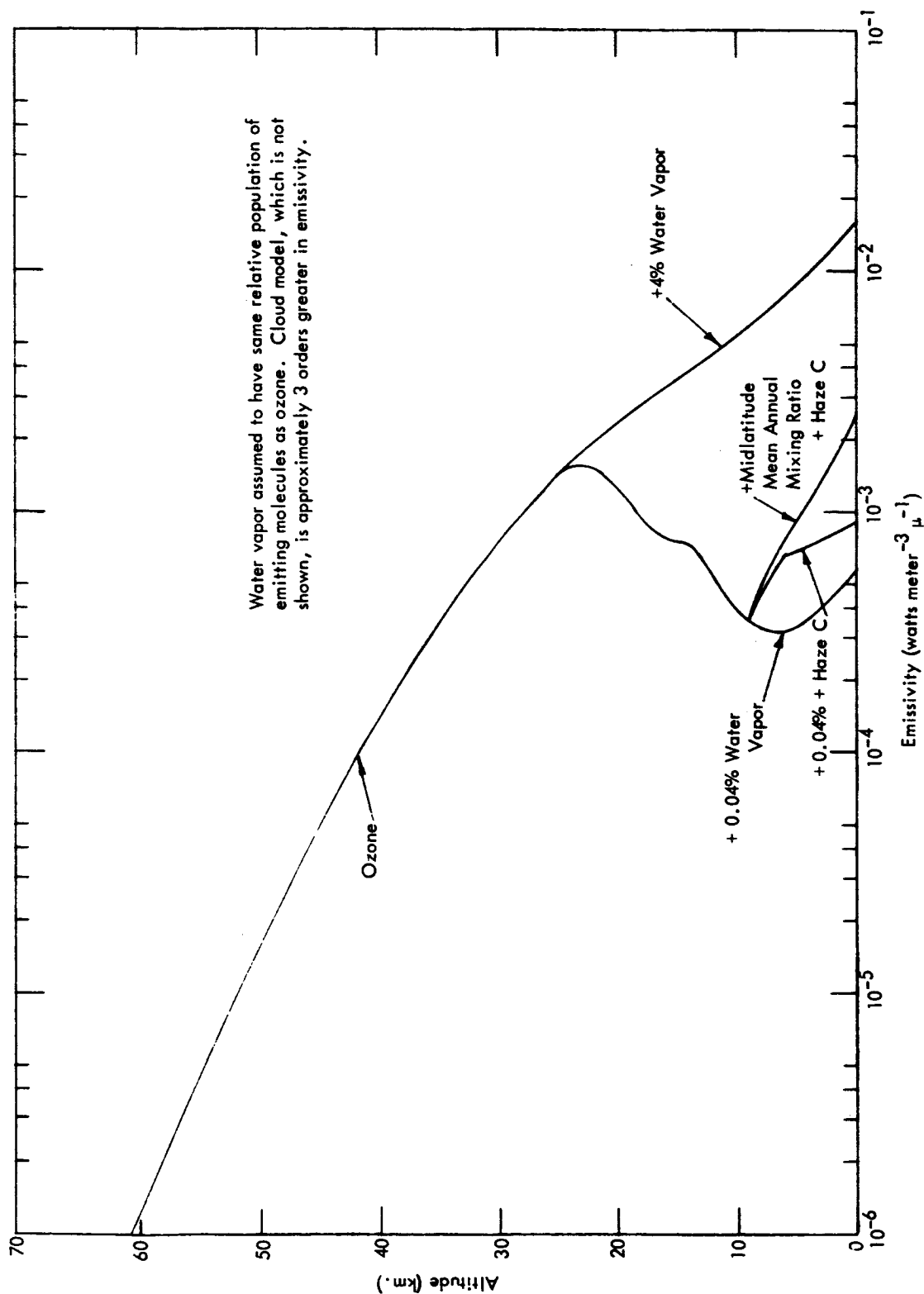


Figure 28 - Emissivity vs. Altitude for a Wavelength of 9.5 μ and Varying Atmospheric Conditions

C. Radiation Sources for Atmospheric Cross-Beam Experiments

The atmospheric and nonatmospheric sources which cover large solid angles as viewed from the earth's surface, from aircraft, or from satellites are all related to the heat balance of the earth. For ultraviolet, visible, and near infrared portions of the spectrum the most obvious source is solar radiation scattered from atmospheric molecules and diffusely reflected from surfaces - clouds, water bodies, vegetated soils, cultural features. The infrared spectrum is a difficult area for finding suitable extended sources because of the vibration-rotation bands of H_2O , CO_2 , O_3 and the pure rotational spectrum of H_2O . Certain specialized atmospheric emissions, such as airglow and aurora, can be used as tracer related sources. Both general extended sources and tracer related sources are discussed in this section.

1. General Extended Sources

General extended sources include skylight (as complicated by Mie scattering from aerosols and diffuse transmittance through clouds), reflected light from various surfaces, and near black body emission from the earth's surface and from clouds. These all show variations in spectral distribution, fluctuations in intensity, and variation of mean intensity with choice of viewing angle. A portion of this nonuniformity is due to meteorological changes. However, variations are also due to other mechanisms, such as the decay of total molecular density with increasing altitude and the variation of soil and cultural conditions on the earth's surface. Natural extended sources will exhibit fluctuations which need to be carefully evaluated in the data reduction of cross-beam results.

a. Skylight: Natural skylight has variable properties depending on the altitude from which viewed, the solar zenith angle, the viewing direction, the aerosol content of the atmosphere, and the albedo of the underlying surface. This radiation is produced by the combined action of Rayleigh and aerosol scattering, molecular absorption, and surface reflectance of sunlight. The absorption by ozone in the ultraviolet (particularly in the Hartley bands) is the primary mechanism competing with scattering in the redistribution of solar energy into skylight. The λ^{-4} dependence of Rayleigh scattering and the small λ dependence of aerosol scattering lead to a wide variation in spectral distribution of skylight within the visible range.

Spectral characteristics of daylight sky have been measured from ground based detectors located up to 1,400 meters above mean sea level.

Winch et al.^{40/} report that the intensity of skylight is greater at 1,400 meters than at lower elevations for the 0.3μ to 0.4μ region. The correlated color temperature of skylight (measurements made with direct solar rays excluded from the spectrometer) has been observed to vary from near 4600°K to over 40000°K .^{41/} At a given ground station, the skylight energy at 0.35μ ranges from about half to at least three times that at 0.7μ which is only part of the reason for the change in correlated color temperature. The most common variations noted in studies in the U.S., Canada, and Great Britain are a variation from yellow to blue (presence or absence of direct sunlight in the view of the spectrometer) and a change from green to pink, which seems to correlate with haze.^{42/} Due to the importance of aerosol scattering in providing sunlight intensity, the highest correlated color temperatures are also associated with the lowest of the clear sky radiances. Henderson and Hodgkiss^{41/} found that with approximately a 6° acceptance angle and a fixed monochromator setting that a random fluctuation of $\pm 10\%$ about mean intensity was experienced in 10 minute observations. Sastri and Das^{43/} report that a dry dust aerosol, blown from a nearby desert, is also able to shift the color balance of skylight.

Jones and Condit^{44/} tabulated skylight illuminances characteristic of different weather conditions. For clear sky conditions, the maximum tabulated illuminances range from 364 foot-lamberts (for sun at horizon) to 7,000 foot-lamberts with the sun 70° from zenith. A factor of 30 between the greatest and least illuminance is also encountered for clear sky conditions and a given solar elevation. For hazy conditions maximum skylight illuminance has been reported as high as 200,000 foot-lamberts in the forward scattered aureole about the sun and a factor of 50 lower in a viewing direction 90° away from the sun. General cloud cover tends to reduce illuminance from the hazy sky values and to switch the maximum intensity from the horizon (characteristic of clear skies) to the zenith (overcast conditions). The diffuse transmittance through moderate cloud cover still provides greater visual illuminance than perfectly clear sky with direct sunlight removed.

A more severe change than that caused by clouds is due to solar eclipse, sunset, or sunrise. During a total eclipse, the zenith skylight drops by 3.5 orders of magnitude at 0.52μ as contrasted to nearly seven orders of magnitude for change from full daylight to night. During eclipse the intensity and spectral distribution are comparable with those observed for solar depression angles of about 5° .^{45/} In both eclipse and twilight there is a spectral shift toward the blue.

Variation in sky brightness as a function of detector altitude has been evaluated from aircraft, balloon, and rocket and estimated from theory at higher altitudes. Under clear sky conditions, aircraft measure-

ments show look-angle variations of approximately 400 to 5,000 foot-lamberts at 1.52 kilometers and 200 to 4,000 foot-lamberts at 6.1 kilometers.^{46/} Recent sounding rocket data^{47/} indicate that the reduction of skylight illumination with altitude can be predicted from a combination of Rayleigh scattering and ozone absorption. These upper atmosphere experimental results are applicable up to 110 kilometers altitude.

In addition to the Rayleigh scattered portion of skylight, there is a significant contribution from aerosols. This contribution is difficult to evaluate, since it does not show a regular variation with altitude. Studies of solar attenuation, searchlight scattering and skylight intensity variation demonstrate that the aerosols are stratified. Such stratification has been determined to at least 30 kilometers altitude.^{48/} Although the solar elevation angle changes the air mass through which Rayleigh scattering takes place, the change in aerosol scattering due to solar elevation is not easy to formulate because of the variation in the aerosol density throughout the atmosphere. Even in the near infrared portion of the spectrum, where water vapor bands are a problem, distinct stratification of aerosols is still measurable.^{49/}

Daytime skylight thus provides a highly variable source. The fall-off of number density of scatterers will reduce skylight intensity at aircraft altitudes. At any particular time, the intensity of the brightest part of the sky is one to two orders of magnitude larger than the least bright parts of the sky center "uniform" aerosol coverage. Aerosol coverage variations change not only the photometric intensity, but also the spectral distribution of the skylight. An order of magnitude change of the ratio of near ultraviolet to near infrared intensity indicates a possible change in required signal if broad band detectors and wavelength dependent tracers are used. A four order of magnitude change in photometric brightness for general daylight sky shows the need for detectors with a wide useful range of signal received or for variable apertures in the detection system. The short term intensity variation noted may be due to multiple systems of turbulence which would be of interest or it may be a problem due to aerosol stratification.

b. Reflected sunlight: For views toward the earth, the problem of source definition becomes more complex. Not only must the albedo of the earth's surface for the specific features viewed and specific angle between surface and viewing system be considered, but a measured change of albedo with solar elevation must also be considered. In addition, the atmospheric scattering will contribute to the overall signal detected from aircraft and satellites.

Coulson^{50/} has reported the reflectance as a function of solar angle, detector angle, and selected wavelengths for several soil types.

Also presented are calculations showing the relative importance of Rayleigh scattering, aerosol scattering and reflected signal as viewed from space. For fixed detector angles and a wavelength of 0.643μ , Coulson reports that the reflectance of sand varies by a factor of three as the source position varied from overhead to 78.5° zenith angle. Airborne studies of albedo^{51,52/} using broadband instruments aboard a light plane and ground clearances near 300 meters have measured average surface albedoes from 9.5% to 69.4% over farmland at various times of the year, and from 2% to 75% over lakes depending on ice cover. Wide variations in average albedo also occur due to land use and snow cover in a given area. The ocean luminance has been reported to increase almost 300% in change of observation altitude from sea level to 6.1 kilometers.^{53/} Reflectance from deep water runs from 1.3% to 103%^{53/} depending on angles of sun and photometer relative to the surface.

The spectral distribution will depend not only on the spectral character of the reflectance from the surfaces viewed, but also on the loss of reflected signal by scattering and absorption, the relative importance of Rayleigh scattering and aerosol scattering, the chance occurrence of specular reflection into the detector, and cloud obscuration of the surface. The intensity will also be variable even for specified photometer acceptance limits, due to transition from open water (3% reflectance) to cropland (10% to 17% reflectance) to desert (24% reflectance) in summer flights.^{52/} Snow and ice cover may further increase reflectance values to $\sim 90\%$.

In a case where atmospheric scattering feeds 2.1×10^{-3} watts $\text{cm}^{-2} \text{sr}^{-1}$ into an orbital detector with bandpass 0.4 to 0.7μ and the atmospheric transmission is 70%, the total signal over open water will approach 2.3×10^{-3} watts $\text{cm}^{-2} \text{sr}^{-1}$ while that over deep snow will be near 9×10^{-3} watts $\text{cm}^{-2} \text{sr}^{-1}$. These variations due to background should be considered in data processing since the signal modulation due to meteorological effects will generally be much smaller, and the effective source distribution is highly variable.

The use of reflected sunlight by aircraft and satellite mounted detectors will also encounter variable intensity. Part of this variation will be due to the underlying surface features, part to the look angle (due to changes in reflectance and in atmospheric scattering), part to the solar elevation (through both atmospheric scattering and surface reflectance variation), and part due to aerosol changes of atmospheric transmittance. The situation is somewhat variable with the wavelength band chosen. Surface reflectance can also be highly variable with wavelength when narrow bandpass systems are used. The problems then become: what portion of the total source is surface reflectance and what is atmospheric when clouds do not interfere; how much does cloud cover distort the signal, and is the effective source position beyond the feature to be studied? The

daytime variability of total signal encountered here should not be as great as for ground-based detectors, since cloud cover will change the effective source height but thick clouds tend to be good diffuse reflectors of sunlight.

c. Thermal radiation: For wavelengths longer than 3μ , the radiance of black body sources at temperatures comparable to normal surface temperatures becomes more important than scattered sunlight. In the infrared spectral region the emission from water vapor, CO_2 and O_3 and the effect of absorption-emission balance leads to interesting problems and possibilities. There are windows in the $3\text{--}4\mu$ region and $8\text{--}12\mu$ region that could be of interest, along with the possibility of tracer related studies in the wings of the molecular band systems. Water vapor and carbon dioxide have only minor absorption in the 8 to 12μ window, but a significant ozone band does occur at 9.6μ . The tendency of the ozone distribution to be concentrated in the 15 to 30 kilometers altitude range means that this feature need not interfere with aircraft observations in this window.

Infrared reflectance spectra of certain rocks indicate that departure from black body emissivity in the $8\text{--}12\mu$ window should be expected. Hovis and Callahan^{54/} report reflectance values within the $8\text{--}12\mu$ window ranging from approximately 5 to 30% for large samples of silicates. In the 8 to 9.5μ region the reflectance of beach sand has been reported^{55/} to exceed 30%. Soil reflectances are often in the 5 to 10% range through the $8\text{--}12\mu$ window.^{55/} Thus the average surface emissivities in the $8\text{--}12\mu$ window can run from near 0.80 to 0.99 depending on surface features.

Further complications arise from the presence of water droplets in the atmosphere. Emission spectra of the atmosphere^{56/} at various zenith angles indicate that the wings of the water-vapor line system will contribute signals in the 8 to 12μ window over long paths. Carlon,^{26/} in an attempt to explain large fluctuations in 10μ signal transmission over a 400 meter path, succeeded in demonstrating that water droplet nucleation in unsaturated vapor strongly affects the 10μ transmission prior to producing a significant effect in the visible. The combination of surface differences in emissivity and temperature with variable atmospheric amounts of vapor, liquid, and solid water at temperatures ranging from 200 to 300°K , can cause variations in received "gray body" radiation in the 8 to 12μ band from about 5×10^{-4} to 4×10^{-3} watts cm^{-2} sr^{-1} . The lower values could result from thick cloud cover at 200°K absorbing radiation from the earth's surface to a greater extent than they re-emit while the higher value would occur with minimal precipitable water over a nonreflecting surface.

Although thermal radiation should be useful as a source regardless of solar position relative to radiating surface, aerosol, or gas, the problem of transmission through the atmosphere still exists. The absorption-

reradiation features within clouds for infrared radiation and within various molecular band systems will affect the spectral region used. Since Mie theory has not been extended to multiple scattering, the scattering effects of clouds in the 3-4 μ and 8-12 μ regions are hard to evaluate, but the absorption is strong enough to limit useful signal transmission through such layers. The major problem with using other infrared regions is the rapid attenuation of an original signal through gas phase absorption-emission processes, thus tending to restrict usefulness of the bands to very short paths or paths free of the primary absorber. However, these short path regions may be valuable for applications where the distant variations would provide overpowering noise.

2. Tracer Related Sources

There are several known emitters that could be used for specific cross-beam studies. The major problems are 1) what sort of interference is encountered with other molecules and particulate matter; 2) is the optical density sufficiently great that absorption-emission equilibrium will limit the useful altitude ranges; and 3) is the variation in signal due to turbulence or population mechanisms sufficiently great to be useful? The types of specific tracers include those with a localized altitude range as well as some with a fairly constant mixing ratio over large altitude ranges, thus opening several regions to observation.

Even the use of ozone as a tracer will involve problems. The analysis procedures for determining ozone distribution over an infrared observatory^{57,58/} are designed to correct for water vapor, condensed water, and the absorption-emission balance through the ozone layer. Since ozone seems significant in the dynamics of the stratosphere^{57/}, techniques to reduce the importance of water vapor effects on the interpretation of the 9-10 μ spectral region should be developed. In observing the nighttime sky at various zenith angles, Bell et al.^{59/} obtained data that suggested strong interference by water vapor and CO₂ minor lines in the 9-10 μ region and a near obscuration of the ozone signals for large air mass paths. Although the ozone picture is very complex, ozone signal will provide about 7.8×10^{-5} watt cm⁻² sr⁻¹ in addition to the H₂O and CO₂ background for vertical viewing and will show a strong departure from secant scaling.

The apparently uniform mixing ratio of CO₂ would tend to make it an undesirable tracer. Similar problems would be encountered with the microwave spectrum of oxygen near 2.5 and 5 millimeters due to the large extent of the emitting region and the temperature effects on line width. However, when the excitation mechanism is not thermal (as in the O₂ bands in airglow) and/or the altitude range of significant density of the emitter is fairly localized (the atomic emission lines in airglow), the possibility

of applying cross-beam techniques to specific problems regarding the emission exists. Aside from ozone emission, the most likely areas are the airglow emitters. Although Wolff^{7/} has used cross-beam techniques to locate the height of the emitting area for OI 5577Å airglow, the problems with cloud obscuration, low intensity level, and the variability of intensity with time and geomagnetic latitude^{60/} must be carefully considered for any specific experiment utilizing airglow as a potential source.

Specific features of the water vapor spectrum may be useful as traces for studies on relatively short paths containing highly variable water vapor concentration. The variations of signal with change of state of the water would need to be studied more extensively than yet reported.^{25/} Experimental evaluation of portions of the water vapor pure rotational and vibrational spectra would be needed to estimate the usefulness of water vapor variability as a tracer.

D. Problems Related to Correlation Volume Definition

The cross-beam correlation experiments are designed to investigate behavior within volume elements of the system under study. The data processing is designed to seek a correlation of fluctuations in either extinction or emission processes. This correlation is assigned to a volume surrounding the minimum separation of the beams. If a pure emission or a pure absorption were the only process available in the portion of the electromagnetic spectrum chosen for the experiment, then assignment of the volume causing a signal would be relatively easy. The fields of view of the two detector systems could be determined geometrically, thus permitting a location of the volume in which minimum beam separation occurred. However, the atmospheric application of cross-beam techniques depends on scattering of radiation and encounters variable refractive indices. Existing models and experiments provide us with some insight into the effects of scattering in providing noise terms and the effects of refractive index variations on beam position and modulation.

Since there will be molecules and aerosols between the volume being examined and the detector, there will be scattering of extraneous radiation into the detector as well as loss of some of the desired radiation. For telescopes with small acceptance angles and the distances involved, a collimated source is impractical. Yet the fine collimation of the detector telescope will not prevent stray light from the 4π steradian, variable-radiance source being scattered into the field of view of the detector by the material between the correlation volume and the telescope.

Although there is no ready indication of the problems to be encountered by scattering from a large source into a well collimated detector, there are some papers which relate to this area. Using a fixed sample and fixed detector acceptance angle, Ivanov and Khairullina⁶¹ have demonstrated on a laboratory scale that increases of source angle produced an apparent increase in transmittance of a turbid medium due to scattering into the detector. Although their experiments did not extend to large source angles, they did demonstrate an increasing error in extinction measurements with enlarged source angles whether the medium was primarily absorptive or essentially a pure scatterer. Steward and Curcio⁶² have reported apparent increased transmittance as a function of increased detector field of view for fixed sources and paths up to 15 kilometers. A similar increase of transmittance should be expected with extended sources.

When the illuminating source consists of scattered radiation, e.g., skylight, the variation of scattering properties beyond the region under investigation can be considered source noise. Yet, additional noise will arise from scattering into the beam between the correlation volume and the detector. Similarly, some signal degradation will occur due to loss of radiation from the beam by scattering. The parameters of importance in evaluating the introduced noise are optical thickness, scattering indicatrices characterizing the path between the correlation volume and detector, sources feeding the scattering volume in terms of radiance and angular distribution, and the size of the acceptance cone for the detector. Knowledge of the optical thickness will permit an evaluation of signal loss and chance of noise developing. The indicatrix and effective noise source for a short segment of the accepted beam will determine the effectiveness of various portions of the source in providing noise. The acceptance cone will dictate how great a portion of the scattered radiation will stay in the beam. The problem then is not a measurement of extinction or transmittance, but an evaluation of noise arising from scattering into each detector field of view. The relation between signal loss and noise input between the correlation volume and the detector is of interest.

A sufficiently detailed model for use in evaluating the importance of scattering is difficult to formulate;* however, certain simplifications can be made. Use of the Rayleigh indicatrix will tend to overestimate the scattering noise if the detector is aimed overhead with overcast sky (the most intense portion is at the zenith with decreasing illumination at the sides). An aerosol indicatrix, with its limited backscatter and strong forward scatter at small angles, could be used in conjunction with a detector aimed at a particularly variable portion in an otherwise uniformly radiant sky. If the indicatrix is uniform in the entire volume from which

* Appendix III of this report presents a model which has been developed to simultaneously account for the principal mechanisms which affect power at the detector.

the noise could arise and if the possible noise source is identical for all points in the volume, then the problem is simplified. For a 2π source of uniform intensity and an albedo of zero on the ground, about half of the signal lost from the beam by outscattering is replaced by inscattered noise. It is possible to devise cases where the scattering of noise into the beam exceeds the loss of signal from the beam due to the intensity distribution of the radiation impinging on the scatterers. The noise contribution of various areas of the source (outside the geometric optics path defined by the collimator) can be estimated from the mean scattering indicatrix and the intensity distribution of the source, since the transmission of the original signal will give an estimate of optical thickness and the indicatrix will show the relative contribution from different portions of the source.

Changes in refractive index of the medium in which the radiation is traveling will cause at least two classes of problems. A progressive change of refractive index, such as can result from cooling of the air, can cause beam wander which will tend to limit the accuracy of triangulation procedures. Microinhomogeneities in refractive index can cause a modulation of total signal in addition to that resulting from the extinction or emission processes in the region of interest. Both of these effects have been observed in experiments with lasers. Observed beam bending on paths of several kilometers has been in the range of 10^{-4} to 10^{-3} radians,^{63,64/} while 5×10^{-5} radians has also been reported^{65/} for a path length of 354 meters. These figures indicate that the refractive errors can be comparable with the angular resolution suggested for useable altitude measurement from satellites.^{66/} However, the reduced atmospheric pressure above ground level may also reduce the beam wander. Since the atmospheric refractive index will normally be approximately 3×10^{-4} greater at sea level than in a vacuum, the beam wander measurements suggest either a large change due to dense aerosols with refractive indices of the particles near 1.3 affecting the average, or a multiplicity of refractive index gradients. The beam studies suggest that part of the modulation is due to local phase changes and much of it is due to small inhomogeneities moving through the path.^{64/} Thus refractive index variations must be considered from both triangulation and noise aspects.

The noise scattered into the beam will cause problems. Part of the noise can come from areas which feed both beams, thus giving a false signal, since the noise would not be completely removed by cross-correlation processing of the detector outputs. This cross-talk feature is difficult to estimate at the present time, but may be one of the problems involved in interpreting present experiments on wind velocity measurement.

E. Optical Collimation Systems

1. Purpose of Collimation

The simplest, idealized cross-beam configuration assumes that the power which arrives at the detector has traversed and/or arisen in a line path so that power variations are due exclusively to atmospheric variations along the line. In practice the electromagnetic power at the detector is controlled by an optical system which admits radiation from some finite viewing angles which may be sufficiently restrictive to constitute a "beam" of relatively small cross section. It is essential to the cross-beam technique that the measured power has arisen in and/or traversed a defined "beam"-like geometry. In the practical case the "beam" cross section replaces a position along the idealized line and an average over the cross section replaces the point value associated with the line.

2. Characteristics of Collimation Systems

The characteristics of collimation systems are often depicted (as they will be here) by rays outside the optical system which define geometric quantities such as "field of view." It must be recalled here that these rays have general validity only for an infinitesimal distance outside the entrance optical element since the optical system can see only that radiation which arrives at the entrance element. The extension of defining rays to large distances is legitimate if the medium is optically uniform or if the effects of nonuniformities are incorporated separately. In the present case the effects of nonuniformities are handled separately as described in the other sections of this report.

Some collimation systems are shown in Figure 29. The three definitive rays shown separate the space around the optical system into regions which are distinguished by the fraction of incident energy from them which is admitted to the detector. Prior to discussing the regions of admittance it is essential to recognize that the entrance ports in Figure 29 are not necessarily located in the instrument. They may be projections of a limiting aperture within the instrument and thus in effect be located some distance outside the instrument. The entrance ports are located outside the instrument in most telescope designs. Consequently, in defining regions of admittance, a distinction must be made between volumes which lie between the entrance pupil and entrance port and volumes which lie beyond the entrance port.

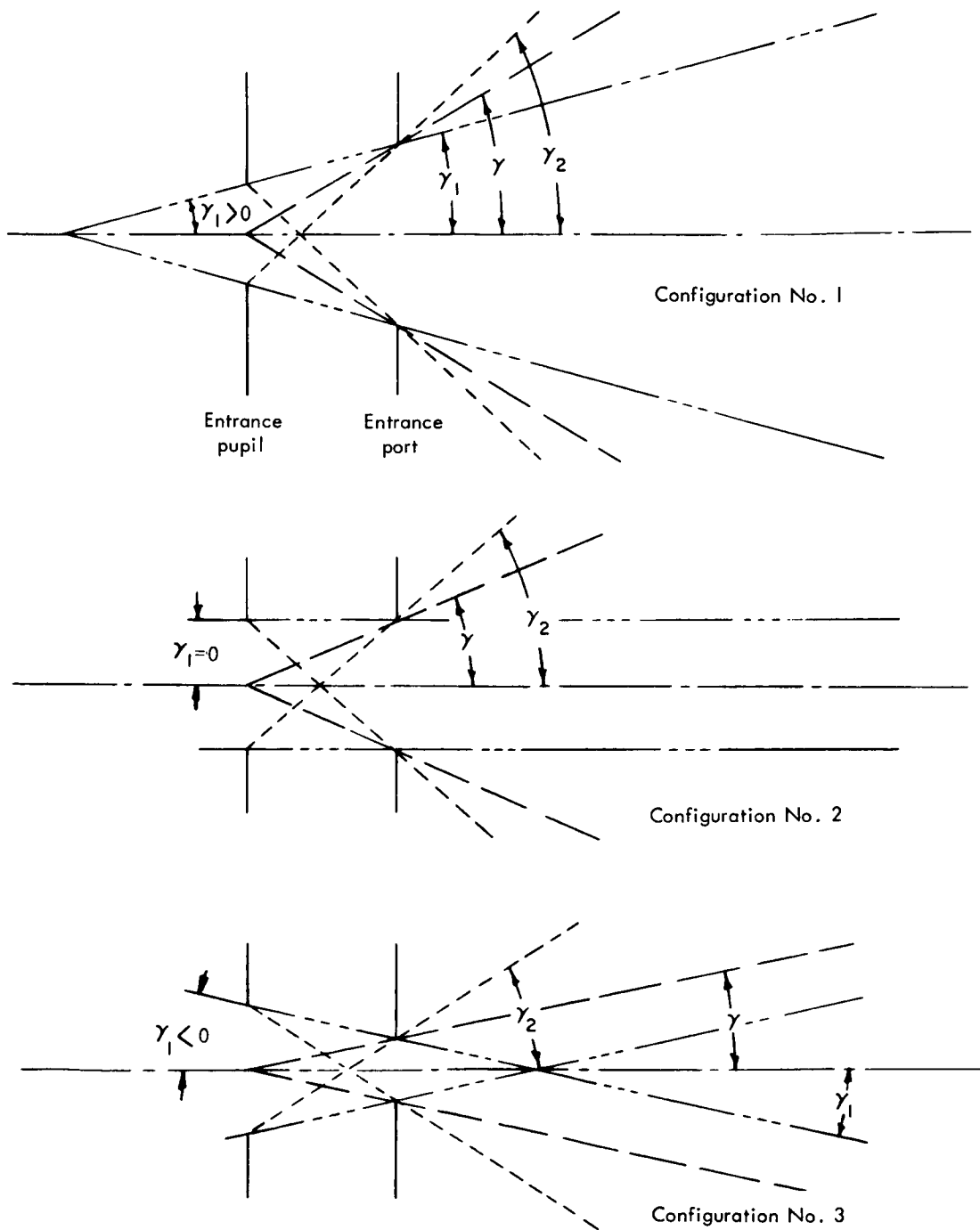


Figure 29 - Fields of View With Multiple Limiting Apertures

Configuration No. 1 in Figure 29 is conventional. Between the pupil and port there is 100% admittance for the region inside ray γ_2 . Outside γ_2 the admittance diminishes until it is 50% at ray γ . Outside ray γ , there is a further reduction in admittance until it reaches zero at ray γ_1 . Beyond the entrance port, ray γ continues defining the 50% admittance locations. However, the meanings attached to rays γ_1 and γ_2 are reversed. The 100% admittance region lies inside ray γ_1 while γ_2 indicates the extreme edge of the fractional admittance region. The telescope employed in atmospheric wind tests has the form of Configuration No. 1 with the effective entrance port located by projection at infinity. (This is the basis of the beam model used in the analysis reported here.)

Configuration No. 2 is a limiting case of No. 1 where the rays γ_1 are parallel to the optical axis. This configuration can be approached but not achieved for a telescope which is focused for great distances.

Configuration No. 3 is unusual in that radiation from distant regions is attenuated by the optical system. In the region bounded by the γ_2 and γ_1 rays there is 100% admittance. Beyond the intersection of γ_1 rays and on the optical axis the percent admittance diminishes with associated reductions for off axis regions.

If we think of the rays in Figure 29 defining a beam, it is apparent that the edge of the beam is characterized by gradual roll-off rather than an abrupt cutoff. It is conventional, however, to treat the 50% admittance ray as defining the field of view.

The above characteristics are generally achieved by multiple limiting apertures in conjunction with refractive lenses or special reflective surfaces. Fields of view depend on the location and size of limiting apertures. For systems which are focused at great distance, the minimum fields are limited to values on the order $1/2$ arc minute half angle. A more typical value is $1/2^\circ$.

The percent admission values shown in Figure 29 are idealized since some losses occur at and within the optical elements. These losses are due primarily to reflection and absorption. In the ultraviolet and visible spectra the losses may be in the vicinity of 5%. However, for this value coated elements would be required and quartz or fused silica transmission elements would be required below 0.25μ . In the infrared at wavelengths $>2 \mu$, transmission losses are a problem so that reflective elements are generally employed with the exception of an entrance element which must be made of a nonsilicate glass for 50 to 90% transmission.

Chromatic aberration may have a slight but probably insignificant effect on system optics over the spectral span likely to be employed.

In some cases the detector may not cover the entire image plane in the optical system. When the system is focused, the detector will "see" a beam with essentially the same angular characteristics as the entire optical system but the entrance port (for the detector) will be reduced in the same ratio as detector area/image plane area. When the system is defocused, the detector will see a beam with the above reduced effective port area and a more extensive roll-off region at its boundaries.

APPENDIX III

ANALYSIS OF POWER FLUCTUATIONS IN AN OPTICAL BEAM

A. Introduction

The cross-beam technique utilizes the covariance of received signal intensities from two intersecting (or nearly intersecting) optical beams to infer certain characteristics of the local fluid flow near the intersection. Paramount to the success of the technique is that this local fluid flow disturbs the local optical properties of the medium. The detected optical signal then contains power fluctuations due to the disturbance in question (as well as due to other causes).

The power in the optical beam, as it approaches the detector, is continually being modified due to several physical processes. These are scattering, both into and out of the beam, absorption, and emission. These fluctuations may (a) provide a source of beam power; (b) generate optical noise; (c) generate the optical signal of interest; and (d) tend to cause the loss, by attenuation, of a signal of interest. It is the purpose of this Appendix to develop usable mathematical expressions to be used in the study of these fluctuations.

In Section B the geometrical model of the optical beam utilized here is presented. Generally, one would not expect great differences in results of later sections if beams with different geometrical arrangements are used, except perhaps close to the optical telescope. The model used here was chosen for its simplicity plus its direct application to systems currently in use in field test operations by NASA and its contractors. Section C presents the mathematical functions used herein for the distribution functions for Rayleigh and Mie scattering.

Section D contains the logical development for the power scattered out of a unit thickness* element of the beam, with specific expressions given for Rayleigh and Mie scattering. Section E gives similar results for the power scattered into the beam. Also, several special types of power sources are considered explicitly, such as the point source, and finite and infinite extended plane sources. In both of these sections, single scattering only is considered. Multiple scattering is considered beyond the scope of

* Measured along the beam.

this work, and not important for clear air situations. For haze and cloud situations where multiple scattering does dominate, the cross-beam technique loses its attractiveness, as even a single scattering model can indicate.

Sections F and G consider the other two modes of power changes, absorption and emission, respectively.

The results of the previous sections are summarized somewhat in Section H where they are combined in the general beam model. The resulting differential equation is solved to give the power at any point along the beam in terms of the beam geometry and atmospheric properties. The solution is a generalization of the well known relation between the beam power and the integrated, generalized extinction coefficient.

The solution in Section H is, in effect, differentiated in Section I to obtain the change in detected beam power corresponding to various perturbations. These relations indicate how a change in any of several quantities (e.g., scattering coefficients, absorption coefficient, source power), effective over a portion of the beam length, modifies the received power at the optical detector.

B. Geometrics

The optical beam used in this study is explained by means of Figure 30. The entrance area is determined by radius of the entrance pupil (objective lens). The field of view is limited by the field stop.

The visibility of any point in the space in front of the objective depends on the lateral position of the point. Ideally, a point outside of the "field of view" is not seen at all; whereas a point within the "field of view" is seen perfectly in the sense that all light emanating from the point and falling on the objective is properly refracted and focused. In actuality, there is also an intermediate region within which a point is seen, but imperfectly.

Figure 30 shows the three general regions of visibility. The portion of space which is perfectly visible is within the cone labeled 100%, while the unseen region is outside the cone frustum labeled 0%. Rather than treating the intermediate region with mathematical precision, it is standard practice to define an idealized field of view by means of the 50% visible line. The approximation consists of assuming the region within this boundary is seen perfectly, while the remainder of the space

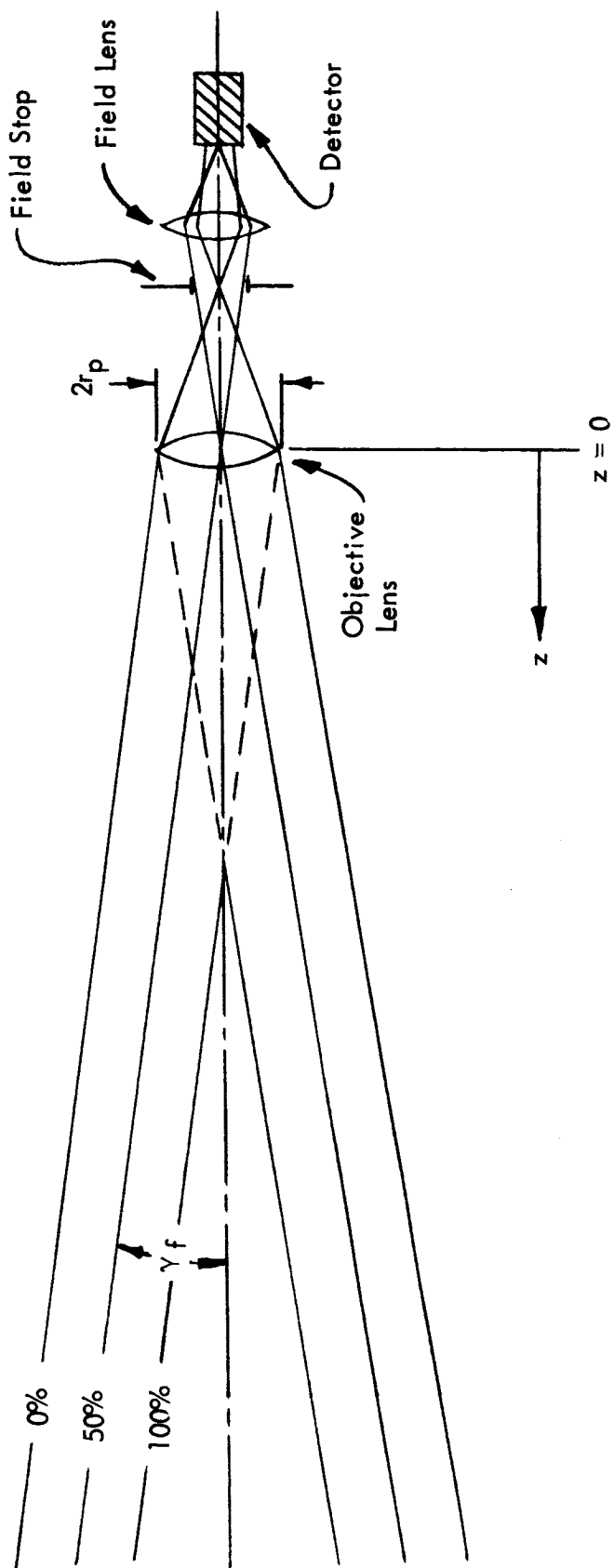


Figure 30 - Geometry of Optical Beam

is not seen. The assumption is expected to lead to inaccuracies only very close to the objective lens, and to have little if any effect well removed (say, 100 diameters) from this area.

We thus define the beam field of view to be the conical region of half angle, γ_f , with apex at the entrance pupil. The entrance pupil has the radius, r_p . The z-axis, in this Appendix, is aligned along the centerline of the beam, directed outward, with origin at the objective lens.

Figure 31 shows an element of volume, dv , in the beam. Its location is defined by the cylindrical coordinates, R , γ_v , z . It may also be located, for convenience, by the spherical coordinates ρ , ϕ_v , γ_v .

The solid angle subtended by the entrance pupil at dv may be obtained by integration over the entrance pupil area. However, that area is not oriented perpendicular, in general, to the vector along ρ . The solid angle subtended to a point on the beam axis is given by (see Figure 32)

$$\Gamma_c = \int_0^{2\pi} \int_0^{\tan^{-1} r_p/z} \sin \beta \, d\beta d\gamma_c \quad (\text{III-1})$$

For a point off the beam axis, such as the location of dv in Figure 31, we make the approximation

$$\Gamma_p = \Gamma_c \cos \phi_v \quad (\text{III-2})$$

In the above developments as well as in much of what follows it is necessary to make simplifying approximations. The philosophy followed is to use approximations that are valid for $z \gg r_p$ but which may be less accurate at small distances from the objective.

As a final preliminary step, we define the "power in the beam." Each volume element, dv , has energy passing through it in all directions. Of this amount, a portion is directed within the solid angle, Γ_p . That is, it is directed toward the entrance pupil. Thus, the power in the beam is the energy per second which passes through an element of volume within the field of view and which is directed toward the entrance pupil.

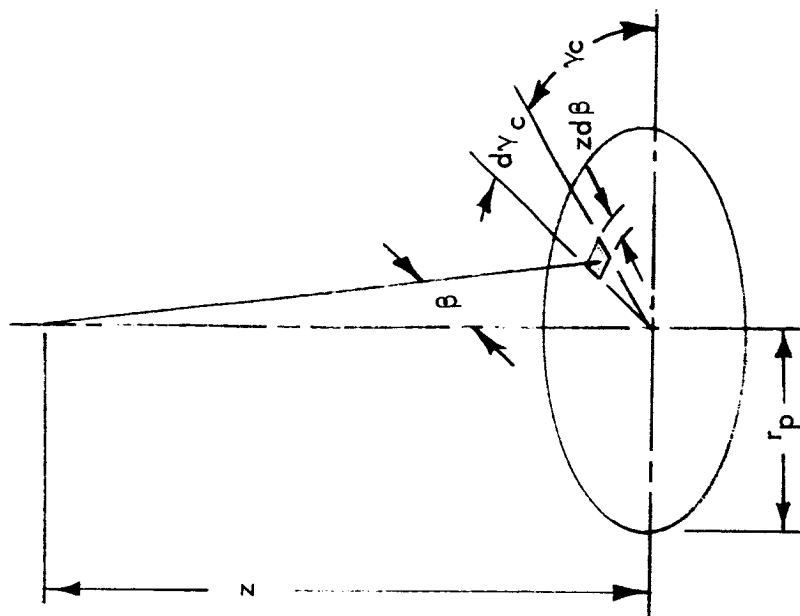
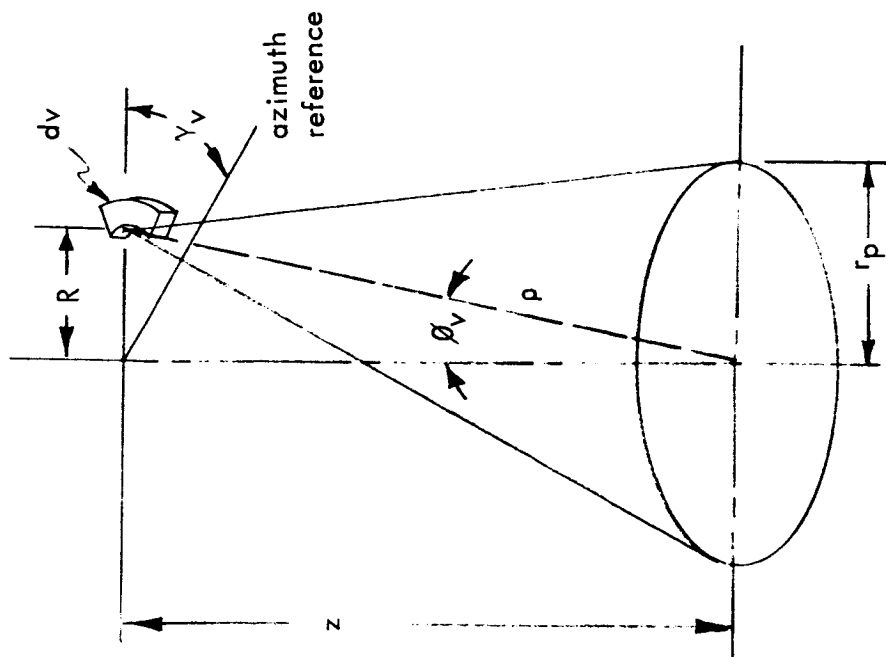


Figure 31 - Location of Element of Beam

Figure 32 - Details of Solid Angle

C. Rayleigh and Mie Scattering Distribution Functions

Radiation is scattered by small particles and aerosols. The two types of scattering usually considered are the Rayleigh and Mie types. The physical (atmospheric) aspects of these scattering modes are discussed elsewhere. Our purpose here is to present the mathematical models of the distribution functions.

The radiation incident on a small volume of scatterers is scattered in all directions. The normalized fraction of the incident radiation scattered in any specific direction is desired. The resultant distribution of intensity* versus direction is known to be dependent only on the polar angle, θ , measured from the direction of the incident radiation.

The Rayleigh scattering model leads to the distribution function

$$P(\theta) = 3/4(1 + \cos^2 \theta) \quad . \quad (III-3)$$

The factor, $3/4$, arises from normalization such that

$$\int_0^{2\pi} \int_0^\pi P(\theta) \sin \theta \, d\theta d\gamma = 4\pi \quad . \quad (III-4)$$

This provides an average of unity per steradian. It should be noted that the Rayleigh model is symmetric in that

$$P(\theta) = P(\pi - \theta) \quad , \quad (III-5)$$

that is, back scattering and forward scattering are equivalent.

The Mie scattering model, used for larger scatterers, tends to be highly directional, with forward scattering preferred. Deirmendjian^{11/} gives curves and tabulations for several wavelengths and polydispersed

* For a specific wavelength and aerosol or particle size distribution.

suspensions. In general, they may be categorized by the large peak in $P(\theta)$ at $\theta = 0$, attenuating to a value of one to five orders of magnitude less at $\theta = \pi/2$, and remaining relatively uniform, with small fluctuations between $\theta = \pi/2$ and $\theta = \pi$. The following approximation was therefore developed:

$$\left. \begin{aligned} P(\theta) &= p_0 e^{-s\theta}, \quad 0 \leq \theta < \pi/2 \\ P(\theta) &= p_0 e^{-s\pi/2}, \quad \pi/2 \leq \theta \leq \pi \end{aligned} \right\} \quad (\text{III-6})$$

where

$$p_0 = 2(s^2+1) / \left[1 + e^{-s\pi/2} (s^2 - s + 1) \right] \quad (\text{III-7})$$

by normalization.

Table XI gives typical values of the parameter πs for specific situations.

TABLE XI

MIE SCATTERING PARAMETER, πs

	<u>Cloud Model</u>	<u>Haze Model C</u>	<u>Clear Air</u>
Visible (0.5μ)	23	14	5
Infrared (10μ)	14	8.5	3

D. Scattering Out of the Beam

Let $E(z)$ be the total power in the beam at any distance, z , from the objective lens. The power is usually expressed in lumens or watts, with watts being used here. The intensity of the beam is given by E_{int} watts/area steradian. Both E and E_{int} are wavelength dependent, but that dependence will be suppressed here. E and E_{int} are related by

$$E(z) = \int E_{\text{int}} \Gamma_p dA \quad (\text{III-8})$$

where the solid angle, Γ_p , subtended by the entrance port or its equivalent is defined by (III-2), and the integral is over the cross section of the beam at z .

The scattering coefficient, k_s , is the fraction of the energy or power scattered in a unit length. It has units of length^{-1} . The power per unit area which is in the beam and incident on a differential volume of thickness unity and area dA , located at R, γ_v, z (see Figure 31), is given by

$$E_{\text{int}} \Gamma_p = E_{\text{int}} \cos \phi_v \int_0^{2\pi} \int_0^{\tan^{-1} r_p/z} \sin \beta d\beta d\gamma_c. \quad (\text{III-9})$$

Carrying out the integration, and approximating $\cos \phi_v$ with the first two terms in the power series expansion for R/z small yields

$$E_{\text{int}} \Gamma_p = E_{\text{int}} (2\pi) \left[1 - \frac{1}{2} (R/z)^2 \right] \left\{ 1 - \left[1 + (r_p/z)^2 \right]^{-\frac{1}{2}} \right\}. \quad (\text{III-10})$$

The total power which was in the beam and is scattered from a slab of unit thickness is thus

$$E_{\text{so}} = \int_0^{2\pi} \int_0^{z \tan \gamma_f} k_s E_{\text{int}} \Gamma_p R dR d\gamma_v \text{ watts}. \quad (\text{III-11})$$

Using (III-10) in (III-11) and assuming k_s and E_{int} are constant over the cross section, we obtain

$$E_{\text{so}} = 4\pi^2 k_s E_{\text{int}} \left\{ 1 - \left[1 + (r_p/z)^2 \right]^{-\frac{1}{2}} \right\} \left\{ \left(\frac{1}{2} \right) z^2 \tan^2 \gamma_f - (1/8) z^2 \tan^4 \gamma_f \right\}. \quad (\text{III-12})$$

Equation (III-12) gives the power scattered from a segment of the beam of unit thickness in the z -direction. This scattered power is written in terms of the input beam intensity, the scattering coefficient,

and factors relating to the beam geometry. The more familiar form of (III-12) occurs if (III-8) is used to replace E_{int} with E . Carrying out this step yields, simply,

$$E_{\text{so}} = k_s E \quad . \quad (\text{III-13})$$

Neither of Eqs. (III-13) or (III-14) is complete for our purposes. Both give the total power scattered from a part of the beam, but not all of that power is scattered out of the beam. That is, some of the power is scattered but remains within the beam and will still be seen by the optical detector.

We require, then, the fraction of the scattered power which is directed toward the objective lens -- that is, lies within the solid angle subtended by the objective lens. For an incident ray at an angle β_d with the vector ρ (see Figure 33), this ratio is

$$R = \frac{1}{4\pi} \int_{\Gamma} P(\theta) d\Gamma \quad , \quad (\text{III-14})$$

Γ being the solid angle subtended by the objective. The total power scattered but retained is then

$$E_{\text{sor}} = \int_0^{2\pi} \int_0^z \tan \gamma_f \left\{ k_s E_{\text{int}} \cos \phi_v \int_0^{2\pi} \int_0^{\tan^{-1} r_p/z} [R \sin \beta \, d\beta d\gamma_c] \right\} R dR d\gamma \quad , \quad (\text{III-15})$$

which is obtained by integrating over all possible incident angles, β , which define the power in the beam passing through dv , and then by integrating over all elements, dv , in a beam cross section.

Now, the ratio R is a complicated expression due to the complexity of the definition of the region of integration in terms of θ . To avoid this unnecessary complication, the following argument is put forth.

The power scattered but retained within the beam, E_{sor} , is of higher order in R/z than E_{so} , so it is sufficient to consider only the first order approximation for E_{sor} . To this end, we neglect the R -dependence of the fraction of power retained, and use that fraction

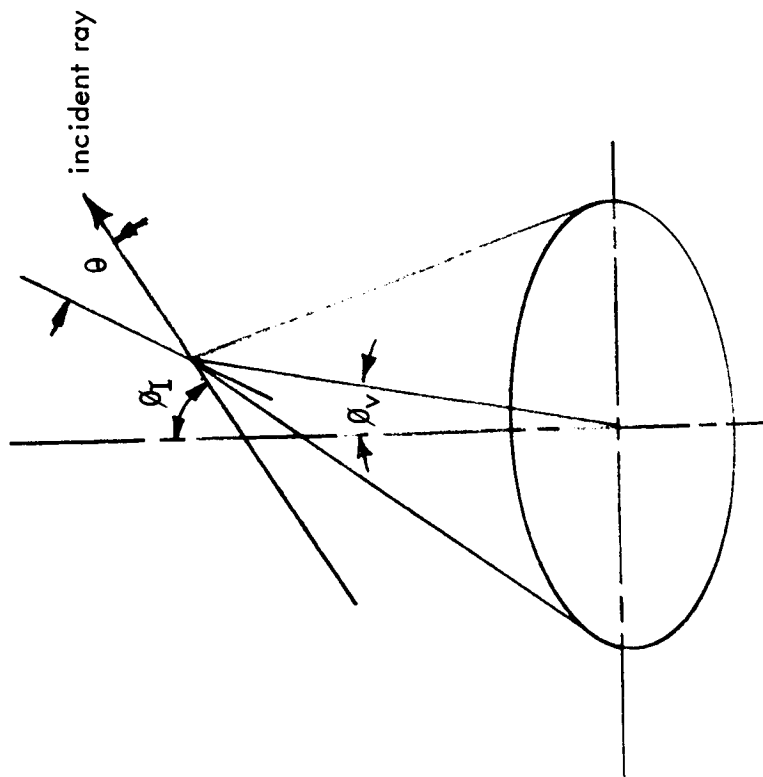


Figure 34 - Power Scattered Into Beam

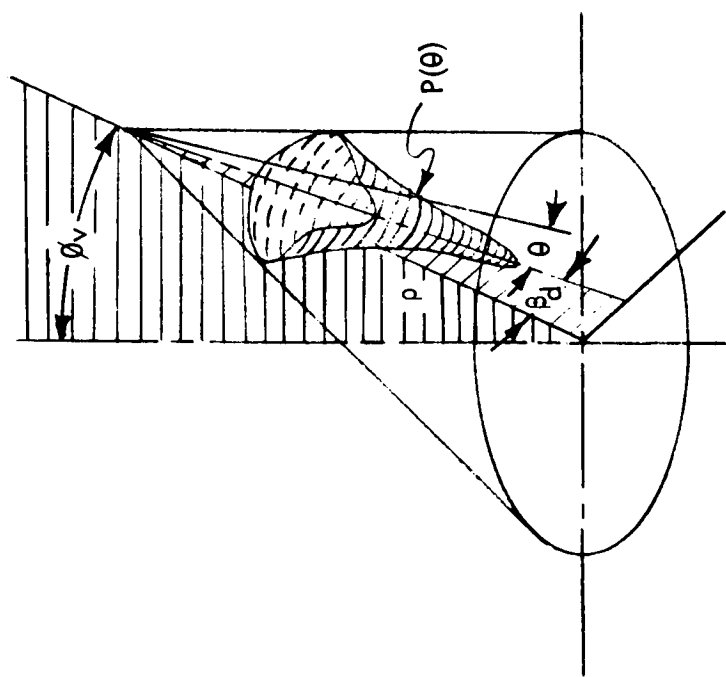


Figure 33 - Power Scattered but Retained
Within Beam

obtained by consideration of a volume element on the beam axis. Also, we neglect the dependence of R on β_d , in spite of the fact that such dependence exists and the configurations can be readily shown as dramatic evidence of such. The rationale of the approach lies in the fact that for large z , the solid angle, Γ , approaches zero so the approximation becomes exact, while for small z , the volume of scatterers approaches zero so that relatively little scattering occurs. Thus, it is assumed that E_{sor} can be suitably approximated by the scattering of a ray incident on a volume element on the beam axis and which is directed toward the center of the objective lens, a slight overestimate.* R then becomes

$$R = \frac{1}{2} \int_0^{\tan^{-1}(r_p/z)} P(\theta) \sin \theta \, d\theta \quad , \quad (III-16)$$

which is dependent only on z . Equation (III-15) then is simply

$$E_{sor} = RE_{so} \quad . \quad (III-17)$$

For future reference, we give explicit forms for R for the two types of scattering.

Rayleigh:

$$R = \frac{1}{2} \left\{ 1 - \frac{3}{4} \left[1 + (r_p/z)^2 \right]^{-\frac{1}{2}} - \frac{1}{4} \left[1 + (r_p/z)^2 \right]^{-3/2} \right\} \quad . \quad (III-18)$$

Mie:

$$R = \frac{1}{2} \frac{P_0}{s^2 + 1} \left\{ 1 - e^{-s \tan^{-1}(r_p/z)} \left[s \left(1 + (z/r_p)^2 \right)^{-\frac{1}{2}} + \left(1 + (r_p/z)^2 \right)^{-\frac{1}{2}} \right] \right\} \quad . \quad (III-19)$$

The power lost from the beam per unit length due to scattering out is then

* Reference to Section C of this Appendix and particularly Table XI indicates the greatest overestimate of power retained after scattering would occur with the cloud model, due to the greater directional preference therein.

$$\frac{dE}{dz} = E_{so} - E_{sor} = k_s E(1 - R) \quad (\text{III-20})$$

E. Scattering into the Beam

Radiation is scattered into the optical beam as well as out of it. This phenomenon causes several effects. First, it serves to generate the beam. That is, unless the telescope is aimed at a specific source, the only energy which enters the optical system* must be scattered into the beam from the direction of a source such as the sun. Secondly, the fluid flow phenomenon of interest may be "seen" by means of this scattered energy, in conjunction with the fluctuations due to scattering out of the beam. Thirdly, a "signal" in the form of power fluctuations moving toward the objective may be diluted by addition of more power fluctuations along the beam.

Consider the incident power in a small solid angle $d\Gamma_I$ centered on a ray through the volume element dv with the direction (ϕ_I, γ_I) (see Figure 34, page 144). ϕ_I is a polar angle measured from the z-axis, γ_I is an azimuthal angle. The incident power is directed away from the objective lens when $\phi_I = 0$. The power incident on dv in this solid angle is

$$E_I(\phi_I, \gamma_I) \cos \phi_I \, dAd\Gamma_I \text{ watts} \quad , \quad (\text{III-21})$$

where E_I is the incident intensity in watts/unit area/steradian. Of this incident power, the amount scattered in the volume dv is

$$k_s \frac{dz}{\cos \phi_I} E_I \cos \phi_I \, dAd\Gamma_I = k_s E_I \, dAd\Gamma_I dz \quad . \quad (\text{III-22})$$

The fraction of the power in (III-22) which is scattered into the beam is given, again, by (III-14)

$$R = \frac{1}{4\pi} \int_{\Gamma} P(\theta) d\Gamma \quad , \quad (\text{III-14})$$

* Energy may also arise from emission, as discussed in Section G of this Appendix.

where the integration is over the solid angle subtended by the entrance pupil (objective lens). Since the angle, ϕ_I , is not in general close to π , the approximation for R used in Section IV is not valid here. Instead, we use

$$R \approx \frac{P(\pi - \phi_I)}{4\pi} \Gamma_P, \quad (III-23)$$

where Γ_P is the solid angle subtended by the entrance pupil and is given in (III-2). The approximation, valid for large z , is equivalent to stating that the ratio, R , is independent of the distance R of the volume element from the beam axis.

Multiplying (III-23) by (III-22) and integrating over the beam cross section of unit thickness gives

$$\frac{dE_{SI}}{d\Gamma_I} = \frac{\pi z^2 \tan^2 \gamma_f}{2} P(\pi - \phi_I) k_s E_I(\phi_I, \gamma_I) \left[1 - \left(1 + (r_P/z)^2 \right)^{-\frac{1}{2}} \right] \left[1 - \frac{1}{4} \tan^2 \gamma_f \right] \quad (III-24)$$

watts per (steradian of incident power). Equation (III-24) must then be integrated over 4π steradians to account for all incident radiation. Specific examples are given next.

1. A Point Source

Let the intensity, E_I , be zero everywhere except for a specific direction (ϕ_I, γ_I) at which it is infinite, but in the form of a dirac delta or impulse function such that

$$\int_0^{2\pi} \int_0^\pi E_I(\phi_I, \gamma_I) \sin \phi_I d\phi_I d\gamma_I = \bar{E}, \quad (III-25)$$

which is the total incident power per unit area. Then, the integral of (III-24) becomes

$$\frac{dE}{dz} = \frac{\pi z^2 \tan^2 \gamma_f}{2} k_s \bar{E} P(\pi - \phi_I) \left[1 - \left(1 + (r_p/z)^2 \right)^{-\frac{1}{2}} \right] \left[1 - \frac{1}{4} \tan^2 \gamma_f \right] \quad (III-26a)$$

watts per unit beam thickness.

2. An Infinite, Plane Source Whose Outward Normal is Directed Toward the Entrance Pupil

The volume, dv , at distance z from entrance pupil, can have power scattered into the beam coming from any portion of the plane except that circle defined by the radius r_m (see Figure 35). Power originating within r_m and directed through dv is already in the beam, by our previous definition. Any scattering of this latter power occurring within dv is thus considered scattering out of the beam (or, scattered and retained) and has already been accounted for.

We assume that r_m is independent of R . (This appears reasonable for $z_{pl} \gg r_p$). The half angle, γ_f , is defined by

$$\tan \gamma_f = r_p/z.$$

We let the incident power intensity be given by

$$E_I(\phi_I) = \begin{cases} \bar{E}/2\pi, & \phi_I \geq \pi/2 \\ 0, & \phi_I < \pi/2 \end{cases} \quad (III-27)$$

so that (III-25) is again satisfied. Equation (III-27) states that the incident power intensity is independent of direction within the hemisphere $\phi_I \geq \pi/2$. That is, the power per steradian is constant.

Integrating (III-24) using (III-27) yields the power increase per unit length of

$$\frac{dE}{dz} = \frac{\pi z^2 \tan^2 \gamma_f}{2} k_s \bar{E} \left[1 - \left(1 + (r_p/z)^2 \right)^{-\frac{1}{2}} \right] \left[1 - \frac{1}{4} \tan^2 \gamma_f \right] Q, \quad (III-26b)$$

where Q is dependent on the scattering model, having the forms

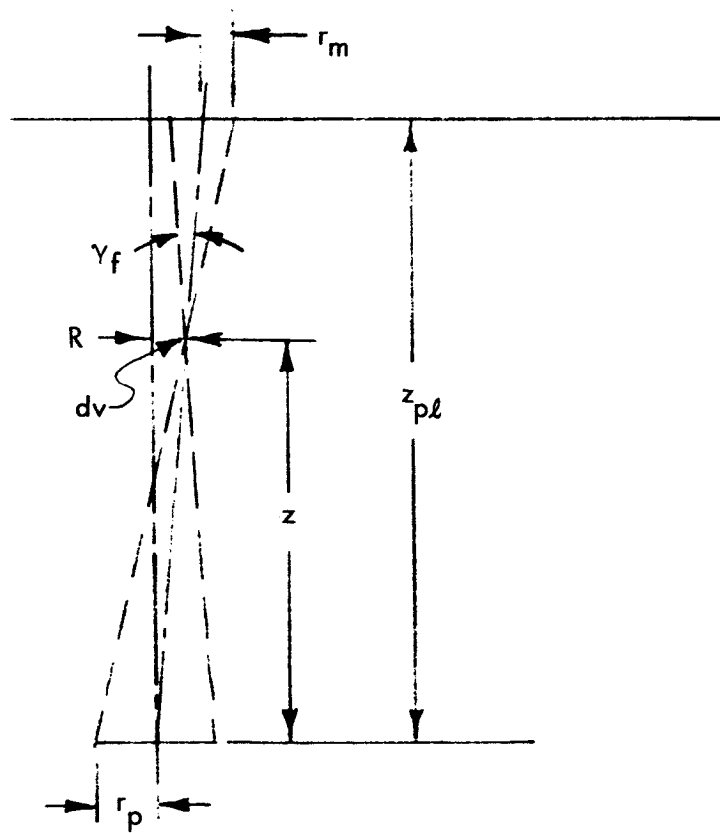


Figure 35 - Power Scattered from a Plane

Rayleigh:

$$Q = \frac{1}{4 \left[(1 + (r_p/z)^2) \right]^{\frac{1}{2}}} \left[\frac{4 + 3(r_p/z)^2}{1 + (r_p/z)^2} \right] \quad (\text{III-28})$$

Mie:

$$Q = \frac{p_0}{s^2 + 1} \left\{ e^{-s \tan^{-1}(r_p/z)} \left[1 + (r_p/z)^2 \right]^{-\frac{1}{2}} \left[r_p s/z + 1 \right] - s e^{-s\pi/2} \right\}. \quad (\text{III-29})$$

3. An Infinite Plane Source Whose Outward Normal Is Directed Away from the Entrance Pupil

This example is similar to example 2 with but two differences. First, back scattering rather than forward scattering is of concern here. $E_I(\phi_I)$ is nonzero over the hemisphere $\phi_I \leq \pi/2$. Secondly, we chose to integrate over the entire hemisphere without excluding the solid angle subtended by the entrance pupil. The result obtained is given by (III-26b) with Q defined as follows

Rayleigh:

$$Q = 1 \quad (\text{III-30})$$

Mie:

$$Q = p_0 e^{-s\pi/2} \quad (\text{III-31})$$

F. Finite Plane Source

A finite plane source which is perpendicular to the beam axis and is circular with its center on the beam axis is readily handled. One simply modifies (III-27) to include a specific angle, $\phi = \phi_M$, as a limiter rather than $\pi/2$. ϕ_M will, in general, depend on z and z_{pl} (see Figure 35). Also, one should define \bar{E} as convenient.

Other finite (or infinite) plane sources can be dealt with in the manner described here, but the integral limits become complicated. Numerical integration may need to be resorted to.

G. Absorption

Of interest here is the loss in beam power due to absorption. Let k_a be the absorption coefficient, with units of length^{-1} . The derivation follows precisely along the lines given in Section D of this Appendix for the power scattered from a unit thickness of the beam, except the correction for power scattered but retained in the beam is not applicable for absorption.

The power lost due to absorption is thus

$$\frac{dE}{dz} = k_a E \quad . \quad (\text{III-32})$$

H. Emission

Power increases may be caused by spontaneous emission at certain wavelengths by various species. The emission is not normally given in terms of a coefficient, k , with units of length^{-1} . Rather, it is convenient to deal with the power, P_e , emitted per unit volume of the atmosphere.

The power emitted into the beam is thus

$$\frac{dE}{dz} = \int_0^{2\pi} \int_0^z \tan \gamma_f P_e(z) \frac{\Gamma_p}{4\pi} R dR d\gamma_v \quad . \quad (\text{III-33})$$

Using (III-2) and retaining second order terms, as before, yields

$$\frac{dE}{dz} = \frac{\pi z^2 \tan^2 \gamma_f}{2} P_e(z) \left[1 - \left(1 + (r_p/z)^2 \right)^{-\frac{1}{2}} \right] \left[1 - \frac{1}{4} \tan^2 \gamma_f \right] \quad (\text{III-34})$$

watts per unit length gained due to emissions.

I. General Beam Model

This section collects together the results of Sections D to G in a unified model. It is convenient at this point to think in terms of a coordinate directed in the opposite direction to z , so that such a coordinate takes on increasing values as the entrance pupil is approached. Let this coordinate be g , defined by

$$g = z_{\max} - z \quad (\text{III-35})$$

where z_{\max} is the (arbitrary) origin for g .

The results of the previous sections can be combined to yield a single expression for the rate of gain in power approaching the entrance pupil. The equation is

$$\frac{dE}{dg} = - \left\{ \sum_{i=1}^6 k_i(g) F_i(g) \right\} E + \sum_{i=1}^6 k_i(g) I_i(g) \quad . \quad (\text{III-36})$$

The first group of terms represents the losses due to scattering out and absorption; the second group represents gains due to scattering in and emission. The summation on i from 1 to 6 is somewhat artificial but is a convenience for distinguishing various effects. The k_i are defined as follows:

$$\begin{aligned}
k_1 &= k_s \text{ (Rayleigh scattering out of beam)} \\
k_2 &= k_s \text{ (Mie scattering out of beam)} \\
k_3 &= k_a \text{ (absorption)} \\
k_4 &= k_s \text{ (Rayleigh scattering into beam)} \\
k_5 &= k_s \text{ (Mie scattering into beam)} \\
k_6 &= P_e \text{ (emission)}
\end{aligned}
\tag{III-37}$$

The first five have units of length^{-1} , the sixth is in watts per unit volume.

Comparing (III-36) with (III-18), (III-19), (III-20), (III-32), (III-26), and (III-34) yields the following definitions:

$$\begin{aligned}
F_1(z) &= 1 - \frac{1}{2} \left\{ 1 - \frac{3}{4} \left[1 + (r_p/z)^2 \right]^{-\frac{1}{2}} - \frac{1}{4} \left[1 + (r_p/z)^2 \right]^{-3/2} \right\} \\
F_2(z) &= 1 - \frac{1}{2} \frac{p_0}{s^2 + 1} \left\{ 1 - e^{-s \tan^{-1}(r_p/z)} \left[s \left(1 + (z/r_p)^2 \right)^{-\frac{1}{2}} + \left(1 + (r_p/z)^2 \right)^{-\frac{1}{2}} \right] \right\} \\
F_3(z) &= 1 \\
F_4(z) &= 0 \\
F_5(z) &= 0 \\
F_6(z) &= 0 \\
I_1(z) &= 0 \\
I_2(z) &= 0 \\
I_3(z) &= 0 \\
I_4(z) &= \bar{E} Q_4 I_6(z) \\
I_5(z) &= \bar{E} Q_5 I_6(z) \\
I_6(z) &= \frac{\pi z^2 \tan^2 \gamma_f}{2} \left[1 - \left(1 + (r_p/z)^2 \right)^{-\frac{1}{2}} \right] \left[1 - \frac{1}{4} \tan^2 \gamma_f \right]
\end{aligned}
\tag{III-38}$$

where

$$\left. \begin{aligned} Q_4 &= 3/4(1+\cos^2 \phi_I) \\ Q_5 &= \begin{cases} p_o e^{-s\pi/2} & , 0 \leq \phi_I \leq \pi/2 \\ p_o e^{-s(\pi-\phi_I)} & , \pi/2 < \phi_I \leq \pi \end{cases} \end{aligned} \right\} \quad (\text{III-39})$$

for a point source. For plane sources, Q_4 is given by (III-28), (III-30), and the like, while Q_5 is given by (III-29), (III-31), or related expressions.

Equation (III-36) is a first order linear differential equation whose solution is

$$E(g_p) = e^{G(g_p)} \left\{ E_o + \int_0^{g_p} e^{-G(g)} \left[\sum_{i=1}^6 k_i(g) I_i(g) \right] dg \right\} \quad (\text{III-40})$$

where

$$G(g) = \int_0^g \left[\sum_{i=1}^6 k_i(g) F_i(g) \right] dg \quad . \quad (\text{III-41})$$

g_p is a particular value of g which is of interest -- generally at the entrance pupil ($z = 0$) . E_o is the power in the beam at the arbitrary reference point, $g = 0$.

It is of interest to note that the first term of (III-40) $e^{-G(g_p)} E_o$, is the relation considered as fundamental to the cross-beam theory. The so-called generalized extinction coefficient, k , is given by

$$k = \sum_{i=1}^6 k_i F_i \quad . \quad (\text{III-42})$$

However, reference to (III-38) shows that the generalized extinction coefficient includes absorption and scattering out of the beam. Emission and scattering into the beam are therefore not included in cross-beam theory with the generalized extinction coefficient.

The second term of (III-40), the integral term, is not part of the usual cross-beam theory. Also, it is this term which contains the effects of emission and scattering into the beam. Often, these effects are considered separately as contributors to "noise", or, in the case of emission, as a tracer. Their integrated effect has not, to the knowledge of the authors, been studied as yet in relation to the cross-beam technique.

J. Beam Power Fluctuations

The previous section presented the relation between received beam power and the various physical processes on which it depends. Now, the quantity of most direct concern in cross-beam work is the change or fluctuation in this power due to local changes in physical processes along the beam path. The relation(s) giving this result is derived here.

We consider a small change, δk_j , in the value of the coefficient k_j . We wish to localize this change to a small interval, δg , located at $g = g_v$. We form $(1+\delta_j)E$ by considering the small incremental changes in various parts of (III-40).

The factor $G(g)$ becomes

$$\left. \begin{aligned} G(g) &\longrightarrow G(g) \quad \text{for } g < g_v \\ G(g) &\longrightarrow G(g) + F_j(g_v) \delta k_j \delta g \quad \text{for } g > g_v + \delta g \\ G(g) &\longrightarrow G(g) + F_j(g_v) \delta k_j (g - g_v) \quad \text{for } g_v \leq g \leq g_v + \delta g \end{aligned} \right\} \quad (\text{III-43})$$

and

$$G(g_p) \longrightarrow G(g_p) + F_j(g_v) \delta k_j \delta g \quad . \quad (\text{III-44})$$

The integral in (III-40) may be written in three parts, with the aid of (III-43) to yield

$$\int_0^{g_p} e^{G(g)} \left[\sum_{i=1}^6 k_i(g) I_i(g) \right] dg \rightarrow$$

$$\begin{aligned} & \int_0^{g_v} e^{G(g)} \left[\sum_{i=1}^6 k_i(g) I_i(g) \right] dg \\ & + \int_{g_v}^{g_v+\delta g} e^{G(g)+F_j(g_v)\delta k_j(g-g_v)} \left\{ \sum_{i=1}^6 [k_i(g) I_i(g)] + I_j(g_v)\delta k_j \right\} dg \\ & + \int_{g_v+\delta g}^{g_p} e^{G(g)+F_j(g_v)\delta k_j\delta g} \sum_{i=1}^6 [k_i(g) I_i(g)] dg \quad . \quad (\text{III-45}) \end{aligned}$$

Equations (III-43) to (III-45) are exact expressions. We now make use of the fact that δk_j is a small change occurring over a small interval δg and retain only the dominant terms (i.e., we neglect higher order terms in δk_j or δg). We thus obtain

$$\begin{aligned} (1+\delta_j)E(g_p) &= e^{-G(g_p)} [1-F_j(g_v)\delta k_j\delta g] \left\{ E_0 \right. \\ &+ \int_0^{g_v} e^{G(g)} \left[\sum_{i=1}^6 k_i(g) I_i(g) \right] dg \\ &+ \int_{g_v}^{g_v+\delta g} e^{G(g)} \left[\sum_{i=1}^6 (k_i(g) I_i(g)) + I_j(g_v)\delta k_j \right] dg \\ &+ e^{G(g_v)} \left[\sum_{i=1}^6 (k_i(g_v) I_i(g_v)) + I_j(g_v)\delta k_j \right] F_j(g_v)\delta k_j \frac{(\delta g)^2}{2} \\ &\left. + \int_{g_v+\delta g}^{g_p} e^{G(g)} [1+F_j(g_v)\delta k_j\delta g] \sum_{i=1}^6 [k_i(g) I_i(g)] dg \right\} . \quad (\text{III-46}) \end{aligned}$$

The next to last line of (III-46) is of higher order in δg so is hereafter dropped. Portions of the integrals with common integrands can be combined to yield

$$(1+\delta_j)E(g_p) = e^{-G(g_p)} [1-F_j(g_v)\delta k_j\delta g] \left\{ E_0 + \int_0^{g_p} e^{G(g)} \left[\sum_{i=1}^6 k_i(g)I_i(g) \right] dg \right. \\ \left. + I_j(g_v)\delta k_j \int_{g_v}^{g_v+\delta g} e^{G(g)} dg + F_j(g_v)\delta k_j\delta g \int_{g_v+\delta g}^{g_p} e^{G(g)} \left[\sum_{i=1}^6 k_i(g)I_i(g) \right] dg \right\}. \quad (III-47)$$

Subtracting (III-40) from (III-47) and retaining only the first order terms in $(\delta k_j\delta g)$ leaves

$$\delta_j E(g_p) = \delta k_j\delta g e^{-G(g_p)} \left\{ -F_j(g_v) \left[E_0 + \int_0^{g_v} e^{G(g)} \left(\sum_{i=1}^6 k_i(g)I_i(g) \right) dg \right] \right. \\ \left. + e^{G(g_v)} I_j(g_v) \right\} \quad (III-48)$$

Finally, the expression in square brackets is seen to be, within a multiplicative factor of $e^{-G(g_v)}$, the power in the beam at g_v , so that (III-48) takes on the simple form

$$\delta_j E(g_p) = \delta k_j\delta g \left\{ e^{-G(g_p)}/e^{-G(g_v)} \right\} \left\{ I_j(g_v) - F_j(g_v)E(g_v) \right\}. \quad (III-49)$$

The terms in (III-49) are easily identified as follows. The loss in beam power at g_p due to an increase δk_j in the scattering out (or absorption) coefficient k_j over a length δg at g_v is given by the factor of (III-49) involving $F_j(g_v)$. The power in the beam at g_v is $E(g_v)$ and the fractional loss of this power, at g_v , is $\delta k_j\delta g F_j(g_v)$.

This effect is then attenuated over the remainder of the beam by the factor

$$\frac{e^{-G(g_p)}}{e^{-G(g_v)}} = e^{-\int_{g_v}^{g_p} \left[\sum_{i=1}^6 k_i(g) F_i(g) \right] dg} \quad (\text{III-50})$$

On the other hand, a gain in beam power occurs with an increase δk_j in the scattering in (or emission) coefficient k_j over the length δg at g_v . The gain is given by the other factor of (III-49), which consists of the gain at g_v , $\delta k_j \delta g I_j(g_v)$, attenuated by the factor in (III-50).

It is also of interest to examine the effect on the observed power of a small change in incident power, $\delta \bar{E}$, on an interval δq at q_v . This can be simulated by using $j = 6$ in (III-49), which corresponds to an incremental change in emission. However, correction must be made for dimensional and geometrical differences. The same change in $E(g_p)$ occurs if

$$\delta k_6 (= \delta P_e) = \delta \bar{E} (k_4 Q_4 + k_5 Q_5) \quad (\text{III-51})$$

That is, a change $\delta \bar{E}$ in incident power is completely equivalent, mathematically, to a change δP_e given by (III-51).

A final statement is made regarding all of the equations developed here. They are in a form readily adaptable to computer programming. Numerical evaluation is necessary because of the variations of the k_j with altitude discussed elsewhere. However, care must be taken in evaluating many of the expressions (and in particular, (III-38)) for large and small values of z . To retain numerical significance it is necessary in many cases to employ series expansions in r_p/z or z/r_p , so that analytical cancellation of terms of like order may be accomplished.

APPENDIX IV

EFFECTS OF NONIDEAL ENVIRONMENTS ON CROSS-BEAM CORRELATIONS

A. Introduction

The basic theory concerning the use of crossed or nearly crossed optical beams for making turbulent flow measurements is discussed in many papers and articles and will, therefore, not be repeated here. In the theory, several simplifying assumptions are made concerning the environment of the beams. These assumptions lead to methods of determining physical quantities of interest in the turbulent flow studies. It is the purpose of this section to relax some of the idealizations and, by example, indicate the changes to be expected in interpretation of the flow properties.

The study of nonideal environments will be limited to fixed beams, for simplicity and ease in interpretation. Let us select a coordinate system aligned with the optical beams. That is, beam number 1 is directed along the x-axis, beam number 2 along the y-axis, and the beam normal, perpendicular to the two beams, is along the z-axis. The intersection of beam 1, the beam normal, and beam 2 translated along the beam normal until it intersects beam 1, is given by the point (x_0, y_0, z_0) . The beam separation is given by the distance, Δz . Furthermore, a time lag is introduced between the signals from the two beams such that the signal from beam 2 is delayed by a time interval, τ , relative to beam 1. Then, it may be shown^{1/} that the covariance of the signal fluctuations is given by

$$G(x_0, y_0, z_0 + \Delta z, \tau) =$$

$$< I_1 > < I_2 > \int_y \int_x \frac{1}{t} \int_0^t k(x, y_0, z_0, t) k(x_0, y, z_0 + \Delta z, t + \tau) dt dx dy . \quad (IV-1)$$

I_1 and I_2 are the beam intensities, which are to be averaged over time. k is the extinction coefficient, which may be caused by either absorption or scattering of power out of the beam. Emission and scattering of power into the beam are not considered here.

The inner integral can be written in terms of the variances of the k 's and the correlation coefficient, R , between them (assuming a sufficiently large integration time), yielding

$$G(x_0, y_0, z_0 + \Delta z, \tau) =$$

$$\langle I_1 \rangle \langle I_2 \rangle \int_y \int_x \left\{ \overline{k^2(x, y_0, z_0)} \overline{k^2(x_0, y, z_0 + \Delta z)} \right\}^{1/2} R(x, y, \Delta z, \tau) dx dy . \quad (IV-2)$$

It is at this point that certain idealizations are made in the basic cross-beam theory. It is implicitly assumed that $\overline{k^2}$ is uniform (homogeneous flow) in some region around the beam normal and explicitly assumed that $R(x, y, \Delta z, \tau)$ is separable so that its dependence on Δz and τ can be removed from under the integral. Further, it is implied that the convection speed of the fluid is uniform and aligned with the z -direction. That is, the effects of other velocity components or of a nonuniform velocity magnitude are not considered.

With the above assumptions, it is possible by analysis of the measured covariance, G , to determine the behavior of the correlation coefficient, R . From this, the following physical quantities can be obtained:

1. z -Component of convection speed, w .
2. Eddy lifetime.
3. Integral scale of turbulence.
4. Power spectrum.

These quantities are obtained from consideration of the family of curves

$$\frac{G(x_0, y_0, z_0 + \Delta z, \tau)}{G(x_0, y_0, z_0 + 0, 0)} \text{ versus } \tau ,$$

with Δz as a parameter, and the envelope to the family. The convection speed, w , is found from

$$w = \frac{\Delta z}{\tau^*} \quad (IV-3)$$

where τ^* is the value of τ at which the member of the family defined by Δz is tangent to the envelope.* The eddy lifetime is obtained by locating the time at which the envelope has decayed to $1/e$ of its value at $\tau = 0$. The integral scale of turbulence is found from

$$L_z = \int_0^\infty \frac{G(x_0, y_0, z_0 + \Delta z, 0)}{G(x_0, y_0, z_0 + 0, 0)} dz, \quad (\text{IV-4})$$

and the power spectrum is obtained from the Fourier transformation of the autocorrelation, $G(x_0, y_0, z_0, \tau)/G(x_0, y_0, z_0, 0)$, which is the member of the family for which $\Delta z = 0$.

The above methods are applied in the present analysis to situations which violate one or more of the assumptions used, but which are certainly to be expected in atmospheric applications.

B. Correlation Coefficient for Extinction Coefficient

The intensity of the turbulence** is indicated by the variance of the extinction coefficient, $\overline{k^2}$, and the correlation coefficient (in space and/or time) between coefficient fluctuations by R . For purposes of this study, the variance and the correlation coefficient are considered independently.

It is necessary to postulate a functional form for R which agrees reasonably well with observations of turbulent flow while, at the same time, is simple enough to allow analytic studies and/or direct physical interpretation. To this end, we first consider the case where there is no time lag. Thus, we require the correlation coefficient between fluctuations at two points in space. For isotropic turbulence (which is assumed here) the correlation coefficient can depend only on the distance, r , between the two points and not the direction of separation. Without loss of generality we locate the origin of the coordinate system so that $x_0 = y_0 = z_0 = 0$ so that

* Often, as an approximation, the value τ' at which the curve attains its maximum is used in place of τ^* .

** We use the term, turbulence, to include any cause of signal fluctuations, whether it be flow turbulence in the usual sense or not.

$$r^2 = x^2 + y^2 + (\Delta z)^2 .$$

Many forms of $R(r)$ have been postulated,^{67/} with the exponential function most common. Except for turbulence in its late stages where it is dominated by viscous effects (low Reynolds number), the form

$$R(x,y,\Delta z,0) = e^{-(x^2+y^2+\Delta z^2)^{1/2}/L} \quad (IV-5)$$

appears acceptable. It fits velocity fluctuation data rather well, and bears a resemblance to pressure fluctuation data. A better fit might be possible by multiplying the right-hand side of (IV-5) by a power series or Fourier series so as to duplicate the phenomena of sign changes in R , which are not possible using (IV-5) alone. It is felt that the attendant analytical complications are not warranted, however, for this study, particularly in light of the lack of agreement among measured correlation data.

The value, L , is included in equation (IV-5) for dimensional purposes, and, furthermore, is the integral scale of turbulence, as application of equation (IV-4) will show.

Equation (IV-5) must be generalized to include effects of time lag and a convection speed of the fluid. Considering, first, just the time lag, experimental evidence indicates that the correlation should decay exponentially with time. This behavior requires a multiplicative factor of $e^{-\tau/T}$ where T is the eddy lifetime. The incorporation of a convection speed requires additional considerations.

Consider a point (a small amount of fluid) located on the x -axis (beam 1), at time $t = 0$, and another point on the y -axis at $t = \tau$. We assume a uniform convection velocity with components u , v , and w in the positive x , y , and z directions, respectively. The sketch shown in Figure 36 shows the projection in the x - y plane of the two points in question at times $t = 0$ and $t = \tau$. The distance, r , between the points is not $(x^2 + y^2 + \Delta z^2)$ but must be modified because of the convection.

The point on the x -axis has coordinates $(x,0,0)$ at time $t = 0$. The point on the y -axis, at time $t = \tau$, has coordinates $(0,y,\Delta z)$. At time $t = 0$, the latter point was located at $(-u\tau, y-v\tau, \Delta z-w\tau)$. The distance between points, at time $t = 0$, is thus given by

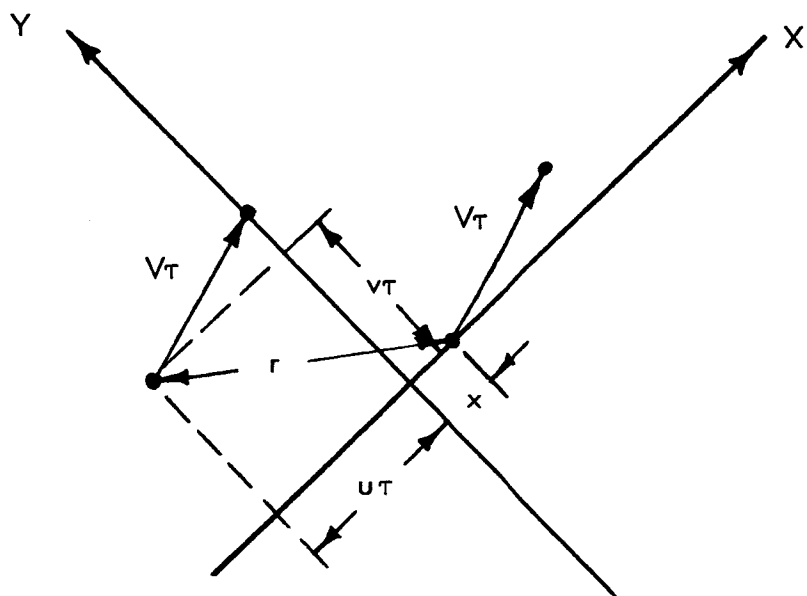


Figure 36 - Effects of Convection on Correlation Coefficient

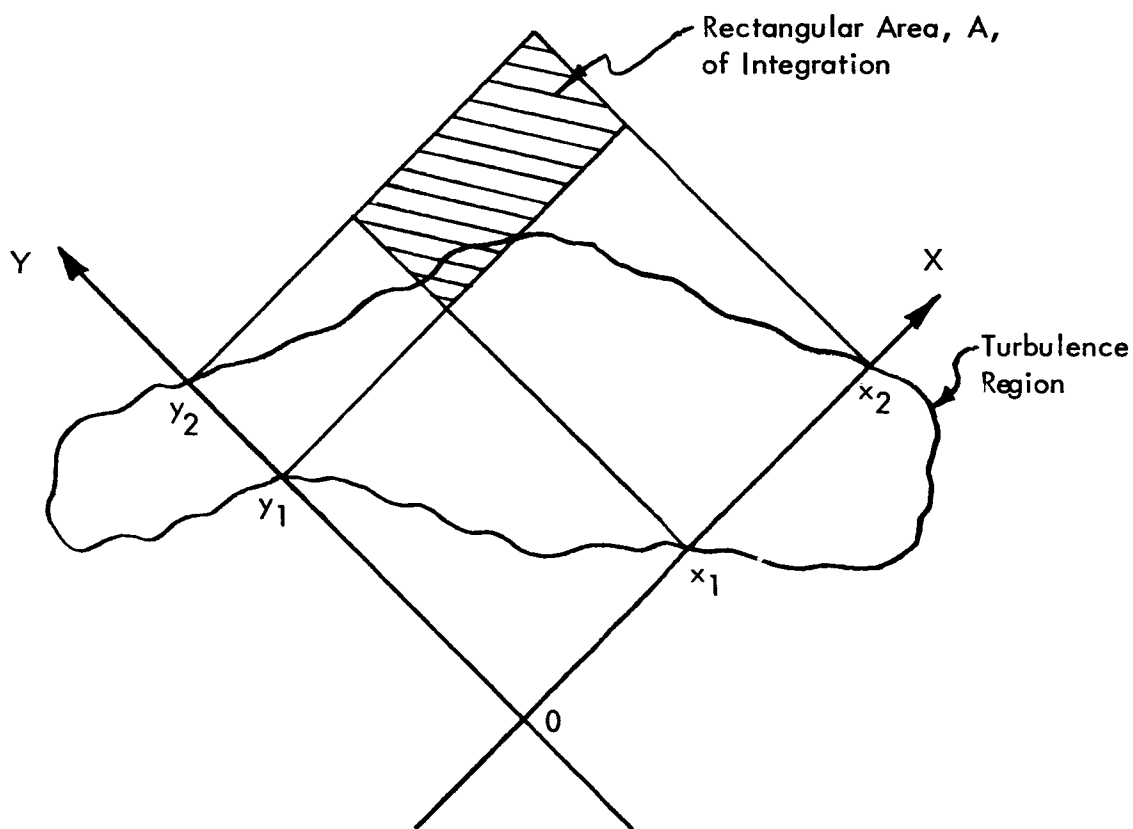


Figure 37 - Relation Between Turbulence Region and Area of Integration

$$r^2 = [x - (-u\tau)]^2 + [0 - (y - v\tau)]^2 + [0 - (\Delta z - w\tau)]^2.$$

or

$$r^2 = (x + u\tau)^2 + (y - v\tau)^2 + (\Delta z - w\tau)^2 \quad . \quad (\text{IV-6})$$

The same result is obtained, for uniform flow, by considering the distance between points at time $t = \tau$. For nonuniform flow, it is proper to consider r as the separation at $t = 0$, as above, where u , v , and w are the velocity components at the point $(0, y, \Delta z)$.

Combining the previous results, we obtain

$$R(x, y, \Delta z, \tau) = e^{-\tau/T_e} - \left\{ [(x + u\tau)^2 + (y - v\tau)^2 + (\Delta z - w\tau)^2]^{\frac{1}{2}} / L \right\} \quad (\text{IV-7})$$

as the general form of the correlation coefficient to be used for study of nonideal situations.

C. Effects of Nonuniform Turbulence

1. Gross Effects Obtained from Analytical Approximations

To determine the types of effects that might result from nonuniform turbulence (more precisely -- nonuniform intensity of turbulence), consider the hypothetical situation where $k = 1$ in some selected region of space and $k = 0$ elsewhere. This problem is an approximation to the physically realizable problem of a localized region of intense turbulence. The actual shape of the region of high turbulence is unimportant at this point.

Let us assume that the x-beam intersects the turbulence such that $k(x, 0, 0) = 1$ for $x_1 \leq x \leq x_2$ while the y-beam is such that $k(0, y, \Delta z) = 1$ for $y_1 \leq y \leq y_2$. Then, dropping x_0 , y_0 , and z_0 , (IV-2) becomes

$$\frac{G(\Delta z, \tau)}{\langle I_1 \times I_2 \rangle} = e^{-\tau/T} \int_{y_1}^{y_2} \int_{x_1}^{x_2} e^{-\left\{ \left[(x+u\tau)^2 + (y-v\tau)^2 + (\Delta z-w\tau)^2 \right]^{1/2} / L \right\}} dx dy . \quad (\text{IV-8})$$

Now, it should be emphasized that, physically, (IV-8) represents a multiple line integral along those portions of the beams which intercept the turbulence region. Mathematically, however, the integral may be looked on as an area integral over the rectangular area defined by x_1 , x_2 , y_1 , and y_2 . Figure 37, page 163, indicates how this area, A, is related to the turbulence region. One should take care in this type of figure not to attach any significance to the intersection of A and the turbulence region, or to otherwise confuse the physical location of turbulence and the mathematical region of integration.

Carrying the mathematical interpretation further, the value of the integral in (IV-8) may be written, using the mean value theorem, as

$$\frac{G(\Delta z, \tau)}{\langle I_1 \rangle \langle I_2 \rangle} = e^{-\tau/T} A e^{-\bar{r}/L} \quad (\text{IV-9})$$

where \bar{r} is the value of r corresponding to the mean value of the integrand in the area, A. For the special case where $\tau = 0$ (or, if the convection speed is zero) r is the distance from the origin, 0, to a point $(x, y, \Delta z)$ in the integration area. Thus, \bar{r} is a representative distance from the origin to the area. It is not the distance to the centroid, although that distance would serve as a first order approximation in an attempt to obtain gross effects.

We now examine the effect, on G , of convection. First, let us consider the transformation

$$\left. \begin{aligned} \xi &= (x+u\tau)/L \\ \eta &= (y-v\tau)/L \\ a &= |\Delta z-w\tau|/L \end{aligned} \right\} \quad (\text{IV-10})$$

Then, (IV-8) becomes

$$\frac{G(\Delta z, \tau)}{\langle I_1 \rangle \langle I_2 \rangle} = e^{-\tau/T_L^2} \int_{\frac{y_1 - v\tau}{L}}^{\frac{y_2 - v\tau}{L}} \int_{\frac{x_1 + u\tau}{L}}^{\frac{x_2 + u\tau}{L}} e^{-(\xi^2 + \eta^2 + a^2)^{\frac{1}{2}}} d\xi d\eta \quad (\text{IV-11})$$

Thus, in terms of the ξ - η plane, the limits of integration are determined not only by the location of the beam intersections with the turbulence region, but also by the time lag, τ . In effect, the velocity components u and v translate the integration region relative to the ξ - η origin. This translation changes the value, \bar{r} , which is indicative of the mean value of the integrand, but does not affect the size of the integration region, which is now

$$A_{\xi\eta} = (y_2 - y_1)(x_2 - x_1)/L^2 \quad (\text{IV-12})$$

The implications of this fact are evident in the example shown in Figure 38. Here is depicted a horizontal "band" of turbulence located just above the beam intersection and translating to the left with speed, V . ($u = -V/\sqrt{2}$, $v = +V/\sqrt{2}$, $w = 0$.) The location of the area, A , is shown at a sequence of times starting at $\tau = 0$. It is obvious that \bar{r} thus first decreases, then increases with time, leading to the conclusion that, barring the factor $e^{-\tau/T}$, the measured covariance, G , would first increase, then decrease with τ . This would be true even for the case $\Delta z = 0$.

Other situations can be looked upon in the same fashion. It is clear that the factor $e^{-\tau/T}$ could, depending on circumstances, dominate the time behavior. Also, the component of convection speed along the beam normal, w (which was neglected in Figure 38), could dominate the picture. Its effect, however, may also be looked upon as a translation of the area, A , but in the z -direction rather than in the z - y plane. In any particular problem, the actual location of the turbulence region, the convection velocity vector, the eddy lifetime and integral scale of turbulence all interact in producing the $G(\Delta z, \tau)$ curves. The important point is that there is apparently no unique inverse transformation that will generate $R(x, y, \Delta z, \tau)$ from the measured covariance, G , when nonuniform turbulence is present.

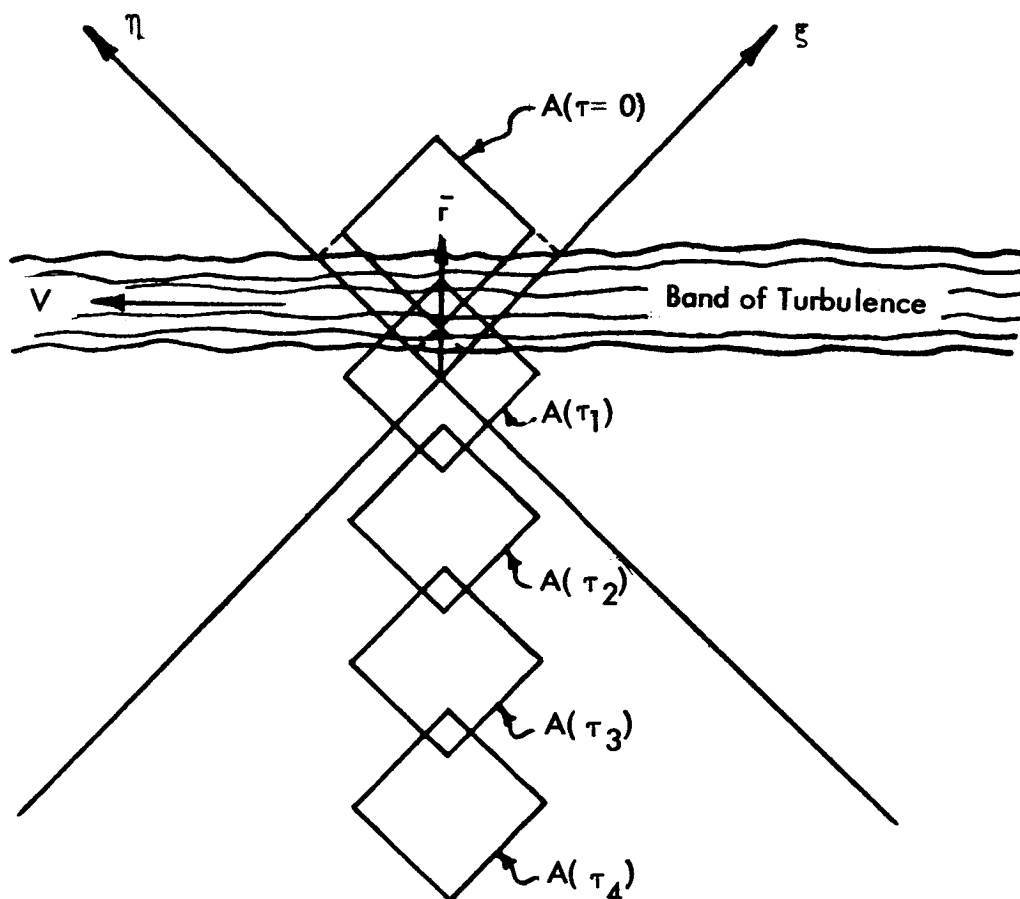


Figure 38 - Effect of Convection on Integration Area

The effect on the determination of convection speed in the z' -direction (see (IV-3)) of nonideal environment can be analyzed. Consider an arbitrary member, $G(\Delta z, \tau)$ of the family of covariance curves, with parameter Δz . Certainly, the point determined by setting $\tau = \Delta z/w$ is a point on that curve. Define the curve, $g(\tau)$ such that

$$g(\tau) = G(w\tau, \tau) . \quad (IV-13)$$

This curve intersects each member of the family at $\tau = \Delta z/w$. The slope of this curve is $dg/d\tau$. The slope of a member of the family is $\partial G(\Delta z, \tau)/\partial \tau$. To prove that the curve $g(\tau)$ is, in fact, tangent to each member of the family at the point $\tau = \Delta z/w$ requires proof of

$$\frac{dg}{d\tau} = \frac{\partial G(\Delta z, \tau)}{\partial \tau} \Big|_{\Delta z = w\tau} . \quad (IV-14)$$

Proof of (IV-14) then shows that the point of tangency, τ^* , satisfies (IV-3).

The proof of (IV-14) is straightforward when $G(\Delta z, \tau)$ is given by (IV-2) and R is taken in the form shown in (IV-7), provided k is independent of Δz and all Δz and τ dependence is as shown explicitly. In other words, (IV-3) holds for arbitrary dependence of k , u , v , and w on x and y .

Before proceeding to exact, numerical evaluations of (IV-8) or (IV-11), we remark that other forms of variation of the extinction coefficient can be readily handled. For example, if the extinction coefficient is equal to k everywhere except in a region (defined by beam intercepts x_1 , x_2 , y_1 , y_2) where it is $k+K$, then

$$\begin{aligned} \frac{G(\Delta z, \tau)}{\langle I_1 \rangle \langle I_2 \rangle} &= K^2 \int_{y_1}^{y_2} \int_{x_1}^{x_2} R(x, y, \Delta z, \tau) dx dy + k^2 \int_{-\infty}^{\infty} \int_{-\infty}^{\infty} R(x, y, \Delta z, \tau) dx dy \\ &+ kK \left\{ \int_{-\infty}^{\infty} \int_{x_1}^{x_2} R(x, y, \Delta z, \tau) dx dy + \int_{y_1}^{y_2} \int_{-\infty}^{\infty} R(x, y, \Delta z, \tau) dx dy \right\} . \quad (IV-15) \end{aligned}$$

2. Specific Examples, Utilizing Numerical Integration

Equation (IV-8) (or, its equivalent, (IV-11)) can be readily evaluated by use of numerical integration procedures. An efficient method is that of Gaussian Quadratures, which compute the integral as a weighted sum of values of the integrand at selected, discrete locations in the domain of integration.^{68/} Care must be taken of the possibility of a derivative discontinuity in the integrand (for example, at $\xi = \eta = a = 0$), or near discontinuity which might occur.

Several situations were studied by means of numerical integration. In all cases, the following values were selected:

$$L = 1,000 \text{ ft.}$$

$$T = 300 \text{ sec.}$$

$$w = 50 \text{ ft/sec}$$

$$x_2 - x_1 = y_2 - y_1 = 3,000 \text{ ft.}$$

Thus, a horizontal band of turbulence is depicted, whose thickness is $3,000\sqrt{2}$ feet, which has a component of convection speed along the beam normal of 50 feet/second. The parameters which were varied were the location of the turbulence band relative to the beam crossing and the u- and v-components of convection speed.

As a first example, we consider the case where the turbulence is centered around the beam normal ($-x_1 = x_2 = -y_1 = y_2 = 1,500$ feet), and has a horizontal convection speed component perpendicular to the beam normal. The numerical values chosen were $u = -20$, $v = 20$. (Any other sign combination such as $u = -20$, $v = -20$ gives the same results for $G(\Delta z, \tau)$.) Figure 39 shows curves for several values of beam separation, Δz , and the envelope to the family. As predicted, the velocity component w can be readily obtained from the value, τ^* , at the tangency point. Note the difference, however, between τ^* and the maximum, τ' . For example, at $\Delta z = 5,000$, $\tau^* = 100$ and $\tau' = 83$, a difference of 17%.

Figure 40 shows the effect of other components of convection speed on the envelope for a centered band of turbulence. The decay of G with τ increases as the component of convection speed perpendicular to the beam normal increases. The apparent eddy lifetime, given by τ at $G = G(0,0)/e$, is correctly T if the velocity vector is in the z-direction. However, T is not obtainable if the direction of the convection speed is unknown.

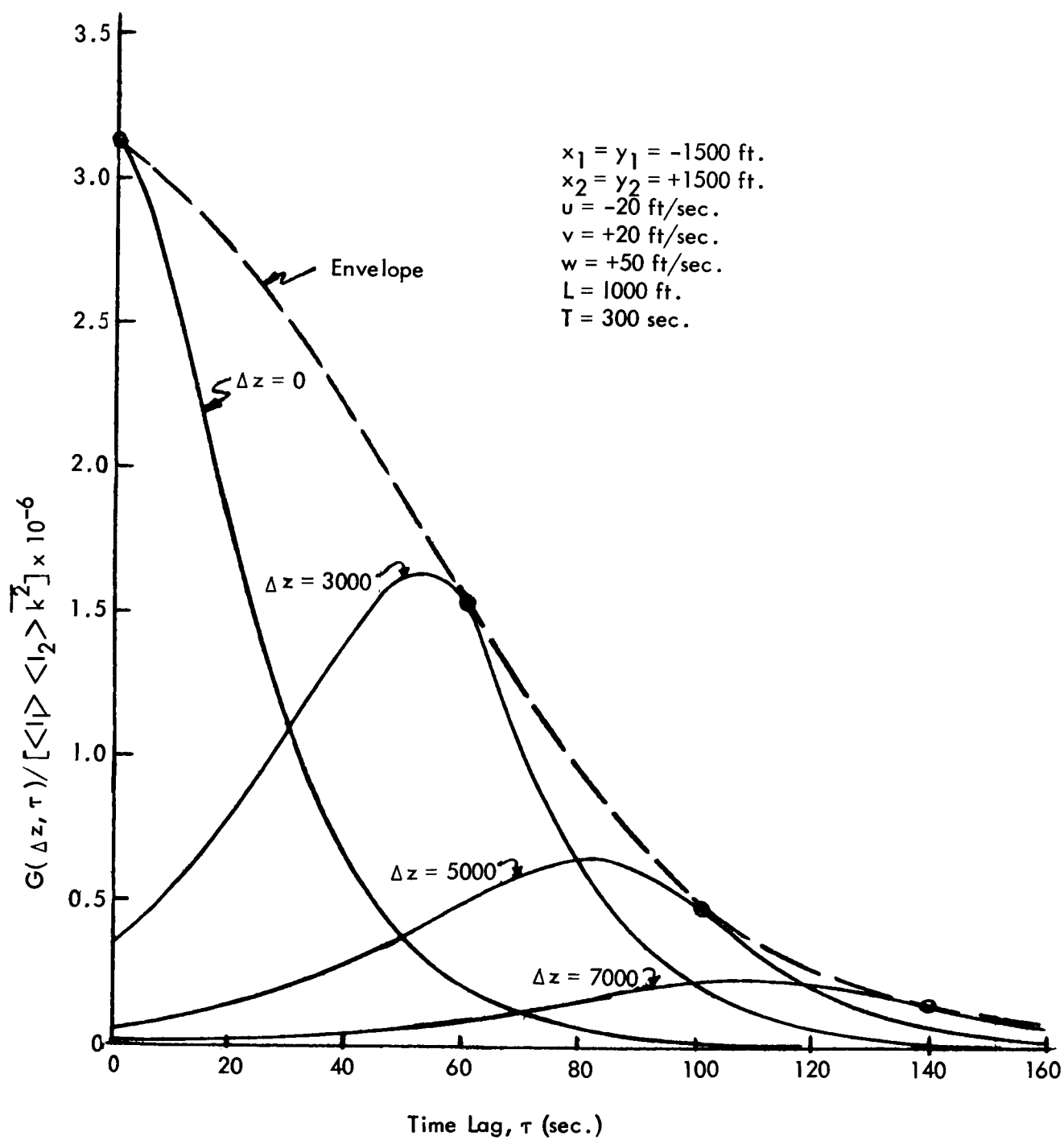


Figure 39 - Covariance for Turbulence Patch Centered Around Beam Normal

$x_1 = y_1 = -1500$ ft.
 $x_2 = y_2 = +1500$ ft.
 $w = 50$ ft/sec.
 $L = 1000$ ft.
 $T = 300$ sec.

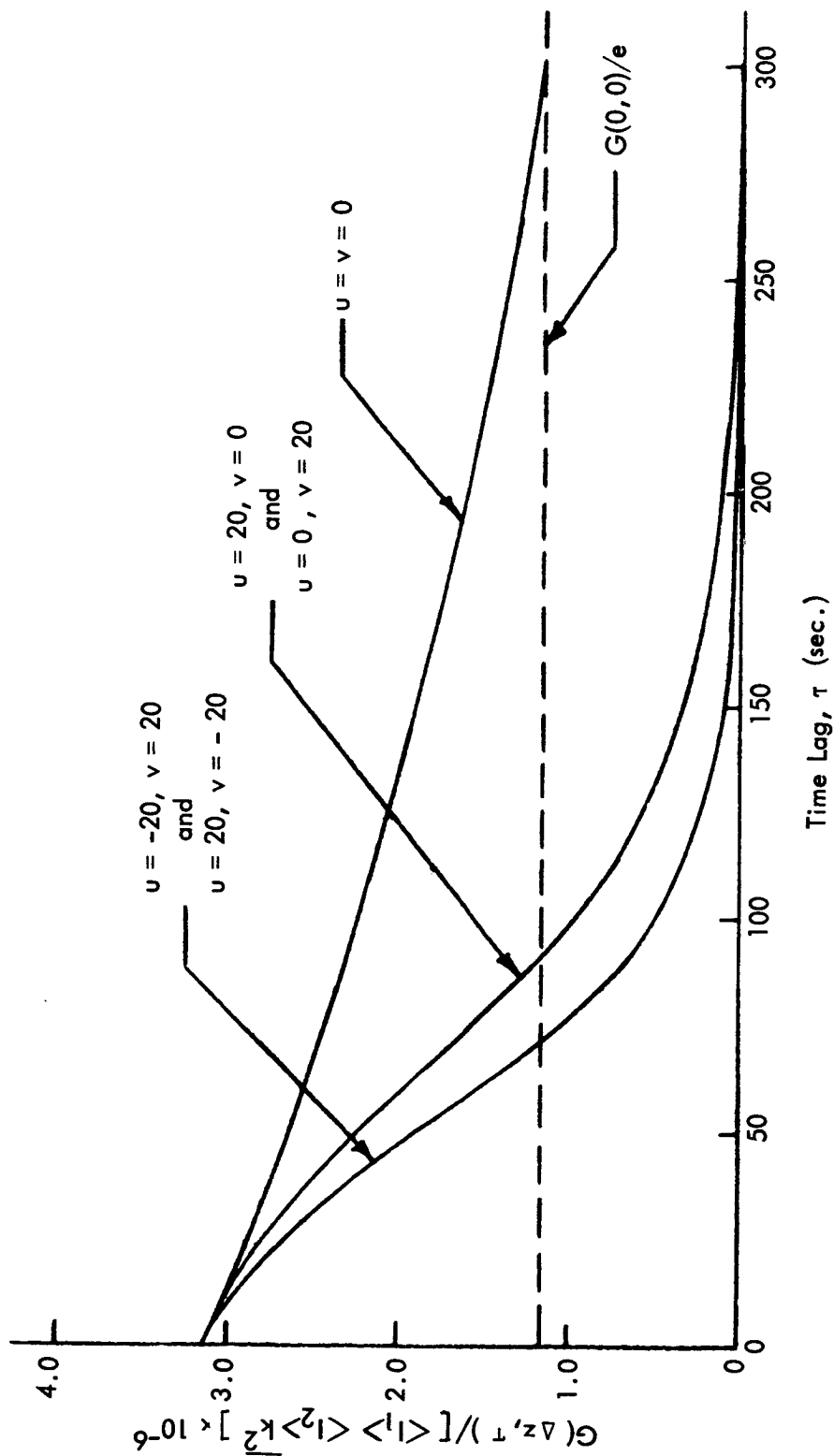


Figure 40 - Effect of Cross Flow on Covariance Envelope for Turbulence Patch Centered Around Beam Normal

The autocorrelation is shown in Figure 41 for three velocity vectors. The change in the autocorrelation is small, compared with changes such as are shown in Figure 40, so are believed to be relatively unimportant. Therefore, the power spectrum should be relatively uninfluenced by velocities perpendicular to the beam normal if the turbulence is centered about the beam normal.

The integral scale of turbulence is obtained by examining $G(\Delta z, 0)$. From (IV-8), we obtain

$$\frac{G(\Delta z, 0)}{\langle I_1 \rangle \langle I_2 \rangle} = \int_{y_1}^{y_2} \int_{x_1}^{x_2} e^{-\left\{ \left[x^2 + y^2 + \Delta z^2 \right]^{\frac{1}{2}} / L \right\}} dx dy \quad (IV-16)$$

which is obviously independent of convection speed.

Next, we consider the effect of the location of the turbulence band with respect to the beam normal. Figure 42 shows results analogous to those of Figure 39, but with the beams crossing below the turbulence, so that $x_1 = y_1 = 1,000$ feet, $x_2 = y_2 = 4,000$ feet. Here, we have again chosen $u = -20$, $v = 20$. (In this case, with the turbulence off center, as opposed to being centered, the signs of the speed components are important in determining the covariance, G .)

The normal velocity component, w , is again obtainable from the tangency points. The envelope is of completely different character, here, as compared to those shown in Figure 40. The phenomena of G increasing with τ before it decreases are as predicted in Section 3a.

Due to the changed shape of the envelope it is obvious that the eddy lifetime cannot be ascertained unless $u = v = 0$. If the convection velocity is directed along the beam normal, (IV-8) may be written

$$G(\Delta z = w\tau, \tau) = e^{-\tau/T} \int_{y_1}^{y_2} \int_{x_1}^{x_2} e^{-\left\{ \left[x^2 + y^2 \right]^{\frac{1}{2}} / L \right\}} dx dy \quad (IV-17)$$

Thus, in this situation, the eddy lifetime may be found from $G = G(\tau = 0)/e$ independently of the location of the turbulence band. Figure 43 shows the envelopes for several selected velocity vectors.

Also evident from Figure 42 is the changed shape of the autocorrelation curve ($\Delta z = 0$). The shape of this curve can be shown to be strongly dependent on the transverse velocity components. An indication of this is evident in the envelopes shown in Figure 43.

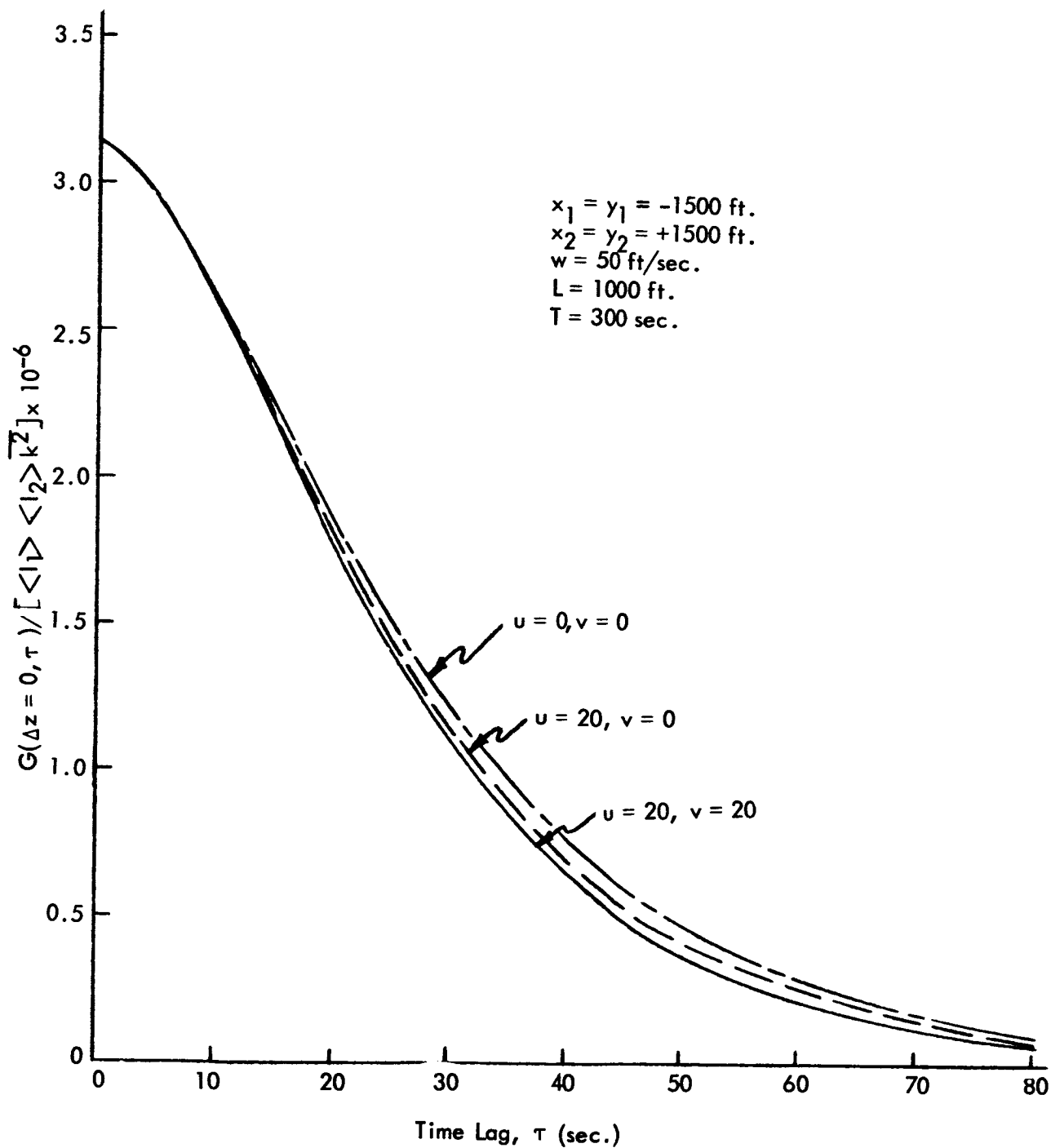


Figure 41 - Effect of Cross Flow on Autocorrelation for Turbulence Patch Centered Around Beam Normal

$x_1 = y_1 = 1000 \text{ ft.}$
 $x_2 = y_2 = 4000 \text{ ft.}$
 $u = -20 \text{ ft/sec.}$
 $v = 20 \text{ ft/sec.}$
 $w = 50 \text{ ft/sec.}$
 $L = 1000 \text{ ft.}$
 $T = 300 \text{ sec.}$

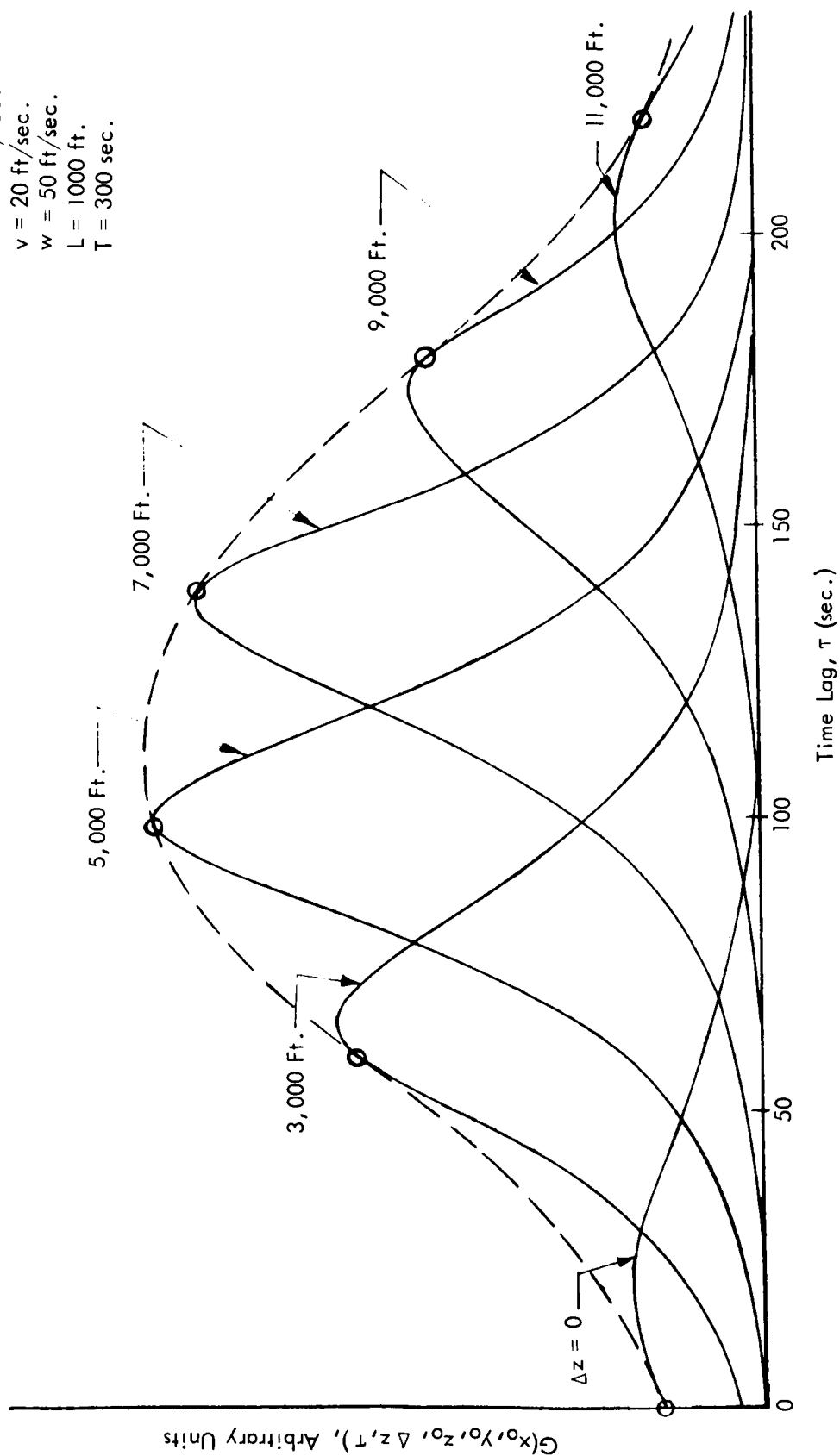


Figure 42 - Covariance for Turbulence Patch Centered Above the Beam Normal with a Horizontal Cross Flow

$x_1 = y_1 = 1000$ ft.
 $x_2 = y_2 = 4000$ ft.
 $w = 50$ ft/sec.
 $L = 1000$ ft.
 $T = 300$ sec.

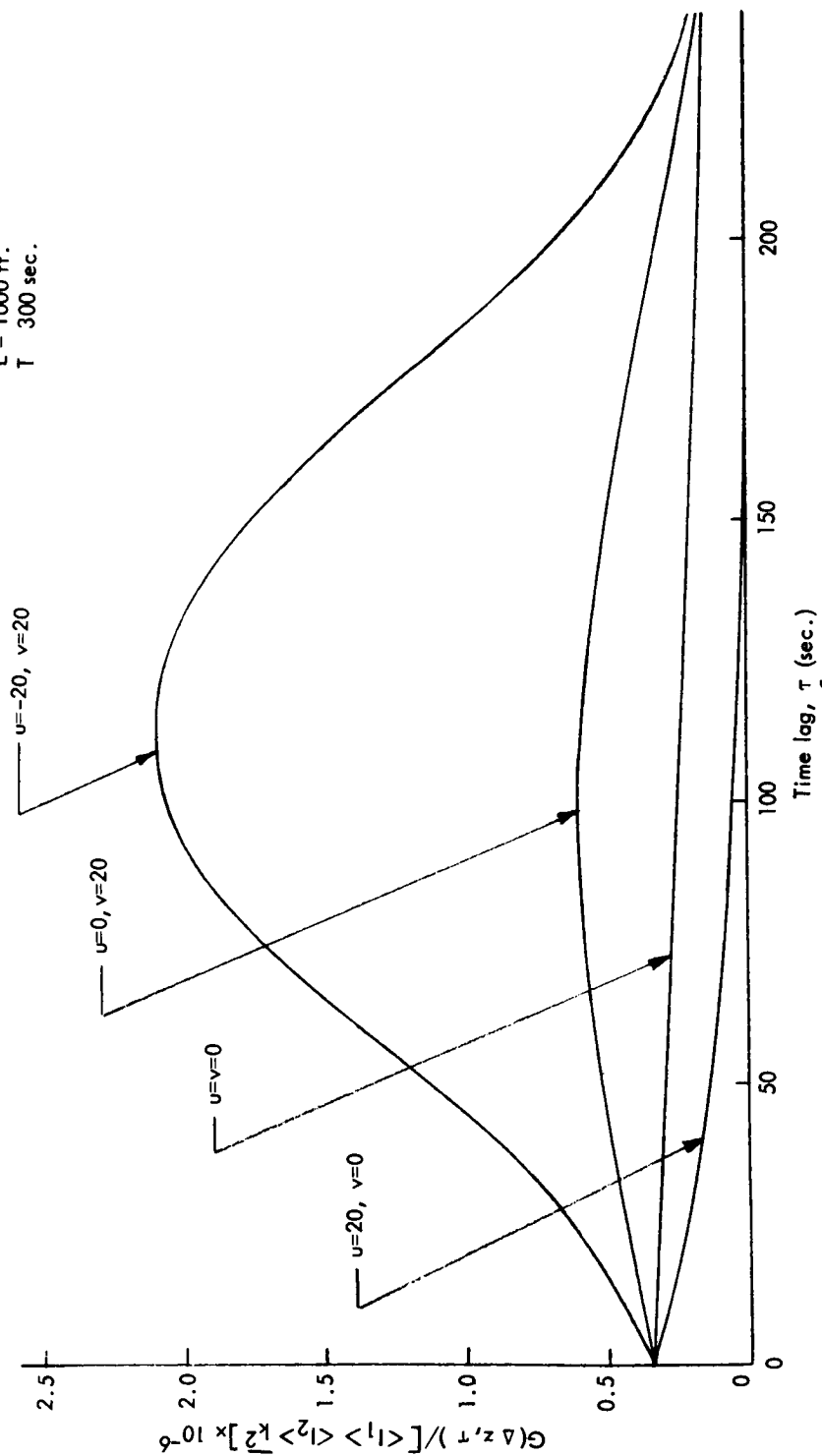


Figure 43 - Effect of Cross Flow on Covariance Envelope for Turbulence
 Patch Centered Above the Beam Normal

Thus, when the turbulence is not centered around the beam normal, the observed power spectrum is influenced by other components of the convection velocity.

Referring again to (IV-16), the determination of the integral scale of turbulence, although independent of convection speed, can be influenced by the turbulence location. Figure 44 shows the covariance plotted against Δz for zero time lag, for the two turbulence band locations considered. (Each curve is normalized to 1 at $\tau = 0$; they actually differ by about an order of magnitude.) It is obvious that the integrals of the curves are unequal. Apparent eddy size is thus dependent on the location of the turbulence relative to the beam normal.

The occurrence of nonuniform turbulence coupled with nonnormal convection speed components appears to cause great difficulty in interpretation of the turbulent flow properties from the beam signal covariance. However, it should be mentioned that the nonuniformity causes one useful effect that does not occur in the ideal case. It is apparently possible to determine the component of convection speed perpendicular to the beam normal. The procedure is outlined below, with the aid of Figure 45.

Curve 1 represents the envelope of the family of curves defined when the beam normal is centered in the turbulent region. The case shown corresponds to Figure 39 where $u = -20$, $v = 20$. Curve 2 is the envelope which would be obtained if $u = v = 0$, with the beam normal at the same location. Curve 3 is obtained when the beam normal is lowered a distance r ($2,500\sqrt{2}$ feet in this example). The peaking effect will be maximized, in general, when the vector \vec{r} is in the direction obtained by reflecting the portion of the velocity vector which is perpendicular to the beam normal about the x-axis. The tangency point between curves 3 and 2 defines a time τ^{**} . That value represents the time required to transport the turbulence a distance r in the x-y plane. (It is simultaneously convected a distance $w\tau^{**}$ in the z-direction.) The component of convection speed in the x-y plane is thus

$$V_{xy} = r/\tau^{**} = 20\sqrt{2} . \quad (\text{IV-18})$$

The actual tangency point cannot be located since curve 2 would be unknown. In its place, the value τ'' corresponding to the maximum in the envelope could be used, as is commonly done in determining w .

Since the convection direction is not known a priori, it appears that the above procedure is still applicable if the direction of \vec{r} is

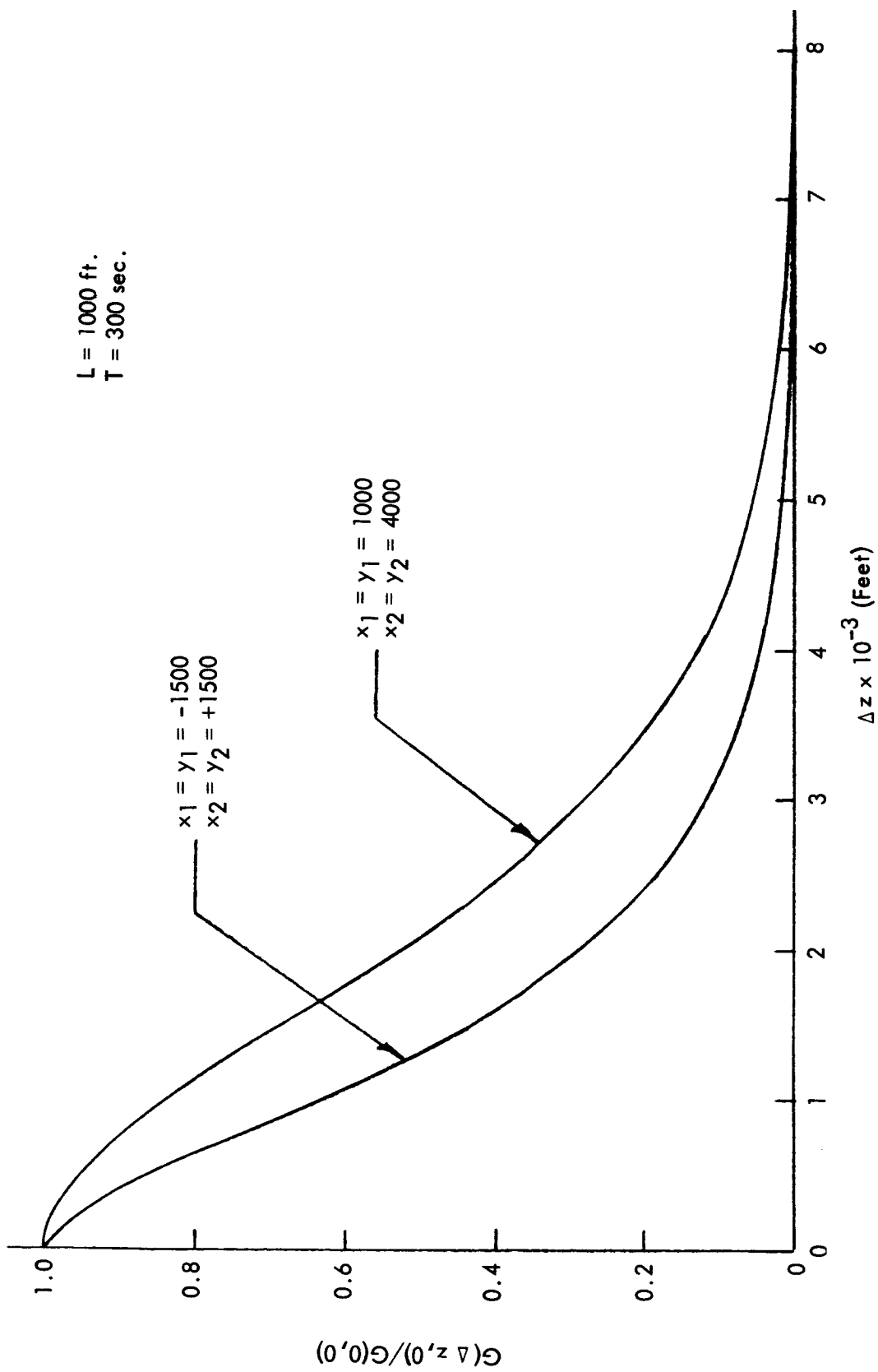


Figure 44 - Effect of Location of Turbulence Relative to Beam Normal on Integral Scale of Turbulence

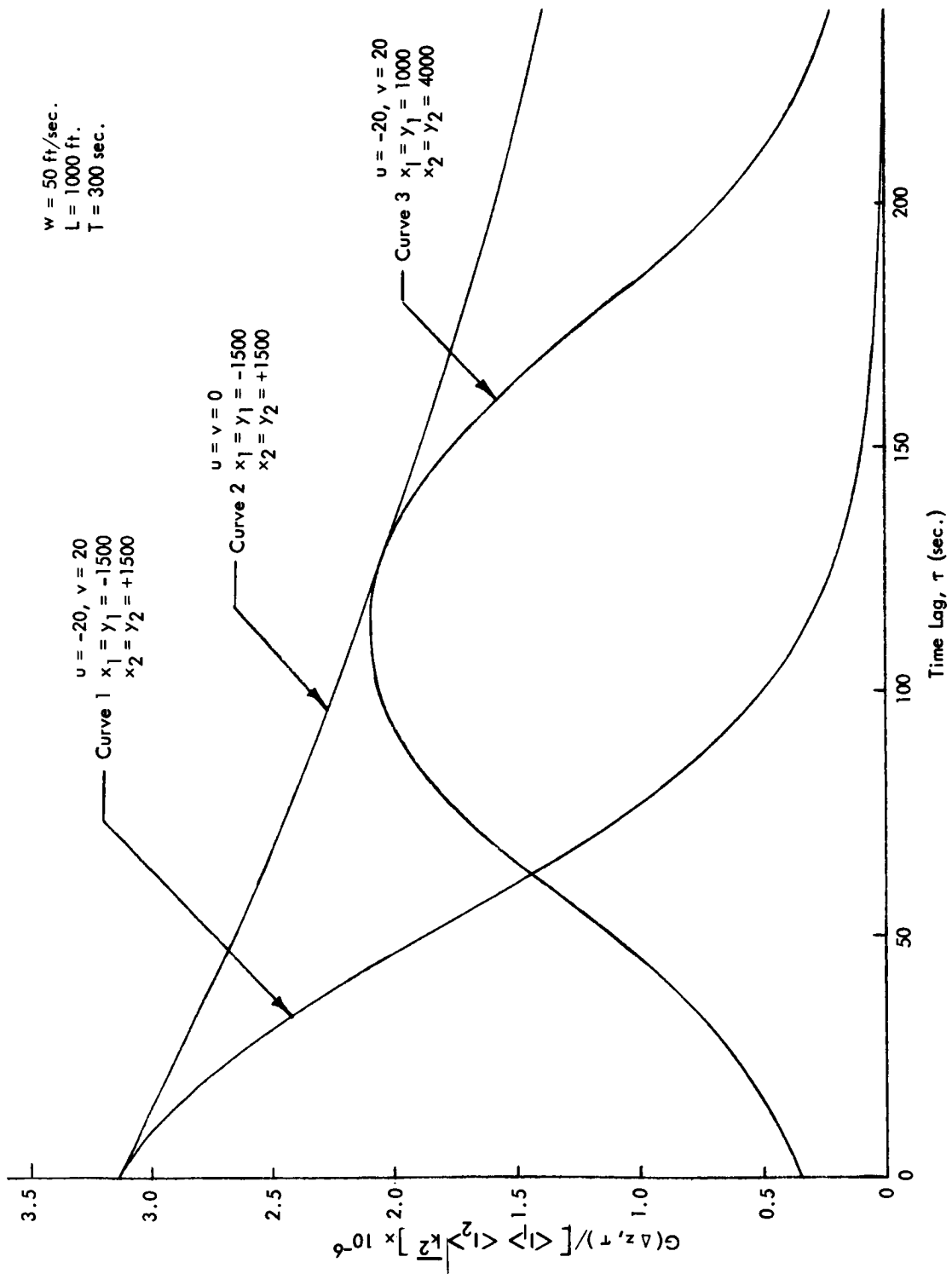


Figure 45 - Determination of Cross Flow Velocity with Nonuniform Turbulence

varied until the highest peak is obtained. τ'' at the peak serves to estimate the speed, V_{xy} , while the direction is obtained by reflecting \vec{r} about the x-axis.*

D. Effect of Wind Shears

The general form of the extinction coefficient,

$$R(x, y, \Delta z, \tau) = e^{-\tau/T_e} - \left\{ \left[(x+u\tau)^2 + (y-v\tau)^2 + (\Delta z-w\tau)^2 \right]^{\frac{1}{2}} / L \right\} \quad (\text{IV-7})$$

is applied to problems involving variable wind speed by simply considering u , v , and w to be functions of position. The exponent in (IV-7) is proportional to the distance at time $t = 0$, between a point on the x-beam at that time and another point which arrives at the y-beam at the later time $t = \tau$. Thus, the convection speeds are to be considered as functions of y and Δz rather than of x .

Two situations are considered. Both involve uniform turbulence with intensity, k . The first situation has no transverse convection ($u = v = 0$) but a w -component of 50 feet/second at $y = 0$ and varying linearly with y (constant shear). The shear was varied from 0 to 0.025 sec⁻¹. The second situation featured a uniform w -component of 50 feet/second but a variable cross flow. The latter was oriented horizontally ($u = -v$) and was defined by

$$V_{xy} = V'_{xy}y \quad (\text{IV-19})$$

where the shear, V'_{xy} , was 0.025 sec⁻¹. Both situations utilized the values

$$L = 1,000 \text{ ft.}$$

$$T = 300 \text{ sec.}$$

To evaluate the effect of the limits on the integrals in (IV-8), both $\pm 4,000$ feet and $\pm 8,000$ feet were used with no significant differences found.

* It is recognized that this procedure is valid only for the extreme, but well defined type of nonuniform turbulence considered here. No attempt at generalization or extrapolation to operational situations is considered, although the concept, in general, seems valid.

Let us consider the effect of the uniform shear in the z-direction and no transverse velocity. First the value of w at the beam normal (50 feet/second) is correctly predicted. This was proven in Section 3a and is shown in Figure 46 for the shear, $w' = 0.025$. Also shown in this figure is the effect of w' on the envelope and hence, on the estimate of the eddy lifetime. It is found that with this type of velocity variation the eddy lifetime is underestimated.

Figure 47 shows the effect of w' on the autocorrelation. Although there is an effect, it is considered small. Thus, the power spectrum will also be affected, but not drastically. The integral scale of turbulence is unaffected by wind speed since it is evaluated at $\tau = 0$.

Turning now to the variable cross flow effects, with uniform w , the results shown in Figure 48 are obtained. The principal conclusions are (a) w is correctly found; (b) eddy lifetime is incorrectly indicated; (c) the autocorrelation and power spectrum is greatly affected, and (d) integral scale of turbulence is unaffected (not shown in figure). The peak in the curve occurs at

$$\tau = \frac{\sqrt{2}}{V'_{xy}}, \quad \Delta z = \frac{w\sqrt{2}}{V'_{xy}}$$

for the beam orientation used (45 degree inclination to the horizontal wind, V_{xy}) and is due to the fact that, at this beam separation and time lag, each particle of fluid which passes the x-beam at $t = 0$ subsequently passes through the y-beam at $t = \tau$. Thus, except for the eddy decay with time, the fluctuations along the entire lengths of the beams are perfectly correlated. This is an extreme case -- this strong peaking would not be expected in real flows. Real shears occurring in the atmosphere could, however, be expected to cause some peaking, depending on beam orientation.

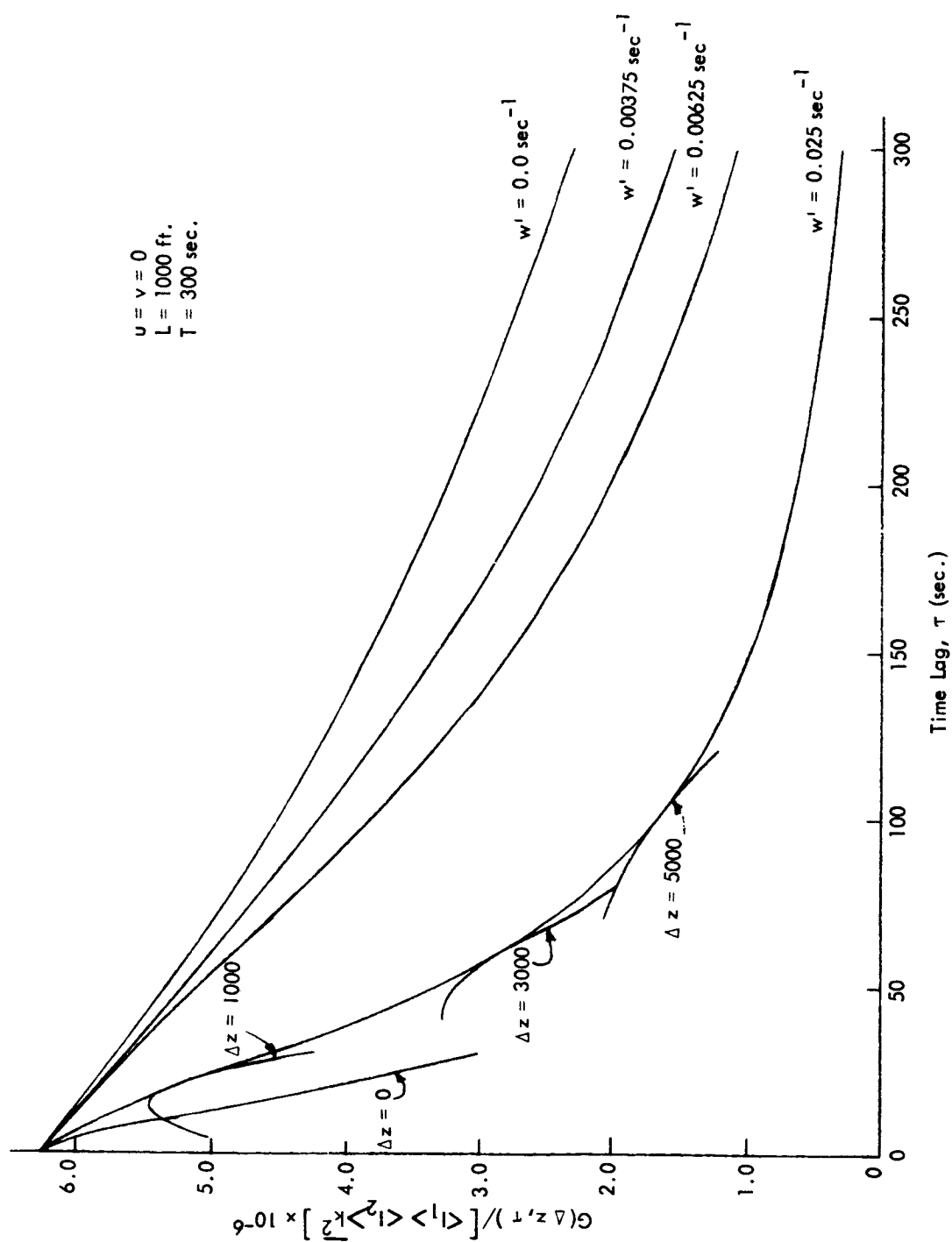


Figure 46 - Effect of Shear, w' , on Correlation Envelope

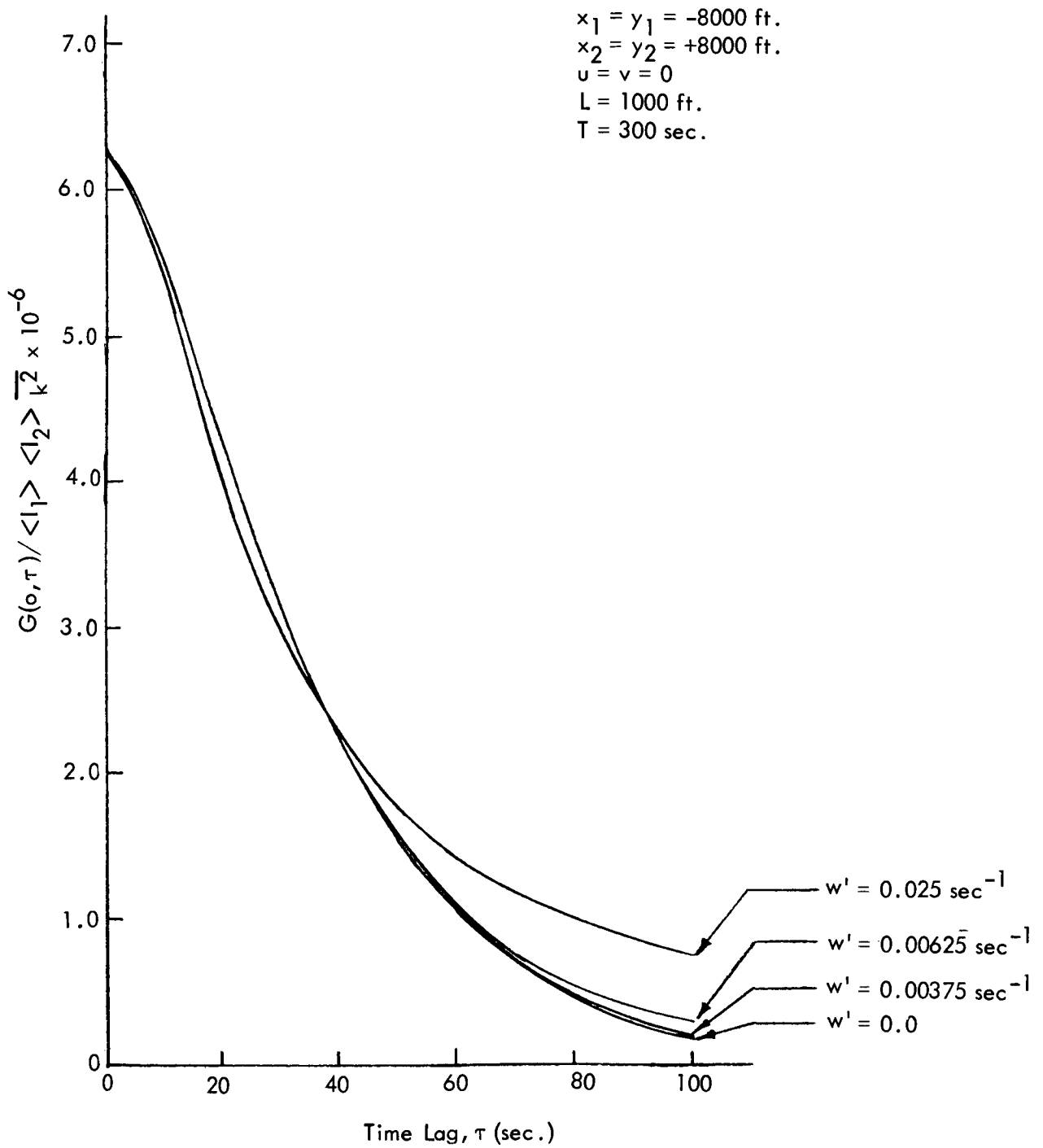


Figure 47 - Effect of Shear, w' , on Autocorrelation

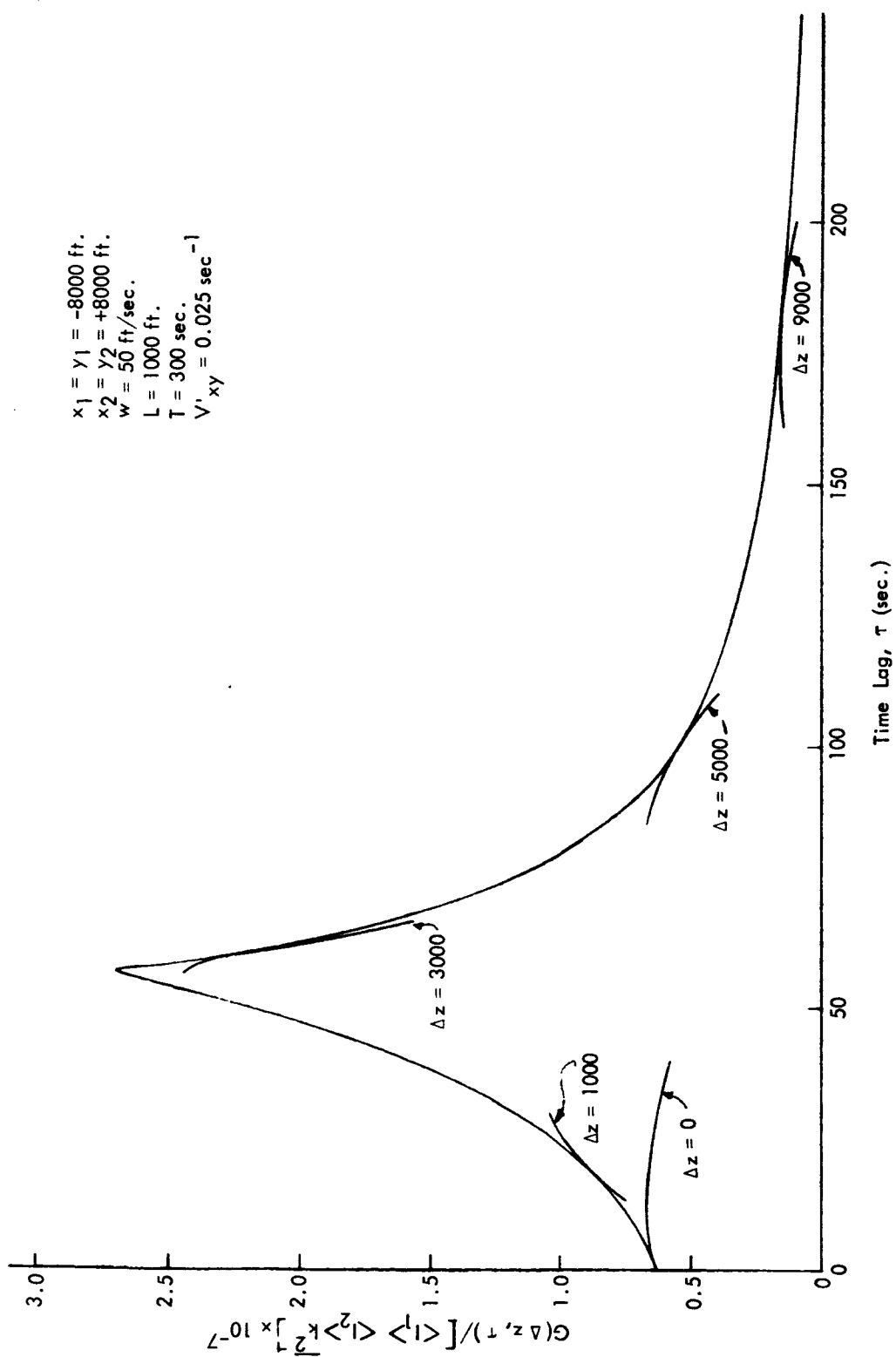


Figure 48 - Effect of Cross Flow Shear on Correlation Envelope

APPENDIX V

EFFECT OF EDDY SIZE AND BEAM DIAMETER ON BEAM POWER

Consider an optical beam of width D measured in the direction of fluid convection speed. We imagine idealized eddies which cause sinusoidal fluctuations in the extinction coefficient, k . We desire the effect on the fluctuation power of the eddy size and beam diameter.

Referring to Figure 49, assume, for simplicity, a beam of rectangular cross section. The total intensity of the beam per unit beam width relative to its average value, is

$$i(t) = \frac{1}{D} \int_0^D \cos \frac{2\pi}{L} (x - Ut) dx ,$$

or,

$$i(t) = \frac{L}{2\pi D} \left\{ \sin \frac{2\pi}{L} (D - Ut) + \sin \frac{2\pi}{L} Ut \right\} .$$

The average power is then

$$P = \lim_{\tau \rightarrow \infty} \frac{1}{2\tau} \int_{-\tau}^{\tau} i^2(t) dt ,$$

or,

$$P = \left(\frac{L}{2\pi D} \right)^2 \left[1 - \cos \frac{2\pi D}{L} \right] .$$

This can be written, as well, in terms of the frequency, ω , of the intensity fluctuations and the time, T , required for a point moving with the fluid to traverse the beam. Thus,

$$D/L = \omega T .$$

Figure 50 shows the relative power in the beam versus $2\pi D/L$ (or $2\pi\omega T$). The power is, of course, zero when the eddy size is equal to the beam diameter. It is obvious that eddies of smaller size than the beam width contribute essentially no power to the beam. Thus, the higher frequency fluctuations, relatively speaking, will not be readily observable.

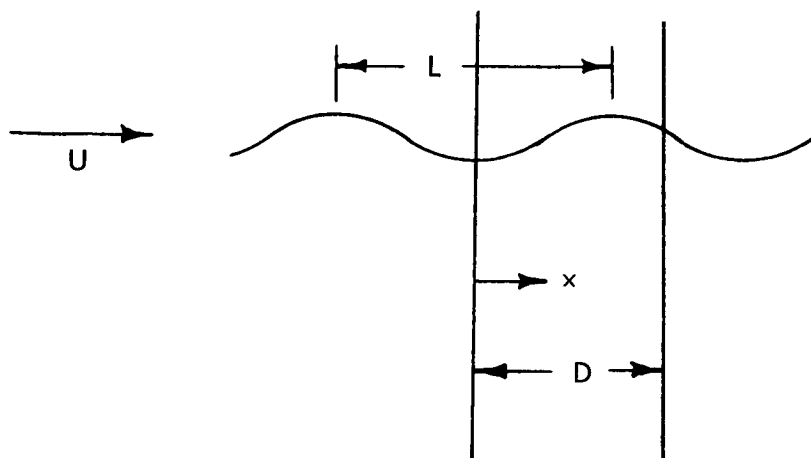


Figure 49 - Eddy Passing Through Optical Beam

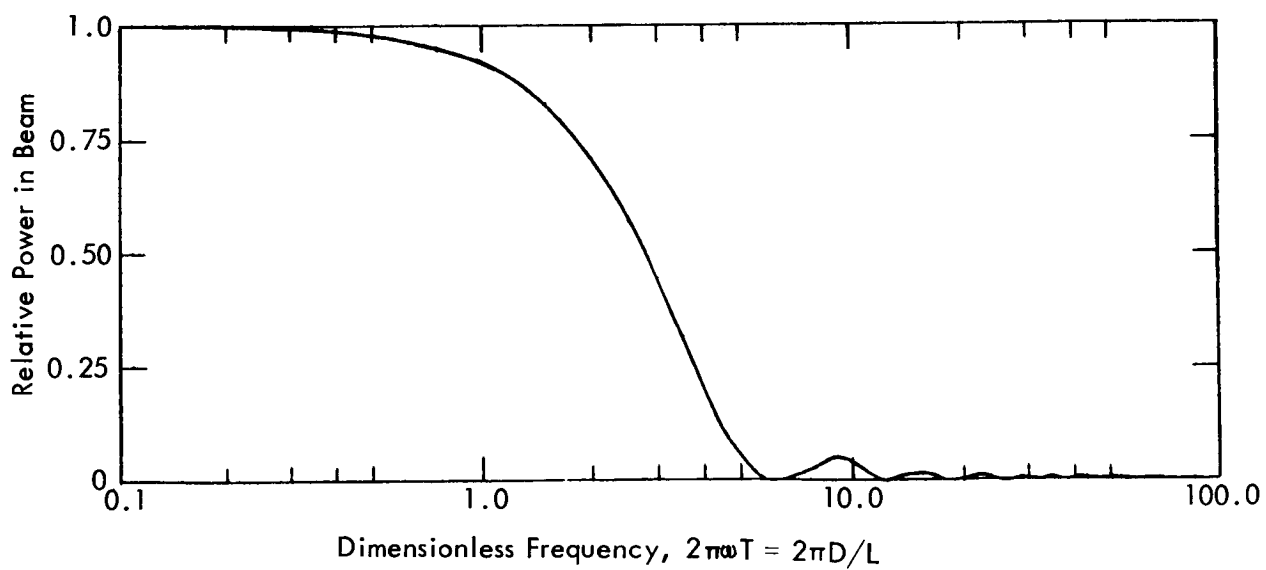


Figure 50 - Power Spectrum for Finite Beam

APPENDIX VI

DETECTOR TECHNOLOGY

It appears that the current state of the art of optical detectors in the visible range of the spectrum is satisfactory for use in cross-beam correlation measurements. That is, the noise that they contribute to the total signal is much less than the atmosphere-generated noise so that the noise limit is set by the atmosphere, not the detection system. In the infrared range, the situation is not as good, with indications being that infrared detectors are only marginal for cross-beam measurements. These statements are based on using a set of fixed beams and with no limitation placed on integration times.

In analyzing the usefulness of an optical detector, three sources of noise must be considered.* These noise sources, discussed below, tend to degrade the usefulness of any detection system and thus are undesirable. For the cross-beam technique, each of two detectors measures the optical power in a given frequency range as a function of time. This power consists of a mean value, $\bar{\phi}$, and fluctuations about the mean. The signals from the two beams are then cross-correlated. We denote by M the fraction of the signal which is correlated, under the assumption that no extraneous correlation arises from the detector system itself. That is, M refers to the correlated signal arising from fluctuations in the atmospheric extinction coefficient in the "correlated region" around the beam intersection or near-intersection.

One of the sources of noise, then, is the portion of the extinction coefficient fluctuation along the optical beam which is uncorrelated.** The ratio of correlated to uncorrelated atmospheric or input signal to the detector is denoted M/M_u . This ratio may be thought of as being related

* Much of this presentation is based on the excellent report by G. Johnson and A.J. Montgomery.⁶⁹ Their notation and approach are followed here.

** There is, of course, no sharp distinction between correlated and uncorrelated fluctuations, as might be implied in the above. Rather, the amount of correlation generally decreases with the distance between the small elements of length of each beam being considered. It is helpful, however, to conceive of "correlated" and "uncorrelated" regions, recognizing that only integrated effects are actually available.

to the number of regions along the beam which are equivalent to the correlated region. Thus, if one assumes each beam sees eleven regions which each generate the same amount of signal fluctuation, but only one of these regions is correlated, then the ratio of uncorrelated to correlated power is

$$M_u^2/M^2 = 10$$

This value seems to be of the order of magnitude that is currently being observed in preliminary experiments.^{70/}

A second source of noise is detector signal shot noise. It is related to the signal intensity, being given by the relation

$$\frac{S}{N_{ss}} = \left[\frac{M^2 \lambda (QE)}{hc(2\Delta f)} \bar{\Phi} \right]^{\frac{1}{2}}$$

where N_{ss} = signal shot noise ,

S = signal ,

λ = optical wavelength ,

QE = quantum efficiency ,

$hc = 1.986 \times 10^{-19}$ micron-joules/photon ,

Δf = bandwidth

and M and $\bar{\Phi}$ are as defined above.

Finally, the detector dark noise, N_d , is that noise which the detector causes in the absence of a signal. It may be expressed in the form

$$\frac{S}{N_d} = D_{\Delta f} M \bar{\Phi}$$

where $D_{\Delta f}$ is the wideband detectivity, in reciprocal watts. It, in turn, is related to other common measures used by detector manufacturers, by the relations

$$D_{\Delta f} = D^* / (A \Delta f)^{\frac{1}{2}}$$

$$D^* = A^{\frac{1}{2}} / \text{NEP}$$

where A is the detector cross-sectional area, D^* is the detectivity in $\text{cm}(\text{cps})^{\frac{1}{2}}/\text{watt}$ for 1 cps bandwidth, and NEP is the noise-equivalent power in rms watts/ $(\text{cps})^{\frac{1}{2}}$.

To illustrate the use of these relationships, two specific detectors are considered for use in a fixed, ground-based detector system. One detector is chosen to operate in the visible spectrum, one in the infrared. The following estimates of mean radiative power, based on a zenith angle of 45° and excellent visibility, are used.*

	<u>Visible</u>	<u>Infrared</u>
Wavelength, microns	0.5	9.6
Wavelength band, microns	0.3	3.0
Background Radiance, watts/ $(\text{cm}^2\text{-micron-steradian})$	6×10^{-3}	2×10^{-4}
Mirror cross section, cm^2	100	100
Field of view, degrees	0.25	0.25
Mean Power, watts	2.7×10^{-6}	0.9×10^{-6}

For use in the visible spectrum, a type S-20 detector made by ITT Industrial Labs is selected as an example. It is a multialkali (Cs-Na-K-Sb) photomultiplier, model FW-143, with the following properties:

* See, for instance, F.R. Krause et al.^{8/} Other estimates, depending on the application, may be used and a similar analysis carried out.

$$A^{\frac{1}{2}} = 0.225 \text{ cm.}$$

$$QE = 20 \text{ percent}$$

$$NEP = 1.1 \times 10^{-15} \text{ watts/cps}^{\frac{1}{2}}$$

A bandwidth of 1,000 cps and a ratio of correlated to mean signal, $M = 0.0001$ (0.01 percent) are selected for this study.* This leads to the following results:

$$D^* = 2.04 \times 10^{14} \text{ cm(cps)}^{\frac{1}{2}}/\text{watt}$$

$$D_{\Delta f} = 2.9 \times 10^{13} \text{ watts}^{-1}$$

$$S/N_{ss} = 1.6 \times 10^3 \bar{\Phi}^{\frac{1}{2}}$$

$$S/N_d = 2.9 \times 10^9 \bar{\Phi}$$

$$S/N_u = \sqrt{M^2/M_u^2} = \sqrt{0.1}$$

The three separate signal-to-noise ratios are shown in Figure 51. It is apparent from the figure that at the anticipated power level the detector adds little noise to the system. It is limited by the atmospheric noise under these conditions. Even if the mean power level decreases by a log, the total noise given by

$$N^2 = N_u^2 + N_{ss}^2 + N_d^2$$

is relatively uninfluenced by detector noise. In that case, the ratio of shot noise to atmospheric noise will be given by

$$\frac{N_{ss}^2}{N_u^2} = 1/10, \text{ approximately.}$$

* These values are felt to be conservative but not unrealistic in light of recent experimental work by IIT Research Institute.^{71/}

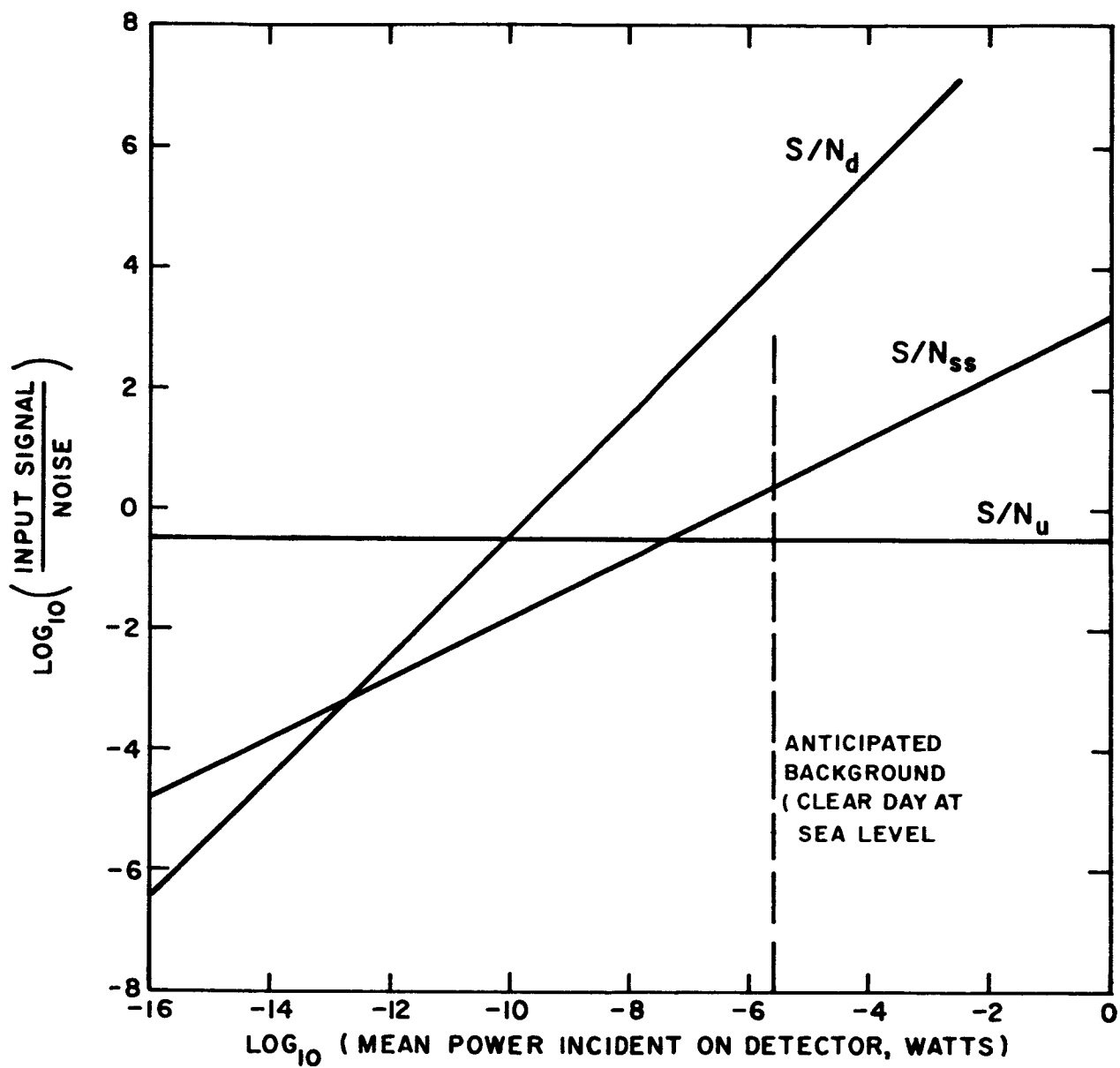


Figure 51 - Signal-to-Noise Ratio in the Visible Spectrum

In the infrared range the detector selected for study is a Ge:Cu detector. The model number of one made by Raytheon is QKN-1009 and it has the following properties:

$$A^{\frac{1}{2}} = 0.044 \text{ cm.}$$

$$QE = 40 \text{ percent}$$

$$NEP = 2.1 \times 10^{-12} \text{ watts/cps}^{\frac{1}{2}}$$

Again, assuming $\Delta f = 1,000 \text{ cps}$ and $M = 0.0001$, we have

$$D^* = 2.1 \times 10^{10}$$

$$D_{\Delta f} = 1.5 \times 10^{10}$$

$$S/N_{ss} = 1.0 \times 10^4 \bar{\Phi}^{\frac{1}{2}}$$

$$S/N_d = 1.5 \times 10^6 \bar{\Phi}$$

$$S/N_u = \sqrt{0.1}$$

Figure 52 shows these ratios and the nominal operating mean power. It appears that, ideally, the system is atmospheric-noise limited. However, a one-half log decrease in either the mean power or the correlated signal level will cause the system to be detector dark-noise limited. Thus, one must consider the detector to be, at best, marginal for this application.

There does not appear to be a significantly better infrared detector on the open market. One should not consider the matter closed, however, even at the present time, until the classified literature in this area is referred to.

It might be expected that the shot noise will not be greatly reduced in future detectors since the quantum efficiency is the only detector factor that might be improved and current detectors have reasonably high efficiencies. Of course, one can lower the detector bandwidth, but then integration time becomes of great concern. The dark noise, N_d , should be expected to be reduced later as lower values of the NEP are attained. Again, the classified literature should be studied in this regard.

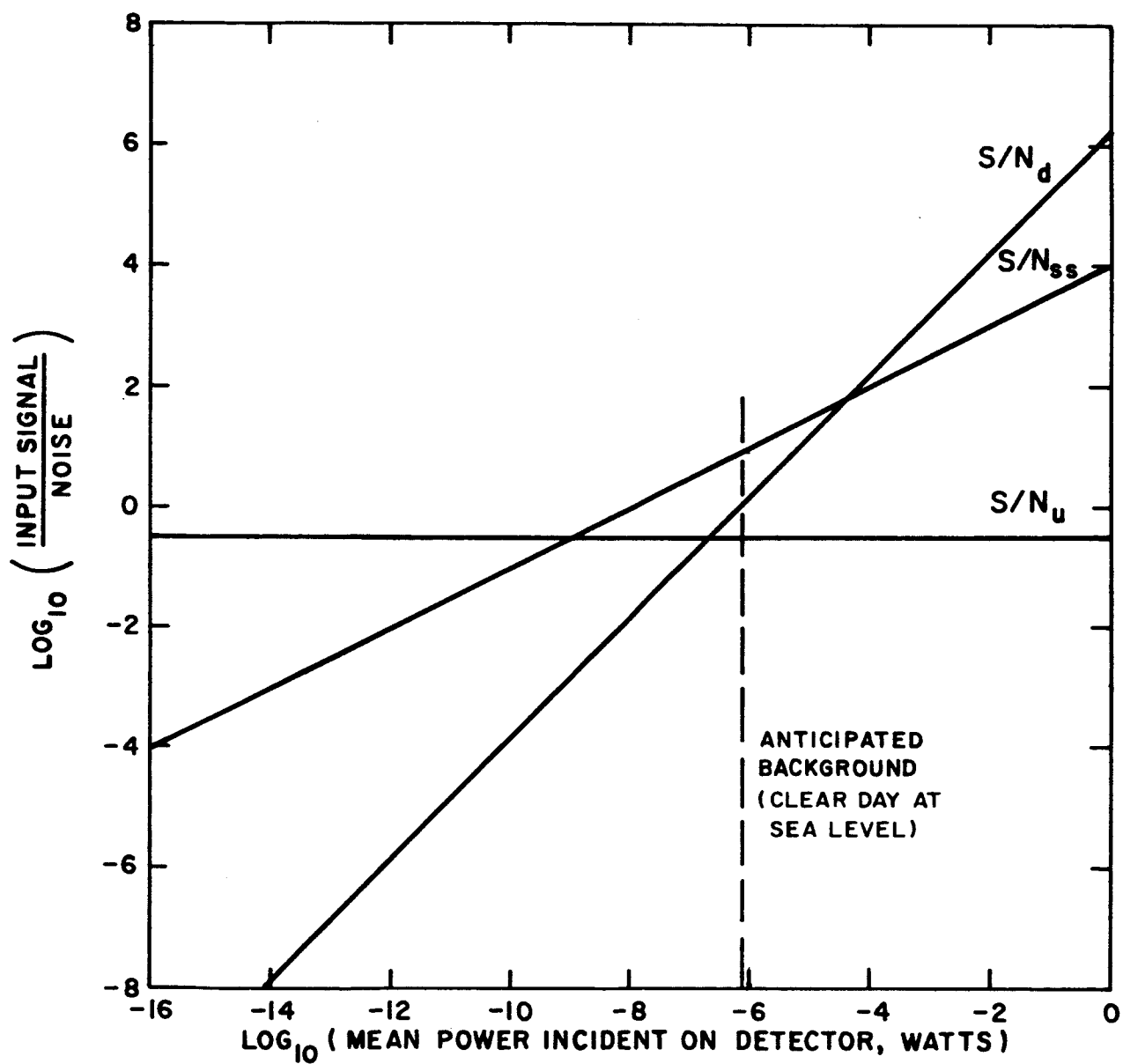


Figure 52 - Signal-to-Noise Ratio in the Infrared Spectrum

APPENDIX VII

INTEGRATION TIME REQUIREMENTS

The cross-correlation, R , between two functions, X_1 , and X_2 is given by

$$R(\tau) = \lim_{T \rightarrow \infty} \frac{1}{T} \int_0^T X_1(t) X_2(t+\tau) dt$$

where τ is the time lag introduced between the two.* In practice, one cannot let T approach infinity, but must accept a finite value. Because of this, the cross-correlation cannot be determined precisely; a certain error will be present. It is the purpose of this discussion to estimate that error as a function of the finite T , the time lag, and the assumed characteristics of the functions.

First of all, it will be assumed that the two functions each contain a common signal, $s(t)$ with the rms value, S , and that they also contain distinct portions, $n_1(t)$ and $n_2(t)$ with rms values N_1 and N_2 . For simplicity it is assumed that $N_1 = N_2 = N$.

The two functions X_1 and X_2 are each assumed to be normal random processes with a flat spectrum over the range of frequencies passed by a filter placed ahead of the correlator. The assumption of normality is not expected to be too restrictive, but the shape of the spectrum is known to be not flat. In fact, initial studies using a single optical beam indicate that the power spectral density decays with frequency to the $-5/3$ to $-6/3$ power.^{70,71/} The assumption of flatness thus leads to the inclusion of more power at the higher frequencies, leading in turn to the expectation of more information per unit time, than truly exists. Thus, from this standpoint, our estimates of integration time will be optimistic (low). However, the general trends will be indicative of the true situation.

A final assumption is that the filter can be considered equivalent (from a transfer function viewpoint) to a low pass RC filter with a full bandwidth , B . (The low pass filter would have half-power points at $\pm B/2$ cps.) The true bandpass filter would be expected to have a flatter

* Much of the basic theoretical development given here is taken from J.S. Bendat.^{72/}

spectrum and sharper cut-off. This assumption compensates, to some extent, for the lack of flatness in the input spectrum but, more importantly, allows the analysis to be carried out with relatively little difficulty. It is recommended, however, that a more detailed study be carried out to confirm the findings given here and, perhaps, to shed more light on the effect of bandwidth and power spectral density on the integration time.

Based on the above assumptions, the ratio of the cross-correlation, R , to the standard error in its estimate, σ is

$$\frac{R}{\sigma} = \frac{e^{-\alpha} \beta^{\frac{1}{2}}}{\left[k + 2(N/S)^2 + (N/S)^4 \right]^{\frac{1}{2}}}$$

where

$$\beta = \pi B T,$$

$$\alpha = \pi B \tau,$$

$$S/N = \text{signal-to-noise ratio},$$

$$k = 1 + e^{-2\alpha} \left[1 + 2\alpha + \alpha^2/\beta \right]$$

and it has been assumed that $\beta \gg 1$. It is noted that

$$\begin{aligned} \lim_{\alpha \rightarrow 0} k &= 2 \end{aligned}$$

$$\begin{aligned} \lim_{\alpha \rightarrow \infty} k &= 1 \\ \alpha &< \beta \end{aligned}$$

so that R/σ is influenced relatively little by k .

Using the normality assumption, the measured value of R lies within a fraction, P , of the true value of R 95 percent of the time if PR is within $\pm 2\sigma$. Using this confidence level and the relation

$$2\sigma = PR$$

leads to

$$Pe^{-\alpha} = 2\beta^{-\frac{1}{2}} \left[k+2(N/S)^2 + (N/S)^4 \right]^{\frac{1}{2}}.$$

In making numerical estimates the values $k = 2$ and $(N/S)^2 = 10$ are used. The time lag, τ , is to be interpreted, for cross-beam applications, as being measured relative to the peak in the correlation curve. That is, the value $\tau = 0$ is used for that actual lag time which corresponds to the translation of an eddy from beam 1 to beam 2. If the beams are physically crossed, the true lag time would also be zero.

Let us first consider the peak in the curve where $\tau = 0$, which is used to determine one component of the convection speed.* For this case, the curve in Figure 53 results. We see that to limit the error to 50 percent (with 95 percent confidence) requires a value of $\beta = 2 \times 10^3$. The correlations recently obtained by IIT Research Institute^{73/} appear to be in this range. The bandwidth used was 1 cps and the integration time corresponded to 10-2/3 min. of data collection.**

To limit the error to 10 percent would require, at the same bandwidth, 25 times as much data (about 4½ hr.). The alternative is to increase the bandwidth. This, apparently, was not possible in the recent experiments because the signal-to-noise ratio deteriorated at the higher frequencies due to detector noise. Thus, it is clear that the required integration time, in practice, is a function of detector noise. That is, it is possible to eliminate such noise by using a narrower bandpass filter (at the lower frequencies) but a severe penalty is thereby paid in integration time requirements.

When the time lag, τ , is introduced, the situation is less satisfactory. Again selecting $(N/S)^2 = 10$ and $k = 2$, we obtain the

* We neglect here the possibility that the tangency point of an individual correlation curve to an envelope of such curves may be displaced from the peak.

** In practice, the data tape was played back to the correlator at 32X recorded speed. Thus, the correlator bandwidth was 32 cps and the actual integration time was 20 sec.

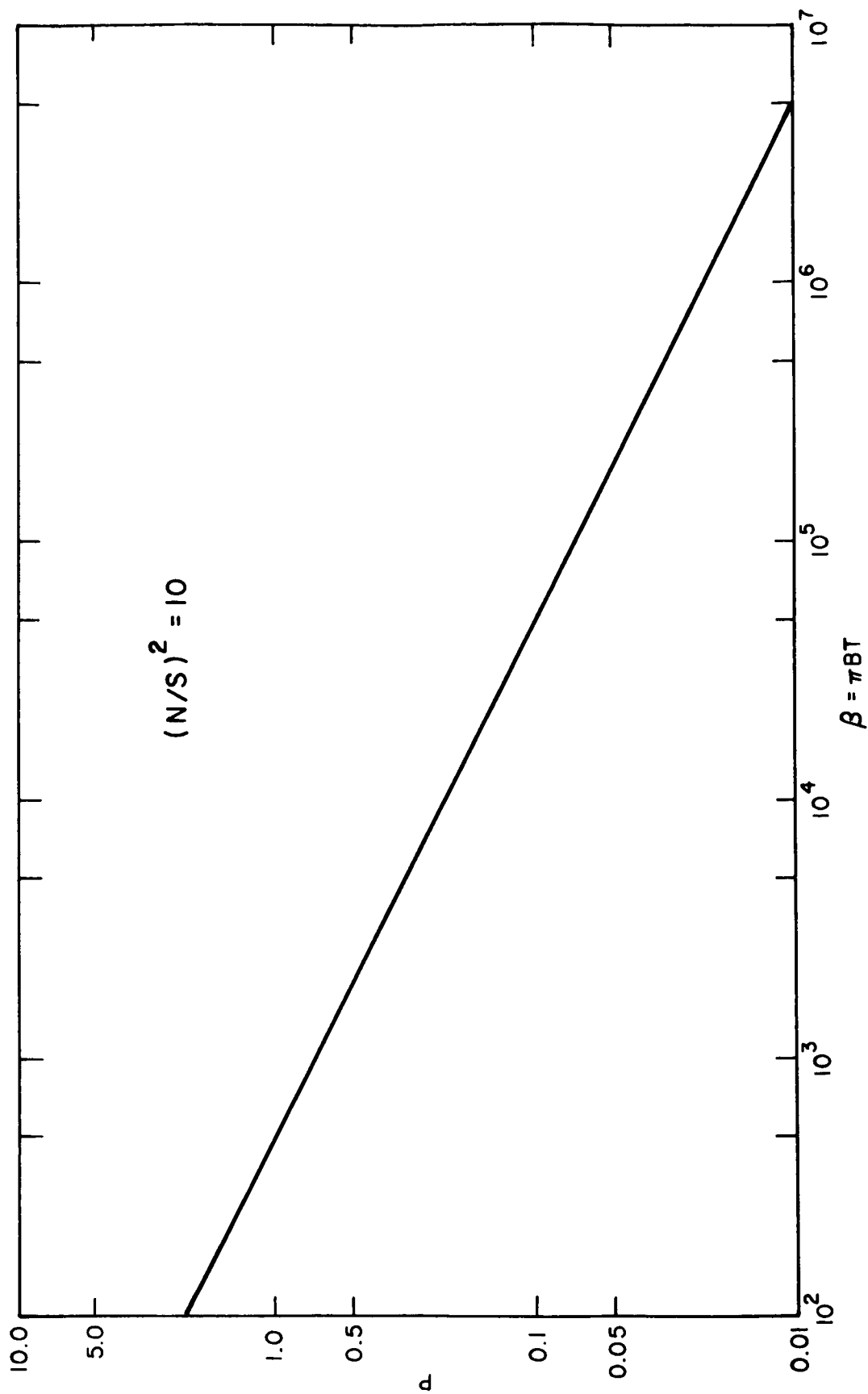


Figure 53 - Maximum Fractional Error, at 95% Confidence Level, in Cross Correlation for Zero Time Lag as a Function of Bandwidth and Integration Time

families of curves shown in Figure 54. The major effect which is noted is the large influence of the time lag on the required integration time to maintain a fixed relative error. A second, less obvious effect is that for a specified integration time and time lag there exists a bandpass which will minimize the error, P .* This bandpass is

$$B = \frac{1}{2\pi\tau}$$

and, for the signal-to-noise values used here, the minimum relative error is

$$P_{\min} = 51.4 \sqrt{\tau/T}$$

For the data presented in Ref. 73 the estimated relative error increases from 50 percent to 100 percent at a time lag of about $\frac{1}{4}$ sec.

The rapid attenuation of precision with time lag, particularly with larger bandwidth filters, leads to speculation that a different approach to locating the peak in the cross-correlation curve might be considered. The current procedure is to compute the correlation at several time lags, with a specified accuracy, then locate the maximum in the resulting curve. An alternative would be to compute the ratio, R/σ , for a specified integration time and for several time lags. The time lag which maximizes R/σ should then correspond to the minimum relative error and, hence, the peak in the correlation vs. τ curve.

In conclusion, it is clear that the problem of integration time is not solved and, furthermore, cannot be considered separately. It is highly dependent on such considerations as input power spectrum, bandwidth selections and detector noise. A major complication is the relative unavailability of data pertaining to input signal fluctuation level and power spectral density. (The current work of IITRI is a start in this direction.) More work needs to be done in such fundamental areas as atmospheric noise generation and random processes. Some light should be shed on the former area by Midwest Research Institute's current studies on atmospheric models; the latter area requires consideration of nonflat power spectra, current filter designs, etc.

* For example, in Figure 54 at $T = 3,000$ sec. (50 min.) and $\tau = 1/4$ sec., the relative error is less for $B = 1$ cps than for $B = 0.1$ or 10 cps.

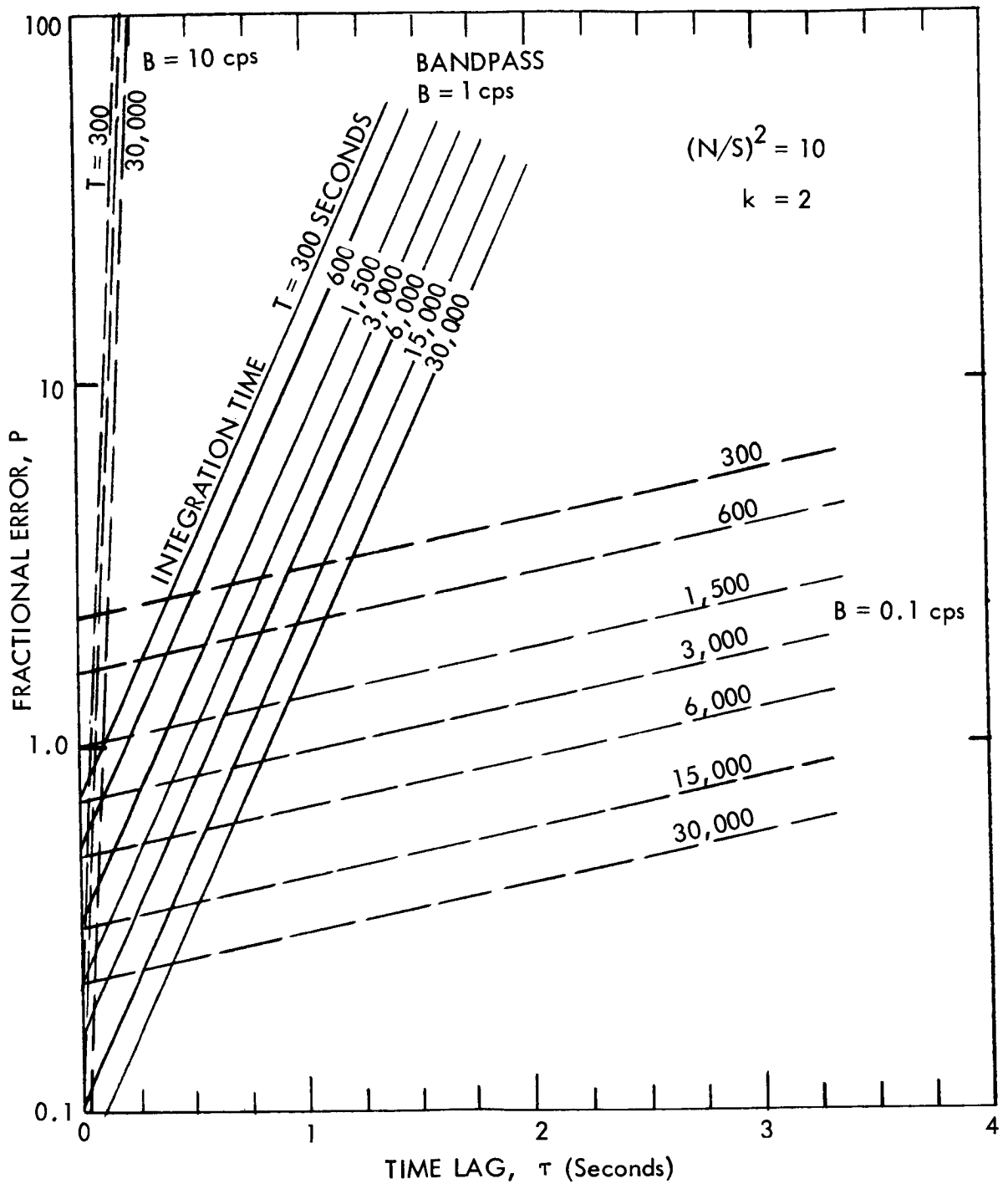


Figure 54 - Error in Correlation Determination vs. Time Lag for Selected Bandpasses and Integration Times

DISTRIBUTION LIST

Final Report, Contract NAS8-21065, Project No. 3042-P

<u>No. of Copies</u>	<u>Recipient</u>
1	National Aeronautics and Space Administration George C. Marshall Space Flight Center Huntsville, Alabama 35812 Attn: PR-SC
1	National Aeronautics and Space Administration George C. Marshall Space Flight Center Huntsville, Alabama 35812 Attn: MS-IL
1	National Aeronautics and Space Administration George C. Marshall Space Flight Center Huntsville, Alabama 35812 Attn: MS-T
2	National Aeronautics and Space Administration George C. Marshall Space Flight Center Huntsville, Alabama 35812 Attn: MS-I
40 + Reproducible	National Aeronautics and Space Administration George C. Marshall Space Flight Center Huntsville, Alabama 35812 Attn: R-AERO-Y Dr. William Vaughan
1	Dr. J. R. Scoggins Department of Meteorology Texas A & M College College Station, Texas 77843

DISTRIBUTION

DEP-T

R-DIR

R-SE

Mr. L. Richard

R-EO

Dr. W. Johnson

Mr. H. Attaya

R-SSL

Dr. Stuhlinger

R-ASTR

Dr. Haeussermann

Dr. R. Decher

R-TEST

Dr. H. Lackner

R-COMP

Mr. J. Jones

Dr. H. Trouboth

I-DIR

Col. O'Connor

MS-IP

MS-IL (8)

R-AERO

Dr. Geissler

Mr. Jean

Mr. Turner

Mr. D. Bean

Mr. W. Vaughan (20)

Mr. Stephens

Mr. Jayroe

Dr. F. Krause (50)

Mr. Mabry

Mr. W. Murphree

Mr. O. Smith

Mr. Fichtl

Mr. R. Smith

R-AERO (Cont'd)

Mr. C. Brown

Mr. Kaufman

Mr. T. Reed

Dr. Heybey

Mr. W. Dahm

Mr. Heaman

EXTERNAL

ESSA

Inst. for Environmental Research

Boulder, Colorado 80302

Attn: Dr. J. Kuettner

ESSA

National Environ. Satellite Center

Suitland, Md.

Attn: Mr. D. Johnson

ESSA

National Bureau of Standards

Boulder, Colorado 80302

Attn: Dr. B. R. Bean

Mr. Andy St. John (25)

Midwest Research Inst.

425 Walker Blvd.

Kansas City, Mo. 64110

IITRI

10 West 35th St.

Chicago, Ill. 60616

Attn: Dr. Fischer (3)

Dr. Montgomery (3)

Mr. R. Sears

Dr. W. Davies

Scientific & Tech. Info. Facility (25)

P. O. Box 33

College Park, Md.

Attn: NASA Rep. (S-AK/RKT)

EXTERNAL DISTRIBUTION (Continued)

Dr. Robert White
Director, ESSA
1410 Gramax Bldg.
8060 13th St.
Silver Springs, Md. 20910

Col. Robert Long
Commanding Officer
Air Force Cambridge Research Labs.
L. C. Hanscom Field
Bedford, Mass. 01731

South Dakota School of Mines & Tech.
Sioux Falls, S. D. 57101
Attn: Dr. Paul Smith

Dept. of Meteorology
Pa. State Univ.
503 Deike Bldg.
Univ. Park, Pa. 16802
Attn: Dr. A. K. Blackadar
Dr. Charles Hosler

Dept. of Meteorology
Univ. of Okla.
Norman, Okla 73069
Attn: Prof. C. C. Lynn
Prof. R. G. Fowler

ESSA
National Severe Storms Lab.
Norman, Okla 73069
Attn: Dr. Lhermitte

ESSA
Atmospheric Physics & Chem. Lab.
Boulder, Col. 80302
Attn: Dr. Helmut Weichman
Mr. Heinz H. Grote

Colorado State Univ.
Dept. of Atmospheric Science
Fort Collins, Col. 80521
Attn: Dr. E. R. Reiter
Dr. Inge Dirmhirn
Prof. Virgil A. Sandborn
Dr. M. M. Siddigui

Inst. of Tech.
St. Louis University
P. O. Box 8020
College Sta.
St. Louis, Mo. 63156
Attn: Dr. Ferdinand C. Bates

Dept. of Meteorology
Texas A&M University
College Station, Texas 77843
Attn: Dr. J. R. Scoggins (4)

NASA Headquarters
Federal Office Bldg. No. 6
Washington, D. C. 20546
Attn: Technical Info. Div. (2)

Ofc. of Adv. Res. & Tech.
Director (2)
Mr. W. McGowan
Dr. W. A. Minzel

Ofc. of Space Sci. & Appl.
Director (2)
Dr. M. Tepper
Mr. J. Lekman
Mr. T. G. George

NASA - Electronic Res. Center
Boston, Mass.
Attn: Dr. Charles E. Leigh

NASA - Langley Res. Center
Langley Sta.
Hampton, Va. 23365
Attn: Mr. H. B. Tolefson

NASA - Goddard Space Flt. Center
Greenbelt, Md. 20771
Attn: Technical Library
Dr. W. Nordburg

Army Missile Command
Redstone Arsenal, Ala. 35809
Attn: Dr. O. Essenwanger
Technical Library